Aalborg Universitet

Stiffness and Damping related to steady state soil-structure Interaction of monopiles

Bayat, Mehdi

STIFFNESS AND DAMPING RELATED TO STEADY STATE SOIL-STRUCTURE INTERACTION OF MONOPILES

BY
MEHDI BAYAT

DISSERTATION SUBMITTED 2015

AALBORG UNIVERSITY
DENMARK

Stiffness and Damping related to steady state soil-structure Interaction of Monopiles

Ph.D. Dissertation
Mehdi Bayat

Dissertation submitted October 06, 2015

Thesis Details

Mandatory page in PhD theses:

The present thesis "Stiffness and Damping related to steady state soil-structure Interaction of Monopiles" is submitted as a partial fulfilment of the requirements for the Danish PhD degree. The work has been carried out in the period April 2012 to September 2015 at the Department of Civil Engineering, Aalborg University, Denmark, under the supervision of Prof. Lars Bo Ibsen and Dr. Lars Vabbersgaard Andersen.

The PhD thesis presents the appropriate model to describe damping effect by applying analytical and numerical methods to get suitable dynamic response to have better design in order to reduce the overall costs. It deals numerical approach and consider the soil medium as a two-phase system consisting of a solid skeleton and a single pore fluid.

The thesis is based on the following collection of scientific papers and reports written by the author of the present thesis and in cooperation with other authors:

◆ Bayat, M., Andersen, L. V. and Ibsen, L. B. (2013). Comparison between dynamic responses of hollow and solid piles for offshore wind turbine foundations. In *Seventh international conference on case histories in geotechnical engineering*, Chicago, USA, pp. 94–108.

◆ Bayat, M., Andersen, L. V., Andersen, S. M. and Ibsen, L. B. (2013). Numerical calculation of damping for monopile foundations under cyclic load during steady-state vibration. In *The fifth international conferences on structural engineering, mechanics and computation*, Cape town, South Africa, pp. 1–6.

◆ Damgaard, M., Bayat, M., Andersen, L. V. and Ibsen, L. B. (2014). Assessment of the dynamic behaviour of saturated soil subjected to cyclic loading from offshore monopile wind turbine foundations. *Computers and Geotechnics* **61**, 116–126.

◆ Bayat, M., Andersen, L. V. and Ibsen, L. B. (2015). $p - y - \dot{y}$ curves for dynamic analysis of offshore wind turbine monopile foundations. *Soil Dynamics and Earthquake Engineering*, In review.

♦ Bayat, M., Andersen, L. V. and Ibsen, L. B. (2015). Influence of pore pressure on dynamic response of offshore wind turbine using poroelastic model. *Computers and Geotechnics*. Early view.

♦ Bayat, M., Ghorashi, S. Sh., Amani, J., Andersen, L. V., Ibsen, L. B., Rabczuk, T., Zhuang, X. and Talebi, H. (2015). Recovery-Based Error Estimation in the Dynamic Analysis of Offshore Wind Turbine Monopile Foundations . *Computers and Geotechnics*, In review.

This thesis has been submitted for assessment in partial fulfillment of the PhD degree. The thesis is based on the submitted or published scientific papers which are listed above. Parts of the papers are used directly or indirectly in the extended summary of the thesis. As part of the assessment, co-author statements have been made available to the assessment committee and are also available at the Faculty. The thesis is not in its present form acceptable for open publication but only in limited and closed circulation as copyright may not be ensured.

Curriculum Vitae

Mehdi Bayat

E-mail: Bayat.me@gmail.com
meb@civil.aau.com
Date of birth: September 6th, 1975
Address: Teglvænget 15, st TV, 9000 Aalborg, Denmark
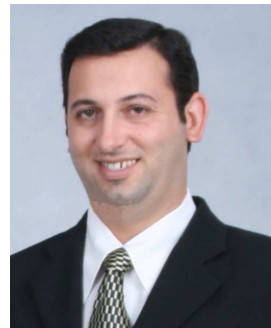
Higher education

2005-2009   **PhD**., Department of Mechanical and Manufacturing Eng. University Putra Malaysia (UPM), Malaysia
Thesis: *Linear and Nonlinear Thermoelastic Analysis of Functionally Graded Materials Axisymmetric Rotating Disks*
CGPA: 4/4

1997-2000   **M.S.**, Mechanical Eng., Applied Design
Sharif University of Technology, Tehran, Iran
Thesis: *The Correction Method to Obtain the Equation of Motion of Rigid Body*
GPA: 16/20

1993-1997   **B.S.**, Mechanical Eng., Applied Design
The University of Guilan, Rasht, Iran
Thesis: *Investigation of Explosive Welding*
GPA: 16.2/20

Research Interests

- Numerical analysis by using: Finite Element Method (Linear/Nonlinear), Extended Finite Elements, Meshfree Methods, Discrete Element Method, Multiscale modelling
- Soil Dynamics, Vibration analysis, Dynamic analysis
- Mathematical Modeling
- Coupling of continuum and Molecular Dynamics
- Composite Materials Analysis such as Functionally Graded Materials

International Academic Activities

2014	**Guest Researcher:** Dept. of Mechanical Eng. and Intelligent, Systems, the University of Electro-communications (UEC), Tokyo, **JAPAN** (Duration: Feb. 2014 – May 2014)
2014	**Guest Researcher:** Dept. of Civil Eng., Bauhaus University Weimar (GRK), Weimar, **Germany** (Duration: May 2013 – Aug. 2013)
2012-2015	**International PhD Candidate:** Dept. of Civil Eng., Aalborg University, Aalborg, **Denmark**
2011-2012	**Research Assistance:** Dept. of Civil Eng., Aalborg University, Aalborg, **Denmark** (Duration: Dec. 2011– March 2012)
2010-2011	**Lecturer:** at Mechanical Dept. University of Malaysia (UM), **Malaysia** (Duration: Dec. 2009 – July 2010)
2009-2010	**Researcher and Visiting Scientific:** Spatial and Numerical Modeling ITMA, UPM, **Malaysia** (Duration: Jan. 2009 – Dec. 2010)
2005-2009	**International PhD Student:** Mechanical Eng. UPM, **Malaysia** (Duration: June. 2005 – Jan. 2009)

Honors

- **Achieving the 4ᵗʰ** place in the national math Olympiad during high school in Karaj city
- **Ranked 1ˢᵗ** during my Bachelor's Degree in the Department of Mechanical Engineering, Guilan University, Guilan, Iran

- **Ranked 17** in the entrance examinations for Master's Degree

Medals

Silver medal	**(2010):** Kasim, N.H.A., Hamdi, M., Rahbari, R.G., Madfa, A.A., **Bayat, M.** "Functionally graded structured dental post (FGSP): A Novel Device to Restore Masticatory Function" 4th – 6th February 2010, Putra World Trade Centre - Kuala Lumpur.
Gold medal	**(2010):** Kasim, N.H.A., Hamdi, M., Rahbari, R.G., Madfa, A.A., **Bayat, M.** "Development of the novel dental post with the functionally graded design to restore endodontically treated teeth" 1st – 3rd April 2010, Innovation and creativity EXPO, Kuala Lumpur, Malaysia.
Gold medal	**(2010):** Kasim, N.H.A., Hamdi, M., Rahbari, R.G., Madfa, A.A., **Bayat, M.** "New generation of dental posts for rehabilitation of endodontically treated tooth" 14 – 16 May 2010, 21st International Invention, Innovation and technology Exabition, ITEX, Kuala Lumpur, Malaysia
Silver medal	**(2010):** Madfa, A.A., Kasim, N.H.A., Hamdi, M., Rahbari, R.G., **Bayat, M.** "A new multilayer composite with functionally graded design for endodontic application" International conference on functional material and devise, 2010, 14-17 June, Terengganu, Malaysia.
Bronze medal	**(2010):** Ali Shahrjerdi, Faizal Mustapha , **M. Bayat**, R.Zahari, S.M.Sapuan, D.L.A. Majid and R.Rahbari G "Hydroxyapatite-titanium functionally graded material via pressure-less sintering" Invention, Research and Innovation Exhibition, Pameran Rekacipta Penyelidikan dan Inovasi (PRPI), 2010, 21-22 July, University Putra Malaysia, Malaysia.

Reviewer

- Soils and Foundations (Elsevier)
- Ships and Offshore Structures (Taylor and Francis)
- Aerospace Science and Technology (Elsevier)
- European Journal of Mechanics - A/Solids (Elsevier)
- Materials and Design (Elsevier)
- Ocean Engineering (Elsevier)
- Applied Ocean Research (Elsevier)
- International Journal of Mechanical Sciences (Elsevier)
- Smart Materials and Structures (IOP)
- Applied mathematical modeling (Elsevier)

- Proceedings of the Institution of Mechanical Engineers, Part B.,(Professional Eng. Publishing)
- Journal of Mechanical Engineering Science - Part C., (Professional Eng. Publishing)
- International Journal of structural stability and dynamics (world scientific)
- Proceedings of the ASME 2010 10th Biennial Conference on Engineering System Design and Analysis, ESDA2010 (ASME)
- Journal of Sustainable Manufacturing and Renewable Energy

Academic Lecturers

2010-2011	**Lecturer:** at Mechanical Dept. University of Malaysia (UM), **Malaysia** (Duration: Jan.n 2009-Dec.2010)
2006-2008	**Teaching Fellow:** Dept. of Mechanical and Manufacturing Faculty of Engineering, UPM, **Malaysia** (Duration: First and second semester 2006/2008)
2000-2005	**Lecturer:** Dept. of Mechanical and Manufacturing at SEMNAN Azad University branch as a full-time academic member, **Iran** (Duration: Sep. 2000 – Sep. 2004)

Industrial Experience

2010-2011	**Research Engineer:** At GL GARRAD HASSAN COMPANY (Duration: Dec. 2010 – DEC. 2011)
2004-2005	**Maintenance Manager:** at SARDSAZ KHODRO IND. COMPANY (Duration: Dec. 2004 - June 2005)
2000-2004	**Engineers / Specialist:** at IRANKHODRO INDUSTRIAL DIES CO (IKID) (Duration: Dec. 2000 - Dec. 2004)
2000	**Engineers / Designer:** at SEPANTA CO. (Duration: Aug. 2000 - Dec. 2000)

Publication

Research Publications more than 50 ISI journals, H-index = 11 (Date: 15-07-2015)
More details are available at:
https://scholar.google.com

Biodata of The Author

Mehdi Bayat (Medi) was born on 6th September, 1975 in Karaj, Iran. He is one of top students in primary and secondary school. In 1990 he entered to high school, he was the top student and in fourth years, he was invited to national mathematics Olympiad, Medi received his fourth degree in that exam, in Karaj city.

He pursued his studies at Gilan Technical University in 1994. He was awarded with a Bachelor degree of Solid Mechanical Engineering 1998. During 4 years study, he was Ranked 1st during Bachelor's Degree and he has been working on the project about explosive welding under supervision of Dr. Darvizeh, who is one of the best professors in Iran, awarded in 1997.

In master entrance exam, he was ranked as seventeenth in Iran and that lead him to continue his study in the best university of Iran: Sharif university of Technology. He has been working in dynamic field.

After graduation he was working as an assistant Professor at Semnan University as a full-time academic member from 2000 to 2004 and also he worked at University of Applied science and Technology, Tehran. He was interested to teach in fields of Strength of materials, Dynamics and Engineering mathematics, Pneumatic, hydraulic and press machine. Moreover, during those years he was working at Iran Khodro Industrial Die Design simultaneously. His industrial experiences are concern with maintenance, transportation and re-installation in boring, milling and press machines and he had cooperation with Scholpp Group in translation and re-installation of 6 CNC machine, such as: Rammatic, Jobs etc in Iran Khodro Industrial Die Design, 2004.

He continued his study in the field of Mechanical Engineering under supervision of Prof. B.B. Sahari, Universiti Putra Malaysia. He achieved full grade A in PhD courses.

He was then proceeded his study in the field of Geotechnical Engineering under supervision of Prof. Lars Bo Ibsen and Dr. Lars Vabbersgaard Andersen at Aalborg University. Medi had produced number of publications during his study.

Preface

I would like to express my deep gratefulness to my supervisor Professor Lars Bo Ibsen for providing me with the opportunity to realise this PhD study and for his kind assistance, support, encouragement and suggestions during the study and preparation of this thesis.

I wish to express my sincere gratitude and appreciation to Dr. Lars Vabbersgaard Andersen for his guidance, critical advice, patience, understanding, encouragement and supervisions throughout the course of the study until the completion of this thesis. I truly appreciate the time he devoted in advising me and showing me the proper directions to continue this research and for his openness, honesty and sincerity. Fruitful discussions, and his constant support and patience over the years have been of invaluable help.

I appreciate the funding support provided by the Department of Civil Engineering, Aalborg University and the Advanced Technology Foundation via the research project Cost Effective Monopile Design. My thanks also go to all colleagues I have worked with, in Aalborg, Weimar and Tokyo, for all help that they have provided. Special thanks are given to all my friends around for pleasant discussion, fruitful and enlightening discussions, moral support and helpfulness during the course of the project.

I wish to express my special thanks and appreciation to my mother and father, who passed away, sibling for their unconditional supports and good cheer.

Words are not enough to thank my lovely wife Maryam for the support she has given me during this long and sometimes difficult journey. I would like to take this opportunity to express my gratitude and the deepest appreciation to Maryam, who has kept me going through it all, with her patience, encouragement, and love, and helping me to keep life in balance. Without her, I would not be able to achieve or enjoy these successes. Though she may not quite realize it yet, my daughter Mana is source of great joys that sustain me and help keep life in perspective.

Aalborg, October 2015 Mehdi Bayat

Summary in English

Renewable or sustainable energy resources gain global interest and are accompanied with less global warming. The cost of energy produced by offshore wind turbines (OWTs) is high compared to conventional sources (coal, oil, etc.). Also it is more expensive than land-based wind turbines (WTs) but since there is limited space on land (where people do not like to have the turbines due to noise and visual impact), OWTs are gaining ground. But the cost of energy (CoE) has to come down to strengthen the competitiveness with fossil fuels.

In order to reduce the CoE, the optimized total weight of turbine and its foundation is demanded which is resulting in a slender system and much more sensitive than non-optimized system to dynamic excitations even at low frequencies. This flexible structure is often exposed to dynamic loads such as wind, waves and, in some regions, earthquakes. OWT foundations undergo translation and rotation due to these applied loads, and the surrounding soil undergoes deformation. The study of the foundation subjected to transient load is important in the context of foundation design especially to work out the stiffness and effective damping due to the surrounding soil. To avert damage of offshore foundation, and obtain a better design, it becomes necessary to identify and quantify the soil-structure interaction and damping effects. The damping level of offshore wind turbines is very important for the fatigue damage accumulated over the lifetime of the structure. Hence, accurate prediction of the damping level is necessary.

The amplitude of the dynamic response of the wind turbine is dependent on the overall damping. Hence, in order to predict accurately the wind turbine lifetime, it is vital to assign the correct damping. The total damping in offshore wind turbines consist of aerodynamic, structural and soil damping. Soil damping comprises radiation and material dissipation. By introducing soil as a porous material, the damping of the seepage can be investigated. The seepage of pore water caused by the deformation of the seabed leads to viscous forces that eventually lead to damping. In order to obtain more precise damping of the seepage, it is important to understand the dynamic interaction between the foundation and the soil. It is important to understand the interaction between the foundations and the dynamic behavior of soil, and soil should be modeled more precisely for that purpose. Generally soil can be considered to be a porous medium consisting of solid phase (soil skeleton) and fluid phase (water

and gas). Determination of the dynamic response of fluid-saturated porous media is an important and not yet fully solved problem in many practical engineering applications.

Unfortunately, accurate and realistic natural frequencies of OWTs as well as soil stiffness and damping cannot be quantified by current methods. The purpose of the current research is to obtain a better understanding of the stiffness and damping of saturated soil, propose an improved methodology for analysis of soil-foundation interaction that accounts for rate-dependent behaviour of saturated soil. Typically, in the design of piles, the soil-structure interaction is incorporated by a so-called Winkler model with springs along the foundation. The increase in stiffness due to high-rate deformation of the saturated soil is not accounted for, and damping is only described in terms of modal damping within each mode. Thus, material damping, viscous damping from seepage and radiation damping are not accounted for explicitly.

Since the stiffness of foundation and subsoil strongly affects the modal parameters, the stiffness of saturated soil due to pore water flow generated by cyclic motion of monopiles is investigated using the concept of a Kelvin model which combines springs and dashpots. In this regard, the coupled equations for porous media are employed in order to account for soil deformation as well as pore pressure. The effects of drained versus undrained behaviour of the soil and the impact of this behaviour on the stiffness and damping related to soil-structure interaction at different load frequencies are illustrated. Based on the poroelastic and Kelvin models, more realistic dynamic properties are presented by considering the effect of load frequency for the lateral loading of monopiles subjected to cyclic loads.

Resumé på dansk

Vedvarende og bæredygtige energiressourcer har global interesse og medfører mindre global opvarmning. Udgifterne til energi der produceres af offshore-vindmøller (OWTs) er høje i forhold til konventionelle energikilder (kul, olie, etc.). Det er ligeledes dyrere end landbaserede vindmøller (WTs), men da der er begrænset plads på land (hvor folk ikke kan lide at have møllerne på grund af støj og visuel effekt), indvinder OWTs terræn. Men udgifterne til energi (CoE) skal mindskes for at kunne styrke konkurrenceevnen i forhold til de fossile brændstoffer.

Med hensyn til reducering af CoE kræves den samlede vægt af møllen og dens fundament optimeret, hvilket medfører et spinklere mere smalt system som er meget mere følsomt end et ikke-optimeret system overfor dynamiske excitationer selv ved lave frekvenser. Denne fleksible struktur er ofte udsat for dynamiske belastninger såsom vind, bølger og i nogle regioner, jordskælv. OWT-fundamenter undergår translation og rotation på grund af disse påførte belastninger, og den omgivende jord undergår deformation. Studiet af de fundament der udsættes for forbigående belastning er vigtig i forbindelse med fundamentdesign specielt med hensygn til bestemmendes af stivhed og effektiv dæmpning forårsaget af den omgivende jord. For at undgå beskadigelse af offshore-fundamentet og for at opnå et bedre design er det nødvendigt at identificere og kvantificere jordstrukturens interaktion og dæmpningseffekter. Dæmpningsniveauet for havvindmøller er meget vigtigt for udmallelsesskader, der akkumuleres over strukturens levetid. Derfor er det nødvendigt at have en nøjagtig forudsigelse af dæmpningsniveauet.

Amplituden af den dynamisk respons af vindmøllen er afhængig af den samlede dæmpning. For at forudsige vindmøllens levetid præcist, er det derfor vigtigt at tildele den korrekte dæmpning. Den samlede dæmpning af havvindmøller består aerodynamisk og strukturel dæmning samt dæmpning i jorden. Sidstnævnte omfatter udstråling og materialedæmpning. Ved at betragte jorden som et porøst materiale kan man undersøge dæmpning pga. sivende porevand. Strømning af porevand forårsaget af deformation af havbunden fører til viskose kræfter, der i sidste ende fører til dæmpning. For at opnå mere præcis dæmpning af udsivning er det vigtigt at forstå den dynamiske interaktion mellem fundamentet og jorden. Det er vigtigt at forstå samspillet mellem fundamenterne og jordens dynamiske opførsel, og jord skal modelleres mere præcist til dette formål. Generelt kan jord anses for at være et porøst medium bestående af en fast fase (jordskelettet) og en væskefase (vand og gas). Bestemmelse

af den dynamiske respons af mættede porøse medier er et vigtig og endnu ikke fuldt løst problem i mange praktiske ingeniørmæssige anvendelser.

Desværre kan præcise og realistiske egenfrekvenser af OWTs samt jordstivhed og dæmpning ikke kvantificeres ved de nuværende metoder. Formålet med den aktuelle forskning er at opnå en bedre forståelse for stivhed og dæmpning af mættet jord og at foreslå en forbedret metode til analyse af jord-fundament interaktionen, der gælder for mættet jords rateafhængige adfærd. Typisk i modelleringen af pæle er jord-struktur interaktionen inkorporeret ved en såkaldt Winkler-model med fjedre langs pælen. Stigningen i stivhed på grund af høj hastighed deformation af den mættede jord er ikke redegjort for, og dæmpning er kun beskrevet i form af modal-dæmpning inden for hver tilstand. Således redegøres der ikke eksplicit for materialedæmpning, viskos dæmpning fra sivende vand og udstråling.

Da stivheden af fundamentet og undergrunden påvirker modale parametre kraftigt, undersøges stivheden af mættet jord, der er forårsaget af porevandsstrømning genereret af cyklisk bevægelse af monopæle, ved hjælp Kelvin-model konceptet, der kombinerer fjedre og svingningsdæmpere. I denne henseende anvendes de koblede ligninger for porøse medier med henblik på redegørelse for jordens deformation samt poretryk. Virkningerne af jordens drænede versus udrænede opførsel og virkningen af denne adfærd på stivhed og dæmpning forbundet med jord-struktur interaktionen ved forskellige belastningsfrekvenser er illustreret. Baseret på poroelasticitet og Kelvin-modeller præsenteres mere realistiske dynamiske egenskaber ved at betragte effekten af belastningsfrekvensen for sidebelastning af monopæle der udsættes for cykliske belastninger.

Contents

CHAPTER 1
Introduction

Wind energy is a type of renewable energy that pumps billions of dollars into the economy. Zero greenhouse gas emissions, low conventional pollutants, affordability, wide availability and wide distribution are characteristics of wind energy as a clean and in-demand energy source (Fthenakis and Kim 2009). Given recent demands for renewable energy, more attention has been paid to wind turbine options. As wind energy pushes to reduce the cost of energy, manufacturers have increasingly sought to increase the size of turbines as well as develop wind farms. In this chapter, a discussion of the different types of wind turbines, their support foundations and applied dynamic lateral load is given with emphasis on the dynamic behaviour of the wind turbine and support structures. The discussion is concluded with a brief overview of the present research. A guide to the remainder of the thesis is provided at the end of the chapter.

1.1 Wind Turbines

The modern era of wind turbine began in 1979 by Danish constructors such as: Kuriant, Vestas, Nordtank and Bonus. These early in-land (onshore) wind turbines generally had small capacities (10 kW to 30 kW) by today's standards, but pioneered the development of the modern wind power industry that we see today. Wind turbines can generally be categorized by whether they are horizontal axis or vertical axis wind turbines (HAWT and VAWT)(Fig. 1.1). The rotational axis of VAWT and HAWT are perpendicular and parallel with the ground respectively. VAWT capable of operating during minimal wind speed and have ability to produce well in tumultuous wind conditions

HAWT   VAWT

Figure 1.1: (a) Horizontal and (b) vertical axis wind turbines (Yahia Baghzouz 2012)

by wind coming from all 360 degrees and they are applicable in small wind projects and because of public ordinances it cannot be placed high enough to benefit from steady wind and also they are not as effective

as HAWT. However HAWT do not produce in turbulent winds well and are generally heavier than VAWT, but they are much more applicable in the big wind industry application because they are able to produce more electricity from a given amount of wind and it is possible to produce as much as possible at all times. Currently small, Intermediate, medium and large-sized wind turbines have generation capacities of less than 100 kW, 250kW, 3MW and more than 3MW, receptively. Today's utility-scale horizontal-axis wind turbine generally has three blades, stall- or pitch-regulated, sweeps a diameter of about 80 to 100 meters, typically start generating electricity at a wind speed of 3 to 5 m/s and generally cut-out at a wind speed of around 25 m/s, has a capacity from 0.5 MW to 3 MW and is part of a wind farm of between 15 and as many as 150 turbines that are connected to the grid (IRENA 2012).

1.1.1 Fundamental elements of a wind turbine

A wind turbine is commonly consist of a rotor (hub and blades), power train, nacelle, generator, tower and support foundation. The blade should be enough stiff and light to have efficient aerodynamic effects and also in order to avoid any resonance, the blade frequency should not be coincide with the frequency at which the blades pass the tower. The shape and material of blade have important roles to capture best possible energy form the wind. A wind turbine with three blades presents efficient aerodynamic effects. Air-foil shapes with a tapered and twisted geometry and composite material are commonly utilized to fabricate desired blades. The steel nacelle structure is a housing for the power train components such as turbine

Figure 1.2: Fundamental elements of a wind turbine. After Vestas Wind Systems A/S (2011).

(and generator) shafts (low (and high)-speed shafts), a gearbox, a yaw drive, brakes, control components and as well as lubrication, and cooling functions. The nacelle located at the top of the tower where the generator is placed and connected to the hub. The nacelle and consequently the rotor shaft aligned with the wind direction by a yaw drive. The nacelle is mounted on a cylindrical and tapered tubular shell tower, the tubular shape permits access from inside the tower to the nacelle and also some devices such as a ladder, powered lift for maintenance, cables for carrying power and control signals are often placed in the tower (Fig. 1.2).

However, the high growth in the installed capacity of offshore wind turbines (wind turbine structure in water), mainly anchored by the ambitious energy and climate change objectives for 2020 by the European Union Committee (2008), causes many challenges within civil engineering and science, and the sector has still not made a definitive breakthrough.

Support Structures fix the wind turbine into the ground. In order to guarantee the stability of the wind turbines, based on the type of wind turbine namely onshore and offshore, different effects and considerations should be taken into account. Based on the size of wind turbine, the dynamic load spreading and the geotechnical site conditions, plate foundations and/or combination of plate and pile foundations are considered to fix onshore wind turbines. Plate foundation is one of the most commonly used foundation, de-

Figure 1.3: Octagonal onshore wind turbine base. (Hamacher 2012)

fines as a large reinforced concrete plate under the earth which forms the footing of the onshore wind turbine. For soft subsoil, the foundation plates are fixed with (inclined and/or vertical) piles into the earth. The foundation for one of the very large turbine with 8 MW and 222 m height which has been installed at østerild wind turbine test field in Denmark is shown in Fig. 1.3. For offshore wind turbine foundations, the other factors like the water depth and the hydrodynamic conditions are important as well. The foundation and/or substructure is defined as as the entire structure to transfer the wind turbine loads to the soil or ground. Not only the dynamic wind load and the geotechnical site conditions are important but also ice loads, sea water loads like: the wave, current and also pore pressure load in saturated soil should be considered for offshore wind turbine foundations. With the anchorage of offshore wind turbines on the seabed, different substructure types such as: grounded and floating designs are considered. The most famous floating designs are: tension leg platform, barge and spar floaters. The grounded designs can be classified into monopod and multipod structures. Different types of grounded offshore wind turbine foundations will be explained in more detail later in this chapter.

1.1.2 Small and large wind turbines

Small wind energy systems can be used in connection with grid-connected systems, or in stand-alone applications that are not connected to the utility grid. A grid-connected wind turbine can reduce your consumption of utility-supplied electricity for lighting, appliances, and electric heat. If the turbine cannot deliver the amount of energy you need, the utility makes up the difference. When the wind system produces more electricity than the household requires, the excess can be sold to the utility. With the interconnections available today, switching takes place automatically. Small onshore wind turbine

Figure 1.4: Proven 6Kw wind turbine at Brill school. (RET 2015)

are typically less than 50 kW in size, but can be as large as 500 kW and are designed to provide electricity for isolated locations, small regions and companies. In all of these applications, the turbine(s) are providing energy for the end user to offset the use of grid power. Small turbines are typically installed as a single unit or in small numbers. The interest is in finding small wind turbines that produce the most energy at low wind levels. Fig. 1.4 shows a proven WT6000 wind turbine installed at Brill's school in 2004 (Renewable Energy Toolkit 2015). The three-bladed turbine has 5.6 m diameter and 9 m height.

More or less the harnessed energy by a wind turbine is approximately commensurate with the swept area by the blades. By increasing the rotor diameter twice, the swept area and consequently the output power is increased by a factor of four. Fig. 1.5 presents the growth in the size of wind blades and turbines (EWEA 2013). In order to extract more energy from the wind, beside improving the size of the wind turbine, some control mechanisms such as yaw and pitch could be supportive. A yaw and pitch are rotational mechanisms to adjust and put the wind turbine rotor and blades to exploit more energy and get efficient rotational speed.
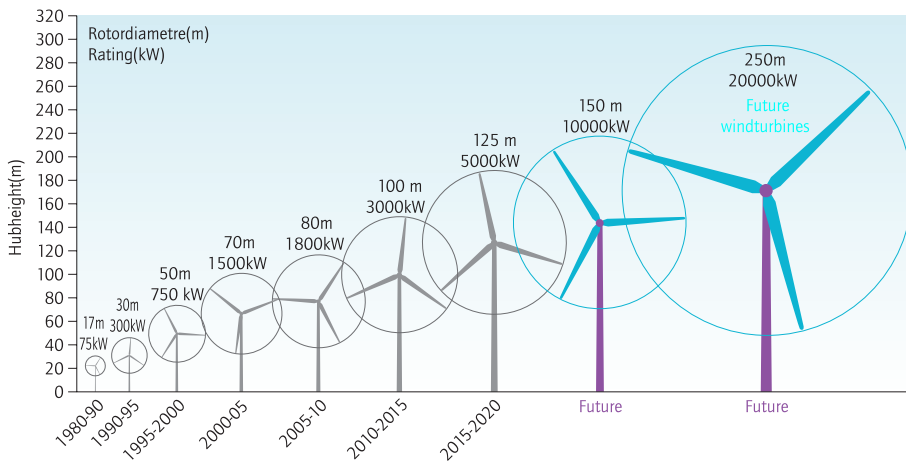
Figure 1.5 Growth in the size of wind turbines since 1985. After EWEA (2013).

A large contribution from wind energy to European power generation is technically and economically feasible. In 2011, installed wind power produced 6.3% of the EU's demand for electricity. EWEA's analysis predicted to produce roughly 14% of the EU's demand in 2020 (EWEA 2013). Large wind turbines have rated capacities ranging from 650 kW to 3 MW (and/or 4 MW) and are designed for using in electricity generating power plants. As wind turbines get larger, worries have emerged that the turbine noise would move down in frequency and that the low-frequency noise would cause annoyance for the neighbours (Møller and Pedersen 2011). The average level of noise from wind turbine can be the same level of noise as a family car travelling at 100 Km/h. Large turbines are typically deployed in either onshore and/or offshore wind farms and are intended to provide wholesale bulk electricity and connect to the

electric power transmission network.

1.2   Advantages of Offshore Wind Turbine

As Fig. 1.5 shows the growth in the size of turbines, this trend is not confined to off-shore, the size of wind turbines installed on-shore has also continued to grow. Larger turbines provide greater efficiency and economy of scale, but they are also more complex to build, transport and deploy. Based on lower cost for transporting, installing and servicing of the wind turbines, majority of them are erected on land so far. Onshore wind energy is one of the most cost-effective and mature of all the renewable technologies. Whilst off-shore wind has high costs, immature tech-nologies and development constraints. At present, one of the most expensive energy technology is offshore wind turbine energy.

Figure 1.6: Offshore wind farm at Anholt. (Dong Energy 2015)

Based on a result of the technical difficulties of offshore turbine construction and con-nection to the National Grid. Offshore wind farms energy is 90% and 50% more expensive than fossil fuel generators and nuclear energies. Wind farms on land are al-most as monetarily cheap as fossil fuels. But, if environmental damage was included, the price of coal would be three times greater than onshore wind energy, according to Friends of the Earth. Over time, offshore wind energy costs should come down, just as onshore has (Boythorpe Wind Energy 2015). The advantage of shifting offshore brings not only higher average mean wind speeds, but also the ability to build very large turbines with large rotor diameters. Offshore wind farms can harness more fre-quent and powerful winds than are available to land-based installations. Consequently, the tower heights, rotor diameters and rated powers of offshore wind turbines have in-creased during recent years in order to capture the more energetic winds that occur at higher elevations and to produce more energy per turbine installation. At this writing, however, the majority of wind turbines is located onshore due to lower installation cost. Nevertheless, the population density and existing buildings limit suitable wind turbine locations on land in many regions of the world. This justifies the development of offshore wind energy and indicates the potential of rapid growth of the market over the next decade. Thirteen offshore wind farms have been constructed in Denmark. Fig. 1.6 shows the biggest wind farm, which has capacity of 400MW is located at Anholt.

Whilst onshore wind has developed into a mature technology, the availability of desir-able sites is diminishing and new locations are becoming harder to develop. Offshore locations offer greater scope in this respect, as well as higher load factors out at sea and the scale effects from building very large wind farms. Offshore wind is steadier

and stronger than on land, and offshore farms have less visual impact, but construction and maintenance costs are considerably higher (Fthenakis and Kim 2009; Gipe 1993). Offshore wind turbine design is a burgeoning area of engineering and young technology. Offshore wind turbine foundations are subjected to time-varying loads from waves, wind and ice, and during operation blade passage across the tower as well as imbalances in the rotor cause cyclic loading. These loads may cause premature failure in the ultimate limit state or the fatigue limit state if resonance occurs or damping is low. Therefore, the certain dynamic response of offshore wind turbine which depends on the soil–structure interaction can play an important role in design step. The average wind turbine size is currently between 2 MW and 3 MW. Whereas, the average turbine capacity is around 4 MW positioned within a average distance of 29 km from shore and located at positions with average water depths less than 16 m. However, the cost of energy for offshore turbines is higher than that for onshore turbines due to large costs in operation and maintenance. In addition, offshore foundations may account for up to 35% of the installed cost (Byrne and Houlsby 2003). Evidently, the biggest challenge in the offshore wind industry is how to reduce the cost of energy. By increasing lifetime span and reducing the maintenance programs and operational costs, the energy cost is going to reduce. Moreover, enhancing the understanding of the dynamic behaviour of wind turbine and the interactive behaviour between the substructure and ground is necessary to have more accurate design of the wind turbine and consequently reducing the overall wind turbine cost. The model can simulate the soil correctly and brings more interrelation effects between the dynamically active wind turbine and support structure therefore being efficient in terms of computational-time is desired.

The research work presented in this dissertation aims to improve the dynamic interaction between the foundation and the soil and illustrates the dynamic response of offshore wind turbines at different load frequencies based on mathematical and numerical approaches. Special focus on soil stiffness and effective damping because of pore water flow generated by cyclic motion of monopile is addressed. The outcomes of this research may directly or indirectly increase (or decrease) the economic feasibility of future offshore wind farms by presenting more accurate soil stiffness and damping which is related to the interrelation effects between the substructure and the subsoil.

1.3   Offshore Wind Turbine Foundations

The main criteria of selecting the most appropriate offshore wind turbine foundations are: the water depth, the hydrodynamic conditions, the geotechnical site conditions and the wind turbine size. The shallow, transitional water depths are limited to 30 m and 50 m respectively. The water depths greater than 50 m is called the 'deep water' environment. In shallow waters, the wave heights are limited by the water depth and there is no particular dynamic effect from waves, wind, ice or combinations thereof. Current commercial grounded offshore foundations are eco-

nomically limited to maximum transitional depths (maximum water depths of 50 m). Floating structures are especially competitive in terms of the levelized cost of energy with grounded foundations in more than 50 m water depth. According to the water depth, the offshore structure can be levelled by two different strategies: moored floating and grounded (and/or fixed) structures. Current moored floating offshore wind turbine technology is not used on a commercial scale. Several prototypes for offshore wind floating foundations can be listed as: tension leg platform, barge and spar floaters which are combination of swaying, buoying and floating concepts. Based on the number of interface between the substructure and seabed, monopod and multipod foundations are defined for grounded structures. The following subsections give introduction to some of the most important and popular grounded offshore wind turbine foundations.
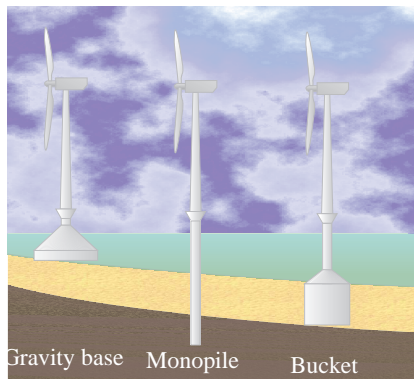
Figure 1.7: Typical monopod substructure concepts for offshore wind turbines.

1.3.1 Monopods

Monopod substructures are defined as having a single interface to the seabed such as: gravity base, monopile and suction caisson monopod foundations (Fig. 1.7). The mentioned monopod substructures are well suited for shallow water depth and sites with water depth ranging from 0 to 25 metres according to the DNV (DNV 2011).

Heavy weight foundations are massive area foundations employed steel or reinforced concrete caissons which are sunk at the location of the plant with the help of ballast. A small skirt around gravity base foundation could make a desired restriction for scouring and also increases the contact area and consequently increases the base shear resistance. Comprehensive preparation works are necessary on the seabed in order to make proper contact for heavy weight foundations such as: removing soft top layers and levelling the seabed. The foundation masses increase disproportionally with bigger water depths and they are applicable for shallow water depths up to 30 m. The Danish offshore wind farm

Figure 1.8: Heavy weight foundations for the Horns Nysted II offshore wind farm. (Bilfinger Construction 2015)

projects Middelgrunden (2001), Nysted (2003),Thornton Bank I (2009) and Nysted II (2010), for instance, employed gravity base foundations. Here, the Nysted II is the largest installed offshore wind farm with gravity based foundations with 207 MW ca-

pacity at positions with average water depths less than 12 m. As it is shown in Fig. 1.8 for Nysted II wind farm, gravity base foundations are used rather than piles due to ice conditions.

Monopile foundations consist of a central large diameter steel pipe which is rammed into the seabed by use of a hydraulic or vibratory hammer which has proved to be the most economical solution. Monopile foundations benefits lie in their simple design, relatively easily installation, favourable fabrication conditions with a considerable automation potential, no big preparation works on the seabed and short installation times (Scharff and Siems 2013a). The area of employment is restricted to a relative low water depth of up to 25 m and with pile diameters of around 4–6 m. However, Scharff and Siems (Scharff and Siems 2013a; Scharff and Siems 2013b) have explored the use of very

Figure 1.9: Monopile foundation for the Horns Reef II offshore wind farm. (Bilfinger Construction 2015)

large monopile foundations in water depth of up to 40 m with diameter up to 10 m and have given two detailed discussions of design examples. Reducing scour around monopiles is desired issue which is related to wave loads and pile diameter. It should be noted that wave loads change intensely with the pile diameter. Another difficultly of monopiles is injecting grout in cold conditions to attach a transition piece on top of the monopile which the transition part is bolted to the wind turbine tower. A transition piece is located between the tower and monopile. Examples of the three largest offshore wind farms by actual energy production since commissioning are Horns Reef I (2002), Nysted 1 (2003) and Horns Reef II (2009). Fig. 1.9 shows one of the monopiles used for the Horns Reef II offshore wind farm.

Suction caisson monopod foundations or bucket foundations consist of a cylindrical, open steel towards the bottom which is drawn into the ground with the negative pressure generated inside the foundation presses after placing on the sea bed. These novel bucket foundations are combining the key benefits of gravity based foundations, a monopile and suction anchor technology (Byrne 2000; Ibsen *et al.* 2003; Houlsby *et al.* 2005). The material at the bottom of the inside of the cylinder supports the foundation and fixes it to the sea bed. Bucket foundations can have a silent installation process and relatively cost-efficient because of avoiding any cranes, pile driving and jack-ups and also they can easily

Figure 1.10: Monopod bucket used as foundation for the Mobile Met Mast at Horns Reef II offshore wind farm. (Universal-Foundation 2015)

be deconstructed. However, the buckling phenomenon during installation can be considerable issue because of the thin shell structure compared to the diameter of the buck (Madsen *et al.* 2013). Prerequisite for bucket foundations are unobstructed conditions of the ground. Bucket foundation can be employed in water depths up to around 40 m. Aalborg University has done a lot of researchs and projects on bucket foundations and recently two bucket foundations have been installed at the Forewind Dogger Bank project in the UK 2013. Moreover, the foundation was used to support the met mast for Horns Rev 2 in 2009 Denmark and a Vestas V90 turbine in Frederikshavn in 2004 Denmark (Fig. 1.10).

1.3.2   Multipod

Multipod foundations refer to the substructure with more than one interface to the seabed and this makes them suitable for deep water depths where there are large bending loads. In the following, only tripods, triples and jackets with piled anchoring are presented. According to DNV (DNV 2011) the water depth for the from 25-40 m and for tripod and jacket (or lattice) support structures is 20-50 m. However these type of foundation can be utilized in shallow depth but they are not suitable at water depth less than 6-7 m especially for tripods and triples cases.

Tripods foundations have a central foundation pipe to absorb the offshore wind turbine which is welded and connected to a three-legged foundation structure made out of steel as shown in Fig. 1.11. Three pipes, which are bucked up among themselves and also with the central pipe and diagonal braces, branch off or sleeves can be vertical or aslant respect to the central pipe. The central column is divided into a triangular frame of steel transition pieces. On each end of the tripod, hulls are fixed to pile with concrete or grouting for the adoption of the foundation poles rammed and/or penetrated into the seabed. According to current technology, tripods are suitable for water depths of 20 to 80 m and can be employed with relatively flat seabed in particular. In large water depths, tripods foundations are more stable than monoplie foundations however there might be more risk for fatigue damage in comparison with

Figure 1.11: Tripod foundations for the ha Ventus offshore wind farm. (Offshore Wind Technology 2015)

jacket foundation. They are less suitable for locations with a stony ground. The six wind turbines in the offshore testing field Alpha Ventus were installed upon tripod foundations.

Tripiles foundations made of three individual steel pipes on which a tripod cross bracing is attached on the water surface and wind turbine is then erected on the tripod cross bracing. The individual pipes could be anchored in a ram depth of up to 30 m. In contrast to monopiles, the individual pipes could have a lower diameter and can be adjusted to the location with regard to wall thickness and length of the individual pipes and then can be rammed more easily. It can be applicable for water depths between 25 and 50 m. As indicated in Fig. 1.12, the tripiles offshore foundations were used for the BARD offshore 1 wind farm in the North Sea 2013 and also with the nearshore test case in Hooksiel 2008.

Figure 1.12: Tripiles foundations for the offshore wind farm BARD Offshore 1 in the North Sea. (Bard 2015)

Jacket foundations are a three or more legged chequered steel construction, see Fig. 1.13. The slender tubular feet take up the jacket poles which are rammed into the seabed. The bracing system between the legs gives the stiffness to the structure, because it actually acts as a buckling resistor of the steel tubular piles inside the legs. The forces are transferred to the seabed by axial forces in the members. The advantages of the jacket foundation are: a light and efficient construction (axial forces) and saves material compared to the monopile or tripod foundations in case of deeper waters and also the large base of the jacket offers a large resistance to overturning moments. There are some disadvantages such as: every node of the trusses needs

Figure 1.13: Jacket foundations for the Ormonde offshore wind farm. (Peire *et al.* 2008b)

to be designed and require many man-hours of welding, resulting in high design costs. Moreover, transportation of the jacket requires a lot more space compared to a monopile and also the maintenance cost is high. Several offshore wind farms make use of the jacket foundation concept, among these the Alpha Ventus (2010), Ormonde (2011), Thorton Bank II (2013) and Nordsee Ost (2013) offshore wind farms.

1.4   Offshore Piles under Cyclic Lateral Loading

The overall loads on a offshore wind turbine can be classified into five categories: a) gravitation and/or inertial loads such as: gravity,breaking, aviation and seismic

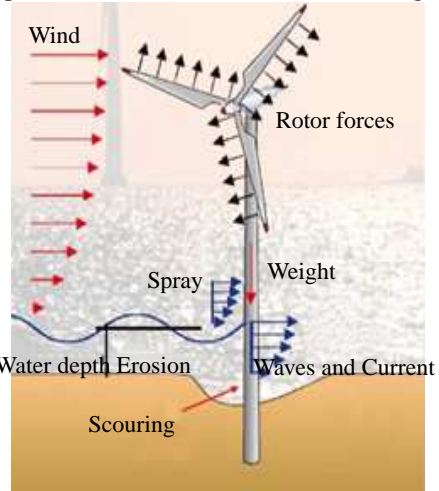activity, b) areodynamic load, c) hydrodynamic loads (wave and current), d) actuation loads like: torque control, yaw and pitch actuator and mechanical braking load, e) other loads such as: wake and impact loads and also tsunami. The mentioned dynamic loads can be in stochastic and/or harmonic forms, cf. Fig. 1.14. According to ICE (IEC 61400-3 2009), these loads are affected and connected with environmental conditions like: a) wind conditions (normal and extreme wind conditions), b) marine conditions such as: marine growth, waves (normal and extreme wave conditions), water and sea level, c) seabed movement and scour, d) other conditions like: air temperature, humidity, solar radiation, rain, hail, snow and ice, chemically and mechanically active substance, salinity causing corrosion, lighting, seismicity causing earthquake, water density and temperature. The variation of environmental conditions can have high impact and

Figure 1.14: Environmental impact and structural loads of an offshore wind turbine (Offshore Wind 2015)

change the structural dynamic properties, for instance, the damping ratios and natural frequencies of the wind turbine. Evidently, the internal forces are not equal to external forces in the presence of the dynamic loads. In DNV (DNV 2011) a limit state design (LSD) is considered in dimensioning step and it was defined as: *A condition beyond which a structure or structural component will no longer satisfy the design requirements*. Based on LSD which needs the design for different set up scenario refer to certain conditions and loads, different limit states categories as: ultimate, fatigue, accidental and serviceability limit states. The Ultimate limit state (ULS) analysis should ensure that the maximum admissible load do not make any collapse and failure in the turbine, foundation and subsoil. Maximum load carrying resistance can be mentioned as: yield and buckling, loss of bearing/overturning, failure of critical components. Fatigue limit state (FLS) is correlated with the metal and welded joints fatigue and failure due to the effect of cyclic loading where materials performance, in high-cycle fatigue situations, is commonly characterized by an S-N curve (or Wöhler curve). The S-N curve presents the magnitude of a cyclic stress (S) against the logarithmic scale of cycles to failure (N). In this writing, focus is on soil modelling and soil-pile interaction, hence the fatigue analysis will not be touch. However, the metal fatigue analysis highly effected by interaction between soil and pile. the effect of cyclic loading can be originated from: repeated wind and wave loading, repeated gravity loading on blade. Accidental limit state (ALS) corresponds to accidental structural damage caused by accidental loads and conditions and also it concerns resistance of damaged structures. Finally, the permanent deformation such as displacement and rotation of structure (such as tilt of turbine due to differential settlement) should not exceed the maximum allowable value in serviceability limit state (SLS). Detailed description about loads on wind turbines is out of the scope of the current thesis. However, a short introduction

to periodic and non-periodic loads on wind turbine blade may be relevant for the understanding the dynamic response of wind turbine. This section provides an overview of the most relevant environmental parameters affecting the dynamic behaviour of offshore wind turbines.

1.4.1   Non-periodic loading

Importance of dynamics loads such as non-periodic loads in design is to increase (or decrease) of maximum load which can affect ULS conditions. A non-periodic load is a function whose value is not repeated at constant intervals (Fig. 1.15). The non-periodic load can be random such as: turbulence and random waves. As an instance, wind turbulence causes non-periodic, stochastic loads on the rotor (Zaaijer, M. 2008). The non-periodic can be classified into transient load (such as step function: start/stop condition, turbine failures, storm front) and short events (such as impulsive load: extreme gust and waves). The starting point for the entire load spectrum of a wind turbine are the loads acting on the rotor. Turbulence is the natural variation of the wind speed about the mean wind speed in a 10-minute period and characterised by the standard deviation. An appropriate distribution model based on the application should be selected to fit data for the standard deviation properly. A log-normal, Weibull, Frechet and normal distribution can be used to provide a good fit to data for the standard deviation. The normal and extreme turbulence models are used to represent turbulent wind speed in terms of a characteristic standard deviation of wind speed. The turbulent wind speed with specific standard deviation is combined with the normal wind profile model to represent the extreme turbulence model. The distribution of energy of the wind turbulence between different frequencies is presented by the spectral density of the wind speed process. The spectral density of the wind speed process is an important parameter and represents how the energy of the wind turbulence is distributed between different frequencies. The spectral density of the wind speed process including wake effects from any upstream wind turbines is ultimately of interest. The Kaimal spectrum and other model spectra are applied to represent the upstream wind field. However, a rotational sampling turbulence due to the rotation of the rotor blades should be added to the turbulence of the upstream wind field. The coherence of the wind and the turbulence spectrum of the wind are of significant importance for determination of tower loads such as the bending moment in the tower. The offshore wind turbine is a dynamic system influenced by the hydrodynamic loading of waves and current. Here, we briefly glimpse the wind, wave and current loads.
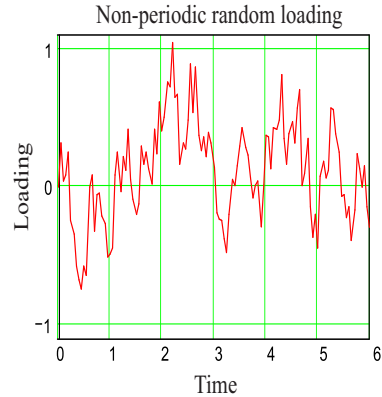
Figure 1.15: Non-periodic stochastic loading (Zaaijer 2008)

Wind load generates the aerodynamic blade loads and also aerodynamic drag forces on tower and nacelle directly. The incoming wind generally decomposed into mean value wind speed and a stochastic turbulence on that. Airfoils shaped blades lead to the lift and drag forces as a result of created pressure and suction on the different sides of the blade surface which make the faster air flow on one side and slower on the other. In an airfoil, one surface of the blade is somewhat rounded, while the other is relatively flat. The two primary aerodynamic blade forces are called lift, which acts perpendicular to the direction of wind flow; and drag, which acts parallel to the direction of wind flow (Fig. 1.16). The projection of lift and drag

Figure 1.16: The two primary aerodynamic blade forces. (Julia Layton 2015)

forces on the desired axes results in the rotation of the rotor and bending in blades.

Wave and current loads originally come from wind while the effect of travelled waves should be considered in wave load and also tidal and storm surge effects need to be considered in calculating current load (Fig. 1.17 Different waves theories like: linear Airy, non-linear Stokes and the stream function wave theories are used to ascertain the wave and particle kinematics and then , as an instance, the Morison equation and/or wave diffraction analysis are utilized to calculate wave-induced loads on an offshore support by considering the size, shape and type of structure. Morison's equation can be applied for slender structure while the wave diffraction analysis shall be performed for large volume structure to catch the correct wave kinematics which disturbed by the presence of the

Figure 1.17: Wave and current load on offshore wind turbine (offshorewind 2015).

structure. In particular, wave radiation forces should be included for floating structures. The wave theory shall be selected with due consideration of the water depth and of the range of validity of the theory. Viscous and potential flow effects have highly influence on the wave-induced loads.

Tidal effects and storm surge effects shall be considered in evaluation of the current velocities. Higher water levels tend to increase hydrostatic loads and also the sea current is considered to vary as a function of depth, consequently, the current

loads on the structure will be increased. The loading from sea currents generated by wind and tides is rather smaller than the wave loads. Note that the summation of the wave-induced water particle velocity and the current velocities present the total water particle velocities. Wave-current interaction is not a research issue in the offshore wind, but should be considered in the design. The occurrence of tidal current simultaneously with sea waves has a significant influence on the fatigue life of the platform (Peters and Boonstra 1988). Wave-current interaction changes the shape of the wave spectrum and the energy content in the wave frequency range of 0.2 - 0.35Hz. This is in the range of natural frequency of fixed offshore wind turbine structures (Peeringa 2014).   .

1.4.2   Periodic loading

A periodic load is a function whose value is repeated at constant time intervals. Some non-harmonic periodic loading in wind turbine structure can be listed as: shear wind, yaw misalignment, tower shadow and rotational sampling of turbulence. In this regards, harmonic loading can be recorded as: gravity loads on blades, mass imbalance rotor, aerodynamic imbalance and small regular waves. Importance of periodic dynamics in design is to increase or decrease of number of load cycles and their amplitudes (affects FLS/Life time). Most of the periodic motions we encounter are circular or semi-circular. The frequency of a periodic excitation should not be equal to natural frequency of system in order to eschew resonance. Evidently, number of blades has a high influence on the vibration behaviour of the wind turbine structure regarding to the internal stresses, structural deformation, resulting ultimate and FLS. The cyclic loads for a three-bladed rotor are much smaller than those produced by the two-bladed rotor since the combined cyclic loads close to the hub somewhat are balanced and symmetric. However the installation can be easy for one-bladed rotor by assembling that on ground but the rotor must move more rapidly to capture same amount of wind and this higher speed means more noise, visual and wildlife impacts and also gearbox ratio would be reduced. Moreover, the added weight of counterbalance negates some benefits of lighter design and one-bladed wind turbine captures 10% less energy than two blade design. For two-bladed wind turbine the advantages and disadvantages are nearly the same as the one-blade wind turbine. In addition, two-bladed wind turbines need teetering hub and/or shock absorbers because of gyroscopic imbalances and the captured energy is 5% less than three blade designs. For a three-bladed wind turbine, the blades rigidly connect to the ductile cast steel hub and the cantilevered boundary conditions are implied to transfer the dynamic loads of the blades to the shaft. Studies have shown that a three bladed wind turbine is more efficient from an aerodynamic point of view. Basically, the individual blade must be stiff and light enough as well as that the frequency of the blade modes does not coincide with the frequency at which the blades pass the tower to avoid fatigue damage of the blades.

Dynamic amplification factor (DAF) is defined for harmonic excitation equal to dynamic amplitude divided by static deformation. In this regard, to reduce the fatigue damage accumulation during the lifetime of the wind turbine structure, the dynamic amplification should be avoided. In turn, the lowest eigenmode of the wind turbine does not coalesce with excitations from the operation frequency of a three-bladed

turbine and waves to elude the resonance. Typically, sea waves have frequencies of 0.20 - 0.25 Hz. This is close to the rotor frequency 1P associated with the cyclic loading generated by mass imbalances in the blades. Furthermore, each time a blade passes the tower, the shadowing effect causes a load on the structure. For a three-bladed wind turbine, this leads to excitation at the blade passing frequency 3P as well as multiples thereof, e.g. at a frequency of 6P. Three classical design approaches as shown in Fig. 1.18, have been defined based on the the natural frequency f_1 which should not coincide with the excitation frequencies of the dominant forces are listed as: "soft-soft" design, where the natural frequency f_1 is less than 1P as well as the frequencies re-lated to the dominant wave action and it is a very soft structure. "soft-stiff" design, where the natural frequency f_1 lies between the frequencies 1P and 3P. "stiff-stiff" design, where the natural frequency f_1 is higher than the blade passing frequency 3P and it is a very stiff structure. Today, a "soft-stiff" design wind turbine is chosen because it needs less amount of steel in comparison with "stiff-stiff" design. On the other hand, designing the wind turbine based on "soft-soft" approach requires a control system to obtain an exclusion window of the rotor rate. Because of high wave loading, the "soft-soft" design may be critical. For larger wind turbines, the first natural frequency and rotation frequency decrease due to longer height and length of hub and blades. Then, there is relatively high risk to fall the hydrodynamic frequency range into 1P.
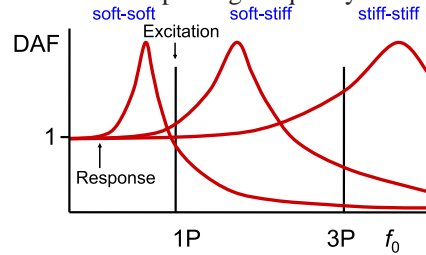
Figure 1.18: Classification for wind turbines (Scharff and Siems 2013).

A "soft-stiff" design requires a very stiff foundation and has major implications for the structural design characteristics of the wind turbine. It is also sensitive to the levels of damping in the design and requires soil characteristics within a particular range, limiting potential sites for offshore wind turbine installation and introducing an implicit reliance on static soil properties to achieve resonance avoidance. In addition, the "soft-stiff" design philosophy does not explicitly treat higher structural modes of the wind turbine's components. A Campbell diagrams is a classical way of representing the dynamics of rotary machinery and utilized to figure out sources of resonance for the "soft-stiff" design. As shown in Fig. 1.19, the lowest natural bending frequencies f_1 of the complete system are adjusted so that they remain above the excitation frequency due to rotor imbalance (1P) and below the excitation frequency due to the blade passing frequency (3P) for the entire operating range of the turbine. Resonance coincidence is represented by the natural frequency f_1 crossing a resonance lines (1P and 3P).
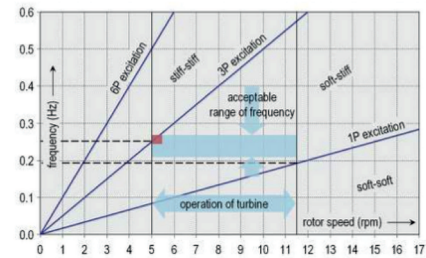
Figure 1.19: Example of Campbell diagram (Rohrmann *et al.* 2010).

Energy dissipation in offshore applications and implementing the proper levels of

damping in the design is an important issue to study the dynamic behaviour of offshore structure. Energy in the offshore foundation and subsoil dissipate through geometry and material damping which are affected by the soil–structure interaction model.

Geometrical damping or radiation of waves away from the foundation presents the attenuation of wave over large area or volume by spreading the energy through the P-, S- and Rayleigh waves propagating. The geometric damping depends on the (1) geometry of the foundation-soil contact area, (2) properties of the structure, and (3) properties of the underlying soil deposits. Material damping defines as a conversion from mechanical energy into thermic energy (heat) which is also called local damping. Soil material damping incorpo-

Figure 1.20: Hysteresis material behaviour (Gordan and Adnan, 2014).

rates the effects of energy dissipation in the soil due to hysteretic or inelastic action on the soil. Material damping is only present in the medium frequency range. The material damping can nearly explained by Mohr Coulomb friction between particles, viscus friction between particles and fluid, molecular collisions or irreversible inter-crystal heat flux. As indicated in Fig. 1.20 material hysteresis represents by the area of the hysteresis loop as measuring of energy dissipation during one cycle and it depends on the magnitude of the cyclic loads acting on the wind turbine structure. As mentioned, the soil–structure interaction model is an interesting challenge that could represent the soil stiffness and damping in saturated soil properly when subjected to dynamic load. The soil model includes combined springs and dashpots, which could be a suitable and more accurate approach to represent interrelation effects between the wind turbine foundation and subsoil to account for soil deformation as well as pore pressure.

1.5   Motivation for Research

As discussed in the previous sections, the costs of large offshore wind turbine are kept as low as possible, and the overall weight of the turbine and foundation is minimized, resulting in a flexible and dynamically active structural system–even at low frequencies. According to this argument, the dynamic amplification of the response from wave- and wind-induced loads become much more important. The highly variable and cyclic loads on the rotor, tower and foundation, caused by wind and wave loads as well as low-frequent excitations from the rotor blades, all demand special fatigue design considerations and create even greater demand for fuller appreciation of how the wind turbine ages structurally over its service life. In this regard, the seepage damping in the subsoil producing from the vibrations on the soil–foundation interface and the dynamic soil behaviour are crucial to consider.

This study aims to evaluate the extension of soil–structure interaction that affects the dynamic structural response of offshore wind turbines which highly depends on

soil stiffness and seepage damping. With this in mind, an appropriate model is needed based on considering the effect of dynamic behaviour of soil–structure interaction. Instead of using a linear/non–linear dry soil model without physical knowledge regarding the dynamic behaviour of offshore monopile wind turbines, saturated soil is modelled based on the coupled equations for porous media to account for soil deformation and pore pressure.

Dynamic analysis of the saturated soil requires an appropriate soil model to reflect the reality to a high degree. However, although a rapid increase in computation power has been observed over the last decades, which continues today, advanced finite element models of wind turbine and substructure combined with the governing equations of motion may not seem feasible to determine the flow around the blades, tower and foundation. Considering that focus is drawn on the soil–structure interaction, special attention is given on modelling techniques of accounting for the dynamic behavior of soil-foundation interaction. The characterisation of poroelastic media and cyclic loading is thoroughly covered in the literature.

1.5.1 Overview of the Thesis

Following the introduction, the structure of the thesis is given below.

◆ **Chapter 2** presents a review of certain soil models proposed in the literature for analysis of soil–structure interaction as well as soil damping and substructure models, mechanics of porous and non–porous media. This chapter further details the implementation of numerical method of porous media and related post–processing error estimation in finite element analysis for the two–phase problem of offshore wind turbine foundations. The review is categorised into different topics within numerical work highlighting the most relevant techniques that during past years have been developed.

◆ **Chapter 3** describes the scope of the thesis. A short summary of the literature review is given which forms the basis for a clear definition of the models used here.

◆ **Chapter 4** contains a summary of the included international conference and journal papers.

◆ **Chapter 5** concludes the thesis with a summary and discussion of the methods and analyses presented in the thesis. The main results achieved in the project are presented and directions for future work are given.

◆ **Appendix A** contains the enclosed conference paper: "Numerical calculation of damping for monopile foundations under cyclic load during steady-state vibration".

◆ **Appendix B** contains the enclosed journal paper: "Assessment of dynamic substructuring of a wind turbine foundation applicable for aeroelastic simulations".

♦ **Appendix C** contains the enclosed journal paper: "Recovery–Based error esti-
mation in the dynamic analysis of offshore wind turbine monopile foundations".

♦ **Appendix D** contains the enclosed journal paper: "$p - y - \dot{y}$ curves for dynamic
analysis of offshore wind turbine monopile foundations".

♦ **Appendix E** contains the enclosed journal paper: "Influence of pore pressure on
dynamic response of offshore wind turbine using poroelastic model".

CHAPTER 2
State of the Art

Offshore wind turbine energy is a burgeoning area of multidisciplinary engineering that is growing rapidly. The annual market for wind energy is estimated to grow to €17 billion with roughly 50% of contributions offshore by 2020 and it is expected to €20 billion with 60% of investments offshore by 2030. Given recent requests for sustainable energy forms such as renewable energy, offshore wind turbines have increasingly been considered, with the majority of research conducted in Europe especially in the North Sea. More than two thirds of total EU wind capacity is currently installed in the three pioneering countries Germany, Spain and Denmark. Denmark provides more than 20% and Spain more than 10% of its electricity demands by wind energy. Offshore wind turbines are subjected to dynamic loads, which makes complicated interactions such as aero- and hydro-dynamics response between different parts of superstructure and substructure. This chapter conducts a survey of current research, findings and knowledge of the dynamic response of offshore wind turbines. The review is classified into different categories, covering different soil–structure interaction methods regarding soil damping, substructure media models such as porous and non-porous media, and numerical simulation and related stress recovery-error estimation in finite element method.

2.1 Overview of the State-of-the-Art

Numerous topics in geotechnical engineering require the use of pragmatic and realistic models for the supporting soil and the soil–structure interface. This media and its interaction require improvement and development that can sometimes modify stress and deformation fields in the entire structural system significantly. The imposed stresses and deformations on the ground by structure with its loading make deformations and movements in the soil, thereby transmitting back additional forces and deformation to the structure. This process continues until full equilibrium of the whole soil–structure sys-
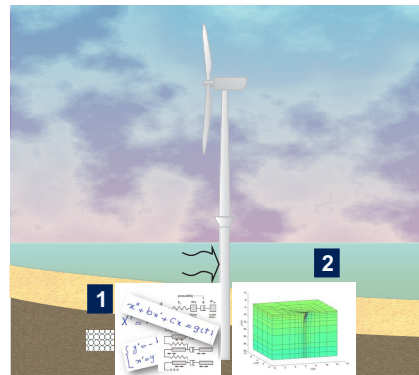
Figure 2.1: Prospective interested subjects in the state-of-the-art.

tem is satisfied, or fails in the case of excessive loading and deformations of the system. The dynamic analysis of offshore foundation requires better understanding of soil behaviour and implementing more realistic soil model to capture more accurate soil stiffness and damping. The chapter aims to present an overview of certain models mentioned in the literature investigate the soil–structure interaction and their application in offshore wind turbine industry. The chapter reviews the work related to the dynamic analysis of offshore wind turbine foundation, *i.e.* numerical methods of evaluating the dynamic soil stiffness and damping as well as numerical approaches of including the frequency dependent natural frequencies of wind turbine structures induced by periodic loadings. In general, this chapter addresses the following topics (Fig. 2.1):

1 **Soil model:** A review of the state-of-the-art is presented. The models may be used to evaluate soil stiffness and damping as well as natural frequency of offshore wind turbines. The importance of soil models such as viscoelastic is highlighted and presented. The dynamic behaviour of soil is investigated.

2 **Computational analysis:** A review of the remarkable numerical and mathematical methods to investigate dynamic behaviour of offshore wind turbine foundation is given. The stress post–processing error estimation regarding to the finite element method is given to provide a better stress field.

2.2   Damping in Offshore Wind Turbines

Dynamic analysis of wind turbine is a challenging and intriguing topic in engineering. Their dynamic response is governed by applied loads, design of wind turbine structure components, *i.e.* blades, tower and foundation. In general, the dampings in offshore wind turbines can be categorize into four separate sources, *i.e.* aero-dynamic, structural, water and soil damping. Evidently, the damping is important in reducing load and therefore extending fatigue lifetime. Thus, the thesis emphasis calculating seepage damping and presenting its effects on dynamic response of offshore wind turbine. By considering more realistic soil damping, the natural frequencies, damping ratios, and mode shapes of the wind turbine can be calculated more precisely. The aim of this section is to present an overview of different models that facilitate soil damping in offshore wind turbine. A further description of different types of damping in offshore wind turbine is also given.

2.2.1   Dissipation of energy in soil

The overall weight of wind turbine is minimized to reduce the overall costs. At present, nearly all large modern wind turbines are characterized by a flexible structure, which makes them more sensitive to dynamic excitation even at low frequencies. Soil damping is important in fatigue damage. Additional research on the soil damping affects is needed for their inclusion as an explicit design factor for offshore wind turbines. In this regard, soil damping can be grouped into two classes based on methods

of dissipating energy, geometrical and material damping.

Geometrical dissipation of energy

In early twenty century, the theoretical work regarding to dissipation of elastic wave energy in elastic bodies presented by Lamb in 1904. Lamb investigated the propagation of tremors over the surface of an elastic solid. Geometrical (radiation) type of damping which is the dispersion of energy by propagating the elastic wave from the source in case of moving vertically cylindrical disk (oscillators) on an elastic half-space was developed by Reißner (1936). One year later Reißner (1937) investigated purely torsional oscillations at the semi-infinite elastic body and showed no surface waves (Rayleigh waves) were developed. The comparison of the energy distribution for compressional, shear and surface waves imposed on the free surface of a semi-infinite solid subjected to a vibrating circular disk were analytically determined and presented by Miller and Pursey (1955). Dissipating energy through spreading Rayleigh, P- and S-waves over a large area or volume is called geometrical damping. Rayleigh waves propagate on the surface, whereas the P- and S-waves spread over the volume (Andersen 2006).

Radiation damping in circular foundation placing on an elastic half-space investigated by Lysmer and Richart, Jr. (1966), Hall, Jr. (1967) , Shah (1968), Luco and Westmann (1971) and Veletsos and Wei (1971). Radiation Damping known as outgoing stress waves from pile-soil interface to infinity that make the loss of energy in the soil-pile system. Berger *et al.* (1977) proposed and investigated energy losing through travelling one-dimensional (1D) P- and SH-waves in the direction of shaking and perpendicular to the pile when the pile cross section moved horizontally. Plane strain conditions were considered by Novak *et al.* (1978) and proposed a more rigorous model to analyse the pile subjected uniform harmonic vibrations in an infinite medium for an isotropic, homogeneous, and linearly elastic soil. Gazetas and Dobry (1984a, 1984b) investigated the propagation of compression-extension and SH-waves in four sections around pile partitioned the quarter planes along and perpendicular to the direction of pile (shaking place). Moreover, parallel setting of dashpots with the nonlinear spring employed by Matlock *et al.* (1978), Nogami *et al.* (1992) , Badoni and Makris (1996) and El Naggar and Novak (1995, 1996) to calculate wave propagation and radiation damping. Meanwhile, in case of end-bearing and groups of vertical floating piles the dispersion relationship due to the interaction between the solid and fluid phases to investigate the waves propagation presented by Boer and Liu (1994). As an alternative, Badoni and Makris (1996), El Naggar and Bentley (2000) and Allotey and El Naggar (2008) employed parallel setting of nonlinear dampers and springs to model radiation damping.

Radiation damping can be offered by a vis-
cous dashpot that reduced at large pile de-
flections and radiation damping does not ap-
pear for frequencies less than the natural fre-
quency of the system. Gazetas (1984) re-
ported the dynamic behaviour of end-bearing
piles subjected to vertical harmonic shear
waves by considering both inertia and kine-
matic interaction, followed by Fan *et al.* (1991)
who studied the kinematic response of piles
groups under the same loading. Meanwhile,
Gazetas and Makris (1991) presented the
dynamic steady-state axial response of pile
groups, accounting for the interaction be-
tween two individual piles. Makris and
Gazetas (1992) proposed a procedure to esti-
mate the dynamic interaction between two vertical piles by introducing the wave field
radiating from an oscillating pile and its effect on another pile, through a single dy-
namic Winkler model, with frequency dependent springs and dashpots. The Winkler
model represents the supporting soil by a set of independent (non)linear elastic springs
perching on a rigid base, will be explained in more details later in this chapter. Later
on, Kavvadas and Gazetas (1993) highlighted the kinematic interaction between the
soil and a pile during seismic excitation consisting of aforementioned wave loading by
performing parametric study. Makris (1994) presented an analytical solution for pile
subjected to the passage of Rayleigh waves by implementing frequency-dependent
springs and dashpots, applicable to near field earthquake response. Makris and Badoni
(1995) extended their earlier work to analyse pile groups subject to obliquely inci-
dent shear and Rayleigh waves and present the wave field radiating and the effect of
this field on an adjacent pile, with spring and dashpot coefficients evaluated from the
techniques described in Makris and Gazetas (1992). Beresnev and Wen (1996) in-
vestigated nonlinear effects in soil dynamic, *i.e.* considering an increase in damping
and shear-wave velocity reduction as excitation strength increases. These effects are
usually ignored in seismological models of ground-motion prediction. A comprehen-
sive survey performed to describe how the presence of elastic nonlinearity affects soil
amplification based on existing geotechnical models and then examined evidence of
nonlinear soil response. Radiation Damping was reported by Wang *et al.* (1998) to
model soil-pile interaction as shown in Fig 2.2). In their model a non-linear spring
represented plastic behaviour of soil in series with Kelvin-Voigt (KV) element to pro-
vide radiation damping for the far field wave propagation. Boulanger *et al.* (1999)
added a gap element to the Wang's *et al.* (1998) model, a non-linear closure spring
in parallel with a non-linear drag spring was included in that gap element as it can be
seen in Model II in Fig 2.2)).

Figure 2.2: One-dimensional soil models; Model I: by Wang *et al.* (1998) and Model II: by Boulanger *et al.* (1999).

Baars (2000) used the concept of damping based on dry particle friction to calculate wave propagation and energy dissipation in soil dynamics and the spring-slider model (as shown in Fig. 2.3) was proposed. A KV material model reflects that the dissipated en-

Figure 2.3: suggested spring slider model (Baars, 2000).

ergy though propagated wave becomes proportional to the frequency of the loading. Whereas, the proposed spring-slider model indicates a damping ratio becomes constant for small deformations for both sand and clay, and independent of frequency or shear strain amplitude. τ is shear stress, $k_1, k_2...k_i$ are spring stiffness and N is constant for sliders that are shown in Fig. 2.3. Kim *et al.* (2000) studied the two dimensional water wave propagation in porous seabed by using boundary element method (BEM) based on integral equation while the numerical results were validated with the analytical solution. Klar and Frydman (2002) combined an explicit two-dimensional (2D) numerical computer code with three-dimensional (3D) model to present the dynamic response of a lateral loaded pile. In 2D model, plane strain boundary value problems and viscoelastic material models regarding to radiation damping were considered for each horizontal soil layer and then in the second model the disregarded shear forces in 2D model which were developed between the horizontal layers were considered in order to couple the behaviour of the horizontal layers.

Non-linear time domain site response analysis is widely used in evaluating local soil effects on propagated ground motion. This approach has generally provided good estimations of field behavior at longer periods but has shortcomings at relatively shorter periods. Viscous damping is commonly employed in the equation of motion to capture damping at very small strains and employs an approximation of Rayleigh damping using the first natural mode only (Hashash and Park 2002). A new formulation for the vis-

Figure 2.4: Multi-degree-of freedom lumped parameter model representation of horizontally layered soil deposit shaken at the base by a vertically propagating horizontal shear wave (Hashash and Park, 2002).

cous damping using the full Rayleigh damping was presented by Hashash and Park (2002) and it was solved numerically at each time step using the Newmark. Their proposed formulation allowed the use of frequency dependent viscous damping. They discretized the geologic column into individual layers using a multi-degree-of freedom lumped parameter model shown in Fig. 2.4.

The comparison between dynamic responses of saturated soil from Biot's and Yamamoto's models has been performed by Lin (2004). The damping of elastic waves in coarse and fine sand with loading frequency have been computed and the representation of viscous and Coulomb friction in both models have also been estimated. Soares and Mansur (2006) modeled time-domain wave propagation in fluid-soil-structure interaction by using iterative procedure in BEM based on different kind of Green functions in order to present linear and non-linear behaviour of elastoplastic regions. Srisupattarawanit *et al.* (2006) applied BEM and a computation method to

compute nonlinear finite amplitude waves in a liquid body of finite depth, in order to be coupled with an elastic structure. The capability for such a coupled simulation to facilitate the fatigue design of offshore wind turbines is important. In the time domain analysis allowing full soil-pile structure interaction, only equivalent viscous damping can be used instead of soil damping ratio. Chang and Nghiem (2010) evaluated the equivalent viscous damping by matching the transfer functions, soil damping ratio and soil damping value in frequency domains.

Chai *et al.* (2011) employed the thin layer stiffness method to present the effective phase velocity of the surface waves and analyse the effects of the body waves based on the calculated phase velocity. Carbonari *et al.* (2011) employed the domain decomposition technique for including radiation damping. In the first step the frequency domain analysis was performed and then time domain finite element program was invoked to evaluate the superstructure response. The presented radiation damping formula by Gazetas and Dobry (1984a, 1984b), has been utilized by many reseachers *i.e.* Mylonakis *et al.* (1997), Liyanapathirana and Poulos (2010) and Dezzi *et al.* (2010), and it was estimated and evaluated by Shadlou and Bhattacharya (2014) for 3D soil–pile dynamic interactions. And also, new formulations were proposed for one- and two-layer soils while plane strain conditions was not considered. Kampitsis *et al.* (2013) utilized linear dashpot to capture radiation damping in far field zone. A hybrid nonlinear spring configuration was employed to capture the near-field plastification of the soil and it was connected in series to an elastic spring-damper model to represent the far-field visco-elastic character of the soil.

Material dissipation of energy

Material damping represents the transformation of mechanical energy into thermic energy. This converting process is irreversible and somewhat relevant to friction and collisions between particles as well as interaction between viscose fluid and particles. It is worth to mention that when two elastic bodies are in contact and are surrounded by a viscous fluid, a force applied in a direction normal to the area of contact will tend to squeeze the flow away from this area. Because of fluid viscosity, the fluid will not move away instantaneously. This type of damping can have important role especially when there is larger deformation of the soil which results to change the first eigenfrequency of the tower mode.

As shown Fig. 2.5, Nogami and Koganai (1988) proposed a Hybrid Dynamic Winkler Model (HDWM) and calculated the flexural response of linear single piles in time-domain by considering plane strain conditions. This model was developed to present the gap and slippage at the soil-pile contact by Nogami *et al.* (1988). Furthermore, This model was then extended by Nogami *et al.* (1992) to analyse the inelastic and nonlin-
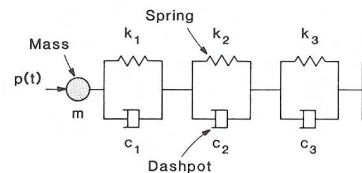
Figure 2.5: Hybrid Dynamic Winkler Model based on Nogami model for Lateral Pile Response (Nogami and Koganai, 1988).

ear dynamic of soil-pile interaction, by dividing the soil medium in two regions. The near and far field regions were presented to show gap element and nonlinear spring in the vicinity of pile shaft and linear elastic behaviour for far field region. In the applied model, the mass of an annular cylindrical region around the pile was included as a soil mass. Based on the same approach, the nonlinear dashpots for the inner field was proposed and implemented to present material damping close to the pile by El Naggar and Novak (1995, 1996) and Mostafa and El Naggar (2002). The concept of near- and far-field by utilizing a nonlinear (linear) spring and a dashpot in parallel for near-field (far-feild) to account for nonlinear soil stiffness and hysteretic damping in near-field and to allow the propagation of waves to infinity to model radiation damping for far-field was implemented by El Naggar and Bentley (2000).

Bardet (1995) applied two phase theory to investigate the damping regarding to the soil-water interaction analytically during steady-state vibration. He studied the influence of water diffusion of a 1D column made of nearly saturated soil. It was shown that the soil-water damping within fully-saturated sand is not negligible compared to structural hysteretic damping. The energy dissipation inherent to material behaviour is called material damping and also the relevant dissipated energy due to soil nonlinear behaviour is known as hysteretic damping. Basically, by allowing the unloading path to be different from the loading path because of nonlinear soil behaviour when a soil is subjected to cyclic symmetric loads a hysteresis cycle is produced in the stress-strain diagram and hysteretic damping equals to the enclosed area Brown *et al.* (Brown, D. A. and O'Neil, M. W. and Hoit, M. and McVay, M. and El Naggar, M. H. and Chakraborty, S. 2001). Material damping was modelled as a viscous dashpot and utilized by Kenny (1954), Achenbach and Sun (1965) in Kelvin model which represents by parallel setting of independent viscous dashpots and the springs. Just to mention a few, the viscous dashpot model in order to show the material damping was employed by other researchers as: Veletsos and Verbic (1973), Weissmann (1973), Luco (1974), Wong and Luco (1985), Sun (2001) and Sun (2002).

Gerolymos and Gazetas (2006) investigated hysteretic loop by considering three foundation soil types such as: very hard, intermediate stiffness and very soft foundation soil to analyse hysteretic damping for a nonlinear-elastic foundation soil. They have shown that large energy dissipation appeared in the soft soil and this hysteretic loop became smaller for hard foundation soil.

Alexander (2010) presented an analytical expressions for the nonlinear resonant frequency of a floating pile by considering the influence of a nonlinear spring and damping with superstructure mass as shown in Fig. 2.6. A strain-dependent nonlinear damping function, near and far-fields concept were employed. Rovithis *et al.* Rovithis:2011 presented analytical expression for dynamic response of inhomogeneous soil under a seismic load and highlighted the effect of hysteretic damping ratio by considering complex shear modulus while hysteretic damping took constant value through depth. De-
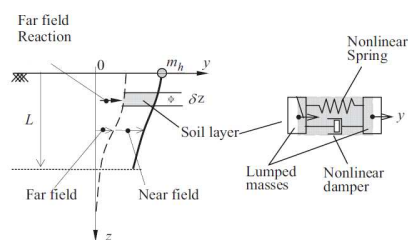
Figure 2.6: Soil model including nonlinear dashpo (Alexander, 2010).

hghanpoor and Ghazavi (2012) applied segment by segment method to determine the stiffness and damping parameters of laterally loaded tapered piles subjected to harmonic vibrations analytically. The soil considered as some elastic horizontal layers that they were homogeneous, isotropic, and linearly visco-elastic. The soil-pile interaction in this method was modelled within each segment and applied via the segment nodes to the analysis of the adjacent segment.

Anoyatis *et al.* (2013) presented the dynamic response of a pile subjected to a harmonic horizontal displacement which was embedded in a homogeneous linear elastic soil and frequency-independent material damping was expressed through a complex-valued shear modulus. Zania (2014) calculated the eigenfrequency and damping ratio of an monopile offshore wind turbine by using a semi-analytical solution based on derived equations by Novak and Nogami (1977) . Hovind and Kaynia (2014) applied three steps method based on superposition to calculate the hysteretic damping for nonlinear soil response by employing nonlinear spring to introduce material damping during the loading cycles. Carswell *et al.* (2015) presented the significance of foundation damping on monopile supported offshore wind turbine by implementing hysteretic damping in a linear elastic 2D finite element model when the model subjected to extreme storm loading. They presented an approach to convert hysteretic energy loss into viscous and rotational dashpots.

2.3   Soil–Structure Interaction

Winkler (1867) formulated the continuous soil reaction based on mechanical spring in order to represent the soil–structure interaction. The stiffness of soil-pile system are figured out and modelled by utilizing a set of independent (non) linear elastic springs resting on a rigid base. The lateral resistance of the pile due to the supporting soil was handled by spring stiffness and called p–y curves, where p and y are representing the lateral resistance per unit length in the horizontal direction and the corresponding displacement of the pile, respectively. The p–y method rely on the American Petroleum Industry (API) has been employed by the off-shore oil and gas industry for designing off-
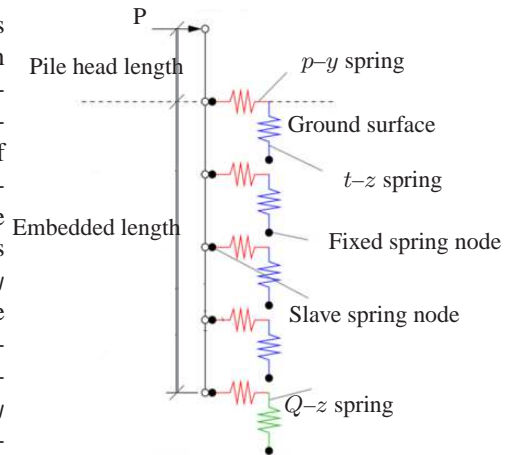
Figure 2.7: Visual representation of p–y,t–z and Q–z methods (OpenSees 2015)

shore piled foundations in the early 1970s (Matlock (1970)). Subsequently, The p–y curves method based on supporting data from Matlock (1970), Cox *et al.* (1974), Reese and Welch (1975), Murchison and O'Neil (1984), Dunnavant and O'Neill (1989) has been extracted and improved for use in offshore wind turbine design standards by API (2000), GL (2005), DNV (2011), and IEC (2009). El Naggar and Bentley (2000) employed the p–y curves method, by equating the two series spring con-

stants for the far and near- fields, the far-field stiffness was known and obtained from a plane strain model. In this way, the nonlinear stiffness of the near field was obtained. In similar fashion, vertical resistance due to skin friction along the pile can be treated with t–z curve and the end bearing resistance at the tip of the pile can be represented by Q–z curves as shown in Fig. 2.7 (Mostafa and El Naggar 2004).

Due to the absence of soil continuum effects and neglecting soil damping as well as the fact that deformations are not directly linked to the number of load cycles in API (2000) methodology, the pile amplitudes close to resonance frequency may not be estimated properly. Accordingly, a mechanism which has included spring-dashpot elements may be used to describe the dissipation effects in the soil. As shown in Fig. 2.8, different combination of the viscous damper with spring can be expressed by the Maxwell and KV models where the viscous damper and spring connected in series and parallel (Kim 2008).
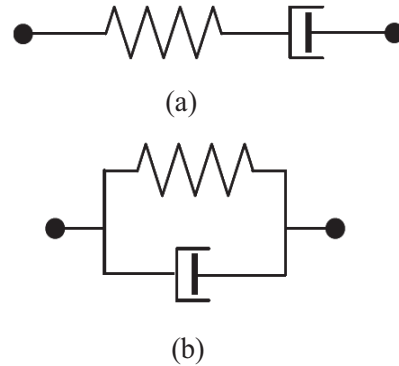
Figure 2.8: Soil model (a) Maxwell (b) Kelvin-Voigt (Kim 2008).

Generalzied KV and Maxwell models are also implemented. Just to mention a few, a KV or Winkler-Voigt model along the foundation has been implemented by many researchers such as (Kenny 1954; Achenbach and Sun 1965; Novak 1974; Sun 2001; Sun 2002; Hirai 2012).

In Winkler model, a plane strain condition is invoked which conducts to represent the soil by a set of independent horizontal layers. This constrain imply that the wave is going to propagate in two dimensional space and the layers work independently. This uncoupled layers concept has been used by many researchers (Baranov 1967; Novak and Beredugo 1972; Novak 1974; Novak 1977; Novak and Howell 1978; Novak *et al.* 1978; Novak and El-Sharnouby 1983), just to mention a few. Some improvement such as varying soil properties through depth has been considered by Novak and El-Sharnouby (1983) and Hirai (2012). To overcome the plane strain restriction, some

coupled mechanism between two adjacent layers were considered by Nogami and Lam (1987), Nogami and Leung (1990), Nogami *et al.* (1992), Nogami (1996). In conjunction with pile foundation model, a beam element supported by (non)linear Winkler foundation (BNWF) model is used by many researchers like: Matlock *et al.* (1978), Matlock Foomatlock:1978b, Nogami *et al.* (1992), Badoni and Makris (1996), El Naggar and Novak (1995, 1996), Wang *et al.* (1998), Boulanger *et al.* (1999), El Naggar *et al.* (2005), Gerolymos Gazetas (2006), Harada *et al.* (2008), Brødbœk *et al.* (2009), Hirai (2012). As in-
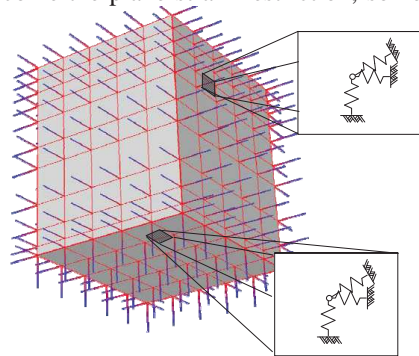
Figure 2.9: Multi-Winkler model of three dimensional soil foundation system (Harada *et al.* 2008).

dicated in Fig. 2.9, Harada *et al.* (2008) presented a multi-Winkler model for nonlinear dynamic and earthquake response of foundations. The nonlinear soil reactions to foundation motions were modelled by using the springs per unit area of interface between soil and foundation with three components corresponding to normal traction and two shear traction on soil-foundation interface.

A set of independent dashpots (viscous dampers) connected in parallel with the independent (non)linear springs is called Winkler-Voigt. They can be used for soil modelling to capture the soil energy dissipation. The Winkler and Winkler-Voigt models are arranged and combined in order to illustrate better soil representation in near and far fields. The Winkler-Voigt model by considering near and far fields concept have been utilized by Matlock *et al.* (1978), Nogami *et al.* (1992), Badoni and Makris (1996), El Naggar and Novak (1995, 1996), Wang *et al.* (1998), Boulanger *et al.* (1999) and Memarpour *et al.* (2012). Nogami *et al.* (1988) developed hybrid near/far field soil-pile interaction models for dynamic loading, as shown in Fig. 2.10. They formulated numerical solutions for single pile and pile group axial and lateral response in the time and frequency domains, incorporating nonlinear soil-pile response, degradation, gapping, slip, radiation damping and loading rate effects. A series connection of gap, plastic and elastic elements which are pointed the area very close to pile, near and far-fields based on the BNWF has been used by Wang *et al.* (1998) and Boulanger *et al.* (1999).
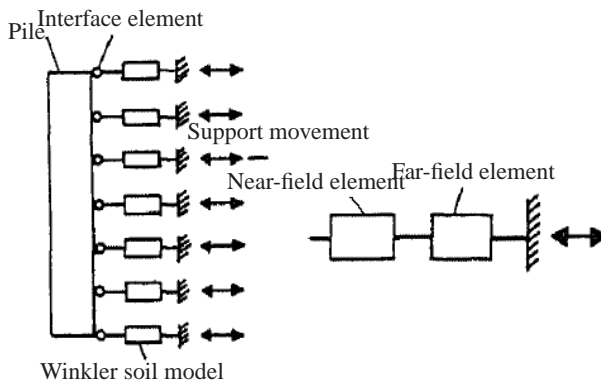
Figure 2.10 Nogami's beam on Winkler foundation soil–pile interaction model. (Nogami *et al.* 1988).

Beside considering the effect of soil stiffness and damping, the contribution of soil inertia can also be important. In the literature we can find some models which attempt to include the soil mass by considering lump-mass. Just to mention a few, El Naggar and Novak (1993, 1995), Pacheco *et al.* (2008), Kouroussis and Verlinden (2015) have considered the effect of soil mass. Some other improvement such as considering nonlinear and frequency-dependent characteristics of the supported soil have been considered like Makris (1994), Hashash and Park (2002) and Kampitsis *et al.* (2013). Hashash and Park (2002) presented a new formulation for the viscous damping using the full Rayleigh damping. Their proposed formu-

Figure 2.11: Soil-pile-structure model (Kampitsis *et al.* 2013).

lation allowed the use of frequency-dependent viscous damping. El Naggar *et al.* (2005) considered the elasto-plastic spring connected in parallel with a dashpot in the Winkler-Voit model. Badoni and Makris (1996), El Naggar and Bentley (2000), Mostafa:2002, Mostafa and El Naggar (2002), Halabian and El Naggar (2002) as well as Allotey and El Naggar (2008) cosidered nonlinear spring and damper in the Winkler-Voigt model. Halabian and El Naggar (2002) modelled the soil stiffness as functions of soil shear wave velocity to account for the soil–structure interaction efficiently. Kampitsis *et al.* (2013) considered a hybrid model consists of a nonlinear *p–y* spring connected in series to the KV element as shown in Fig. 2.11. The nonlinear spring represents the plastic soil behaviour in the near-field and viscoelastic characteristic of the soil presented by the KV model.

Another category of soil–structure interaction problems is called lumped-parameter models. In this family, soil characteristics are frequency-independent and real number but not necessarily positive parameters, and these combination of masses, dashpots and springs are calculated based on minimizing the total square errors between the dynamic stiffness and obtained results from applied methods such as: closed-form solutions, FEM, BEM and on-site measurement results. Simple and high-order lumped-parameter models were considered by many researchers such as: Wolf and Somaini (1986), Nogami and Konagai (1986), Wolf (1994), Francisco *et al.* (1990), Jean *et al.* (1990), Wolf (1991a, 1991b), Wolf (1997), Wu and Chen (2001), Wu and Lee (2002) and Wu and Lee (2004), just to mention a few. As shown in Fig. 2.12 in lumped-parameter models, an additional degree of freedom is considered for a mass and it is not directly attached to the foundation node but rather is connected to it through a dashpot. Nogami and Konagai (1986) connected a mass at the end of three KV models which was in a series form to represent the subgrade reaction of soil surrounding single piles as shown in Fig. 2.12. The dynamic stiffness and damping of soil-foundation systems are represented by impedance functions. In simple or semi-empirical lumped-parameter models, the coefficients of the masses, dashpots
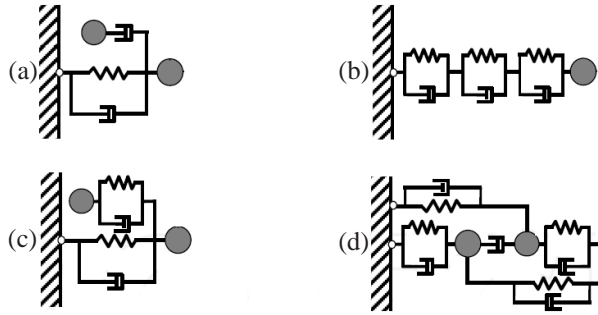
Figure 2.12 Lumped parameter models proposed by: (a) Meek and Veletsos (1974); Wolf and Somaini (1986); (b) Nogami and Konagai (1986, 1988), (c) Francisco *et al.* (1990) and (d) Jean *et al.* (1990)

and springs are usually determined by minimizing the errors from the target (exact) impedance functions. It depends on how significantly an optimal fit can be obtained by using curve-fitting techniques of the impedance functions, which is obtained from lumped-parameter models with the corresponding target impedance functions. This model is reported by Meek and Veletsos (1974), Wolf and Somaini (1986), Nogami and Konagai (1986, 1988), Francisco *et al.* (1990), Jean *et al.* (1990), Wu and Chen (2001), Taherzadef *et al.* (2009) and Saitoh (2011). The impedance parameters like dynamic-stiffness coefficients in high-order or systematic lumped-parameter models are approximated as a ratio of two polynominals, which is then formulated as a partial-fraction and/or parallel-fraction expansions whose each term is represented by a discrete model comprising parallel-form and/or series-form lumped-parameter models. In systematic lumped-parameter models would be needed to approximate the rigorous impedance functions by using specific functions such as the ratio of two polynominals. Wolf (1991a, 1991b) employed partial-fraction expansions and parallel-form lumped-parameter models. Later, Wu and Lee (2002) utilized series-form lumped-parameter models for approximating the flexibility functions instead of using dynamic-stiffness. And also, Wu and Lee (2004) and Zhao and Du (2008) alternatively used a continued-fraction expansion for different lumped-parameter models. Moreover, other transformation procedures based on a modal expansion and conventional complex modal analysis were proposed to construct an exact (closed-form) solution for lumped-parameter models from the original systems by Saitoh (2011, 2012).

Finally, it should be noted that due to the unbounded nature of a soil medium, the computational size regarding to large model can be very large. For this reason, it is important to present some simple mathematical models which reduce the computational cost as well as increase the accuracy of results. In order to pass outgoing wave motions through the boundary without being reflected form soil layer and model boundaries, artificial or transmitting boundary conditions are considered. The related boundaries regarding to bounded domain problems in FEM simulation must be modelled such that, the energy crosses them without reflection and special conditions must be specified at the boundaries. Generally, these can be classified into local or global boundary conditions, where the local degree of freedom in neighbouring to bound-

aries or all degree of freedom are involved. The importance of global transmitting boundaries or absorbing boundaries has been reported in the past and consequently a number of methods have been developed and proposed for constructing absorbing boundaries by Lysmer and Kuhlemeyer (1969), Clayton and Enguist (1977) and Reynolds (1978). Later, many different methods have been reported in the literature to present and model absorbing boundary conditions in FEM such as Bamberger *et al.* (1988), Kim *et al.* (1996), Krenk *et al.* (1999), Semblat and Broist (2000), Kellezi (2000) and Krenk and Kirkegaard (2001). Morover, another methods such as applying damping solvent stepwise extraction methods based on complex frequencies for time domain analysis and semi-infinite elements have been proposed and used to provide a more efficient and accurate way to calculate the interaction forces of the unbounded soil within the framework of finite elements by , Li *et al.* (2008), Kausel (2010), Xunqiang *et al.* (2013) and Dassault Systèmes Simulia Corp (2012).

2.4   Mechanics of Porous and Non–porous Media

The soil behaviour is typically represented by continuum mechanics based on material behaviour of continuum media by employing stress-strain relationships. Saturated soil is often idealized as a two-phase medium comprising deformable soil skeleton and pore fluid, which may be sufficient for quasi-static properties, but which may not be enough to capture the dynamic properties for high frequency loads. Liquefaction in earthquakes is such a case where the modelling of soil as a solid skeleton fails: The structural changes go beyond more nonlinearities in the small deformation approximation of conventional solids. Particulate models (e.g. grain by grain in the discrete element models) are still not in a stage where they can be used to model larger volumes, but at least for the surroundings of piles, they are likely to give more realistic behaviour for the damping than continuum solid models. The intricate dependence of soil stiffness on density, stress and direction of stretching is often neglected. However, on length scales, much greater than inter-particle distances, continuum mechanics theories point out good accuracy. Also fundamental physical laws can be employed easily to derive the governing equations and describe the material behaviour.

2.4.1   Continuum Mechanics for Porous Media

Biot (1941a) presented his theory to calculate consolidation settlement of a soil under a rectangular load distribution. Biot (1941b) applied his theory based on continuum mechanics regarding to three-dimension based on the number of physical constants, which were necessary to determine the properties of the soil. The physical constants defined the physical proportions of an isotropic soil in the equilibrium conditions. Later, Biot (1955) implemented direct method and

Figure 2.13: Schematic representation of the region of contact between grains with viscouse fluid and the corresponding spring-dashpot model (Biot 1962b).

extended his previous derivation to the general case of anisotropy. And then, theories of the propagation of stress waves in a porous elastic solid containing a compressible viscous fluid for low and high frequency ranges developed by Biot (1956a, 1956b), where the material described by four non-dimensional parameters and a characteristic frequency. Biot's papers on wave propagation proposed the idea of representing the pores by small cylinders. The cylinder diameter became the key parameter needed to quantify permeability (Biot 1956a). Biot used the cylinder diameter to extend his theory to include turbulent flow beyond a defined transition frequency (Biot 1956b). Biot (1962b) investigated the visco-elasticity, anisotropy and solid dissipation in porous media by applying acoustic propagation theory. The Maxwell element which represents the dashpot and spring in series was implemented with Biot (1962a) in order to include the fluid-solid interaction. In these cases, the properties of the fluid and solid phase are not considered separately. Biot (1962b, 1962a) considered the model as shown in Fig. 2.13. to represent the contact between two elastic grains and a fluid.

Fukuo (1969) derived the dynamic theory for the deformation of a granular solid saturated with a liquid, assuming that the liquid filling up the pore space was a Newtonian viscous fluid and the skeleton constituted by solid particles was a linear visco-elastic solid. The theory consists of three fundamental equations which are the equations of motion of liquid and skeleton and the equation of continuity between the particles and liquid. Prevost (1982) analysed the response of saturated porous medium viewed as a two-phase system by the use of finite element method (FEM). Bardet (1992) proposed a viscoelastic model for a saturated poroelastic materials that obeyed the two-phases formulation of Biot and solved them analytically. Furthermore, Bardet and Sayed (1993) presented exact and approximate expressions for the velocity and attenuation of the low frequency compressional waves within nearly saturated poroelastic media based on the Biot's two-phase theory. The results were validated with the three-phase theory of Vardoulakis and Beskos (1986). Two phase theory of Biot was applied to investigate the damping regarding to the soil-water interaction analytically during steady-state vibration by Bardet (1995). Many other researchers have used the concept of porous media and continuum mechanics to investigate the behaviour of saturate soil such as: Kim *et al.* (2000), Soares and Mansur (2006) and Srisupattarawanit *et al.* (2006). Kim *et al.* (2000) studied the 2D wave propagation in porous seabed by using BEM based on integral equation while the numerical results were validated with an analytical solution. Based on Stoll's reports (1985) for saturated soil and the theoretical formulation of Biot (1962b), the Kelvin-Voigt-Maxwell-Biot (KVMB) model was formulated by Michaels (2006). This model behaves very much like the KV model, but splits the mass into two parts, and is a re-arrangement of the elements in series (similar to a Maxwell body) as shown in Fig. 2.13. When relating this KVMB model to a saturated soil, porosity can be used to define the mass ratio (frame to pore fluid). The dashpot is an expression of the permeability which controls the relative motion between frame and pore fluid. Furthermore, Michaels (2008) implement a model to capture equivalent viscosity by using viscosity as the specific soil property. Wang *et al.* (2008) developed an analytical solution to investigate the torsional vibration of an end bearing pile embedded in a homogeneous poroelastic medium and subjected to a time-harmonic torsional loading. The poroelastic medium

was modelled by using Biot's two-phase linear theory and the pile was modeled by one-dimensional elastic beam theory. Zhou *et al.* (2009) presented a semi-analytical method to solve the dynamic response of a pair of parallel elliptic tunnels embedded in an infinite poroelastic medium which was described by Biot's poroelastic theory. Badia *et al.* (2009) applied FEM to simulate the interaction between a fluid and a poroelastic structure due to the fact that both subproblems are indefinite. They designed residual-based stabilization techniques for the Biot system, motivated by the variational multiscale approach. Lo *et al.* (2010) presented a theoretical analysis for the dynamic response of a semi-infinite fluid-bearing porous medium to external harmonic loading based on the decoupled poroelasticity equations of Biot. Qiu (2010) presented a theoretical investigation on Biot flow induced damping for a saturated soil column/layer under shear wave excitations.

Based on continuum mechanics, three coupled and dynamic formulations are presented based on the soil and pore fluid (water) displacements and the pore water pressure. They are the $\mathbf{u}-P-\mathbf{U}$, $\mathbf{u}-P$ and $\mathbf{u}-\mathbf{U}$, where $\mathbf{u}$, P, and $\mathbf{U}$ are the soil skeleton displacement, pore water pressure and displacement, respectively. Zienkiewicz (1982) developed the FEM discretization to present the behaviour of various classes of soil and rock, or concrete as a two-phase medium composed of a solid skeleton and an interstitial fluid. Zienkiewicz and Shiomi (1984) modified the equations of motion in an innovative way, presenting a continuum model for the soil skeleton and pore fluid media that is called $\mathbf{u} - P - \mathbf{U}$. Prevost (1985) incorporated a semi-discrete finite element (FE) procedure with an implicit-explicit time integration algorithm to analyse wave propagation in fluid-saturated porous media, which was modelled in the $\mathbf{u} - P$ format. In the $\mathbf{u} - P$ formulation, if the fluid phase is considered incompressible, then the Ladyzenskaja-Babuska-Brezzi (LBB) condition needs to be satisfied (Brezzi (1974), Ye (1998), Zienkiewicz *et al.* (1999) and Bathe (2001)). In this case, the element type for the displacement and pore pressure fields requires special consideration, to prevent volumetric locking (Zienkiewicz *et al.* (1999) and Zienkiewicz and Taylor (2000)). The restrictions imposed by the LBB condition exclude the use of elements with equal order interpolation for pressures and displacements. Considering this restriction for monolithic algorithm, a simple model for numerical analyses is the $\mathbf{u} - P$ formulation that neglects the relative acceleration of the fluid with respect to the solid skeleton. This model is especially useful for low-frequency analysis. The contribution of the solid acceleration is neglected in the fluid mass balance. This omission was investigated by Chan (1988), who found the omitted contribution to be insignificant. Zienkiewicz *et al.* (1990) studied the transient and static response of saturated soil, which they modelled soil as a two-phase material based on the $\mathbf{u} - P$ formulation for porous media. Pastor *et al.* (1990) used a generalized plasticity approach to describe the behaviour of soil in the $\mathbf{u} - P$ formulation under transient loading. Oka *et al.* (1994) applied FEM and finite difference method (FDM) to investigate numerically the governing equations of soil skeleton and pore water obtained through application of the two-phase mixture theory by using a $\mathbf{u} - P$ formulation. Elgamal *et al.* (2002, 2003) implemented the $\mathbf{u} - P$ model for a two-phase (solid-fluid) problem with multi-surface plasticity, using a finite element method (FEM) to highlight the effect of excitation frequency. Jeremi *et al.* (2008) modeled a coupled porous

solid-fluid base on $\mathbf{u} - P - \mathbf{U}$ dynamic field equations while water accelerations to be taken into account and applied standard FEM. Later, Cheng and Jeremic (2009) used a fully coupled, inelastic $\mathbf{u} - P - \mathbf{U}$ formulation to simulate the dynamic behaviour of piles in liquefiable soils subjected to seismic loading. Niemunis and Cudny (2008) presented two FE-solutions of the coupled analysis of solid deformation and pore fluid behaviour. They were presented: $\mathbf{u} - P$ and $\mathbf{u} - P - \mathbf{U}$. Khiavi *et al.* (2009) presented the equations of motion of the soil mixture which was coupled with the global mass balance equations. The weighted residual standard Galerkin method with 8-noded elements was used for developing finite element code for $\mathbf{u} - P - \mathbf{U}$ model. The analysis was carried out in time domain considering earthquake excitation and Newmark time integration scheme. Researchers have attempted to solve these coupled equations by various numerical methods. For example, Lu and Jeng (2010) investigated the porous soil which governed by the $\mathbf{u} - P$ formulation, using the BEM. Samimi and Pak (2012) solved the $\mathbf{u} - P$ formulation by applying the Element-Free Galerkin method.

The difficulty of LBB condition can be solved by implementing appropriate stabilization techniques such as fractional step algorithm which was developed for soil mechanics by Pastor *et al.* (1999). Later, the generalized fractional step method proposed by Pastor *et al.* (2000), was modified by Li *et al.* (2003). Recently, Soares *et al.* (2014) described an edge-based smoothed meshfree technique by presenting an independent spatial discretization for each phase of the model.

2.4.2   Mechanics of Non–continuum for Porous Media

Soil's behaviours have been simulated by continuum soil model which is not able to model soil properly and it cannot suffice for soils however it can provide useful arguments. Continuum soil models need a set of complex constitutive relationships, which are mathematical formula that relate the stress tensor to the strain tensor, dependent on independent variables and constants, which sometimes have no clear physical meaning. The continuum approach lacks some of the required characteristics, since it does not provide information about grains and contact orientations. Continuum soil model mechanics is not the case with dissipative systems like rearranging soils (Gudehus 2011). This has led to the method composed of distinct particles that interact with their neighbours through contact mechanisms which is called discrete element method (DEM).

Regardless of the nature of the soil, which is discrete in nature, they interact only at the contact points. The assumptions in DEM have striking attempt to reproduce the soil's behaviour verisimilitude in a way that cannot be achieved by continuum approaches. DEM was originally developed by Cundall (1971, 1974) and proposed by Strack and Cundall (1978) for a dry environment initially. It was extended to account for the effects of pore fluid by M. Hakuno and Y. Tarumi (1988) for the first time which assumed fluid behaves as a perfectly elastic material by apportioning elastic properties to fluid phase (Hakuno and Tarumi 1988; Hakuno 1995). Nakase *et al.* (1999) used the same method to calculate the pore pressure by FDM. Sithram and Dinesh (2003) implemented the 3D DEM to analyse sphere particles. Furthermore, Dinesh *et al.* (2004) implemented the results from cyclic triaxial test to results from Sithram and

Dinesh (2003) to estimate the shear modulus and damping ratio. Jiang and Yu (2006) analysed the non-coaxiality of granular materials by introducing different contact laws to present effective stress and bonding effect in natural soils. The literature review for DEM has presented by Zhanping You (2007), Donze *et al.* (2008) and Bobet (2010). Kumari and Sitharam (2010) investigated the effect of particle shape on the behaviour of soils by particle flow code (PFC3D). Soroush and Ferdowsi (2011) employed the variation of hysteretic micromechanical parameters by. Andrade et al. (2012) and employed the DEM and captured particle morphology by using Non-Uniform Rational Basis-Splines. Ng and Matuttis (2012) developed a FEM to Matuttis Hans-Georg's Group two dimensional in order to have Newtonian fluid between the polygon particles. Ng and Matuttis (2013a) extended their work to simulate free surfaces. Ng and Matuttis (2013b) improved two dimensional program by adding shadow effect in order to avoid any flogging liquid between particles. Baohui *et al.* (2014) analysed sea ice dynamics by using DEM.

2.5 Numerical Analysis of Porous Media

In this section the different numerical methods, formulations and simulation codes regarding to the soil as a two-phase problem and foundation behaviours are reviewed. The simulation procedure can be done in time and/or frequency domains based on type of loadings. For harmonic loadings the frequency analysis can be useful in terms of computation time. Beside analytical approaches to solve the mathematical formulation which results in a highly coupled and non-linear system, requiring specific numerical techniques are highlighted. Several numerical methods have been proposed and implemented for porous media such as: FEM, Meshless, Isogeometric, BEM, DEM and FDM. On the other hand, some of mentioned method have been developed and grown up well which make appropriate simulation codes and user friendly software.

2.5.1 Numerical methods for Porous Media

Among all the available numerical techniques, few are widely accepted in engineering practice due to computationally expenses and the conceptual complexity. It can be a convenient method to discretise a wind turbine structure and surrounding supported soil into a number of elements with appropriate boundary conditions to describe the dynamic behaviour of foundation and soil. Finite element procedure is one of the most stable and concrete approach to solve the equations of motion. FEM as a straightforward and approachable manner has been used by Lysmer *et al.* (1974) to analyse soil–structure systems by discretising the foundation and the structure. Wong and Luco (1978) presented dynamic response of rectangular foundations to obliquely incident seismic waves, and also for dynamic analysis employed by Achmus *et al.* (2009), Li *et al.* (2011), Ibsen *et al.* (2012), Sørensen and Ibsen (2013) and Zhang *et al.* (2013), just to mention a few.

Brown and Shie (1991) utilized 3D FEM to model a laterally loaded pile in clay soil. Astley (2000) reviewed the application of infinite elements for wave problems

and illustrated the wave propagation toward infinity as the shape functions of the displacements. Nikolaou *et al.* (2001) employed 3D FEM with BNWF model to study Kinematic pile bending during earthquakes in layered soil. Andersen and Nielsen (2003) applied FEM and presented a solution in the frequency domain of an elastic half-space to a moving force on its surface. The latter model has been coupled with an FE scheme for the analysis of the shielding efficiency of trenches and barriers along a railway track by Andersen and Nielsen (2007). The time domain response of a jacket offshore tower while the soil resistance to the pile movement was modelled using p–y and t–z curves to account for soil nonlinearity and energy dissipation, was presented by Mostafa and El Naggar (2004) by employing FEM. Abbas *et al.* (2008) employed 3D FEM and investigated the effect of cross sectional shape on the response of a laterally loaded pile and obtained that the square pile has higher bending resistance to the lateral load compared to the circular pile. Khiavi *et al.* (2009) employed the weighted residual standard Galerkin method with 8-node elements to solve the equations of motion of the soil mixture which was coupled with the global mass balance equations while the Newmark time integration scheme was employed. Begum and Muthukkumaran (2008) investigated a lateral loaded long flexible pile by considering plane strain conditions and elastic-plastic Mohr Coulomb model by the use of 2D FEM for located pile on a sloping ground in cohesionless soil. Maiorano *et al.* (2009) utilized a quasi 3D FEM to perform dynamic analyses in the time domain and evaluate kinematic bending moments developing during earthquakes for single pile and pile groups. Dezi *et al.* (2010) used 3D FEM and BNWF to evaluate the bending moments induced by the transient motion for single piles. Georgiadis and Georgiadis (2010) improved p–y curve method by taking into account the inclination of the slope and adhesion of the pile slope interface by using 3D FEM for piles in sloping ground under undrained lateral loading condition. Thavaraj *et al.* (2010) employed quasi 3D FEM to present the dynamic nonlinear effective stress analysis of pile foundation under earthquake excitation. The time domain results for soil foundation structure interaction by considering the dependency of the foundation on the excitation frequency were presented by Cazzani and Ruge (2012) by using FEM. Laora *et al.* (2013) investigated Kinematic effects at the head of a flexible pile and elucidated the role of a number of key phenomena controlling the amplitude of kinematic bending moments at the pile head by using 3D elastodynamic FEM. Shahir *et al.* (2014) employed FEM to simulate the behaviour of the two-phase porous medium of saturated sandy soil under earthquakea by considering fully coupled $\mathbf{u} - P$ formulation. Hovind and Kaynia (2014) presented the three-step method based on the principle of superposition for nonlinear analyses of offshore wind turbine skirted foundation while two steps have been done by FEM. Cuéllar *et al.* (2014) investigated the cyclic soil behaviour in the frame of the theory of plasticity by adopting appropriate finite element formulations. Bisoi and Haldar (2014) studied the dynamic behaviour of offshore wind turbine by using BNWF and FEM in time domain to investigate the effect of different parameters, such as rotor and wave frequencies and geometry of monopile (thickness and diameter). Maste *et al.* (2014) carried out the analysis of group of piles in time domain by using FEM and developed soil–structure interaction model and it was validated with obtained FEM results by Sawant and Shukla (2012). Ghandil and Behnamfar (2015)

implemented FEM by considering modified equivalent linear method to analyse the dynamic behaviour of the near-field of foundation by including inelastic soil–structure interaction. Carswell *et al.* (2015) used FEM by employing several software packages to highlight the significance of foundation damping on monopile wind turbine foundations subjected to extreme storm loading.

In order to model the unbounded soil more precise and satisfy the radiation condition automatically; the BEM is a powerful tool and the boundaries of the unbounded soil are discretized (Beer *et al.* (2008)). However, the BEM has its limitation regarding to solve the complicated practical engineering problems owing to its reliance on the fundamental solution for many cases (Dominguez 1993; Manolis and Beskos 1988). Alternatively, the hybrid techniques are more precise where the unbounded soil is modelled by BEM and bounded structures with an adjacent irregular soil simulated by FEM.

Dominguez (1978) employed BEM to compute the dynamic stiffness of embedded rectangular foundations to travelling waves in the frequency domain. Karabalis and Beskos (1985) investigated the dynamic behaviour of flexural foundation plate subjected to external forces and obliquely incident seismic waves in time domain by using BEM-FEM. Gaitanaros and Karabalis (1988) presented the dynamic response of 3D flexible foundations of arbitrary shape subjected to obliquely incident seismic waves and external forces by implementing BEM-FEM, while both relaxed and completely bonded boundary conditions were considered. Kaynia and Kausel (1991) presented dynamic response analysis of piles and pile groups in a layered soil media by the use of BEM. Zhang *et al.* (1995) utilized 3D BEM-FEM while the coupling between 3D boundary and infinite boundary elements was developed to simulate the infinite and irregular canyons. The results for the seismic analysis of arch dam-canyon interaction presented in the time domain. Beskos (1997) performed a comprehensive review of applied 3D time/frequency domain FEM-BEM methods to solve elasto-dynamic problems. The multiple reflection of different kinds of waves in finite and semi-infinite domains may lead to instability problems. Yu *et al.* (1998) presented time weighting algorithm to improve the stability of the time response for the dynamic analysis. Ahmad and Banerjee (1988) presented the direct boundary element formulation to analysis 3D solids by using a time-stepping scheme to solve the boundary initial value problem. Rizos and Wang (2002) employed coupled BEM-FEM methodology to perform dynamic analysis regarding to 3D wave propagation and soil–structure interaction in time domain. Yazdchi *et al.* (1999) performed transient dynamic and seismic forces analysis of an elastic structure embedded in a homogeneous by considering non-zero initial conditions, while the BEM and FEM were coupled through equilibrium and compatibility conditions at the soil–structure interface. BEM and FEM were employed to model the semi-infinite far and near fields, receptively. And also, a two and three- dimensional combined FEM-BEM have been carried out for two railway tunnel structures by Andersen and Jones (2006). Then the steps in the FEM-BEM were discussed, and the problems in describing material dissipation in the moving frame of reference were investigated by Andersen *et al.* (2007). A BEM-FEM coupling model and a beam according to the Bernoulli hypothesis, for the time harmonic dynamic analysis of piles and pile groups embedded in an elastic half-space was em-

ployed by Padron *et al.* (2007). Later, Padron *et al.* (2008) improved their work by implementing a 3D BEM-FEM to study the dynamic behaviour of piled foundations in presence of a rigid bedrock. And also, Padron *et al.* (2010) extended their work to highlight the influence of inclined piles on deep foundations. Genes (2012) presented harmonic and transient dynamic response of large scale 2D structures by proposing an algorithm for parallel use of BEM-FEM and scaled boundary FEM. Romero *et al.* (2013) presented the dynamic analysis of soil-foundation interaction by considering nonlinear soil–structure contact in time domain by using BEM-FEM. Galvin and Romero (2014) developed 3D BEM-FEM analysis in time domain in MATLAB.

Basically, the mesh indicates the connectivity between the corresponding neighbouring nodes. The meshing process is one of the most cumbersome step in the entire numerical analysis as mentioned by Owen (1998). Instead of using a mesh, a set of geometrically unconnected nodes can be used for the global domain discretization, resulting in the meshless or meshfree methods. In addition to bypass in mesh creation, using overlapping domains in meshfree methods, which gives more support nodes for each point, allowing a richer approximation and avoiding any artificial discontinuity in the field. More details about meshless regarding to reviewing different types of meshless, advantage of using meshless and comparison between them have been presented by Li and Liu (2007), Daniel and Orden (2007) and Trobeca *et al.* (2007), respectively. Belytschko *et al.* (1995) proposed the element-free Galerkin method and coupled it with FEM for both elastostatic and elastodynamic problems, including a problem with crack growth. Karim *et al.* (2002) analysed the saturated porous elastic soil layer under cyclic loading by using a two dimensional mesh free Galerkin method with incorporated periodic conditions. A meshless method was an effective alternative, because it is difficult for FEM to analyse the problems associated with the moving boundary. Lei-na and Xi-ping (2009) applied the element free Galerkin method to simulate the response of the seabed under wave actions, especially for the critical cases with incompressible pore water and impervious soil skeleton. Augarde and Heaney (2009) reviewed and presented the application of meshless method in geotechnical problems specially when it is involved with nonlinear material and geometric. Soares (2013) formulated an edge-based smoothed weak meshless formulation by Delaunay triangulation to perform an iterative dynamic analysis of linear and nonlinear fully saturated porous media. FDM is the oldest method and it is based upon the application of a local Taylor expansion to approximate the differential equations. The FDM uses a topologically square network of lines to construct the discretization of the partial differential equations. On the side of FDM, it is conceptually simpler and easier to implement than FEM. Finite elements has the benefit of being very flexible, for example the grids may be very non-uniform and the domains may have arbitrary shapes. Stevens and Krauthammer (1998) used FDM-FEM to analyse buried structures subjected to earthquakes while FDM was used to analyse wave propagation in continuous media with nonlinear constitutive properties and large strain deformations and FEM used for structure analysis. Ng and Zhang (2001) investigated the performance of the sleeved and unsleeved piles constructed on a cut slope using 3D FDM. Andersen *et al.* (2012) used FDM to analyse a nonlinear stochastic p–y curve for calculation of the monopile response. Nowamooz *et al.* (2015) employed FDM to present the heat dis-

tribution throughout the unsaturated soil while its thermal diffusivity varies with time and depth. Indraratna *et al.* (2015) utilized DEM-FDM to study the deformation of a single stone column installed in soft ground. Isogeometric methods is very close to FEM and computer aided design. That is why, it can addresses a very accurate description of complex geometries. The term iso- is used to indicate that the same functions, that are used to describe the geometry and unknown variables. Zhang *et al.* (2009) formulated a coupling material point method to predict the dynamic response of saturated soil and the contact/impact behavior between saturated porous media and solid bodies. Irzal *et al.* (2013) implemented an isogeometric analysis to predict the behaviour of a deformable fluid-saturated porous medium, using non-uniform rational B-splines.

Besides all numerical methods, there are also several analytical solutions for these type of problems. Boer and Liu (1994) presented an analytical solution based on the geometrically and physically linear theory to investigate the wave propagation in an incompressible liquid saturated porous medium when governed by a set of linear coupled partial differential equations. Peng and Yu (2011) obtained an analytical solution of the torsional impedance saturated soil by using transfer matrix method. The effects of important parameters such as frequency and the rigidity ratio of different soil layers at the top of the pile were analyzed. Wang *et al.* (2008) developed an analytical solution to investigate the torsional vibration of an end bearing pile embedded in a homogeneous poroelastic medium and subjected to a harmonic torsional loading by using the separation of variables technique. Belotserkovets and Prevost (2011) developed a full-analytical method and an exact unique solution of the coupled thermo/hydro/mechanical response of a fluid saturated porous sphere subject to a pressure stress pulse on the outer boundary. The method of solution was based on the Laplace transformation method. Li and Zhang (2010) presented an analytical solution in frequency domain by means of a variable separating method and then a semi-analytical solution was obtained using a numerical convolution method. Chai *et al.* (2011) employed the thin layer stiffness method, the matrix stiffness of the thin layer for PSV and analytical expressions for the effective phase velocity of the surface waves to illustrate the effects of the body waves on the observed phase velocity through the phase analysis of the vibrations of both the surface waves and the body waves. The plane wave assumption was applied to account for higher modes. The multichannel analysis of surface waves was used to obtain the dispersion images of the modes by Strobbia and Foti (2006) and Bodet *et al.* (2009), for more details see the references therein.

2.5.2   Simulation codes regarding to Porous Media

At the present time, there are several codes and software to model wind turbine and soil, which describe some of soil properties to a sufficient degree and wind turbine problems with different degree of detail. Some commercial software such ANSYS and ABAQUS originated for structures and then they have been extended to include different models of soil to simulate onshore and offshore wind turbine foundations. And also, some other software which are more specific to model buildings, wind turbines and supported soil can be listed as Plaxis, FLAC, SHAKE-91, OpenSees,

OpenSeesPL, FLEX5, FAST, HAWC2 and ROSAP, just to mention a few. Different methods to simulate the dynamic response of offshore wind turbines subjected to combined wind and wave loads in an integrated and/or superimposed manner have been proposed. In order to reduce costs of offshore wind energy, accurate modelling of the dynamic response of offshore wind turbines and supported soil are necessary to improve their design. Therefore, simulation codes need to take a system approach for predicting aerodynamic, hydrodynamic loads and also soil damping much more precisely. Below, a short review of researches that have used simulation codes such as ANSYS and ABAQUS are given.

Rovithis *et al.* (2009) performed parametric analyses of coupled soil-pile-structure systems subjected to seismic loading by using 3D finite element model in ANSYS. Laora *et al.* (2012) investigated the behaviour of a kinematically stressed pile in layered soil by using ANSYS, while both pile and soil are idealized as linearly viscoelastic materials. Hemmat *et al.* (2012) simulated the stress-sinkage behavior of a silty clay loam soil by using ANSYS, while the soil was modelled as a 2D axisymmetric structure. Xunqiang *et al.* (2013) employed ANSYS to present nonlinear seismic analysis of large 3D structures while the soil was bounded with artificial dampers. Wang *et al.* (2013) utilized ANSYS to do frequency domain analysis of soil pile interaction when it was founded on viscous-elastic soil layer and hysteretic damping has been considered for both the soil and the structures. Vasilev *et al.* (2015) implemented BEM-FEM through ANSYS to study seismic response of a soil–structure system when BEM was used to model infinite far-field media.

Johnson *et al.* (2001) presented a surface interaction model between pile and soil in ABAQUS. Memarpour *et al.* (2012) investigated the lateral behaviour of offshore pile foundations under cyclic lateral loads by using BNWF and ABAQUS. Su and Li (2013) investigated the response of a single pile subjected to lateral loadings using ABAQUS. Kampitsis *et al.* (2013) used an advanced beam model for the soil-pile-structure kinematic and inertial interaction by using SHAKE91 (Shake 1991) to analyse the seismic site response without the presence of the structure. The obtained excitation motions was employed in OpenSees (opensees 2005) to analyse the soil-pile-structure system. The calculations of the site response and the soil-pile-structure interaction were performed in a fully coupled manner with ABAQUS (ABAQUS 2009). Bhowmik *et al.* (2013) investigated the nonlinear behavior of single hollow pile in layered soil subjected to varying levels of horizontal dynamic load by the use of ABAQUS while the Mohr-Coulomb plasticity model was employed to simulate the soil. Gu *et al.* (2014) investigated the behaviour of pile group under eccentric lateral loading by using ABAQUS. Mendoza *et al.* (2015) presented the behaviour of groups of helical screw piles while the hypoplasticity constitutive model was considered for soil by employing ABAQUS. Wang *et al.* (2015) employed different pile and soil contact interface models to calculate conductor lateral displacement and vertical bearing capacity using ABAQUS by writing corresponding computer programs of constitutive model of interface model.

Several coupled pore pressure/displacement elements (*i.e.* CPE4P, CPE6MP, CAX8RP and CINAX5R) have been implemented in ABAQUS. Static and quasi-static soil analysis such as consolidation can be done systematically. But fully dynamic soil analysis

is not possible for lack of inertia effect. For example a steady-state, coupled pore fluid diffusion/stress analysis needs to be performed in several increments and steps with appropriate time step to allow ABAQUS to resolve the high degree of nonlinearity in the problem. The full effect of inertia does not considered in dynamic soil analysis, it is fitted for the cases with low frequency loadings. However, ABAQUS provides a library of pipe-soil interaction elements to present the ground behaviour and soil-pipe interaction. But, these elements have only displacement degrees of freedom at their nodes. Therefore, after performing preliminary analysis in ABAQUS in order to have full dynamic soil analysis in frequency domain the in-house FE code is developed. More information of the developed codes and techniques can be found in the included Papers 4, 5 and 6.

2.6   Post-processing in Finite Element Method

To improve the efficiency of numerical approaches, it is important to calculate and reduce the errors. For as long as physical events have been computationally simulated, the numerical error of such calculations has been a major concern. Discretization error is inherited in these simulations, arising from the discretization process of the continuum domain. As a result, not all of the information characterized by the partial differential or integral equations can be obtained. Especially for the dynamic analysis of complex problems with many degrees of freedom, adaptive refinement procedures in regions where there are large gradients in the changes between the nodal variables need to be used. This requirement is because of the limitations of the speed and memory of available computers. The error can be in conjunction with the adaptive refinement procedure to obtain the desired accuracy for design purposes with less computational effort.

   To check the accuracy of numerical solutions based on the classical energy norm, error estimation methods are used. These methods can be categorized into two classes: residuals-based and recovery-based. In residual-based methods, the residuals of a differential equation and its boundary conditions are considered as error criteria. In the residuals-based method, the residual of the differential equation or some function of the residual is used as a measure of the error (Babuska (1975), Babuska and Rheinboldt (1978) and Babuska and Rheinboldt (1979)). The recovery-based approach uses the error in gradient of the solution as the error estimator and comparing to the residual based error estimation, it is easy to implement in FE simulation. In recovery-based method by comparison between obtained results from FEM and the recovered solution, which is obtained by using recovery techniques in a postprocessing procedure, the error can be estimated. It is well known that the calculated FE stresses at the Gauss points based on nodal displacement do not have continuity between elements. Zienkiewicz and Zhu (1987) as pioneer in the recovery technique and error estimation used nodal averaging to modify the finite element solution. Later, the most famous ZZ (Z2) superconvergent patch recovery technique (SPR) was proposed and implemented by Zienkiewicz and Zhu ((1992a), (1992b), (1992c)). The ZZ error estimator (Zienkiewicz and Zhu, (1987), (1992a), (1992b)) is a recovery-based method that is

used in conjunction with the SPR, weighted super-convergence path recovery (WSPR) and L2-projection. The theory of super-convergence is that to have more accurate results in Gauss points to recover the results at nodal points and the rate of convergence has a maximum value. The numerical results in Babuska *et al.* (994a, 994b, 1997) showed that a recovery technique with a standard SPR. A comprehensive survey of the error estimation in FEM has been presented by Babuska *et al.* (1986). Chung and Belytschko (1998) presented local and global error estimates for the element-free Galerkin method. El-Hamalawi and Bolton (2002) presented and developed the consolidation super-convergent patch recovery with equilibrium and boundaries method for using in plane-strain coupled-consolidation axisymmetric geotechnical problems. The original SPR method is based on a least-squares fit of derivatives at the optimal sampling points. The technique states that if the gradients at some points are super-convergent, then any gradient field resulting from a polynomial fit to these values will be super-convergent (*i.e.* Babuska *et al.* (1996) ; Barlow(1976); Levine (1985); Mackinnon and Carey (1989); Prathap (1996), Oh and Batra (1999); Lin and Zhang (2004)). Ullah and Augarde (2013) implemented Meshless and SPR method to present an efficient computational modelling of problems including both material and geometric nonlinearities.

SPR method has been extended and improved by many researchers, for example Mukherjee and Krishnamoorthy (1998), Wiberg *et al.* (1995) and Gu *et al.* (2004) proposed a weighted patch recovery scheme (WSPR). And also, incorporating the equilibrium and boundary condition with patch recovery was presented by Blacker and Belytschko (1994), Park *et al.* (1999), Zienkiewicz *et al.* (1999), Boroomand *et al.* (2004); Rodenas *et al.* (2006), Khoei *et al.* (2008)). The main objective of the recovery process is to overcome this difficulty and make a smoothed continuous stress field between elements. In the standard SPR technique, all sampling points have similar properties in the patch, which may yield to significant errors, particularly at the edges of a crack (Khoei *et al.* (2008)). For elements located on high-gradient regions with insufficient sampling points, the points of the nearest patch must be used, with the definition of a weight function for the SPR procedure. Tang and Sato (2004, 2005, 2013) studied error estimation and adaptive mesh refinement on seismic liquefaction, seeking to improve the numerical results for large deformation in a soil-pile interaction problem. Estimation the global error has been used extensively in mesh-based and meshless methods based on residual-based (Afshar *et al.* (2012)) and recovery-based (Bordas and Duflot (2007)) techniques. Nazem *et al.* (2012) used an h-adaptive FEM to tackle the penetration and indentation problems of geomechanics in the presence of inertial forces. They compared three alternative error estimation techniques, based on the energy norm, the Green-Lagrange strain, and the plastic dissipation.

CHAPTER 3
Scope of the Thesis

As reviewed and mentioned in Chapter 2, scientists and researchers have developed and implemented several mathematical methods and numerical approaches either by their own developed codes or commercial software packages to analyse dynamic behaviour of offshore foundations and consider the soil–structure interaction and soil damping. To the best of the author's knowledge, accurate and realistic natural frequencies of OWTs as well as soil stiffness and damping cannot be quantified by current methods. The current research aims to obtain a better understanding of the stiffness and damping of saturated soil, propose an improved methodology for analysis of soil-foundation interaction that accounts for rate-dependent behaviour of saturated soil. This chapter clarifies the overall objectives and specific aim of the present dissertation based on the literature review and mentioned discussions from Chapter 2. The main idea and focus of the research project as well as its innovation and contribution to the offshore wind industry are highlighted.

3.1 Main Findings of the State-of-the-Art

The design process of offshore wind turbines begins with site selection, in which external conditions such as aerodynamic and hydrodynamic loads are assessed as well as geotechnical conditions. Commonly, by selecting the size of wind turbine, an initial design of the wind turbine tower is presented and, consequently, evaluating initial loads on the foundation is given to select and design foundation initially. Afterward, by considering different load cases and assessing geohazards for certain foundations, an iterative design process between tower and foundation is implemented to find the optimum design. During this procedure, performing geotechnical and structural analyses are considered until a satisfactory design is found. The design procedure for monopile foundation based on the fixed ratio of pile diameter to thickness until to get the desired natural frequency is sketched in Fig. 3.1 presented by Segeren and Diepeveen (2014). In the iteration procedure, monopile geometry is modified and varied until the desired natural frequency is obtained. As discussed in the previous chapter, the methods and procedures to model the foundation and supported soil have a substantial in reducing computational times as well as having an appropriate design and cost-effective foundation. Commonly, beam theories such as Bernoulli-Euler or Timoshenko are implemented in 2D (and/or 3D) FE codes to model piled foundations. Moreover, the damping in offshore wind turbines is significant in the fatigue perspective.
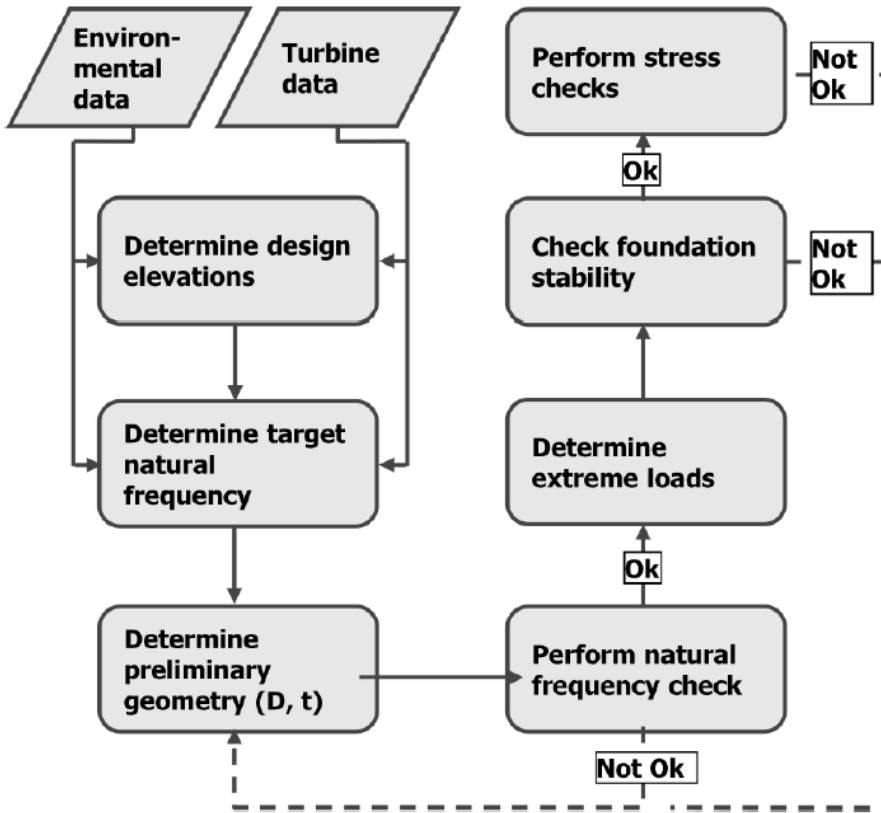
Figure 3.1 Design of offshore monopile wind turbine foundations (Segeren and Diepeveen 2014).

Offshore wind turbines are subjected to highly dynamic loads. Therefore, modelling of the wind turbine foundation is important to capture all dynamic effects properly; *i.e.* dynamic soil stiffness and damping in the presence of pore pressure should reflect reality as close as possible. Moreover, damping in offshore wind turbines is an important parameter in fatigue analysis. Evidently, damping has a great effect on the magnitude of the wind turbine response, and has a considerable influence on the natural frequency of wind turbine system. As shown in Fig. 3.1, to perform design evaluations and determine target natural frequency, the dynamic effects regarding foundation and supported soil must be calculated and captured properly within the numerical approach. Therefore, modelling soil–structure interaction properli is essential, as is obtaining accurate and realistic dynamic soil stiffness and damping, which results in fatigue damage. Fatigue damage increases with decreased damping. Soil damping by Rayleigh damping is commonly presented as a linear combination of the mass and stiffness. The design regulations recommend the use of p–y and t–z curve methods to include the soil–structure interaction for offshore wind turbines. The p–y

curve method was developed for small-diameter (D = 0.32 m, D from 0.5 to 3 m), long, flexible and slender piles with length-to-diameter ratios (L/D) generally larger than 12 in the oil and gas industry. Rigid monopiles with L/D < 12 and diameters from 3.5 to 7 m are typically used for offshore wind turbines.

Offshore wind turbine structures are sensitive to rotations and dynamic changes in the pile-soil system. The effect of load rate is not concerned in the p–y curve method. Furthermore, this effect does not account dynamic soil stiffness because inertia effects and it does not assign a well-defined representation of the soil damping. To incorporate the effect of load frequency and pore pressure, the coupled equations are needed to illuminate the behaviour of different states in the soil.

Equivalent system comprising equivalent masses and springs at pile-cap level can be constructed by using Winkler model approach. However, current Winkler models do not consider the effect of pore pressure and load frequency. To overcome this problem, an improved methodology to analyse soil–foundation interaction that accounts for rate-dependent behaviour of saturated soil will be proposed. The increase in stiffness because of high-rate deformation of the saturated soil is not accounted for, and damping is only described in terms of modal damping within each mode. Thus, material damping, viscous damping from seepage and radiation damping are not accounted for explicitly. Given that the stiffness of foundation and subsoil strongly affects the modal parameters, the stiffness of saturated soil because of pore water flow generated by cyclic motion of monopiles is investigated using the concept of a Kelvin model that combines springs and dashpots. In this regard, the coupled equations for porous media are employed to account for soil deformation as well as pore pressure. The effects of drained versus undrained behaviour of the soil and the impact of this behaviour on the stiffness and damping related to soil–structure interaction at different load frequencies are illustrated.

3.2   Aim and Objectives

For the past decade, the number of installed offshore wind turbine have greatly increased, as has the size of the turbines. The more efficient design with higher capacity wind turbines consist of larger rotor diameters and higher hubs affected by modeling the dynamic of the pile-soil interaction. As the size of offshore wind turbines increase, the structure should undergo larger fatigue loads. The level of damping, including structural and soil damping as well as aerodynamic damping, is vital to improve current design practices to be cost-effective and provide a safe and economical design.

The objective of this thesis is to more closely examine the dynamic behaviour of saturate soil that support structures for offshore wind turbines and improve the knowledge of the soil damping. Representing the soil–structure interaction properly, can directly affect (a) the natural frequency of wind turbine system (b) the dynamic soil stiffness and damping (c) the life time of wind turbine (d) and finally, the cost of wind turbine. The main objectives of the study are listed as follows:

◆ To evaluate the effect of loss factor and other soil properties on the dynamic soil

stiffness and the phase angle of the dynamic stiffness for different load frequencies. The results for hollow and solid cylinders are presented by employing mathematical approach based on Somigliana's identity, Betti's reciprocal theorem and Green's function.

◆ To demonstrate damping and stiffness of saturated soil within the seabed when the monopile is subjected to a cyclic motion and considering the effect of the generated pore water flow. FEM in ABAQUS and Kelvin-Winkler model are employed for two dimensional analyses. Input files format for ABAQUS are coding; by utilizing Python and MATLAB, the desired results are presented.

◆ To extract p–y–$\dot{y}$ curves for offshore monopiles subjected to cyclic loads, a two-dimensional finite-element program is developed for analysis of a segment of an offshore monopile foundation placed in different depths. The response to cyclic loading is analysed by employing coupled equations based on the **u**-p formulation, *i.e.* accounting for soil deformation as well as pore pressure.

◆ To illustrate the effect of pore pressure by implementing a poroelastic model to present more realistic dynamic properties and compare them with results obtained by p–y curve method, finite-element programs are developed to analyse an offshore monopile foundation placed in different depths

◆ To investigate the dynamic behaviour of soil around monopile foundation subjected to cyclic loads and present stress recovery techniques based Zienkeiwicz-Zhu (ZZ) error estimator namely, super-convergent patch recovery (SPR), weighted super-convergent patch recovery (WSPR), and L2-projection techniques.

From the soil dynamic and geotechnical perspective, this study primarily aims to calculate seepage damping, to present the effect of pore water pressure, and to investigate the effect of material damping on soil stiffness and natural frequency of offshore wind turbine system. The novelty of this PhD research can be highlighted by (a) calculating soil damping during cyclic loading based on numerical approach by employing Kelvin-Winkler model (b) parametric study to investigate the soil–structure interaction and its influence on the dynamic response of the soil and the natural frequency of wind turbine (c) elucidate the effect of load frequency on soil stiffness and damping and natural frequency of offshore wind turbine supported by monopiles.

CHAPTER 4
Summary of Included Papers

The present research project is based on six scientific peer-reviewed papers, including four journal papers and two conference papers that can be found in the enclosed appendices. The papers fulfill the listed objectives of the PhD project by employing mathematical and mostly numerical approaches to elucidate the groundwater behavior and the impact of such behaviour on the stiffness and damping related to soil-structure interaction at different load frequencies. In the following chapter, the main results and employed methodologies in the articles are demonstrated.

4.1 Overview of Publications

This dissertation focuses on the behaviour of the saturated soil surrounding to offshore monopile wind turbines based on mathematical modelling and numerical methods, cf.
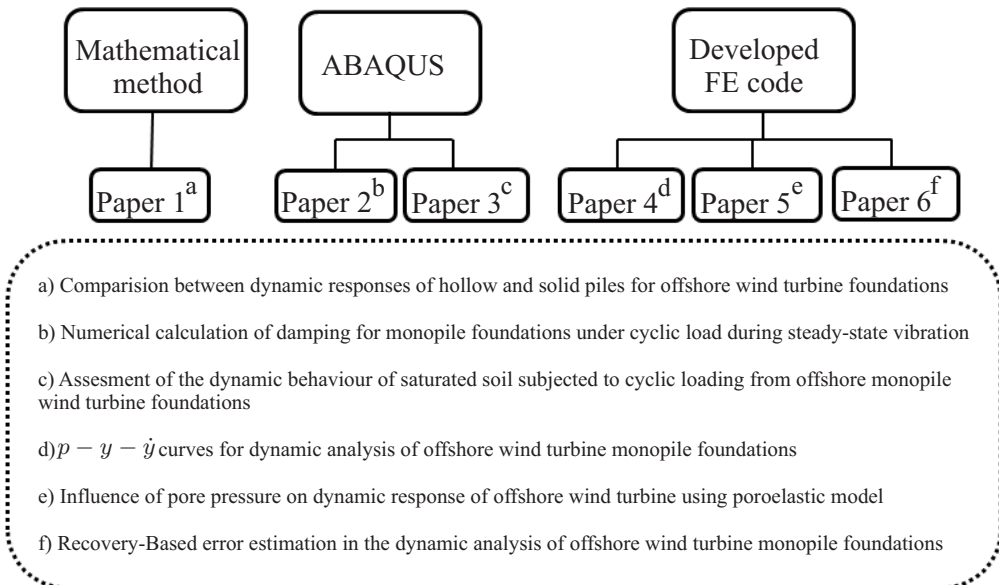

Figure 4.1 Overview of research topics and scientific papers.

Fig. 4.1. FEM in ABAQUS and developed FEM code are used to evaluate more realistic dynamic properties for offshore wind turbine foundations by considering the effect of load frequency for lateral loading of monopiles subjected to cyclic loads. First, the effect of soil damping and other soil properties on the dynamic behaviour of offshore monopile wind turbine foundations are illustrated. Secondly, FEM in ABAQUS is employed to calculate the soil damping and then in-house FE code is developed to illustrate the effects of drained versus undrained behaviour of the soil and the effect of this behaviour on the stiffness and damping related to soil-structure interaction at different load frequencies. Finally, different stress recovery techniques based on the Zienkeiwicz-Zhu (ZZ) error estimator are employed to recover the stresses at nodal points in the FEM.

4.1.1   Paper 1

Published in *Seventh international conference on case histories in geotechnical engineering*, May 2013, Chicago, Pages 94–108.

Paper 1: "Comparison between dynamic responses of hollow and solid piles for offshore wind turbine foundations" presents the effects of basic factors such as geometry, damping, Young's modulus, and Poisson's ratio on dynamic behavior of soil. The pile is modeled as smooth long hollow and solid cylinders and the dynamic excitation is applied vertically. The exact solutions and elastic responses are obtained in viscoelastic media and frequency domain. The vertical loads are applied on the surface along the entire interface by considering rough and full contact between the soil and structure. Long tabular and solid piles are investigated via integral method along with Betti's reciprocal theorem, Somigliana's identity and Green's function. Modes of resonance and anti-resonance are identified and presented.

Main Results

The following main findings from *Paper 1* can be stated as follows:
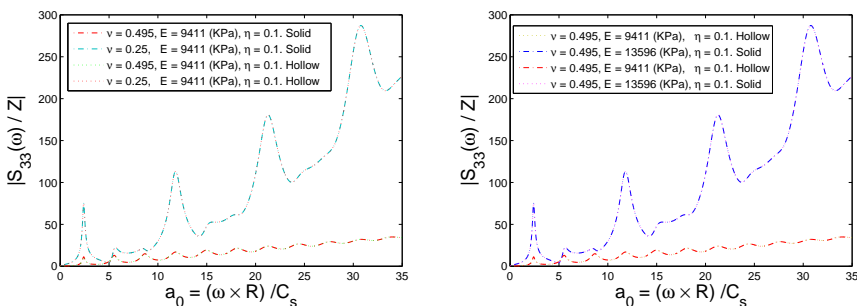
Figure 4.2 *Paper 1* — Comparison between normalized dynamic stiffness per unit length of an infinite hollow and solid cylinders due to dynamic vertical loadings.

◆ The dynamic soil stiffness and phase angle in a hollow or solid cylinder are independent of the soil's material properties *i.e.* Young's modulus and Poisson's ratio, whereas it is dependent on the load frequency and loss factor. The dynamic soil stiffness increases with the increase of the load frequency until reaching a peak point then decreases to a local minimum for certain value of frequency. This procedure is repeated periodically for hollow and solid cylinders as shown in Fig. 4.2.

◆ The phase angle fluctuates around line $\pi/2$ and the amount of fluctuating around this line decreases with the increase of load frequency for hollow cylinder and by increasing the loss factor it converges to line $\pi/2$, whereas the phase angle does not converge to certain value in solid cylinder.

The results reveal that the presented approach gains the physical understanding for offshore foundation in the geo-mechanics field.

The results reveal that the presented approach gains the physical understanding for offshore foundation in the geo-mechanics field.

4.1.2 Paper 2

Published in *The fifth international conferences on structural engineering, mechanics and computation*, Cape town, South Africa, pp. 1–11.

Paper 2: "Numerical calculation of damping for monopile foundations under cyclic load during steady-state vibration " demonstrates dynamic responses of an isotropic saturated elastic soil medium due to pore water flow generated by the cyclic motion of a monopile. The concept of a Kelvin-Voigt model is employed and combined with a 2D FE model of the pile in ABAQUS to calculate seepage damping and dynamic stiffness of saturated soil within the seabed. The two-dimensional analysis of each individual soil layer is performed in ABAQUS by coding input files, utilizing Python scripting in ABAQUS and MATLAB. To calculate desired results, the Python program is employed so that it can be called from MATLAB, then the program executes ABAQUS, MATLAB is used for post processing. The pore pressure and displacement at the exterior boundary is considered zero. Symmetry of the solution is applied across the center line of the model, whereas for the semi-circle carve, the sinusoidal periodic displacement in horizontal direction is applied as shown in Fig. 4.3(a). A sinusoidal forced displacement is applied and the simulation is conducted within 12 second. The seepage damping is calculated based on the phase shift between the applied forced displacement and mean value of the reaction force at the semi-circle boundary. A parametric study is performed to illustrate the effects of model size, soil properties (*i.e.* Young's modulus, grain bulk modulus, void ratio, and permeability), load frequency, and amplitude on the soil stiffness and damping.

Main Results

The following main findings from *Paper 2* can be stated:

♦ The effect of permeability is highlighted and by increasing the permeability the damping increases. In addition, for specific values of permeability, the maximum damping occurs. However, for further increasing permeability, the damping decreases as shown in Fig. 4.3(b). Stiffness decreases with increasing permeability.

♦ The variation of soil stiffness and damping due to periodic loading for different values of the void ratio, Young's modulus and load's amplitude and frequency are illustrated.

4.1.3 Paper 3

Published in *Computers and Geotechnics*, Volume 61, May 2014, Pages 116–126, DOI: 10.1016/j.compgeo.2014.05.008.

Paper 3: "Assessment of the dynamic behaviour of saturated soil subjected to cyclic loading from offshore monopile wind turbine foundations" is one of two papers employing ABAQUS to investigate the soil damping of saturated soil owing to pore water flow generated by cyclic motion of monopiles. This study highlight the effect of pore water pressure, and addresses calculating natural frequency of offshore wind turbine via three methods. (a) Full-scale measurement by free vibration tests, (b) using a beam on a nonlinear Winkler foundation model with soil-pile interaction recommended by the design regulations, and (c) recalculating the frequency by using improved soil stiffness, the influence of pore water flow is considered by using the concept of a Kelvin model that combines spring and dashpot.

Main Results

The main findings from *Paper 3* are as follows:

♦ A beam on a nonlinear Winkler foundation model based on the incorporated $p - y$ curves recommended by the design regulations consequently underestimates the
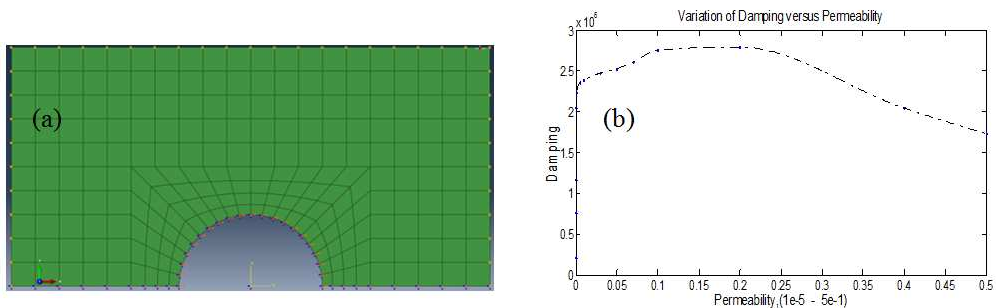
Figure 4.3 *Paper 2* — (a) Geometry, discretization and boundary conditions for the soil model (b) Variation of seepage damping versus variation of the permeability.

eigenfrequency related to the lowest eigenmode of offshore wind turbine structure installed on monopile foundations compared to full-scale measurements. This discrepancy is reduced by considering the influence of pore water pressure for cohesionless soils as shown in Fig. 4.4.

♦ For low and high values of soil permeability, indicating fully undrained and drained soil behaviour, respectively, soil stiffness is independent of the frequency of the forced displacement.

4.1.4 Paper 4

Submitted to *Soil Dynamics and Earthquake Engineering*, In review.

Paper 4: "$p - y - \dot{y}$ curves for dynamic analysis of offshore wind turbine monopile foundations" presents an improved $p - y$ curve method by considering the influence of excitation frequency. Coupled equations based on the $\mathbf{u} - P$ formulation are employed and 2D FE code is developed to analyse a segment of an offshore monopile foundation placed in different depths. The effects of drained and undrained behaviour of the soil and the effect of this behaviour on the stiffness and damping related to soil-structure interaction at different soil depths and load frequencies are illustrated. A parametric study is performed to extract $p - y - \dot{y}$ curves for lateral loading of monopiles subjected to cyclic loads.

Main Results

The most important conclusions from *Paper 4* are stated below:

♦ The soil stiffness reduction onsets in transient region from silt to sandy soil; it occurs in sandy soil for all values of load frequencies as shown in Fig. 4.5.
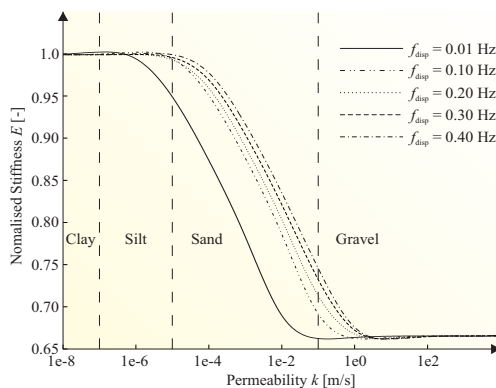
Figure 4.4 *Paper 3* — Variation of soil stiffness versus permeability for different forced displacement frequencies.

◆ The maximum equivalent damping almost occurs in transient region, primarily in the sandy soil regime, and the maximum damping moves toward the coarse (sandy) soil by increasing the load frequency as shown in Fig. 4.5.

4.1.5 Paper 5

Submitted to *Soil Dynamics and Earthquake Engineering*, In review.

"Influence of pore pressure on dynamic response of offshore wind turbine using poroelastic model" illustrates the effect of pore pressure by implementing a poroelastic model to present more realistic dynamic properties and compare them with results from $p - y$ curve method. Two different finite element programs are developed and combined analyse an offshore monopile foundation as shown in Fig. 4.6. The response to cyclic loading is analysed by employing a Winkler foundation model based on nonlinear $p - y$ curve method. Moreover, a two phase system consisting of a solid skeleton and fluid phase, based on $\mathbf{u} - P$, is implemented to perform free vibration tests to evaluate the eigenfrequencies. Furthermore, a simple model of an offshore wind turbine is constructed with equivalent masses, dashpots and springs providing the foundation response at the pile-cap level via Winkler and Kelvin model.

Main Results

The most relevant conclusions from *Paper 5* are listed below:

◆ In comparison between loose, medium dense, and dense sandy soil, the damping ratio becomes smaller for medium dense and dense sandy soil. Furthermore, the natural frequencies for dense sandy soil are greater than those of the other soil types.
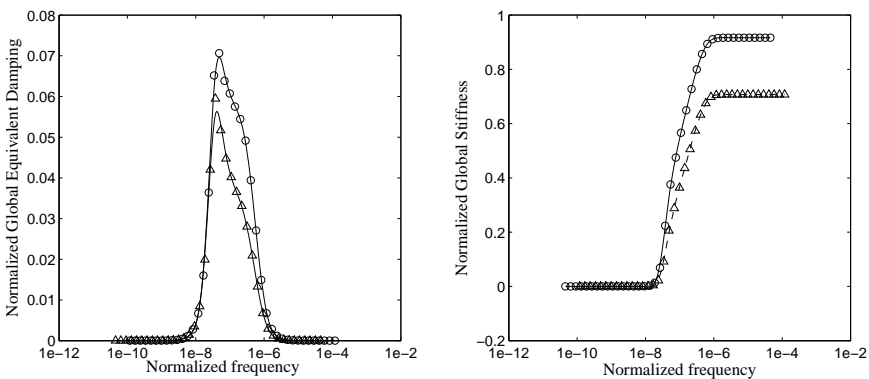

Figure 4.5 *Paper 4* — Variation of soil stiffness and damping versus normalized load frequency.
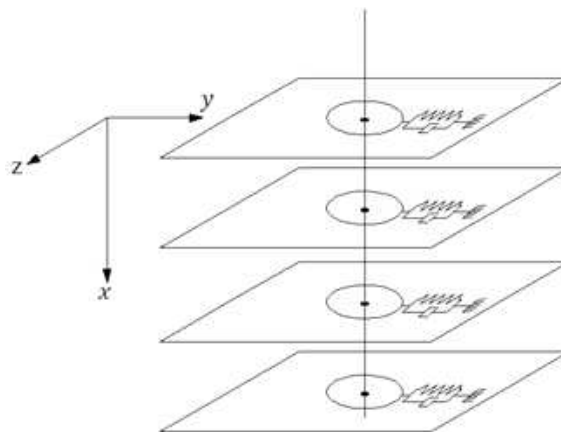
4.1.6 Paper 6

Submitted to *Ocean Engineering*, In review.

Paper 6: "Recovery-Based Error Estimation in the Dynamic Analysis of Offshore Wind Turbine Monopile Foundations " presents the response in terms of pore water pressure, stress and strain distribution in an elastic porous medium at regions around the monopile foundation. Different stress recovery techniques based on the Zienkeiwicz-Zhu error estimator namely, super-convergent patch recovery, weighted super-convergent patch recovery, and L2-projection techniques are also investigated to recover the stresses at nodal points in the finite element method. The convergence of the dynamic problem is also studied. The results are verified with findings in the literature.

Main Results

The most important findings from *Paper 6* are listed below:

◆ The convergence rate is 0.5 for all presented recovery procedures applied for solving the coupled dynamic equations for the 2D monopile model.

◆ For a given simulation time, the difference between the minimum and maximum shear stress values is constant. The maximum (or minimum) shear stress occurs at the center line of the model and varies harmonically with the corresponding behaviour of the load as shown in Fig. 4.7. The direction of the shear stress at the center line is independent of the direction of movement; it always takes both positive and negative values.

Figure 4.6 *Paper 5* — Kelvin model consisting of a spring and a dashpot in each depth.
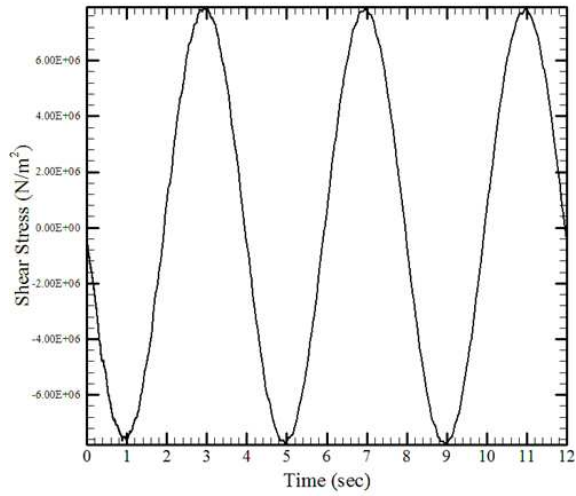
Figure 4.7 *Paper 6* — Kelvin model consisting of a spring and a dashpot in each depth.

CHAPTER 5
Conclusions and Future Directions

The dynamic soil behavior and the effect of the soil–structure interaction on the behaviour of monopiles foundations of offshore wind turbines have been studied. The numerical analyses incorporated with poroelastic media is employed to improve the understanding of groundwater behavior and elucidate the dynamic behaviour of monopile foundations subjected to cyclic loadings. The present chapter summarizes the main findings of the results and proposes some suggestions for further work.

5.1 Overall Conclusions

At present, offshore wind turbines have grown much larger then onshore wind turbines to capture economies of scale. Offshore wind turbines generate more electricity than those on land because the wind at sea is typically stronger and more constant than that onshore. Therefore, using the computational model to compute the damping effect, dynamic response for different kinds of loading such as wind, water and earthquake are necessary to improve the model in order to reduce the overall costs as well as the uncertainty. The fatigue life of offshore wind turbines strongly depends on the dynamic behaviour of the structures including the underlying soil. To avert damage of offshore foundation and better design, identifying and quantifying the soil–structure interaction and damping effect, is is necessary. For offshore wind turbines, dynamic loading and fatigue are much greater problems than they are on land. Wave-induced oscillations introduce unwanted accelerations on the entire of the structure. For a deep water foundation installation, the major part of the structure is under water, and the water provides not only support to the structure but also considerable damping for the wave induced vibrations. Thus, understanding how the soil behaves as regards damping is critical. Fatigue problems are an important issue for offshore wind turbines in comparison with inshore wind turbines, given unsteady forces from earthquake and different direction of water and wind waves. Besides the aerodynamic damping in wind turbine structure, effective damping from saturate soil is essential in properly presenting the dynamic responses of structure. Saturated soil can be idealized as two-phase media comprising deformable soil skeleton and pore fluid. The dynamic

response of the saturated soil is especially important to understand the deformations and pore water pressures generated by dynamic loads.

Damping of wind turbine structures comprises gyroscopic, structural, aerodynamic and additional damping. The additional damping for offshore support structures is higher than that for onshore support structures. Two components such as material (internal) damping and radiation (geometrical) damping represent the soil damping. Material damping is inherent within the material and is occurs because of viscous and hysteretic effects, whereas the radiation damping is because of loss of energy affected by radial propagation of elastic waves from the immediate vicinity of the source of vibration. Soil as viscoelastic model can be represented with the combination of spring and dashpot by considering elastic continuum theory. In this regard, numerical methods can be implemented to investigate the dynamic behavior of the soil (seepage damping, dynamic soil stiffness), foundation and interaction between soil and foundation.

Generally, the soil–structure interaction is incorporated by a so-called Winkler model with static springs along the foundation and soil damping applied as modal damping. Flexible and complex loaded offshore wind turbines are coupled with supported soil, and the related dynamic responses become highly dependent on the foundation. Therefore, to propose improved design guidlines for overall cost reduction, we must present a better understanding of the damping from saturated soil via particulate simulation, and deeper understanding of the damping effects in offshore wind turbine foundations. The main conclusions of the project are summarized below.

♦ The absolute value of normalized dynamic stiffness and phase angle for an infinite hollow and solid cylinder because of dynamic vertical load are independent of soil material properties such as Young's modulus and Poisson's ratio. However, these factors are dependent on loss factor. In comparison between the absolute value of the dynamic stiffness for solid and hollow cylinders, the stiffness indicates greater values for solid cylinder when the same value of soil properties and large values of normalized frequency are considered.

♦ For two-dimensional analysis of each individual soil layer subjected to cyclic load, the permeability of the seabed strongly influences the damping of wind-turbine-tower vibrations. Furthermore, the pore water flow generated by the cyclic motion is important in determining soil stiffness and damping.

♦ Low and high values of the soil permeability (in a two-dimensional analysis) indicate fully undrained and drained soil behaviour, respectively. Soil stiffness is independent of the frequency of the forced displacement. In the transient state between fully undrained and drained soil behaviour, the frequency of the forced displacement greatly influences stiffness. For increasing forced displacement frequency [0.01; 0.4] Hz, pore pressure in both the fluid and solid phase will increase, resulting in a stiffness increase.

♦ $p - y - \dot{y}$ curves have been extracted and the effect of load frequency has been highlighted. We conclude that soil stiffness and damping for the transient re-

gion, which is located between loose and dense soil, are highly affected by load frequency.

♦ Even at frequencies related to the first and second modes of an offshore monopile wind turbine, soil stiffness, damping and natural frequencies of wind turbine are frequency dependent especially when placed in sandy soil. Contrary to the results of the equivalent soil stiffness at pile cap the equivalent dashpots and masses at pile cap are highly dependent on soil type.

♦ The convergence rate for two–dimensional saturated porous soils is 0.5 for SPR, WSPR and L2 projection post processing recovery methods in FEM.

This PhD thesis has calculated the seepage damping and proposed a $p-y-\dot{y}$ curve to promote improved understanding of soil–structure interaction. The study has shown the importance of load frequency, the interrelation effects between the foundation and subsoil that change system stiffness and damping as well as natural frequency of system because of the frequency-dependent dynamic stiffness of the soil–foundation system.

5.2   Recommendations for Further Research

Some suggestions for further work are listed as follows:

♦ Developing a three dimensional numerical model for offshore wind turbine foundations subjected to cyclic loadings by using different soil layers and appropriate material model along the depth of foundation to calculate dynamic soil stiffness and damping.

♦ Finding the dynamic response of wind turbines installed on different types of offshore foundations as well as different soil conditions, then presenting the effect of load parameters such as load amplitude and frequency on soil damping and stiffness.

♦ Implementing absorbing boundary conditions to reduce the model size and therefore decrease the time simulation for different soil layers

♦ Developing meshless, isogeometric and discrete element methods to calculate soil response in different type soil layers and foundations as well as different dynamic loads such as cyclic, impact and earthquake.

♦ In the present research, a Kelvin model has been employed to interpret each soil depth. Further studies can focus on a combination of Kelvin model and mass in series form, plus Kelvin model and mass once again to evaluate each parameter and compare the results for further investigation.

♦ Analyzing vibration (installation) of different offshore foundations such as bucket (monopod), monopile and tripod are points of interests for further study.

Bibliography

Abbas, J. M., Chik, Z. H., and Taha, M. R. (2008). Single pile simulation and analysis subjected to lateral load. *Electronics Journal of Geotechnical Engineering* **13**, 1–15.

Achenbach, J. D. and Sun, C. (1965). Dynamic response of beam on viscoelastic subgrade. *Journal of Engineering Mechanics* **91**(5), 61–76.

Achmus, M., Yu-Shu, K., and Abdel-Rahman, K. (2009). Behavior of monopile foundations under cyclic lateral load. *Computers and Geotechnique* **36**(5), 725–735.

Afshar, M. H., Amani, J., and Naisipour, M. (2012). A node enrichment adaptive refinement in discrete least squares meshless method for solution of elasticity problems. *Engineering Analysis with Boundary Elements* **36**(3), 385–393.

Ahmad, S. and Banerjee, P. K. (1988). Time-domain transient elastodynamic analysis of 3-d solids by bem. *International Journal for Numerical Methods in Engineering* **26**(8), 1709–1728.

Alexander, N. A. (2010). Estimating the nonlinear resonant frequency of a single pile in nonlinear soil. *Journal of Sound and Vibration* **329**(8), 1137–1153.

Allotey, N. and El Naggar, M. H. (2008). Generalized dynamic Winkler model for nonlinear soil–structure interaction analysis. *Canadian Geotechnical Journal* **45**(4), 560–573.

Andersen, L. and Jones, C. J. C. (2006). Coupled boundary and finite element analysis of vibration from railway tunnels-a comparison of two-and three-dimensional models. *ournal of sound and vibration* **293**(3), 611–625.

Andersen, L. and Nielsen, S. R. K. (2003). Boundary element analysis of the steadystate response of an elastic half-space to a moving force on its surface. *Eng Anal Bound Elem* **27**(1), 23–38.

Andersen, L. and Nielsen, S. R. K. (2007). Stochastic nonlinear *p–y* analysis of laterally loaded piles. In *Proceedings of the 11th international conference on soil dynamics and earthquake engineering*, Berkeley, CA, USA, pp. 869–876.

Andersen, L., Nielsen, S. R. K., and Krenk, S. (2007). Numerical methods for analysis of structure and ground vibration from moving loads. *Computers and Structures* **85**(1-2), 43–58.

Andersen, L. V. (2006). Linear elastodynamic analysis. DCE Technical Memorandum No. 3, Aalborg University.

Andersen, L. V., Vahdatirad, M. J., Sichani, M. T., and Sørensen, J. D. (2012). Natural frequencies of wind turbines on monopile foundations in clayey soils—a probabilistic approach. *Computers and Geotechnics* **43**, 1–11.

Anoyatis, G., Laora, R. D., Mandolini, A., and Mylonakis, G (2013). Kinematic response of single piles for different boundary conditions: Analytical solutions and normalization schemes. *Soil Dynamics and Earthquake Engineering* **44**, 183–195.

API (2000). Recommended practice for planning, designing and constructing fixed offshore platforms, RP2a-WSD. American Petroleum Institute, Dallas, Texas, USA.

Augarde, C. and Heaney, C. (2009). The use of meshless methods in geotechnics. In *Proceedings of the 1th International Symposium on Computational Geomechanics*, Juan-les-pins, Paris, pp. 311–320.

Baars, S. V. (2000). Frictional soil damping versus viscous soil damping. Technical Memorandum, Laboratoire 3SR, ENPG, Grenoble, France.

Babuska, I. (1975). *The Self Adaptive Approach in the Finite Element Method, In Mathematics of Finite Elements and Applications* (1 ed.). Academic Press, London.

Babuska, I. and Rheinboldt, W. C. (1978). A posteriori error estimates for the finite element method. *International Journal for Numerical Methods in Engineering* **12**(10), 1597–1615.

Babuska, I., Strouboulis, T., Upadhyay, C., and Gangargj, S. (1996). Computer-based proof of the existence of superconvergence points in the finite element method; superconvergence of the derivatives in finite element solutions of laplace's, poisson's, and the elasticity equations. *Numerical Methods for Partial Differential Equations* **12**, 374–392.

Babuska, I., Strouboulis, T., and Upadhyay, C. S. (1994a). A model study of the quality of a posteriori error estimators for linear elliptic problems. error estimation in the interior of patchwise uniform grids of triangles. *Computer Methods in Applied Mechanics and Engineering* **114**(3-4), 307–378.

Babuska, I., Strouboulis, T., and Upadhyay, C. S. (1997). A model study of the quality of a posteriori error estimators for finite element solutions of linear elliptic problems, with particular reference to the behaviour near the boundary. *International Journal for Numerical Methods in Engineering* **40**(14), 2521–2577.

Babuska, I., Strouboulis, T., Upadhyay, C. S., Gangaraj, S. K., and Copps, K. (1994b). Validation of a posteriori error estimators by numerical approach. *International Journal for Numerical Methods in Engineering* **37**(7), 1073–1123.

Babuska, I., Zienkiewicz, O. C., Gago, J., and Oliveira, E. A. (1986). *Accuracy estimates and adaptive refinements in finite element computations* (1 ed.). Wiley, New York.

Babuska, I. and Rheinboldt, W. C. (1979). Reliable error estimation and mesh adaptation for the finite element method. Technical Report, Maryland university college park institution for physical science and technology.

Badia, S., Quaini, A., and Quarteroni, A. (2009). Coupling biot and navier-stokes equations for modelling fluid-poroelastic media interaction. *Journal of Computational Physics* **228**(21), 7986–8014.

Badoni, D. and Makris, N. (1996). Nonlinear response of single piles under lateral inertial and seismic loads. *Soil Dynamics and Earthquake Engineering* **15**(1), 29–43.

Bakmar, C. L. (2009). Recent experience and challenges ahead. In *Hamburg Offshore Wind*, Hamburg, pp. 1–37.

Bamberger, A., Chalindars, B., Joly, P., Roberts, J. E., and Teron, J. L. (1988). Radiation boundary conditions for elastic wave propagation. *SIAM Journal of Scientific Statisitics and Computation* **9**(6), 1016–1049.

Baohui, L., Hai, L., L. Yu, Anliang, W., and Shunying, J. (2014). Amodified discrete element-model for sea ice dynamics. *Acta Oceanologica Sinica* **33**(1), 56–63.

Baranov, V. A. (1967). On the calculation of excited vibrations of an embedded foundation. In *Voprosy Dinamiki i Prochnosti*, Polytechnic Institute, Riga, pp. 195–209.

Bardet, J. P. (1992). A viscoelastic model for the dynamic behavior of saturated poroelastic soils. *Treansactions of the ASME* **59**, 128–135.

Bardet, J. P. (1995). The damping of saturated poroelastic soils during steady-state vibrations. *Applied Mathematics and Computation* **67**(1-3), 3–31.

Bardet, J. P. and Sayed, H. (1993). Velocity and attenuation of compressional waves in nearly saturated soils. *Soil Dynamics and Earthquake Engineering* **12**, 391–401.

Barlow, J. (1976). Optimal stress location in finite element models. *International Journal for Numerical Methods in Engineering* **10**(2), 243–251.

Bathe, K.J. (2001). The inf-sup condition and its evaluation for mixed finite element methods. *Computers and Structures* **79**, 243–252.

Beer, G., Smith, I., and Duenser, C. (2008). *The Boundary Element Method with Programming* (1 ed.). Springer-Verlag Wien.

Begum, N. A. and Muthukkumaran, K. (2008). Numerical modeling for laterally loaded piles on a sloping ground. In *Proceedings of the 12th International Conference of International Association for Computer Methods and Advances in Geomechanics*, Goa, India, pp. 1–5.

Belotserkovets, A. and Prevost, J.H. (2011). Thermoporoelastic response of a fluid-saturated porous sphere: An analytical solution. *International Journal of Engineering Science* **49**(12), 1415–1423.

Belytschko, T., Organ, D., and Krongauz, Y. (1995). Coupled finite element – element-free galerkin method. *Computational mechanics* **17**, 186–195.

Beresnev, I. A. and Wen, K. L. (1996). Nonlinear soil response – a reality? *Bulletin of the Seismological Society of America* **86**(6), 1964–1978.

Berger, E., Mahin, S. A., and Pyke, R. (1977). Simplified method for evaluating soil–pile–structure interaction effects. In *Proceedings of the 9th Offshore Technology Conference*, Houston, Texas, pp. 589–598.

Bhowmik, D., Baidya, D. K., and Dasgupta, S. P. (2013). A numerical and experimental study of hollow steel pile in layered soil subjected to lateral dynamic loading. *Soil Dynamics and Earthquake Engineering* **53**, 119–129.

Biot, M. A. (1941a). Consolidation settlement under a rectangular load distribution. *Journal of Applied Physics* **12**(5), 426–430.

Biot, M. A. (1941b). General theory of three-dimensional consolidation. *Journal of Applied Physics* **12**(2), 155–164.

Biot, M. A. (1955). Theory of elasticity and consolidation for a porous anisotropic solid. *Journal of Applied Physics* **26**(2), 182–185.

Biot, M. A. (1956a). Theory of propagation of elastic waves in a fluid-saturated porous solid, i. low-frequency range. *JOURNAL OF THE ACOUSTICAL SOCIETY OF AMERICA* **28**(2), 168–178.

Biot, M. A. (1956b). Theory of propagation of elastic waves in a fluid-saturated porous solid, ii. higher frequency range. *JOURNAL OF THE ACOUSTICAL SOCIETY OF AMERICA* **28**(2), 179–191.

Biot, M. A. (1962a). Generalized theory of acoustic propagation in porous dissipative media. *JOURNAL OF THE ACOUSTICAL SOCIETY OF AMERICA* **34**(9), 1254–1264.

Biot, M. A. (1962b). Mechanics of deformation and acoustic propagation in porous media. *JOURNAL of Applied Physics* **34**(4), 1482–1498.

Bisoi, S. and Haldar, S. (1997). Boundary element methods in dynamic analysis: Part ii (1986–1996). *Applied Mechanics Reviews* **50**, 149–197.

Bisoi, S. and Haldar, S. (1998). Time weighting in time domain bem. *Engineering Analysis with Boundary Elements* **22**, 175–181.

Bisoi, S. and Haldar, S. (2014). Dynamic analysis of offshore wind turbine in clay considering soil–monopile–tower interaction. *Soil Dynamics and Earthquake Engineering* **63**, 19–35.

Blacker, T. and Belytschko, T. (1994). Superconvergent patch recovery with equilibrium and conjoint interpolant enhanements. *International Journal for Numerical Methods in Engineering* **37**, 517–536.

Bobet, A. (2010). Numerical methods in geomechanics. *The Arabian Journal for Science and Engineering* **35**(1), 27–48.

Bodet, L., Abraham, O., and Clorennec, D. (2009). Near-offset effects on rayleigh-wave dispersion measurements: physical modeling. *Journal of Applied Geophysics* **68**(1), 95–103.

Boer, R. D. and Liu, Z. (1994). Plane waves in a semi-infinite fluid saturated porous medium. *Transport in Porous Media* **16**, 147–173.

Bordas, S. and Duflot, M. (2007). Derivative recovery and a posteriori error estimate for extended finite elements. *Computer Methods in Applied Mechanics and Engineering* **196**, 3381–3399.

Boroomand, B., Ghaffarian, M., and Zienkiewicz, O. (2004). On application of two superconvergent recovery procedures to plate problems. *International Journal for Numerical Methods in Engineering* **61**, 1644–1673.

Boulanger, R. W., Curras, C. J., Kutter, B. L., Wilson, D. W., and Abghari, A. (1999). Seismic soil–pile–structure interaction experiments and analysis. *Journal of Geotechnical and Geoenvironmental Engineering* **125**(9), 750–759.

Boythorpe Wind Energy (2015). Onshore vs offshore wind energy. `http://www.boythorpewindenergy.co.uk/wind-turbine-advice/onshore-vs-offshore-wind-energy`. Accessed: 2015.

Brezzi, F. (1974). On the existence, uniqueness, and approximation of saddle-point problems arising from lagrange multipliers. *Mathematical Modelling and Numerical Analysis* **8**(2), 129–151.

Brødbœk, K. T., Møller, M., Sørensen, S. P. H., and Augustesen, A. H. (2009). Review of p-y relationships in cohesionless soil. Technical Report, Dept. of Civil Engineering, Aalborg University.

Brown, D. A. and Shie, C. F. (1991). Some numerical experiments with a three-dimensional finite element model of a laterally loaded pile. *Computers and Geotechniques* **12**, 149–162.

Brown, D. A. and Shie, C. F. (2000). Infinite elements for wave problems: a review of current formulations and an assessment of accuracy. *International Journal for Numerical Methods in Engineering* **49**(7), 951–976.

Brown, D. A. and O'Neil, M. W. and Hoit, M. and McVay, M. and El Naggar, M. H. and Chakraborty, S. (2001). Static and dynamic lateral loading of pile groups. Technical Report, Short Course, National Cooperative Highway Research Program, NCHRP Report 461, Transportation Research Board National Research Council, National Academy Press, Washington, D.C.

Byrne, B. W. (2000). *Investigations of suction caissons in dense sand*. PhD thesis, University of Oxford, England.

Byrne, B. W. and Houlsby, G. T. (2003). Foundations for offshore wind turbines. *Philosophical Transactions of the Royal Society of London* **361**, 2909–2930.

Carbonari, F., S. ans Dezi and Leoni, G. (2011). Seismic soil–structure interaction in multi-span bridges: Application to a railway bridge. *Soil Dynamics and Earthquake Engineering* **31**(9), 1137–1153.

Carswell, W., Johansson, J., Løvholt, F., Arwade, S. R., Madshus, C., DeGroot, D. J., and Myers, A. T. (2015). Foundation damping and the dynamics of offshore wind turbine monopiles. *Renewable Energy* **80**, 724–736.

Cazzania, A. and Ruge, P. (2012). Numerical aspects of coupling strongly frequency-dependent soil-foundation models with structural finite elements in the time-domain. *Soil Dynamics and Earthquake Engineering* **37**, 56–72.

Chai, H. Y., Phoon, K. K., Wei, C. F., and Lu, Y. F. (2011). Analysis of effects of active sources on observed phase velocity based on the thin layer method. *Journal of Applied Geophysics* **73**(1), 49–58.

Chan, A. H. C. (1988). *A unified finite element solution to static and dynamic in geomechanics*. PhD thesis, University College of Swansea, England.

Chang, N. Y. and Nghiem, H. M. (2010). Viscouse damping for time domain finite element analysis. In *Proceedings of the 5th International Conference on Recent Advances in Geotechnical Engineering and Soil Dynamics Structural Dynamics*, San Diego, California, pp. 1–8.

Cheng, Z. and B., Jeremic (2009). Numerical modeling and simulation of pile in liquefiable soil. *Soil Dynamics and Earthquake Engineering* **29**, 1405–1416.

Chung, H. J. and Belytschko, T. (1998). An error estimate in the efg method. *Computational Mechanics* **21**, 91–100.

Clayton, R. and Engouist, B. (1977). Boundary conditions for the numerical solution of wave propagation problems. *Bulletin of the Seismological Society of America* **67**(6), 1529–1540.

Cox, W. R., Reese, L. C., and Grubbs, B. R. (1974). Field testing of laterally loaded piles in sand. In *Proceedings of the Sixth Annual Offshore Technology Conference*, Houston, Texas.

Cuellar, P., Mira, P., Pastor, M., Merodo, J. A. F., Baeßler, M., and Rucker, W. (2014). Single pile simulation and analysis subjected to lateral load. *Electronics Journal of Geotechnical Engineering* **59**, 75–86.

Cundall, P. A. (1971). A computer model for simulating progressive, large-scale movements in blocky rock systems. In *Proceedings symposium of the international Society of Rock Mechanics*, Nancy, Franch, pp. 132–150.

Cundall, P. A. (1974). A computer model for rock-mass behaviour using interactive graphics for the input and output of geometrical data. Report for the Missouri River Division, U.S. Army Corps of Engineers, University of Minnesota.

Dassault Systèmes Simulia Corp (2012). Abaqus 6.12 analysis user's manual. Technical Report, Dassault Systèmes Simulia Corp.

Dehghanpoor, A. and Ghazavi, M. (2012). Response of tapered piles under lateral harmonic vibrations. *International Journal of GEOMATE* **2**(2), 261–265.

Dezi, F., Carbonari, S., and Leoni, G. (2010). Kinematic bending moments in pile foundations. *Soil Dynamics and Earthquake Engineering* **30**, 119–132.

Dezzi, F., Carbonari, S., and Leoni, G. (2010). Kinematic bending moments in pile foundations. *Soil Dynam. Earthquake Engng* **30**(3), 119–132.

DNV (2011). Design of offshore wind turbine structures. DNV-OS-J101. Det Norske Veritas Classification A/S, Høvik, Norway.

Dominguez, J. (1993). *Boundary elements in dynamics* (1 ed.). Computational Mechanics Publications, Southampton.

Donze, F. V., Richefeu, F., and Magnier, S. A. (2008). Advances in discrete element method applied to soil, rock and concrete mechanics. *Electronic Journal of Geotechnical Engineering* **1**, 1–44.

Dunnavant, T. W. and O'Neill, M. W. (1989). Experimental p–y model for submerged stiff clay. *Journal of the Geotechnical Engineering Division, ASCE* **115**(1), 95–114.

E., Reißner V. (1936). Stationare, axialsymmetrische durch eine schuttelnde masse erregte schwingungen eines homogenen elastischen halbraumes. *Ingenieure-Archiv* **7**(6), 381–396.

E., Reißner V. (1937). Freie und erzwungene torsionsschwingungen des elastischen halbraumes. *Ingenieure-Archiv* **8**(4), 229–245.

El-Hamalawi, A. and Bolton, M. D. (2002). An error estimate in the efg method. *Computers and Geotechnics* **29**, 587–607.

El Naggar, M. and Novak, M. (1995). Nonlinear lateral interaction in pile dynamics. *Soil Dynamics and Earthquake Engineering* **14**(2), 141–157.

El Naggar, M. and Novak, M. (1996). Nonlinear analysis for dynamic lateral pile response. *Soil Dynamics and Earthquake Engineering* **15**(4), 233–244.

El Naggar, M. H. and Bentley, K. J. (2000). Dynamic analysis for laterally loaded piles and dynamic p–y curves. *Canadian Geotechnical Journal* **37**(6), 1166–1183.

El Naggar, M. H. and Novak, M. (1993). Nonlinear axial interaction in pile dynamics. *Journal of Geotechnieal Engineering* **120**(4), 678–696.

El Naggar, M. H., Shayanfar, M. A., Kimiaei, M., and Aghakouchak, A. A. (2005). Simplified BNWF model for nonlinear seismic response analysis of offshore piles with nonlinear input ground motion analysis. *Canadian Geotechnical Journal* **42**(2), 365–380.

Elgamal, A., Yang, Z., and Parra, E. (2002). Computational modeling of cyclic mobility and post-liquefaction site response. *Soil Dynamics and Earthquake Engineering* **22**(4), 259–271.

Elgamal, A., Yang, Z., Parra, E., and Ragheb, A. (2003). Modeling of cyclic mobility in saturated cohesionless soils. *International Journal of Plasticity* **19**(6), 883–905.

EWEA (2013). The European offshore wind industry - key trends and statistics 2013. Technical Report, European Wind Energy Association.

Fan, K., Gazetas, G., Kaynia, A., Kausel, E., and Ahmad, S. (1991). Kinematic seismic response analysis of single piles and pile groups. *Journal of Geotechnical Engineering* **117**, 1860–1879.

Francisco, C. P., de Barros, F. C. P., and Enrique, J. E. (1990). Discrete models for vertical vibrations of surface and embedded foundations. *Earthquake Engineering and Structural Dynamics* **19**(2), 289–303.

Fthenakis, V. and Kim, H. C. (2009). Land use and electricity generation: A life cycle analysis. *Renewable and Sustainable Energy Reviews* **13**(6), 1465–1474.

Fukuo, Y. (1969). Visco-elastic theory of the deformation of a confined aquifer. *Bulletin of the Disaster Prevention Research Institute* **18**(4), 1–13.

Gaitanaros, A. P. and Karabalis, D. L. (1988). Dynamic analysis of 3-d flexible embedded foundations by a frequency domain bem-fem. *Earthquake Engineering and Structural Dynamics* **16**(5), 653–674.

Galvin, P. and Romero, A. (2014). A matlab toolbox for soil–structure interaction analysis with finite and boundary elements. *Soil Dynamics and Earthquake Engineering* **57**, 10–14.

Gazetas, G. (1984). Seismic response of end-bearing single piles. *Soil Dynamics and Earthquake Engineering* **3**, 82–932.

Gazetas, G. and Dobry, R. (1984a). Horizontal response of piles in layered soils. *Journal of Geotechnical Engineering, ASCE* **110**(1), 20–40.

Gazetas, G. and Dobry, R. (1984b). Simple radiation damping model for piles and footings. *Journal of Engineering Mechanics, ASCE* **110**(6), 937–956.

Gazetas, G. and Makris, N. (1991). Dynamic pile-soil-pile interaction. part i: Analysis of axial vibration. *Earthquake Engineering and Structural Dynamics* **20**(2), 115–132.

Genes, M. C. (2012). Dynamic analysis of large-scale ssi systems for layered unbounded media via a parallelized coupled finite-element/boundary-element/scaled boundary finite-element model. *Engineering Analysis with Boundary Elements* **36**(5), 845–857.

Georgiadis, K. and Georgiadis, M. (2010). Undrained lateral pile response in sloping ground. *Journal of Geotechnical and Geoenvironmental Engineering* **136**(11), 1489–1500.

Gerolymos, N. and Gazetas, G. (2006). Analysis of effects of active sources on observed phase velocity based on the thin layer method. *Soil Dynamics and Earthquake Engineering* **26**(5), 363–376.

Ghandil, M. and Behnamfar, F. (2015). The near-field method for dynamic analysis of structures on soft soils including inelasticsoil-structure interaction. *Soil Dynamics and Earthquake Engineering* **75**, 1–17.

Gipe, P. (1993). The wind industry's experience with aesthetic criticism. *Leonardo* **26**(3), 243–248.

GL (2005). Rules and guidelines iv industrial services. Technical Standard, Germanischer Lloyd Wind Energie GmbH.

Gu, H., Zong, Z., and Hung, K. (2004). A modified superconvergent patch recovery method and its application to large deformation problems. *Finite Elements in Analysis and Design* **40**, 665–687.

Gu, M., Kong, L., Chen, R., Chen, Y., and Bian, X. (2014). Response of 1×2 pile group under eccentric lateral loading. *Computers and Geotechnics* **57**, 114–121.

Gudehus, G (2011). *Physical Soil Mechanics* (1 ed.). Springer-Verlag Berlin Heidelberg.

Hakuno, M. (1995). Simulation of the dynamic liquefaction of sand. In *In Ishihara, editor, Earthquake Geotechnical Engineering*, Rotterdam, Balkema, pp. 857–862.

Hakuno, M. and Tarumi, Y. (1988). Sand liquefaction analysis by granular assembly simulation. In *Proceedings of Ninth World Conference on Earthquake Engineering*, Tokyo, Japan, pp. 231–236.

Halabian, M. and El Naggar, M. H. (2002). Effect of non-linear soil–structure interaction on seismic response of tall slender structures. *Soil Dynamics and Earthquake Engineering* **22**(8), 639–658.

Hall, Jr., J. R. (1967). Coupled rocking and sliding oscillations of rigid circular footings. In *Proceedings International Symposium on Wave Propagation and Dynamic Properties of Earth Materials*, University of New Mexico Press, Albuquerque, pp. 139–148.

Harada, T., Nonaka, T., Wang, H., Magoshi, K., and Iwamura, M. (2008). A nonlinear dynamic soil foundation interaction model using fiber element method and its application to ninlinear earthquake response analysis of cable stayed bridge. In *The 14th World Conference on Earthquake Engineering*, Beijing, China, pp. 1–8.

Hashash, Y. M. A. and Park, D. (2002). Viscous damping formulation and high frequency motion propagation in non-linear site response analysis. *Soil Dynamics and Earthquake Engineering* **22**(7), 611–624.

Hemmat, A., Nankali, N., and Aghilinategh, N. (2012). Simulating stress–sinkage under a plate sinkage test using a viscoelastic 2d axisymmetric finite element soil model. *Soil and Tillage Research* **118**, 107–116.

Hirai, H. (2012). A Winkler model approach for vertically and laterally loaded piles in nonhomogeneous soil. *International Journal for Numerical and Analytical Methods in Geomechanics* **36**(17), 1869–1897.

Houlsby, G. T., Kelly, R. B., Huxtable, J., and Byrne, B. W. (2005). Field trials of suction caissons in clay for offshore wind turbine foundations. *Géotechnique* **55**(4), 287–296.

Hovind, E. and Kaynia, A. M. (2014). Earthquake response of wind turbine with non-linear soil-structure interaction. In *Proceedings of the 9th International Conference on Structural Dynamics*, Porto, Portugal, pp. 623–630.

Ibsen, L. B., Barari, A., and Larsen, K. A. (2012). Modified vertical bearing capacity for circular foundations in sand using reduced friction angle. *Ocean Engineering* **47**, 1–6.

Ibsen, L. B., Schakenda, B., and Nielsen, S. A. (2003). Development of the bucket foundation for offshore wind turbines: A novel principle. In *Proceedings of the US Wind Energy Conference*, Boston, pp. 1–12.

IEC 61400-3 (2009). Wind turbines - part 3: Design requirements for offshore wind turbines. Technical Standard, European Committee for Electrotechnical Standardization.

Iglesias, D. and Orden, J. C. G. (2007). A meshfree application to the nonlinear of flexible multibody systems. In *Actas da DSM2007, Conferencia Nacional de, Dinamica de Sistemas Multicorpo*, Guimaraes, Portugal, pp. 1–7.

Indraratna, B., Ngo, N. T., Rujikiatkamjorn, C., and Sloan, S. W. (2015). Coupled discrete element–finite difference method for analysing the load-deformation behaviour of a single stone column in soft soil. *Computers and Geotechnics* **63**, 267–278.

IRENA (2012). Renewable energy technologies: Cost analysis series. Technical Report, International Renewable Energy Agency.

Irzal, F., Remmers, J. J. C., Verhoosel, C. V., and Borst, R. d. (2013). Isogeometric finite element analysis of poroelasticity. *International Journal for Numerical and Analytical Methods in Geomechanics* **37**(12), 1891–1907.

J, Dominguez (1978). Response of embedded rectangular foundations to travelling wave. Technical report R78–24, Departament of Civil Engineering, Cambridge, Massachusetts, USA.

Jean, W. Y., Lin, T. W., and Penzien, J. (1990). System parameters of soil foundations for time domain dynamic analysis. *Earthquake Engineering and Structural Dynamics* **19**(4), 541–553.

Jeremi, B., Cheng, Z., Taiebat, M., and Dafalias, Y. (2008). Numerical simulation of fully saturated porous materials. *International Journal for Numerical and Analytical Methods in Geomechanics* **32**(13), 1635–1660.

Jiang, M. and Yu, H. S. (2006). Application of discrete element method to geomechanics. In *Modern Trends in Geomechanics, Springer Proceedings in Physics Volume 106*, pp. 241–269.

Johnson, K., Karunasena, W., Sivakugan, N., and Guazzo, A. (2001). Modeling pile-soil interaction using contact surfaces. *Computational Mechanics–New Frontiers for the New Millennium* **1**, 375–380.

Kampitsis, A. E., Sapountzakis, E. J., Giannakos, S. K., and Gerolymos, N. A. (2013). Seismic soil–pile–structure kinematic and inertial interaction—A new beam approach. *Soil Dynamics and Earthquake Engineering* **55**, 211–224.

Karabalis, D. L. and Beskos, D. E. (1985). Dynamic response of 3-d flexible foundations by time domain bem and fem. *Soil Dynamics and Earthquake Engineering* **4**(2), 81–101.

Karim, M. R., Nogami, T., and Wang, J. G. (2002). Analysis of transient response of saturated porous elastic soil under cyclic loading using element-free galerkin method. *International Journal of Solids and Structures* **39**(24), 6011–6033.

Kausel, E. (2010). Complex frequencies in elastodynamics, with application to the damping-solvent extraction method. *Journal of Engineering Mechanics* **136**(5), 641–652.

Kavvadas, M. and Gazetas, G. (1993). Kinematic seismic response and bending of free-head piles in layered soil. *Geotechnique* **43**, 207–222.

Kaynia, A. M. and Kausel, E. (1991). Dynamics of piles and pile groups in layered soil media. *Soil Dynamics and Earthquake Engineering* **10**, 386–401.

Kellezi, L. (2000). Local transmitting boundaries for transient elastic analysis. *Soil Dynamics and Earthquake Engineering* **19**(7), 533–547.

Kenny, J. T. (1954). Steady-state vibrations of beams on elastic foundation for moving load. *Journal of Applied Mechanics* **21**(4), 359–364.

Khiavi, M. P., Gharabaghi, A. R. M., and Abedi, K. (2009). Dynamic analysis of porous media using finite element method. *International Scholarly and Scientific Research and Innovation* **3**(10), 1166–1170.

Khoei, A., Azadi, H., and Moslemi, H. (2008). Modeling of crack propagation via an automatic adaptive mesh refinement based on modified superconvergent patch recovery technique. *Engineering Fracture Mechanics* **75**, 2921–2945.

Kim, I. Y. (2008). *Advanced numerical and experimental transient modelling of water and gas pipeline flows incorporating distributed and local effects*. PhD Thesis, The University of Adelaide, Adelaide, Australia.

Kim, J, Varadan, V. V., and K., Varadan V. (1996). Finite element modelling of scattering problems involving infinite domains using drilling degrees of freedom. *Computer Methods in Applied Mechanics and Engineering* **134**(1–2), 57–70.

Kim, M. H., Koo, W. C., and Hong, S. Y. (2000). Wave interactions with 2d structures on/inside porous seabed by a two-domain boundary element method. *Applied Mathematical Modelling* **22**(5), 255–266.

Klar, A. and Frydman, S. (2002). Three-dimensional analysis of lateral pile response using two-dimensional explicit numerical scheme. *Journal of geotechnical and geoenvironmental engineering* **128**(9), 775–784.

Kouroussis, G. and Verlinden, O. (2015). Prediction of railway ground vibrations: Accuracy of a coupled lumped mass model for representing the track/soil interaction. *Soil Dynamics and Earthquake Engineering* **69**, 220–226.

Krenk, S., Kellezi, L., Nielsen, S. R. K., and Kirkegaard, P. H. (1999). Finite elements and transmitting boundary conditions for moving loads. In *Proceedings of the 4th European Conference on Structural Dynamics, Eurodyn '99*, Praha, pp. 447–452.

Krenk, S. and Kirkegaard, P. H. (2001). Local tensor radiation conditions for elastic waves. *Journal of Sound and Vibration* **247**(5), 875–896.

Kumari, S. D. and Sitharam, T. G. A. (2010). Effect of particle shape on the cyclic stress-strain behaviour of granular media. In *Indian Geotechnical Conference, IGS Mumbai Chapter*, IIT, Bombay, India, pp. 16–18.

Laora, R. D., Mandolini, A., and Mylonakis, G. (2012). Insight on kinematic bending of flexible piles in layered soil. *Soil Dynamics and Earthquake Engineering* **43**, 309–322.

Laora, R. D., Mylonakis, G., and Mandolini, A. (2013). Pile-head kinematic bending in layered soil. *Earthquake Engineering and Structural Dynamics* **42**, 319–337.

Larsen, J. W. (2005). *Nonlinear dynamics of wind turbine wings*. PhD thesis, Aalborg University, Denmark.

Lei-na, H. and Xi-ping, Y. (2009). An enhanced element-free galerkin method for dynamic response of poroelastic seabed. *Journal of hydrodynamics* **21**(3), 429–435.

Levine, N. (1985). Superconvergent recovery of the gradient from piecewise linear finite-element aproximations. *IMA Journal of numerical analysis* **5**, 407–427.

Li, J., Lin, G., and Chen, J. (2008). An improved numerical time-domain approach for the dynamic dam-foundation-reservoir interaction analysis based on the damping solvent extraction method. In *The 14th World Conference on Earthquake Engineering*, Beijing, China, pp. 1–8.

Li, M., Zhang, H., and Guan, H. (2011). Study of offshore monopile behaviour due to ocean waves. *Ocean Engineering* **38**, 1946–1956.

Li, Q. and Zhang, Z. (2010). Dynamic response of pile in saturated porous medium considering radial heterogeneity by pile driving. *Soil Dynamics and Earthquake Engineering* **13**, 1–16.

Li, X. K., Han, X. H., and Pastor, M. (2003). An iterative stabilized fractional step algorithm for finite element analysis in saturated soil dynamics. *Computer Methods in Applied Mechanics and Engineering* **192**, 3845–3859.

Lin, M. (2004). Comparison of the dynamic response of a saturated soil between two models. *Science in China Ser. D Earth Sciences* **47**(6), 551–558.

Lin, R. and Zhang, Z. (2004). Natural superconvergent points of trianglar finite elements. *Numerical Methods for Partial Differential Equations* **20**, 864–906.

Liyanapathirana, D. and Poulos, H. (2010). Dynamic stiffness of pile in a layered elastic continuum. *Comput. Geotech* **37**(1), 115–124.

Lo, W. C., Chen, C. H., and Yeh, C. L. (2010). Analytical solution for the dynamic response of a saturated poroelastic half-space to harmonic stress loading. *Journal of Hydrology* **387**, 233–243.

Lu, J. F. and Jeng, D. S. (2010). Dynamic response of an offshore pile to pseudo-stoneley waves along the interface between a poroelastic seabed and seawater. *Soil Dynamics and Earthquake Engineering* **30**(4), 184–201.

Luco, J. E. and Westmann, R. A. (1971). Dynamic response of circular footings. *Journal of Engineering Mechanics, ASCE* **97**(5), 1381–1395.

Lucu, J. E. (1974). Impedance functions for a rigid foundation on a layered medium. *Nuclear Engineering and Design* **31**(2), 204–217.

Lysmer, J. and Kuhlemeyer, R. L. (1969). Finite dynamic model for infinite media. *Journal of the Engineering Mechanics Division, ASCE* **95**(4), 859–878.

Lysmer, J. and Richart, Jr., F. E. (1966). Dynamic response of footings to vertical loading. *Journal of Soil Mechanics, ASCE* **92**(1), 65–91.

Lysmer, J. and Udaka, T. and Seed, H. B. ans Hwang, R. (1974). A computer program for complex response analysis of soil–structure systems. Technical Report, Earthquake Engineering Research Center, University of California, Berkeley.

Mackinnon, R. and Carey, G. (1989). Superconvergent derivatives: a taylor series analysis. *International Journal for Numerical Methods in Engineering* **28**, 489–509.

Madsen, S., Andersen, L. V., and Ibsen, L. B. (2013). Numerical buckling analysis of large suction caissons for wind turbines on deep water. *Engineering Structures* **6**, 443–452.

Maiorano, R. M. S., de Sanctis, L., Aversa, S., and Mandolini, A. (2009). Kinematic response analysis of piled foundations under seismic excitation. *Canadian Geotechnical Journal* **46**, 571–584.

Makris, N. (1994). Analysis of effects of active sources on observed phase velocity based on the thin layer method. *Earthquake Engineering and Structural Dynamics* **23**(2), 153–167.

Makris, N. and Badoni, D. (1995). Seismic response of pile groups under oblique-shear and rayleigh waves. *Earthquake Engineering and Structural Dynamics* **24**(4), 517–532.

Makris, N. and Gazetas, G. (1992). Dynamic pile–soil–pile interaction. part ii: lateral and seismic response. *Earthquake Engineering and Structural Dynamics* **21**(2), 145–162.

Manolis, G. D. and Beskos, D. E. (1988). *Boundary element methods in elastodynamics* (1 ed.). Unwin-Hyman, London.

Maste, J., Salunke, P. J., and Gore, N. G. (2014). The near-field method for dynamic analysis of structures on soft soils including inelasticsoil-structure interaction. *International Journal of Recent Technology and Engineering* **3**(2), 7–9.

Matlock, H. (1970). Correlation for design of laterally loaded piles in soft clays. In *2nd Offshore Technology Conference*, Houston, Texas, pp. 577–594.

Matlock, H., Foo, S. H., and Bryant, L. L. (1978). Simulation of lateral pile behavior. In *Proceedings of Earthquake Engineering and Soil Dynamics, ASCE*, New York, pp. 600–619.

Meek, J. W. and Veletsos, A. S. (1974). Simple models for foundations in lateral and rocking motion. In *Proc., 5th World Conf. on Earthquake Engrg.g*, Rome, Italy.

Memarpour, M. M., Kimiaei, M., Shayanfar, M., and Khanzadi, M. (2012). Cyclic lateral response of pile foundations in offshore platforms. *Computers and Geotechnics* **42**, 180–192.

Mendoza, C. C., Cunha, R., and Lizcano, A. (2015). Mechanical and numerical behaviour of groups of screw (type) piles founded in a tropical soil of the midwestern brazil. *Computers and Geotechnics* **67**, 187–203.

Michaels, M. P. (2006). Relating damping to soil permeability. *International Journal of Geotechnics* **6**(3), 158–165.

Michaels, M. P. (2008). Water, inertial damping and the complex shear modulus. *Geotechnical earthquake engineering and soil dynamics* **181**, 1–10.

Miller, G. F. and Pursey, H. (1955). On the partition of energy between elastic waves in a semi-infinite solid. *Proc. Roy. Soc.* **233**(1192), 56–69.

Møller, H. and Pedersen, C. P. (2011). Low-frequency noise from large wind turbines. *Acoustical Society of America* **129**(6), 3727–3744.

Mostafa, Y. E. and El Naggar, M. H. (2002). Dynamic analysis of laterally loaded pile groups in sans and clay. *Canadian Geotechnical Journal* **39**(6), 1358–1383.

Mostafa, Y. E. and El Naggar, M. H. (2004). Response of fixed offshore platforms to wave and current loading including soil-structure interaction. *Soil Dynamics and Earthquake Engineering* **24**(4), 357–368.

Mukherjee, S. and Krishnamoorthy, C. S. (1998). A weighted element patch based superconvergent stress extraction strategy. *Communications in Numerical Methods in Engineering* **14**(8), 731–749.

Murchison, J. M. and O'Neill, M. W. (1984). Evaluation of p–y relationships in cohesionless soils. In *Analysis and Design of Pile Foundations. Proceedings of the Symposium in Conjunction with the ASCE National Convention*, pp. 174–191.

Mylonakis, G., Nikolaou, A., and Gazetas, G. (1997). Soil–pile– bridge interaction: kinematic and inertial effects. part i: soft soil. *Earthquake Engng Struct* **26**(3), 3337–359.

Nakase, H., Takeda, T., and Oda, M. (1999). A simulation study on liquefaction using dem. In *In Seco e Pinto, editor, Earthquake Geotechnical Engineering*, Rotterdam, Balkema, pp. 637–642.

Nazem, M., Kardani, M., Carter, P., and Sheng, D. (2012). A comparative study of error assessment techniques for dynamic contact problems of geomechanics. *Computers and Geotechniques* **40**, 62–73.

Ng, C. W. W. and Zhang, L. M. (2001). Three-dimensional analysis of performance of laterally loaded sleeved piles in sloping ground. *Journal of Geotechnical and Geoenvironmental Engineering* **127**(6), 499–509.

Ng, S. H. and Matuttis, H. G. (2012). Two-dimensional microscopic simulation of granular particles in fluid. *Theoretical and Applied Mechanics* **60**, 105–115.

Ng, S. H. and Matuttis, H. G. (2013a). Polygonal particles in fluids. In *AIP Conference Proceedings*, Japan, pp. 1138–1139.

Ng, S. H. and Matuttis, H. G. (2013b). Simulating free boundaries in 2d fem flow simulation with direct timeintegration of the surface velocities. *Algorithms and Computational Mathematics and Numerical Analysis* **7**(3), 287–300.

Niemunis, A. and Cudny, M. (2008). On fe modelling of fully saturated soils. pp. 15–18.

Nikolaou, S., Mylonakis, G., Gazetas, G., and Tazoh, T. (2001). Kinematic pile bending during earthquakes: analysis and field measurements. *Geotechnique* **51**, 425–440.

Nogami, T. (1996). Simplified subgrade model for three-dimensional soil–foundation interaction analysis. *Soil Dynamics and Earthquake Engineering* **15**(7), 419–429.

Nogami, T. and Konagai, K. (1986). Time domain axial response of dynamically loaded single piles. *Journal of Engineering Mechanics, ASCE* **112**(11), 1241–1249.

Nogami, T. and Konagai, K. (1988). Time domain axial response of dynamically loaded single piles. *Journal of Engineering Mechanics, ASCE* **144**(9), 1512–1525.

Nogami, T., Konagai, K., and Otani, J. (1985). Computer-aided studies of complex soil moduli. In *Conference Proceeding Paper, Part of: Measurement and Use of Shear Wave Velocity for Evaluating Dynamic Soil Properties*, New York, NY, USA, pp. 18–33.

Nogami, T., Konagai, K., and Otani, J. (1988). Nonlinear pile foundation model for time-domain dynamic response analysis. In *Proceedings of ninth world conference on earthquake engineering*, Tokyo-Kyoto, Japan, pp. 593–598.

Nogami, T. and Lam, Y. (1987). A two parameter layer model for analysis of slab on elastic foundation. *Journal of the Engineering Mechanics Division, ASCE* **113**(9), 1279–1291.

Nogami, T. and Leung, M. B. (1990). Simplified mechanical subgrade model for dynamic response analysis of shallow foundations. *Earthquake Engineering and Structural Dynamics* **19**(7), 1041–1055.

Nogami, T., Otani, J., Konagai, K., and Chen, H-L. (1992). Nonlinear soil–pile interaction model for dynamic lateral motion. *Journal of Geotechnical Engineering, ASCE* **118**(1), 89–106.

Nogami, T., Zhu, J. X., and Itoh, T. (1992). First and second order dynamic subgrade models for dynamic soil–pile interaction analysis. In *Geotechnical Special Technical Publication on Piles under Dynamic Loads*, Polytechnic Institute, Riga, pp. 187–206.

Novak, M. (1974). Dynamic stiffness and damping of piles. *Canadian Geotechnical Journal* **11**(4), 574–598.

Novak, M. (1977). Vertical vibrations of floating piles. *Journal of the Engineering Mechanics Division, ASCE* **103**(1), 153–168.

Novak, M. and Beredugo, Y. O. (1972). Vertical vibration of embedded footings. *Journal of the Soil Mechanics and Foundation Division, ASCE* **98**(12), 1291–1310.

Novak, M. and El-Sharnouby, B. (1983). Stiffness constants of single piles. *Journal of the Geotechnical Engineering Division, ASCE* **109**(7), 961–974.

Novak, M. and Howell, J. F. (1978). Dynamic response of pile foundations in torsion. *Journal of the Geotechnical Engineering Division, ASCE* **104**(5), 535–552.

Novak, M. and Nogami, T. (1977). Soil–pile interaction in horizontal vibration. *Earthquake Engineering and Structural Dynamics* **5**(3), 263–281.

Novak, M., Nogami, T., and Aboul-Ella, F. (1978). Dynamic soil reactions for plane strain case. *Journal of the Engineering Mechanics Division, ASCE* **104**(4), 953–959.

Nowamooz, H., Nikoosokhan, S., Lin, J., and Chazallon, C. (2015). Finite difference modeling of heat distribution in multilayer soils with time-spatial hydrothermal properties. *Renewable Energy* **76**, 7–15.

offshorewind (2015). Structural health monitoring. `http://www.offshorewind.biz/2013/11/15/new-developments-in-field-of-structural-health-monitoring/`. Accessed: 2015.

Oh, H. S. and Batra, R. (1999). Locations of optimal stress points in higher-order elements. *Communications in numerical methods in engineering* **15**, 127–136.

Oka, F., Yashima, A., Shibata, T., Kato, M., and Uzuoka, R. (1994). Fem-fdm coupled liquefaction analysis of a porous soil using an elasto-plastic model. *Applied Scientific Research* **52**(3), 209–245.

Owen, S. J. (1998). A survey of unstructured mesh generation technology. In *Proceedings of 7th International Meshing Roundtable*, Sandia National Laboratories, pp. 239–2678.

Pacheco, G., Suarez, L. E., and Pando, M. (2008). Dynamic lateral response of single piles considering soil inertia contributions. In *The 14th World Conference on Earthquake Engineering*, Beijing, China, pp. 12–17.

Padron, L. A., Aznarez, J. J., and Maeso, O. (2007). Bem–fem coupling model for the dynamic analysis of piles and pile groups. *Engineering Analysis with Boundary Elements* **31**, 473–484.

Padron, L. A., Aznarez, J. J., and Maeso, O. (2008). Dynamic analysis of piled foundations in stratified soils by a bem–fem model. *Soil Dynamics and Earthquake Engineering* **27**, 333–346.

Padron, L. A., Aznarez, J. J., and Maeso, O. (2010). Dynamic stiffness of deep foundations with inclined piles. *Earthquake Engineering and Structural Dynamics* **39**, 1343–1367.

Park, H. C., Shin, S. H., and Lee, S. W. (1999). A superconvergent stress recovery technique for accurate boundary stress extraction. *International Journal for Numerical Methods in Engineering* **45**, 1227–1242.

Pastor, M., Li, T., Liu, X., and Zienkiewicz, O.C. (1999). Stabilized low-order elements for failure and localization problems in unsaturated soils and foundations. *Computer Methods in Applied Mechanics and Engineering* **174**, 219–234.

Pastor, M., Li, T., Liu, X., Zienkiewicz, O. C., and Quecedo, M. (2000). A fractional step algorithm allowing equal order of interpolation for coupled analysis of saturated soil problems. *Mechanics of Cohesive-frictional Materials* **5**(7), 511–534.

Pastor, M., Zienkiewicz, O. C., and Chan, A. H. C. (1990). Generalized plasticity and the modeling of soil behavior. *International Journal for Numerical and Analytical Methods in Geomechanics* **14**(3), 151–190.

Peeringa, J. M. (2014). Fatigue loading on a 5mw offshore wind turbine due to the combined action of waves and current. In *Conference Series 524, The Science of Making Torque from Wind 2014*, Copenhagen, Denmark.

Peire, K., Nonneman, H., and Bosschem, E. (2008). Ormonde offshore wind farm. In *Found Ocean*, UK, pp. 1–8.

Peng, H. and Yu, J. (2011). Dynamic torsional impedance of piles in layered saturated soil. *The Electronic Journal of Geotechnical Engineering* **16**, 1147–1161.

Peters, H.C. and Boonstra, H. (1988). Fatigue loading on a single pile platform due to combined action of waves and currents. In *Proceedings of the fifth international conference on the Behaviour of Offshore Structures*, Tronheim, Norway.

Prathap, G. (1996). Barlow points and gauss points and the aliasing and best fit paradigms. *Computers and Structures* **58**, 321–325.

Prevost, J. H. (1982). Nonlinear transient phenomena in saturated porous media. *Computer Methods in Applied Mechanics ans Engineering* **30**(1), 3–18.

Prevost, J. H. (1985). Wave propagation in fluid-saturated porous media: An efficient finite element procedure. *Soil Dynamics and Earthquake Engineerin* **4**(4), 183–202.

Qiu, T. (2010). Analytical solution for biot flow–induced damping in saturated soil during shear wave excitations. *JOURNAL OF GEOTECHNICAL AND GEOENVIRONMENTAL ENGINEERING* **136**(11), 1501–1508.

Reese, L. C. and Welch, R. C. (1975). Lateral loading of deep foundation in stiff clay. *Journal of the Geotechnical Engineering Division, ASCE* **101**(7), 633–649.

Renewable Energy Toolkit (2015). Small wind turbine. `http://renewablestoolkit.instituteforsustainability.org.uk`. Accessed: 2015.

Reynolds, A. C. (1978). Boundary conditions for the numerical solution of wave propagation problems. *Geophysics* **43**(6), 1099–1110.

Rizos, d.C. and Wang, Z. (2002). Coupled b.e.m.-f.e.m. solutions for direct time domain soil-structure interaction analysis. *Engineering Analysis with Boundary Elements* **26**, 877–888.

Rodenas, J., Tur, M., Fuenmayor, F., and Vercher, A. (2006). Improvement of the superconvergent patch recovery technique by the use of constraint equations: the spr-c technique. *International Journal for Numerical Methods in Engineering* **70**, 705–727.

Rohrmann, R. G, Thons, S., and Rucker, W. (2010). Integrated monitoring of offshore wind turbines – requirements, concepts and experiences. *Structure and Infrastructure Engineering* **16**(5), 575–591.

Romero, A., Galvin, P., and Dominguez, J. (2013). 3d non-linear time domain fem–bem approach to soil–structure interaction problems. *Engineering Analysis with Boundary Elements* **37**(3), 501–512.

Rovithis, E. N., Pitilakis, K. d., and Mylonakis, G. E. (2009). Seismic analysis of coupled soil-pile-structure systems leading to the definition of a pseudo-natural ssi frequency. *Soil Dynamics and Earthquake Engineering* **29**, 1005–1015.

Saitoh, M. (2011). Lumped parameter models representing impedance functions at the interface of a rod on a viscoelastic medium. *Journal of Sound and Vibrations* **330**(9), 2062–2072.

Saitoh, M. (2012). Lumped parameter models representing impedance functions at the end of a finite beam on a viscoelastic medium. *Computers and Structures* **92–93**, 317–327.

Samimi, S. and Pak, A. (2012). Three-dimensional simulation of fully coupled hydro-mechanical behavior of saturated porous media using element free galerkin (efg) method. *International Journal of Computers and Geotechnics* **46**, 75–83.

Sawant, V. A. and Shukla, S. k. (2012). Finite element analysis for laterally loaded piles in sloping ground. *Coupled Systems Mechanics* **1**(1), 59–78.

Scharff, R. and Siems, M. (2013a). Monopile foundations for offshore wind turbines — solutions for greater water depths. *Steel Construction* **6**(1), 47–53.

Scharff, R. and Siems, M. (2013b). Pushing the limits — mega monopile foundations for offshore wind turbines. *Steel Construction* **6**(3), 178–185.

Segeren, M. L. A. and Diepeveen, N. F. B. (2014). Influence of the rotor nacelle assembly mass on the design of monopile foundations. *HERON* **59**(1), 17–36.

Semblat, J. F. and Broist, J. J. (2000). Efficiency of higher order finite elements for the analysis of seismic wave propagation. *Journal of Sound and Vibration* **231**(2), 460–467.

Shadlou, M. and Bhattacharya, S. (2014). Dynamic stiffness of pile in a layered elastic continuum. *Geotechnique* **64**(4), 3030–319.

Shah, P. M. (1968). *On the dynamic response of foundation systems*. PhD Thesis, Rice University, Houston, Texas.

Shahir, H., Mohammadi-Haji, B., and Ghassemi, A. (2014). Employing a variable permeability model in numerical simulation of saturated sand behaviour under earthquake loading. *Computers and Geotechnics* **55**, 211–223.

Sitharam, T. G. and V., Dinesh S. (2003). Numerical simulation of liquefaction behaviour of granular materials using discrete element method. *Indian Academy of Sciences. (Earth and planetary sciences)* **112**(3), 479–484.

Soares, J. D. (2013). Iterative dynamic analysis of linear and nonlinear fully saturated porous media considering edge-based smoothed meshfree techniques. *Computer Methods in Applied Mechanics and Engineering* **253**(1), 73–88.

Soares, J. D., Großeholz, G., and Estorff, O. V. (2014). A more flexible and effective analysis of porous media considering edge-based smoothed meshfree techniques. *Journal of Computational Mechanics* **53**(6), 1265–1277.

Soares, J. D. and Mansur, W. J. (2006). Dynamic analysis of fluid–soil–structure interaction problems by the boundary element method. *Journal of Computational Physics* **219**(2), 498–512.

Sørensen, S. P. H. and Ibsen, L. B. (2013). Assessment of foundation design for offshore monopiles unprotected against scour. *Ocean Engineering* **63**, 17–25.

Soroush, A. and Ferdowsi, B. (2011). Three dimensional discrete element modeling of granular media under cyclic constant volume loading: A micromechanical perspective. *Powder Technology* **212**, 1–16.

Srisupattarawanit, T., Niekamp, R., and Matthies, H. G. (2006). Simulation of nonlinear random finite depth waves coupled with an elastic structure. *Computer Methods in Applied Mechanics and Engineering* **195**(23-24), 3072–3086.

Stevens, D. J. and Krauthammer, T. (1998). A finite difference/finite element approach to dynamic soil-structure interaction modelling. *Computers and Structures* **29**(2), 199–205.

Strack, O. D. L. and Cundall, P. A. (1978). he discrete element method as a tool for research in granular media. Part I. Report to National Science Foundation, NSF Grant ENG76-20711, University of Minnesota.

Strobbia, C. and Foti, S. (2006). Multi-offset phase analysis of surface wave data (mopa). *Journal of Applied Geophysics* **59**(4), 300–313.

Su, D. and Li, j. H. (2013). Three-dimensional finite element study of a single pile response to multidirectional lateral loadings incorporating the simplified state-dependent dilatancy model. *Computers and Geotechnics* **50**, 129–142.

Sun, L. (2001). A closed-form solution of Bernoulli-Euler beam on viscoelastic foundation under harmonic line loads. *Journal of Sound and Vibrations* **242**(4), 619–627.

Sun, L. (2002). A closed-form solution of beam on viscoelastic subgrade subjected to moving loads. *Computers and Structures* **80**(1), 1–8.

Taherzadef, R., Clouteau, D., and Cottereau, R. (2009). Simple formulas for the dynamic stiffness of pile groups,. *Earthquake Engineering and Structural Dynamics* **38**(15), 1665–1685.

Tang, X. and Sato, T. (2004). Adaptive mesh refinement and error estimate for 3-d seismic analysis of liquefiable soil considering large deformation. *Journal of Natural Disaster Science* **26**, 37–48.

Tang, X. and Sato, T. (2005). H-adaptivity applied to liquefiable soil in nonlinear analysis of soil–pile interaction. *Soil Dynamics and Earthquake Engineering* **25**(7), 689–699.

Tang, X. and Sato, T. (2013). Numerical simulation on seismic liquefaction by adaptive mesh refinement due to two recovered fields in error estimation. *Soil Dynamics and Earthquake Engineering* **49**, 109–121.

Thavaraj, T., Finn, W. D. L., and Wu, G. (2010). Seismic response analysis of pile foundation. *Geotechnical and Geological Engineering* **28**, 275–286.

Ullah, Z. and Augarde, C. E. (2013). Finite deformation elasto-plastic modelling using an adaptive meshless method. *Computers and Structures* **118**, 39–52.

V., Dinesh S., Sitharam, T. G., and Vinod, J. S. (2004). Dynamic properties and liquefaction behaviour of granular materials using discrete element method. *Current science, special section: Geotechnics and earthquake Hazard* **87**(10), 1379–1387.

Vardoulakis, I. and Beskos, D. E. (1986). Dynamic behavior of nearly saturated porous media. *Mechanics of Materials* **5**, 87–108.

Vasilev, G., Parvanova, S., Dineva, P., and Wuttke, F. (2015). Soil-structure interaction using bem–fem coupling through ansys software package. *Soil Dynamics and Earthquake Engineering* **70**, 104–117.

Veletsos, A. S. and Verbic, B. (1973). Vibration of viscoelastic foundations. *Earthquake Engineering and Structural Dynamics* **2**(1), 87–102.

Veletsos, S. and Wei, Y. (1971). Lateral and rocking vibration of footings. *Journal of Soil Mechanics and Foundation Engineering Division, ASCE* **97**(9), 1227–1248.

Wang, H. F., Lou, M. L., Chen, X., and Zhai, Y. M. (2013). Structure–soil–structure interaction between underground structure and ground structure. *Soil Dynamics and Earthquake Engineering* **54**, 31–38.

Wang, K., Zhang, Z., Leo, C. J., and Xie, K. (2008). Dynamic torsional response of an end bearing pile in saturated poroelastic medium. *Computers and Geotechnics* **35**, 450–458.

Wang, S., Kutter, B. L., Chacko, M. J., Wilson, D. W., Boulanger, R. W., and Abghari, A. (1998). Nonlinear seismic soil–pile–structure interaction. *Earthquake Spectra* **14**(2), 377–396.

Wang, y., Gao, D., and Fang, J. (2015). Finite element analysis of deepwater conductor bearing capacity to analyze the subsea wellhead stability with consideration of contact interface models between pile and soil. *Computational Mechanics–New Frontiers for the New Millennium* **126**, 48–54.

Weissmann, G. F. (1973). Torsional vibrations of circular foundations. *Journal of Soil Mechanics, ASCE* **97**(9), 1293–1316.

Wiberg, N. E., Abdulwahab, F., and Ziukas, S. (1995). Improved element stresses for node and element patches using superconvergent patch recovery. *Communications in Numerical Methods in Engineering* **11**, 619–627.

Winkler, E. (1867). *Die Lehre von Elasticzitat und Festigkeit (On Elasticity and Fixity)*. Prague.

Wolf, J. P (1991a). Consistent lumped-parameter models for unbounded soil: Frequency-independent stiffness, damping and mass matrices. *Earthquake Engineering and Structural Dynamics* **20**(1), 33–41.

Wolf, J. P (1991b). Consistent lumped-parameter models for unbounded soil: Physical representation. *Earthquake Engineering and Structural Dynamics* **20**(1), 11–32.

Wolf, J. P. (1994). *Foundation Vibration Analysis Using Simple Physical Models*. Englewood Cliffs, NJ: Prentice-Hall.

Wolf, J. P. (1997). Spring-dashpot-mass models for foundation vibrations. *Earthquake Engineering and Structural Dynamics* **26**(9), 931–949.

Wolf, J. P. and Somaini, D. R. (1986). Approximate dynamic model of embedded foundation in time domain. *Earthquake Engineering and Structural Dynamics* **14**(5), 683–703.

Wong, H. and Luco, J. (1985). Tables of impedance functions for square foundations on layered media. *Soil Dynamics and Earthquake Engineering* **4**(2), 64–81.

Wong, H. L. and Luco, J. E. (1978). Dynamic response of rectangular foundations to obliquely incident seismic waves. *Earthquake Engineering and Structural Dynamics* **6**(1), 3–16.

Wu, W-H. and Chen, C-Y. (2001). Simple lumped-parameter models of foundation using mass-spring-dashpot oscillators. *Journal of the Chinese Institute of Engineers* **24**(6), 681–697.

Wu, W-H. and Lee, W-H. (2002). Systematic lumped-parameter models for foundations based on polynomial-fraction approximation. *Earthquake Engineering and Structural Dynamics* **31**(7), 1383–1412.

Wu, W-H. and Lee, W-H. (2004). Nested lumped-parameter models for foundation vibrations. *Earthquake Engineering & Structural Dynamics* **33**(9), 1051–1058.

Xunqiang, Y., Jianbo, L., Chenglin, W., and Gao, L. (2013). Ansys implementation of damping solvent stepwise extraction method for nonlinear seismic analysis of large 3-d structures. *Soil Dynamics and Earthquake Engineering* **44**, 139–152.

Yazdchi, M., Khalili, N., and Valliappan, S. (1999). Dynamic soil-structure interaction analysis via coupled finite-element- boundary-element method. *Soil Dynamics and Earthquake Engineering* **18**(7), 499–517.

Ye, X. (1998). Domain decomposition for a least-square finite element method for second order elliptic problem. *Applied Mathematics and Computation* **91**, 233–242.

Zaaijer, M. (2007-2008). Loads, dynamics and structural design. Note on Offshore Wind Farm Design, Delft University of Technology.

Zania, V. (2014). Natural vibration frequency and damping of slender structures founded on monopiles. *Soil dynamics and Earthquake Engineering* **59**, 8–20.

Zhang, C. H., Jin, F., and Pekau, O. A. (1995). Time domain procedure of fe-be-ibe coupling for seismic interaction of arch dams and canyons. *Earthquake Engineering and Structural Dynamics* **24**, 1651–1666.

Zhang, H. W., Wanga, K. P., and Chen, Z. Z. (2009). aterial point method for dynamic analysis of saturated porous media under external contact/impact of solid bodies. *Computer Methods in Applied Mechanics and Engineering* **198**(17-20), 1456–1472.

Zhang, Y., Jeng, D. S., Gao, F. P., and Zhang, J. S. (2013). An analytical solution for response of a porous seabed to combined wave and current loading. *Ocean Engineering* **57**, 240–247.

Zhanping, Y. (2007). Recent developments in distinct element methods in the civil engineering graduate education and research. In *Proceedings of the 2007 ASEE North Midwest Sectional Conference*, Houghton, Michigan, pp. 1–9.

Zhao, M. and Du, X. (2008). High-order lumped-parameter model for foundation based on continued fraction. In *14th World Conference on Earthquake Engineering*, Beijing, Chaina.

Zhou, X. L., Wang, J. H., and Jiang, L. F. (2009). Dynamic response of a pair of elliptic tunnels embedded in a poroelastic medium. *Journal of Sound and Vibration* **325**(4-5), 816–834.

Zienkiewicz, O., Boroomand, B., and Zhu, J. (1999). Recovery procedures in error estimation and adaptivity part i: Adaptivity in linear problems. *Computer Methods in Applied Mechanics and Engineering* **176**, 111–125.

Zienkiewicz, O. C. (1982). Basic formulation of static and dynamic behaviours of soil and other porous media. *Applied Mathematics and Mechanics* **3**(4), 457–468.

Zienkiewicz, O. C., Chan, A. H. C., Pastor, M., Paul, D. K., and Shiomi, T. (1990). Static and dynamic behaviour of soils: A rational approach to quantitative solutions. i. fully saturated problems. *Proceedings of the Royal Society of London. Series A, Mathematical and Physical Sciences* **429**(1877), 285–309.

Zienkiewicz, O. C., Chan, A. H. C., Pastor, M., Schrefler, B. A., and Shiomi, T. (1999). *Computational Geomechanics with Special Reference to Earthquake Engineering*. John Wiley, New York.

Zienkiewicz, O. C. and Taylor, R. L. (2000). *The finite element method. The basis, vol. 1*. London: Butterworth Heinemann.

Zienkiewicz, O. C. and Zhu, J. Z. (1987). A simple error estimator and adaptive procedure for practical engineering analysis. *International Journal for Numerical Methods in Engineering* **24**(2), 337–357.

Zienkiewicz, O. C. and Zhu, J. Z. (1992a). The super convergent patch recovery and a posteriori error estimate. part 1: The recovery technique. *International Journal for Numerical Methods in Engineering* **33**, 1331–1364.

Zienkiewicz, O. C. and Zhu, J. Z. (1992b). The super convergent patch recovery and a posteriori error estimate. part 2: Error estimates and adaptivity. *International Journal for Numerical Methods in Engineering* **33**, 1365–1382.

Zienkiewicz, O. C. and Zhu, J. Z. (1992c). The superconvergent patch recovery (spr) and adaptive finite element refinement. *Computer Methods in Applied Mechanics and Engineering* **101**(1-3), 207–224.

Appendix

APPENDIX A
Comparison between dynamic responses of hollow and solid piles for offshore wind turbine foundations
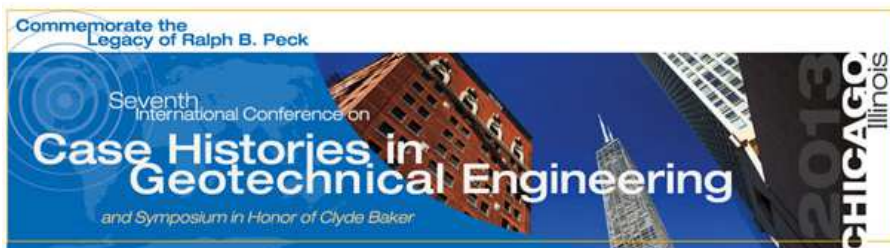
Authors:
Mehdi Bayat, Lars Vabbersgaard Andersen and Lars Bo Ibsen

A.1   Author's Right

COPYRIGHT TRANSFER AGREEMENT

PROCEEDINGS TITLE: Seventh International Conference on Case
Histories in Geotechnical Engineering, Wheeling, IL (Chicago Area) –
April 29-May 4, 2013

MSS Title: COMPARISON BETWEEN DYNAMIC RESPONSES OF HOLLOW AND SOLID PILES FOR OFFSHORE WIND
TURBINE FOUNDATIONS **Paper No.** ___2.23___

Author(s): Type name and address of all authors, and **attach each author's written consent** to this Copyright
Transfer Agreement:
M. Bayat; L.V. Andersen; L.B. Ibsen
Department of Civil Eng., AAU, Aalborg, DK-9000, Denmark

The author(s) warrants that the above-cited manuscript (hereinafter, "the Work") is the original work of the author(s) and
has never been published in its present form.

The undersigned, with the consents of all authors (attached hereto), hereby grants and assigns exclusively to the Curators
of the University of Missouri, a public corporation, on behalf of the Missouri University of Science and Technology, all
rights in the Work and all revisions thereof and derivative works therefrom, throughout the world, including but not
limited to all rights of copyright (including any renewals, extensions or revivals of copyright, together with all rights
enjoyed by an author under the laws of the U.S. and foreign countries), the right to grant any part or all of these rights to
third parties, and all rights to the title of the Work, subject to the following:

The undersigned author and all co-authors retain the right to revise, adapt, prepare derivative works, present orally, or
distribute the work provided that all such use is for the personal noncommercial benefit of the author(s) and is consistent
with any prior contractual agreement between the undersigned and/or co-authors and their employer(s).

[Note: A work prepared solely by an employee or officer of the U.S. Government as a part of his or her official duties is
not protected by copyright. If the Work falls within this category, check this box and return the form unsigned. ___]

SIGN HERE FOR COPYRIGHT TRANSFER

M. Bayat
Print Author's Name

Signature of Author (in ink)

Date: _____25-09-2012_____

Return form to: Missouri S&T's Distance & Continuing Education office along with your manuscript
(email to 7icchge@mst.edu).

Note: If the manuscript is not accepted for this conference or is withdrawn prior to its acceptance, this transfer
will be null and void.

COMPARISON BETWEEN DYNAMIC RESPONSES OF HOLLOW AND SOLID PILES FOR OFFSHORE WIND TURBINE FOUNDATIONS

M. Bayat
Dept. of Civil Eng., Aalborg University
Aalborg, Denmark

L. V. Andersen, L. B. Ibsen
Dept. of Civil Eng., Aalborg University
Aalborg, Denmark

ABSTRACT

The offshore wind energy industry is turning out ever larger numbers of offshore wind turbines every year. One way to achieve a cost-effective design is to have a better understanding of the dynamic response of offshore structures. That is why it is getting more and more important to understand the dynamic behavior of soil and interaction between soil and piles. To avert damage to offshore foundation, it becomes necessary to identify and quantify the soil-structure interaction and the related damping effects on the system. In this study, a single pile is investigated by means of boundary integral equations. The pile is modeled as a solid or hollow cylinder and the dynamic excitation is applied vertically. The surface along the entire interface is considered rough and with full contact between the soil and the structure. Somigliana's identity, Betti's reciprocal theorem and Green's function are employed to derive the dynamic stiffness of pile, assuming that the soil is a linear viscoelastic medium. The dynamic stiffness is compared for solid and hollow cylinders by considering different values of material properties including the material damping. Modes of resonance and anti-resonance are identified and presented. It is observed that the absolute value of normalized dynamic stiffness is independent of Young's modulus and Poisson's ratio, whereas it is dependent on the soil's damping.

INTRODUCTION

There are more than 7,000 offshore structures around the world. Structures to support wind turbines come in various shapes and sizes; the most common are Monopile, Jacket, Tripod, Gravity base and Floating structures (see Fig. 1). Based on dimensions of pile it can be solid and hollow cylinder. The tendency of large-size offshore wind turbines have increased during the last 10 years. As wind turbines get larger and are located in deeper water, jacket structures are expected to become more attractive. Generally, a fixed platform is described as consisting of two main components; the substructure and the superstructure. Superstructure or 'topsides' is supported on a deck, which is mounted on the jacket structure. Substructure is either a tubular or solid cylinder.

Support structures for offshore wind turbines are highly dynamic, having to cope with combined wind and hydrodynamic loading and complex dynamic behavior from the wind turbine. The offshore jacket platform is a complex and nonlinear system, which can be excited with harmful vibration by the external loads. It is vital to capture the integrated effect of the total loads. However, the total loading can be significantly less than the sum of the constituent loads. This is because the loads are not coincident, and because of the existence of different kinds of damping such as aerodynamic and soil damping which damps the motions due to the different loads. The dynamic stiffness indicates the stability and resonance behavior. In fact, the overall weight of the modern wind turbines is minimized, which makes it more flexible and corollary more secretive to low frequency dynamic. Another side, wave propagation in elastic and viscoelastic medium are considerable issues especially when there is an earthquake. In modern offshore wind turbines, instabilities or stability occur due to the coupled damping of the upper side of the wind turbine and the lower part of that as the foundation. Most of the failure phenomena are caused by fatigue while the first natural frequency plays an important role. In this aspect, stiffness has a predominant role to evaluate the first natural frequency. The first estimation for stiffness of foundation comes through the analysis of soil-structure interaction. Applying inaccurate algorithms in the soil-structure media may also occur when two different numerical methods are coupled, e.g. the boundary element method (BEM) and the finite element method (FEM); this problem

may become even more serious when coupled algorithms and different physical media are considered simultaneously in the same analysis as it was mentioned by Jr and Mansur [2006]. Soil-structure interaction (SSI) can be analyzed based on two methods namely substructure and direct methods which are highlighted by Wolf [1985]. Maheshwari and Khatri [2011] analyzed a SSI for a combined footing and supporting column on soft soil by using an iterative Gauss Elimination technique while the footing was modeled as a beam having finite flexural rigidity. Srisupattarawanit et al. [2006] applied BEM and a computation method to compute nonlinear random finite depth waves in order to be coupled with an elastic structure. Guenfoud et al. [2009] employed Green's function to solve the integrals resulting from Lamb's problem in order to study the interaction between soil and structures subjected to a seismic load. Padron et al. [2009] studied the SSI between nearby pile supported structures in a viscoelastic half-space by using BEM-FEM in the frequency domain. Genes [2012] applied a parallelized coupled model based on BEM-FEM to analyze the SSI for arbitrarily shaped, large-scale SSI problems and validation was shown. Comprehensive reviews in applying different methods pertain to SSI have been done by Mpahmoudpour et al. [2011].
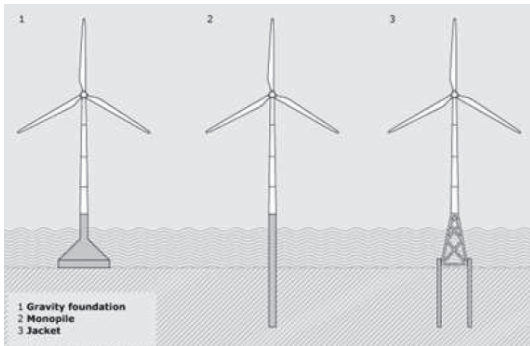
Fig. 1. Different types of offshore wind foundation.

Zienkiewicz [1982] developed the FEM discretization to present the behavior of various classes of soil and rock. He presented a concrete as two-phase medium composed of a solid skeleton and an interstitial fluid. Karim et al. [2002] analyzed the saturated porous elastic soil layer under cyclic loading by using a two-dimensional mesh free Galerkin method by having periodic conditions. A meshless method was an effective alternative, because it is difficult for FEM to analyze the problems associated with the moving boundary. The time domain response of a jacket offshore tower while the soil resistance to the pile movement was modeled using p–y and t–z curves to account the soil nonlinearity and energy dissipation, was presented by Mostafa and Naggar [2004] by employing a FE package in order to do parameters study. Andersen and Nielsen [2003] applied FEM with transmitting boundary element and presented a solution in the frequency domain of an elastic half-space to a moving force on its surface. And also, a two- and three-dimensional combined

FEM and BEM have been carried out for two railway tunnel structures in order to investigate what reliable information can be gained from a two-dimensional model to aid a tunnel design process or an environmental vibration prediction based on 'correcting' measured data from another tunnel in similar ground in research by Andersen and Jones [2003]. Then the steps in the FEM and BEM formulations were discussed, and the problems in describing material dissipation in the moving reference frame investigated by Andersen et al. [2007]. Badia et al. [2009] applied FEM to simulate the interaction between a fluid and a poroelastic structure due to the fact that both subproblems are indefinite. Andersen et al. [2012] used numerical method to analyze a nonlinear stochastic p–y curve for calculating the monopile response. The time-domain results for soil-foundation-structure interaction by considering the dependence of the foundation on the frequency of excitation were presented by Cazzania and Ruge [2012] by using FEM. Also, due to the unbounded nature of a soil medium, the computational size of these methods is very large. For this reason, it is important to establish some simple mathematical models which reduce the computational cost of analysis as well as increase the accuracy of results.

There are several analytical solutions for this type of problem. Peng and Yu [2011] obtained the analytical solutions of the torsional impedance saturated soil by using transfer matrix method. The effects of important parameters such as frequency and the rigidity ratio of different soil layers at the top of the pile were analyzed. Belotserkovets and Prevost [2011] developed a full-analytical method and an exact unique solution of the coupled thermo/hydro/mechanical response of a fluid saturated porous sphere subject to a pressure stress pulse on the outer boundary. The method of solution was based on the Laplace transformation method. Prakash and Puri [2006] presented methods for determining the dynamic response of machine foundations subjected to harmonic load. The soil stiffness was considered frequency independent for design of machine foundations. Li and Zhang [2010] presented an analytical solution in frequency domain by means of a variable separating method and then a semi-analytical solution was obtained using an numerical convolution method. Chai et al. [2011] employed the thin layer stiffness method, the matrix stiffness of the thin layer for P–SV and analytical expressions for the effective phase velocity of the surface waves to illustrate the effects of the body waves on the observed phase velocity through the phase analysis of the vibrations of both the surface waves and the body waves.

It may be noted that existing literature on offshore monopile foundations as cited above have been solved experimentally or theoretically based on numerical and analytical methods. To the best of our knowledge, no work has been reported till date that analyzes offshore foundation as long hollow and solid cylinders by using appropriate mathematical approach and employing the Green's function and integral method. This study attempts to concentrate on this investigation. In this paper, offshore foundations in an elastic and viscoelastic

media are investigated by modeling that as long tabular and solid piles. The integral method along with the Betti's reciprocal theorem, Somigliana's identity and Green's function are employed. The vertical loads are applied on the surface along the entire interface by considering rough and full contact between the soil and structure. The effect of material properties such as Young's modulus and Poisson's ratio on dynamic stiffness and phase angle are illustrated. This work aims to investigate the effect of some basic factors such as geometry, damping and frequency on stiffness, phase velocity in a pile. The exact solutions are obtained in elastic and frequency domain. Modes of resonance and anti-resonance are identified and presented.

GENERAL DEFINITION OF MODEL

Consider a thin axisymmetric circular cylinder with small wall thickness and radius R, as shown in Fig. 2. This cylinder is subject to harmonically varying forced displacement with the cyclic frequency ω and applied in the x_3 direction, along the center axis of the cylinder. In this case, pure antiplane shear wave propagation (SH-waves) occur which means that there is no displacement in the x_1 or x_2 directions. Axial symmetry in geometry and loading is assumed and cylindrical coordinates are considered.
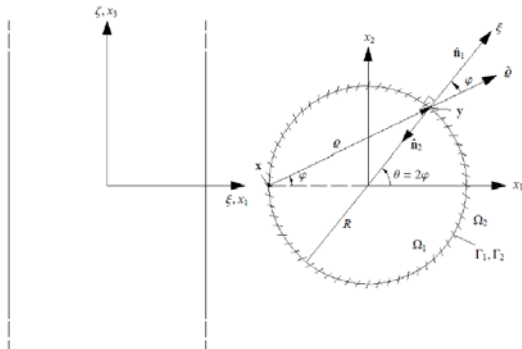
Fig. 2.Cross section of tubular offshore wind turbine foundation.

THEORETICAL FORMULATION AND EQUILIBRIUM EQUATIONS

Somigliana's identity is based on the dynamic reciprocity theorem and the fundamental solution which is used for wave propagation in elastic media. The three-dimensional frequency-domain version of Somigliana's identity reads:

$$\mathsf{C}(x) \cup_i (x, \omega) + \int_\Gamma P_{il}^*(x, \omega; y) \cup_l (y, \omega) d\Gamma(y) =$$
$$\int_\Gamma \cup_{il}^* (x, \omega; y) P_l(y, \omega) d\Gamma(y) +$$
$$\int_\Omega \cup_{il}^* (x, \omega; y) \rho B_l(y, \omega) d\Omega(y) \qquad (1)$$

where
$$\cup_{il}^* (x, \omega; y) = \int_{-\infty}^\infty u_{il}^*(x, t; y, 0) e^{-i\omega t} dt \qquad (2a)$$

$$P_{il}^*(x, \omega; y) = \int_{-\infty}^\infty p_{il}^*(x, t; y, 0) e^{-i\omega t} dt \qquad (2b)$$

$\mathsf{C}(x)$ is a coefficient dependent a the position (x). In particular, for any interior point within the domain Ω, the constant takes the value $\mathsf{C}(x) = 1$. Actually, the value of $\mathsf{C}(x)$ simply corresponds to the part of the point that is included in the domain Γ. Hence, $\mathsf{C}(x) = 0$ at an exterior point, and $\mathsf{C}(x) = 1/2$ for a point on a smooth part of the boundary Γ. A detailed derivation for a smooth part of a surface can be found in the work by Dominguez [1993].

And also, by assuming the surface and body quantities in the physical state vary harmonically with at the circular frequency ω, then:

$$u_l(x, t) = \cup_l (x, \omega) e^{-i\omega t}, \ p_l(x, t) = P_l(x, \omega) e^{-i\omega t},$$
$$b_l(x, t) = B_l(x, \omega) e^{-i\omega t} \qquad (3)$$

where $u_l(x, t)$ are the components of the displacement field, $p_l(x, t)$ is the surface traction and $b_l(x, t)$ is the load per unit mass in coordinate direction i. Vector x is the position in space and t is the time. Furthermore, based on Caushy's law the relation between surface traction and the Caushy stress (σ_{ij}) tensor is: $p_i(x, t) = \sigma_{ij}(x, \omega) n_j(x)$.

$\cup_{il}^* (x, \omega; y)$ and $P_{il}^*(x, \omega; y)$ are the Green's functions for the displacements and the surface traction in the frequency domain or, in other words, they are the Fourier transforms of $u_{il}^*(x, t; y, 0)$ and $p_{il}^*(x, t; y, 0)$, respectively. It can be mentioned here that the Green's function for a vector field is a second-order tensor with the components $g_{il}(x, t; y, \tau)$ which provide the response at the point x and time t in coordinate direction i due to a unit magnitude concentrated force acting at the point y and time τ in coordinate direction l. Hence, whereas the displacement field $\mathbf{u}(x, t)$ is a vector field with the components $u_i(x, t)$, the corresponding Green's function is a tensor field $\mathbf{u}^*(x, t; y, \tau)$ with the doubly indexed components $u_{il}^*(x, t; y, \tau)$.

FREQUENCY- DOMAIN EQUATION OF MOTION FOR SH-WAVES

The antiplane shear assumption induces the displacement components u_1 and u_2 which are identically equal to zero and partially derivatives with respect to x_3 vanish, only the displacement component u_3 in the direction out of the (x_1, x_2) plane exists and it is constant in along the x_3 direction. In the case of elastodynamics, this corresponds to the propagation of SH-waves in the (x_1, x_2) plane. When antiplane shear is considered, only the third component of the displacement field is different from zero. This holds for both the physical field and the Green's function. Hence, Somigliana's identity simplifies to a scalar integral equation as:

$$\mathsf{C}(x) \cup_3 (x, \omega) + \int_\Gamma P_{33}^*(x, \omega; y) \cup_3 (y, \omega) d\Gamma(y) =$$
$$\int_\Gamma \cup_{33}^* (x, \omega; y) P_3(y, \omega) d\Gamma(y) +$$

$$\int_\Omega \cup_{33}^* (\boldsymbol{x}, \omega; \boldsymbol{y}) \, \rho B_3(\boldsymbol{y}, \omega) d\Omega(\boldsymbol{y}) \tag{4}$$

SOLUTION FOR A HOLLOW CYLINDER

By considering smooth interfaces, Somigliana's identity (4) for the two domains Ω_1 and Ω_2 o(as shown in Fig. 2) reduces to:

$$\tfrac{1}{2}\cup_3^{(1)} (\boldsymbol{x},\omega) + \int_{\Gamma_1} P_{33}^*(\boldsymbol{x},\omega;\boldsymbol{y}) \cup_3^{(1)}(\boldsymbol{y},\omega)d\Gamma(\boldsymbol{y}) =$$
$$\int_{\Gamma_1}\cup_{33}^*(\boldsymbol{x},\omega;\boldsymbol{y})P_3^{(1)}(\boldsymbol{y},\omega)d\Gamma(\boldsymbol{y}) \tag{5}$$
$$\tfrac{1}{2}\cup_3^{(2)} (\boldsymbol{x},\omega) + \int_{\Gamma_2} P_{33}^*(\boldsymbol{x},\omega;\boldsymbol{y}) \cup_3^{(2)}(\boldsymbol{y},\omega)d\Gamma(\boldsymbol{y}) =$$
$$\int_{\Gamma_2}\cup_{33}^*(\boldsymbol{x},\omega;\boldsymbol{y})P_3^{(2)}(\boldsymbol{y},\omega)d\Gamma(\boldsymbol{y}) \tag{6}$$

where $\cup_3^{(1)}(\boldsymbol{x},\omega)$ and $\cup_3^{(2)}(\boldsymbol{x},\omega)$ are the displacements in the x_3-direction along the boundaries Γ_1 and Γ_2, respectively, whereas $P_3^{(1)}(\boldsymbol{y},\omega)$ and $P_3^{(2)}(\boldsymbol{y},\omega)$ are the corresponding surface tractions.

Green's function

The fundamental solution for the antiplane displacements is (Domínguez [1993]):

$$\cup_{33}^*(\boldsymbol{x},\omega;\boldsymbol{y}) = \frac{1}{2\pi\mu}K_0(\mathrm{i}k_s\varrho), \ \varrho = |\boldsymbol{x}-\boldsymbol{y}|, \ \mathrm{i} = \sqrt{-1} \tag{7}$$

where, μ is the shear modulus, K_m represents the modified Bessel function of the second kind and order m and k_s is the wavenumber. The relation between wavenumber and phase speed c_s is:

$$k_s = \frac{\omega}{c_s}$$

where c_s is dependent on the material properties, and it is defined as:

$$\begin{cases} \text{For hysteretic material damping}: c_s^2 = (1+\mathrm{i}\eta)\frac{\mu}{\rho} \\ \quad \text{For materials without damping}: \quad c_s^2 = \frac{\mu}{\rho} \end{cases} \tag{9}$$

where η is the loss factor and ρ is the material density. For a homogeneous isotropic linear elastic material, the generalized Hooke's law forming the relation between stresses, $\sigma_{ij}(\boldsymbol{x},t)$, and strains, $\epsilon_{ij}(\boldsymbol{x},t)$, simplifies to

$$\sigma_{ij}(\boldsymbol{x},t) = \lambda \Delta(\boldsymbol{x},t)\delta_{ij} + 2\mu \, \epsilon_{ij}(\boldsymbol{x},t) \tag{10}$$

where λ and μ are the Lame constants, δ_{ij} is Kronecker delta and $\Delta(\boldsymbol{x},t) = \epsilon_{kk}(\boldsymbol{x},t)$ is the dilation. Substituting the fundamental displacements $\cup_{33}^*(\boldsymbol{x},\omega;\boldsymbol{y})$ from Eq. 7 into Hooke's law (Eq. 10) and applying Caushy's stress law the fundamental surface shear stresses is obtained:

$$P_{33}^*(\boldsymbol{x},\omega;\boldsymbol{y}) = -\frac{\mathrm{i}k_s}{2\pi}\frac{\partial\varrho}{\partial n}K_0(\mathrm{i}k_s\varrho), k_s = \sqrt{\frac{\omega^2\rho}{\mu}} \tag{11}$$

$\frac{\partial\varrho}{\partial n}$ defines the partial derivative of the distance ϱ between the source and observation points, $\boldsymbol{x}$ and $\boldsymbol{y}$, in the direction of the outward normal:

$$\frac{\partial\varrho}{\partial n} = \begin{cases} \hat{\varrho}(\boldsymbol{x},\boldsymbol{y}) \cdot \hat{\boldsymbol{n}}(\boldsymbol{y}) = \cos(\varphi) & for \ \boldsymbol{x} \in \Gamma_1 \\ -\hat{\varrho}(\boldsymbol{x},\boldsymbol{y}) \cdot \hat{\boldsymbol{n}}(\boldsymbol{y}) = -\cos(\varphi) & for \ \boldsymbol{x} \in \Gamma_1 \end{cases}$$
(12a)

where
$$\hat{\varrho}(\boldsymbol{x},\boldsymbol{y}) = \frac{\boldsymbol{x}-\boldsymbol{y}}{|\boldsymbol{x}-\boldsymbol{y}|}$$
(12b)

Here φ is the angle between the distance vector $\varrho = \varrho\hat{\varrho}$ and the normal vector $\hat{\mathrm{n}}$.

Continuity conditions

The continuity conditions for the displacements across the interface for the forced displacement with constant amplitude $\hat{\cup}_3$ and in phase along the cylindrical interface, $\Gamma \equiv \Gamma_1$, provides the result:

$$\cup_3^{(1)}(\boldsymbol{x},\omega) = \cup_3^{(2)}(\boldsymbol{x},\omega) = \hat{\cup}_3(\omega), \boldsymbol{x} \in \Gamma \tag{13a}$$
$$P_3^{(1)}(\boldsymbol{y},\omega) = \hat{P}_3^{(1)}(\omega), \boldsymbol{x} \in \Gamma \tag{13b}$$
$$P_3^{(2)}(\boldsymbol{y},\omega) = \hat{P}_3^{(2)}(\omega), \boldsymbol{x} \in \Gamma \tag{13c}$$

Substituting the continuity conditions (Eq. (13)) into Eqs. 5 and 6, by having the constant amplitude for the forced displacement yield a set of linear integral equations:

$$\hat{\cup}_3(\omega)\left(\tfrac{1}{2} + \int_\Gamma P_{33}^*(\boldsymbol{x},\omega;\boldsymbol{y})d\Gamma(\boldsymbol{y})\right) =$$
$$\hat{P}_3^{(1)}(\omega)\int_\Gamma \cup_{33}^*(\boldsymbol{x},\omega;\boldsymbol{y})d\Gamma(\boldsymbol{y}) \tag{14}$$
$$\hat{\cup}_3(\omega)\left(\tfrac{1}{2} - \int_\Gamma P_{33}^*(\boldsymbol{x},\omega;\boldsymbol{y})d\Gamma(\boldsymbol{y})\right) =$$
$$\hat{P}_3^{(2)}(\omega)\int_\Gamma \cup_{33}^*(\boldsymbol{x},\omega;\boldsymbol{y})d\Gamma(\boldsymbol{y}) \tag{15}$$

Analysis

According to the frequency-domain equation of motion for each domain, inside and outside of the hollow cylinder, the dynamic stiffness can be obtained. Eliminating $P_{33}^*(\boldsymbol{x},\omega;\boldsymbol{y})$ from equations 14 and 15, the constant amplitude can be written in terms of the traction on the interface, as follows:

$$\hat{\cup}_3(\omega) = 2\hat{P}_3(\omega)\int_\Gamma \cup_3^*(\boldsymbol{x},\omega;\boldsymbol{y})d\Gamma(\boldsymbol{y}) \tag{16}$$

where the mean traction on either side of the interface ($\hat{P}_3(\omega)$) is:

$$\hat{P}_3(\omega) = \tfrac{1}{2}(\hat{P}_3^{(1)}(\omega) + \hat{P}_3^{(2)}(\omega)) \tag{17}$$

The general dynamic stiffness ($S_{33}(\omega)$) per unit surface of the interface related to displacement along the cylinder axis for arbitrary geometry of the infinite cylinder becomes:

$$S_{33}(\omega) = 2L_\Gamma \frac{\hat{P}_3(\omega)}{\hat{\cup}_3(\omega)} = \frac{L_\Gamma}{\alpha}, \alpha = \frac{1}{2}\frac{\cup_3(\omega)}{\hat{P}_3(\omega)} = \int_\Gamma \cup_3^*(\boldsymbol{x},\omega;\boldsymbol{y})d\Gamma(\boldsymbol{y})$$

where L_Γ is the length of the interface Γ, measured in the (x_1, x_2) plane. In the presented case, an offshore foundation is considered as an infinite circular cylinder with the radius R that is with $L_\Gamma = 2\pi R$. In order to compute α, the cylindrical polar coordinates $\alpha(\xi, \theta, \zeta)$ are introduced (see Fig. 2) such that:

$$x_1 = \xi \cos(\theta), x_2 = \xi \sin(\theta), x_3 = \zeta \qquad (19)$$

In these coordinates, the boundary Γ is defined by $\xi = R$, $0 \leq \theta < 2\pi, \infty < \zeta < \infty$.

In particular, when an observation point x with the plane coordinates $(x_1, x_2 = (-1,0)$ is considered (see Fig. 2), the distance ϱ between the source and observation point becomes:

$$\varrho = R \frac{\sin 2\varphi}{\sin \varphi} = 2R\cos \varphi \qquad (20)$$

Making use of the fact that $\theta = 2\varphi$, Eq. 16 may then be evaluated as:

$$\alpha = \frac{1}{2\pi\mu} \int_0^{2\pi} K_0(ik_s\varrho)Rd\theta = \frac{R}{\pi\mu} \int_0^\pi K_0(2ik_sRcos\varphi)d\varphi = \frac{R}{\mu} J_0(k_sR)K_0(ik_sR) \qquad (21)$$

Here, J_0 is the Bessel function of the first kind and order 0. It is noted that $K_0(ik_sR) \rightarrow \infty$ for $k_s \rightarrow \infty$. Hence, $S_{33}(\omega) \rightarrow 0$ $\omega \rightarrow 0$. Furthermore, $J_0(k_sR)$ has a number of zeros for $\eta = 0$ and $k_s > 0$. At the corresponding frequencies, $S_{33}(\omega)$ becomes singular.

SOLUTION FOR A SOLID CYLINDER

Based on Somigliana's identity for smooth surface of the rigid cylinder as mentioned above, one domain would be considered for the solid cylinder. By representing the equation of motion for one domain:

$$\frac{1}{2} \cup_{s3}^{(2)} (x, \omega) + \int_{\Gamma_2} P_{33}^* (x, \omega; y) \cup_{s3}^{(2)} (y, \omega)d\Gamma (y) = \int_{\Gamma_2} \cup_{33}^* (x, \omega; y)P_{s3}^{(2)}(y, \omega)d\Gamma (y) \qquad (22)$$

Considering a constant amplitude for the forced displacement and in phase along the cylindrical interface provides the result as:

$$\hat{\cup}_{s3} (\omega) \left(\frac{1}{2} - \int_\Gamma P_{33}^* (x, \omega; y)d\Gamma (y) \right) = \hat{P}_{s3}^{(2)}(\omega) \int_\Gamma \cup_{33}^* (x, \omega; y)d\Gamma (y) \qquad (23)$$

The general dynamic stiffness $S_{33}(\omega)$ per unit length along the cylinder of the infinite cylinder becomes:

$$S_{S33}(\omega) = 2L_\Gamma \frac{\hat{P}_{s3}(\omega)}{\hat{\cup}_3(\omega)} = \frac{L_\Gamma}{\alpha_s}, \alpha_s = \frac{1}{2} \frac{\cup_{s3}(\omega)}{\hat{P}_3(\omega)} = \frac{\int_\Gamma \cup_3^*(x,\omega;y)d\Gamma (y)}{\left(\frac{1}{2} - \int_\Gamma P_{33}^*(x,\omega;y)d\Gamma (y) \right)} \qquad (24)$$

by substituting the relation for fundamental surface shear stress, the dynamic stiffness can be written as:

$$S_{S33}(\omega) = \frac{L_\Gamma}{\alpha_s} = \frac{2\pi R}{\alpha_s}, \alpha_s = \frac{1}{2} \frac{\cup_{s3}(\omega)}{\hat{P}_3(\omega)} = \frac{\frac{R}{\pi\mu} \int_0^\pi K_0(2ik_sRcos\varphi)d\varphi}{\left(\frac{1}{2} + \int_0^\pi \frac{Rik_s}{\pi\mu}K_1(2ik_sRcos\varphi)d\varphi \right)} \qquad (25)$$

Then

$$\alpha_s = \frac{\frac{R}{\pi\mu} \int_0^\pi K_0(2ik_sRcos\varphi)d\varphi}{\left(\frac{1}{2} + \frac{R}{\pi} \int_0^\pi ik_scos(\varphi)K_1(2ik_sRcos\varphi)d\varphi \right)}$$

NUMERICAL RESULTS

For numerical illustration of the elastic solutions of this study, a thin long hollow and solid cylinders with mean radius $R = 3.0(m)$ is considered. The material properties are considered as (Liingaard and Andersen [2007]):

Table 1. *Material Properties*

Density $(\frac{kg}{m^3})$	Young's Modulus $(\frac{N}{m^2})$	Loss factor
1861	9411×10^3	Between: 0.01~0.1
	13596×10^3	

Results and Discussion for Hollow cylinder

In the following, results are presented in non-dimensional frequency $a_0 = \frac{\omega R}{c_s}$ and the normalized dynamic stiffness $\left| \frac{S_{33}(\omega)}{Z} \right|$, where $Z = 4\pi(1 + i\eta)\mu$. Different values of material properties such as Young's modulus, loss factor and Poisson's ratio are considered.
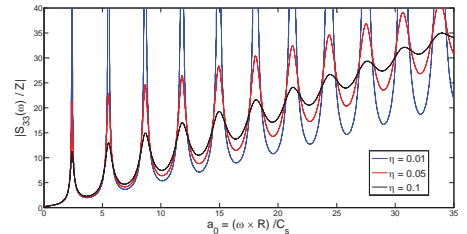
Fig. 3. Normalized dynamic stiffness per unit length of an infinite cylinder due to dynamic vertical load in the axial direction for different values of the loss factor, when $E = 9411 \times 10^3$ and $\nu = 0.495$.

Fig. 3 illustrates the normalized dynamic stiffness based on the small deformation theory due to different frequencies of the axial force. The value of stiffness increases with the increase of the load frequency until reaching a peak point then decreases to a local minimum for certain value of frequency

and again increases with the increase of the load frequency to next peak point. This procedure is repeated periodically with the frequency. The local peak point for dynamic stiffness decreases with increasing loss factor, whilst the local minimum point of the stiffness increases with decreasing the loss factor. It can be noticed that the turning point at which the concave curve changes into a convex curve is the same for all different loss factors.
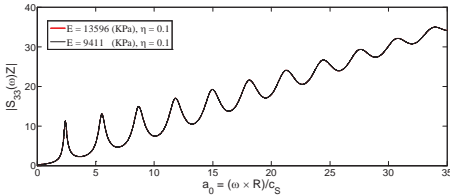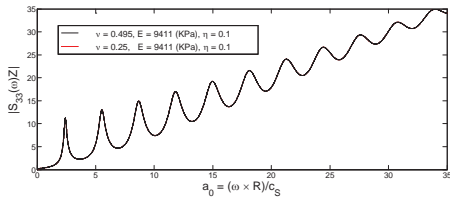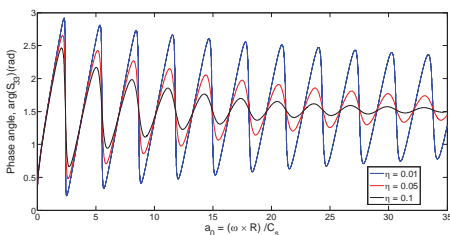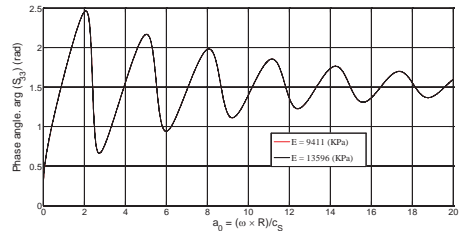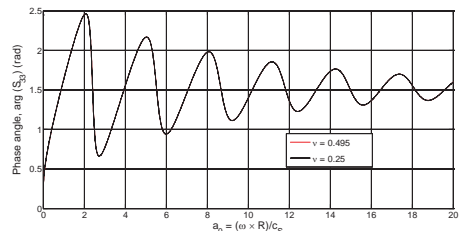

Fig. 4. Normalized dynamic stiffness per unit length of an infinite hollow cylinder due to dynamic vertical load in the axial direction for different values of the Young's modulus $E = 9411 \times 10^3$, $E = 13596 \times 10^3$ when loss factor $\eta = 0.1$ and $\nu = 0.495$.

Fig. 4 shows the effect of Young's modulus on variation of the dynamic stiffness versus load frequency. The normalized dynamic stiffness has the same value as the soil with lower Young's modulus for all values of load frequency.
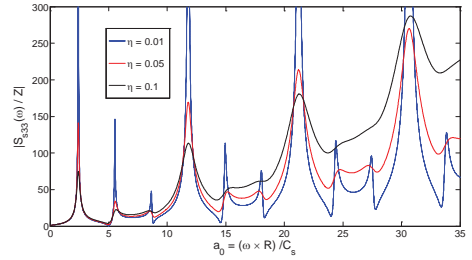

Fig. 5. Normalized dynamic stiffness per unit length of an infinite hollow cylinder due to dynamic vertical load in the axial direction for different values of the Poisson's ratio $\nu = 0.25$, $\nu = 0.495$ when loss factor $\eta = 0.1$ and $E = 9411 \times 10^3 N/m^2$

The variation of the dynamic stiffness with load frequency is shown in Fig. 5 for different value of Poisson's ratio. It is observed that the normalized dynamic stiffness is independent from some material properties of soil such as Poisson's ratio and Young's modulus.
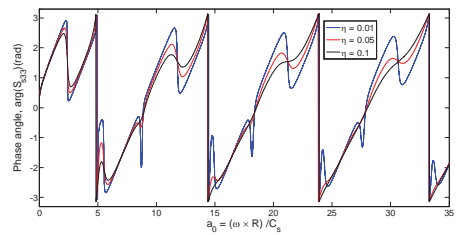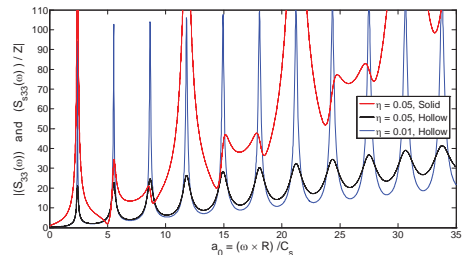

Fig. 6. Phase angle of an infinite hollow cylinder due to dynamic vertical load in the axial direction for different values of the loss factor when the Young's modulus $E = 9411 \times 10^3 \ N/_{m^2}$ and $\nu = 0.495$.

Fig. 6 compares the phase angle for different values of loss factor versus non-dimensional load frequency. As it is seen, the phase angle oscillating around line $\frac{\pi}{2}$ and the amount of fluctuating around this line decreases with the increase of load frequency. It can be noted that the absolute value of phase angle respect to central line (line $\frac{\pi}{2}$) decreases with the increase of loss factor.

Fig. 7. Phase angle of an infinite hollow cylinder due to dynamic vertical load in the axial direction for different values of the Young's modulus $E = 9411 \times 10^3 N/m^2$ and $E = 13596 \times 10^3 N/m^2$ when loss factor $\eta = 0.1$ and $\nu = 0.495$.

Fig. 8. Phase angle of an infinite hollow cylinder due to dynamic vertical load in the axial direction for different values of the Poisson's ratio $\nu = 0.25$ and $\nu = 0.495$ when $E = 9411 \times 10^3 N/m^2$ and the loss factor $\eta = 0.1$.

Figs. 7 and 8 concern the comparison of phase angle for dynamic stiffness versus non-dimensional load frequency for different values of Young's modulus and Poisson's ratio, respectively. In contrast with the results for different values of loss factor, other material properties such as Young's modulus and Poisson's ratio do not have any effect on phase angle like the results reported in Dominguez [1993], Liingaard, and Andersen [2007].
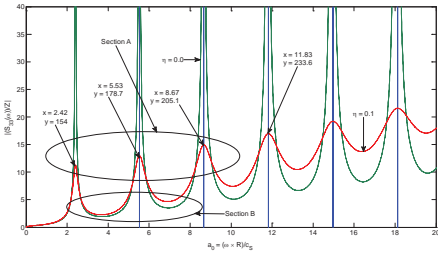
Fig. 9. Normalized dynamic stiffness versus different values of load's frequencies by having different values of loss factor $\eta = 0.0$ and $\eta = 0.1$ when $v = 0.495$ and $E = 9411 \times 10^3 \, N/m^2$.
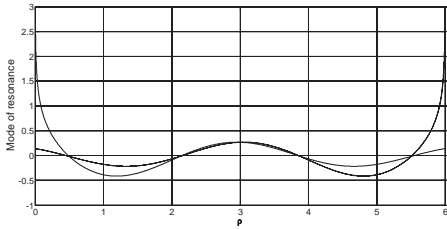
Fig. 10. Scaled mode shape resonance due load with non-dimensional frequency $a_0 = 5.53$ when loss factor $\eta = 0.1$ and $E = 9411 \times 10^3 \, N/m^2$.

To present the mode of resonance and anti-resonance, the load frequencies related to minimum and maximum value of the dynamic stiffness are needed. In order to calculate the related frequency, the maximum non-dimensional frequencies for $\eta = 0.1$ is shown in Fig. 9, which is related to section A. For anti-resonance, the frequency related to minimum stiffness in section B as shown in Fig. 9 is needed. Fig. 10 presents the schematic wave mode inside the hollow cylinder versus ϱ ($\varrho = 2Rcos\phi$, from Eq. 20). The value of non-dimensional frequency is taken from section A in Fig. 9, here $a_0 = 5.53$ is considered. Actually, by selecting each value of a_0 to correspond with peak point (such as: $a_0 = 2.42$, (or $a_0 = 5.53$), (or $a_0 = 8.67$), (or $a_0 = 11.83$), the resonance mode can be seen. The continuous line in Fig. 10 represents the wave motion from the left hand side of cylinder to right hand side, and the dash line represents the wave motion from right to left hand side of the hollow cylinder. As seen, the wave motion on left hand side and right hand side have the same sign, both of them are positive which means resonance phenomena. The anti-resonance mode can be seen by selecting the minimum frequencies from section B.

Results and Discussion for Solid cylinder
Figs. 11 and 12 show the effect of loss factor on the dynamic stiffness and the phase angle of the dynamic stiffness versus non-dimensional frequency.

Fig. 11. Non-dimensional dynamic stiffness per unit length of an infinite cylinder due to dynamic vertical load in the axial direction for different values of the loss factor, when $E = 9411 \times 10^3$ and $v = 0.495$.

Fig. 12. Phase angle of an infinite solid cylinder due to dynamic vertical load in the axial direction for different values of the loss factor when the Young's modulus $E = 9411 \times 10^3 \, N/m^2$ and $v = 0.495$.

As it can be seen form Fig. 11, the rate of increasing the normalized stiffness for smaller value of the loss factor is higher than those for soil with greater value of the loss factor. Moreover, it is seen that by increasing the loss factor the number of local maximum decrease. Fig. 12 shows that at any local maximum of the phase angle, the peaks decrease by increasing the loss factor and the reverse manner happen at local minimum.

Comparison between Hollow and Solid cylinders
In the following figures, results for hollow and solid cylinders versus non-dimensional frequency in presentence of different loss factor, Young's modulus and Poisson's ratio are presented.

Fig. 13. Comparison between normalized dynamic stiffness

per unit length of an infinite hollow and solid cylinder due to dynamic vertical load for different values of the loss factor versus non-dimensional frequency
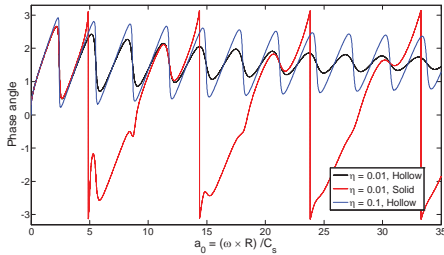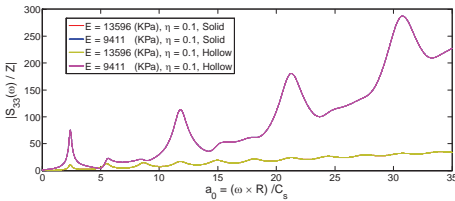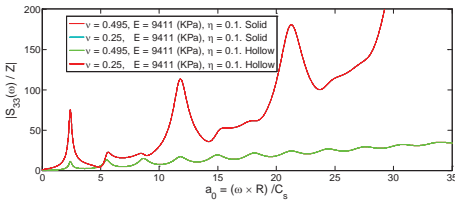

Fig. 14. Comparison between phase angle of an infinite hollow and solid cylinder due to dynamic vertical load for different values of the loss factor versus non-dimensional frequency

Fig. 15. Comparison between normalized dynamic stiffness per unit length of an infinite hollow and solid cylinder due to dynamic vertical load for different values of the Young's modulus

Fig. 16. Comparison between normalized dynamic stiffness per unit length of an infinite hollow and solid cylinder due to dynamic vertical load for different values of the Poisson's ratio

As it is seen from Fig. 13, the numbers of peaks for hollow and solid cylinders are the same. In some peaks, when the frequency is small the stiffness in solid cylinder is greater or smaller than those in hollow cylinder. However for bigger values of frequency ($a_0 > 9$) the stiffness in solid cylinder is greater than hollow cylinder when $\eta = 0.05$. Fig. 14 shows the phase angle in hollow cylinder tends to oscillate around line $\frac{\pi}{2}$ and converges to this line, whilst the behavior of phase angle in solid cylinder in completely different, it is moving periodically without any convergence. It can be seen from Figs. 15 and 16 the stiffness in solid cylinder is greater than those in hollow cylinder by considering the loss factor equal to 0.1.

CONCLUSIONS

Offshore wind turbine foundations are modeled as smooth long hollow and solid cylinders while it is subjected to dynamic vertical excitation. The mathematical approach like boundary integral method is employed to find the exact dynamic stiffness of offshore foundation, phase angle, resonance and anti-resonance mode. The offshore foundation is considered in a viscoelastic media and elastic responses are presented by using the Betti's reciprocal theorem, Somigliana's identity and Green's function. The behavior of the soil with damping and without damping is explored. The effects of material properties such as Young's modulus and Poisson's ratio on dynamic behavior of soil are investigated. The results for the soil with loss factor are validated and compared. Some general observations of this study can be summarized as:

✓ The dynamic stiffness increases with the increase of the load frequency until reaching a peak point then decreases to a local minimum for certain value of frequency and again increases with the increase of the load frequency to next peak point for hollow and solid cylinder. This procedure is repeated periodically. The result is similar to hollow cylinder which reported in Liingaard and Andersen [2007].

✓ The local peak point of the dynamic stiffness decreases with increasing loss factor in solid and hollow cylinder. The turning point which the concave curve changes into convex curve happens in the same pint for all different loss factors in hollow cylinder while this turning point is not the same for solid cylinders for certain frequency.

✓ The Dynamic stiffness and phase angle in a hollow or solid cylinder is independent of the soil's material properties such as Young's modulus and Poisson's ratio whilst it is dependent on loss factor.

✓ The phase angle fluctuates around line $\frac{\pi}{2}$ and the amount of fluctuating around this line decreases with the increase of load frequency for hollow cylinder and also by increasing the loss factor it converges to line $\frac{\pi}{2}$, whilst the phase angle does not converge to certain value in solid cylinder.

It is observed that a mathematical approach that pertains to the vertical vibration analysis of foundation provides good understanding about the behavior of soil beside the wave propagation and different modes of the wave. The results reveal that the presented approach gains the physical understanding for offshore foundation in the geo-mechanics field.

REFERENCES

Jr, D.S. and W.J. Mansur [2006], "*Dynamic analysis of fluid-soil-structure interaction problems by the boundary element method*" J. of Comput., No. 219, pp. 498-512.

Wolf, J.P [1985]. "*Dynamic Soil-Structure Interaction*", Prentice-Hall, Englewood Cliffs, NJ.

Maheshwari, P. and S. Khatri [2011]. "*A nonlinear model for footings on granular bed-stone column reinforced earth beds*", Appl. Math. Model., No. 35, pp. 2790-2804.

Srisupattarawanit, T., R. Niekamp and H.G. Matthies [2006], "*Simulation of nonlinear random finite depth waves coupled with an elastic structure*", Comput. Methods Appl. Mech. Engrg., Vol., 195, pp. 3072-3086.

Guenfoud, S., M.N., Amrane, V. Bosakov and N. Ouelaa [2009], "*Semi-analytical evaluation of integral forms associated with Lamb's problem*", Soil Dyn. and Earthquake Engrg., Vol., 29(3), pp. 438-443.

Padron, L.A., J.J. Aznarez and O. Maeso [2009], "*Dynamic structure–soil–structure interaction between nearby piled buildings under seismic excitation by BEM–FEM model*", Soil Dyn. and Earthquake Engrg., Vol. 29(6), pp. 1084-1096.

Genes M.C. [2012]. "*Dynamic analysis of large-scale SSI systems for layered unbounded media via a parallelized coupled finite-element/boundary-element/scaled boundary finite-element model*", Engrg. Anal. with Bound. Elem., Vol. 36(5), pp. 845-857.

Mahmoudpour, S., R. Attarnejad, and C. Behnia [2011], "*Dynamic Analysis of Partially Embedded Structures Considering Soil-Structure Interaction in Time Domain*", Hindawi Publishing Corporation, Math. Prob. in Engrg, Article ID 534968, 23 pages.

Zienkiewicz, O.C. [1982]. "*Basic Formulation of Static and Dynamic Behaviours of Soil and Other Porous Media*", Appl. Math. and Mech., Vol., 3(4), pp. 457-468.

Karim, M.R., T. Nogami and J. G. Wang [2002]. "*Analysis of transient response of saturated porous elastic soil under cyclic loading using element-free Galerkin method*", Int. J. of Solids and Struct., Vol., 39, pp. 6011- 6033.

Mostafa, Y.E. and M.H. El Naggar [2004]. "*Response of fixed offshore platforms to wave and current loading including soil-structure interaction*", Soil Dyn. and Earthquake Engrg., Vol., 24(4), pp. 357-368.

Andersen. L and S.R.K. Nielsen [2003], "*Boundary element analysis of the steady state response of an elastic half-space to a moving force on its surface*", Eng. Anal. Bound. Elem., Vol., 27(1), pp. 23-38.

Andersen, L. and C.J.C. Jones [2006], "*Coupled boundary and finite element analysis of vibration from railway tunnels-a comparison of two-and three-dimensional models*", J. Sound Vib., Vol., 293(3), pp 611–25.

Andersen, L., S.R.K. Nielsen and S. Krenk [2007]. "*Numerical methods for analysis of structure and ground vibration from moving loads*", Comput. and Struct., Vol., 85, pp.43-58.

Badia, S., A. Quaini and A, Quarteroni [2009]. "*Coupling Biot and Navier-Stokes equations for modelling fluid-poroelastic media interaction*", MSC, Vol., 65, pp. 1-39.

Andersen, L.V., M.J. Vahdatirad, M.T. Sichani and J.D. Sørensen [2012]. "*Natural frequencies of wind turbines on monopile foundations in clayey soils A probabilistic approach*" Comput. and Geotech., No. 43, pp. 1-11.

Cazzania, A. and P. Ruge [2012]. "*Numerical aspects of coupling strongly frequency-dependent soil–foundation models with structural finite elements in the time-domain*", Soil Dyn. and Earthquake Engrg., Vol., 37, pp. 56-72.

Peng, H and J. Yu [2011]. "*Dynamic Torsional Impedance of Piles in Layered Saturated Soil*", EJGE, Vol., 16, pp. 1147-1161.

Belotserkovets, A and J. H. Prevost [2011]. "*Thermoporoelastic response of a fluid-saturated porous sphere: An analytical solution*", Int. J. of Engrg. Sci., Vol., 16, pp. 3981-3989.

Li, Q. and Z. Zhang [2010]. "*Dynamic Response of Pile in Saturated Porous Medium Considering Radial Heterogeneity by Pile Driving*", Soil Dyn. and Earthquake Engrg., Vol., 13, pp. 1-16.

Chai, H.Y., K.K. Phoon, C.F. Wei and Y.F. Lu [2011], "*Analysis of effects of active sources on observed phase velocity based on the thin layer method*", J. Appl. Geophy., Vol., 73, pp. 49–58.

Dominguez, J [1993], "*Boundary elements in dynamics*", Computational Mechanics Publications, Southampton, ISBN = 0-444-88820-9.

Liingaard, L.I.M. and L. Andersen [2007], *Impedance of flexible suction caissons*, Earthquake Engrg. and Struct. Dyn., Vol. 36, 2249-2271.

Prakash, S. and V. K. Puri [2006], "*Foundations for vibrating machines*" SERC J. of Struct. Engrg., Vol., 33(1), pp. 13-29.

Numerical calculation of damping for monopile foundations under cyclic load during steady-state vibration

Authors:
Mehdi Bayat, Lars Vabbersgaard Andersen, Søren Mikkel Andersen, and Lars Bo Ibsen

B.1 Author's Right

Dear Mehdi,

This is fine with us. Could you please made credit to the source file, including a copyright notice?

Kind regards,

Léon Bijnsdorp

From: Alphose Zingoni [mailto:alphose.zingoni@uct.ac.za]
Sent: vrijdag 10 juli 2015 16:47
To: Mehdi Bayat
Cc: Bijnsdorp, Leon
Subject: Permission to Include SEMC 2013 Proceedings Paper in PhD Thesis

Dear Mehdi

As you intend to include the content of your research paper (published in the Proceedings of the SEMC 2013 International Conference) in your own PhD thesis, I do not think this is a problem, according to the terms of the Copyright Transfer Agreement that you signed. However, the publisher (CRC Press/Taylor & Francis) needs to be informed, and so I am copying this email to Leon Bijnsdorp at Taylor & Francis. If there is anything else that needs to be done, he will let you know.

Good luck with your PhD submission!

Kind regards

Alphose

Prof. A. Zingoni, PhD, DIC, CEng, FSAAE, FIABSE, FIStructE
Chair & Editor, SEMC 2016 International Conference
Department of Civil Engineering, University of Cape Town
Rondebosch 7701, Cape Town, SOUTH AFRICA
Tel: (27) (21) 650 2601; Email: alphose.zingoni@uct.ac.za
SEMC 2016 Conference website: http://www.semc.uct.ac.za

From: Mehdi Bayat [mailto:meb@civil.aau.dk]
Sent: Friday, July 10, 2015 3:54 PM
To: Alphose Zingoni
Subject: SEMC 2013 Paper 415

10 July 2015

Prof. Alphose Zingoni,
Editor-in Chief
Fifth International Conference on Structural Engineering, Mechanics and Computation (SEMC 2013)

Ms. Ref. No. : SEMC 2013/415
Subject: Permission to include contents of the manuscript, "Numerical calculation of damping for monopile foundations under cyclic load during steady-state vibration", in the PhD thesis dissertation.

Dear Professor Zingoni,

I am Mehdi Bayat, a PhD student at the Aalborg University (AAU). I am pleased to inform you that the article mentioned as above and that has been published in SEMC 2013 is a part of my PhD dissertation work.

It is therefore requested that I may kindly be granted due permission to use the contents of the said article and make it a part of my PhD dissertation. This dissertation is likely to be submitted to the Aalborg University for the award of the PhD degree.

Thanks for your kind cooperation,

Sincerely yours,

Mehdi Bayat

Offshore Foundations Group, Geotechnical Engineering Research Group,
Division of Structures, Materials and Geotechnics,
Department of Civil Engineering,
Sofiendalsvej 9-11,
DK-9200 Aalborg SV,
Denmark

UNIVERSITY OF CAPE TOWN

Taylor & Francis
Taylor & Francis Group

A.A. Balkema Publishers – Taylor & Francis The Netherlands

Consent to Publish & Transfer of Copyright
for Contributors to Books

In order to protect the Work against unauthorised use and to authorise dissemination of the Work by means of offprints, legitimate photocopies, microform editions, reprints, translation, document delivery, and secondary information sources such as abstracting and indexing services including data bases, it is necessary for the author(s) to transfer the copyright in a formal written manner.

The Consent ensures that the Publisher has the author's permission to publish the Work.

Title of Contribution

Numerical Calculation of Damping for Monopile Foundations under

Author(s)   *Cyclic loading during steady-state vibration*

M. Bayat, L.-V. Andersen, S.M. Andersen, L.B. Ibsen

Name of Book / Conference

SEMC 2013

1. The Author hereby assigns to the Publisher the copyright to the Contribution named above whereby the Publisher shall have the exclusive right to publish the said Contribution in print and in electronic form and translations of it wholly or in part throughout the World during the full term of copyright including renewals and extensions and all subsidiary rights.

2. The Author retains the right to republish the Contribution in any printed collection consisting solely of the Author's own Works without charge and subject only to notifying the Publisher of the intent to do so and ensuring that the publication by the Publisher is properly credited and that the relevant copyright notice is repeated verbatim.

3. The Author guarantees that the Contribution is original, has not been published previously, is not under consideration for publication elsewhere, and that any necessary permission to quote from another source has been obtained. (A copy of any such permission should be sent with this form.)

4. The Author declares that any person named as co-author of the Contribution is aware of the fact and has agreed to being so named.

5. The Author declares that, if the Consent to Publish form has been downloaded from the Publisher's website or sent by e-mail, the form has not been changed in any way without the knowledge of the Publisher.

To be signed by the Author, also on behalf of any co-authors.

Name _*M. Bayat*_   Date *28-02-2013*

Signature _*Mehdi Bayat*_

Please return this signed form promptly to the editor of the book / conference. Thank you.

Numerical calculation of damping for monopile foundations under cyclic load during steady-state vibration

M. Bayat, L.V. Andersen, S.M. Andersen & L.B. Ibsen
Department of Civil Engineering, Aalborg University, Aalborg, 9000, Denmark

ABSTRACT: Dynamic loading and fatigue has significant effects on offshore wind turbine foundations. To obtain a proper design of a turbine and its foundation it is therefore important to understand how the structure and soil interact regarding damping. Especially, this paper demonstrates the damping and stiffness of the saturated soil within the seabed due to pore water flow generated by the cyclic motion of a monopile. The concept of a Kelvin-Voigt model is employed and combined with a Finite Element Method (FEM) model of the pile. The two-dimensional analysis of each individual soil layer is performed in ABAQUS by coding input files, utilizing Python and MATLAB. A parametric study is performed to illustrate the effects of model size, soil properties such as permeability, void ratio, Young's modulus, bulk modulus, and load parameters such as amplitude and frequency. It is found that by increasing the bulk modulus, the damping and stiffness in the soil increase; however, the increase is small. Further, it is observed that Young's modulus has a significant effect on the dynamic response of the soil. Finally, the permeability of the seabed has a strong influence on the damping of wind-turbine-tower vibrations.

1 INTRODUCTION

The recent developments of offshore industries such as offshore wind turbine foundations and also structures for oil and gas extraction lead to a growing demand for realistic predictions of the behavior of offshore structures. As the use of offshore foundations increases, new methodologies need to be developed to characterize and analyze offshore structural components due to dynamic loads.

Dynamic behavior of offshore structures is one of the most important parts in the design of such structures. The dynamic response varies significantly in time and is affected by inertial, damping and kinematic effects as well as the stiffness of the structure and the underlying soil. Large shear strains (greater than 10^{-4}%), pile–soil interaction, dynamic load rates and nonlinear material behavior lead to nonlinearity in the dynamic response (Ahangar et al. 2011). Dynamic analysis is carried out theoretically by numerical methods, analytical or semi-analytical methods.

In the case of analytical methods, Nogami & Konagai (1987) implemented nonlinear conditions in the time domain for dynamic response of pile foundations subjected to harmonic and transient load. Kazama & Nogami (1991) described the dynamic behavior of saturated two-phase layered media. They found that the permeability and loading rate (loading frequency) are critical factors to control the dynamic behavior of saturated soil. Bea (1992) described the effects of cyclic loadings on the axial capacity of piles driven in cohesive soils and supporting offshore platforms. An advanced analytical procedure was developed to estimate pile penetration and to evaluate the pile performance when a platform is subjected to intense cyclic loading. Bea (1992) found that loading rates, the ratio of steady to cyclic load amplitudes, the sequencing and numbers of cycles of loading, and the relative pile–soil stiffness are all important parameters that determine the pile performance. Chang et al. (2000) analyzed the time-dependent damping model by employing integration technique, an alternative time-dependent damping model was proposed by Chang & Yeh (1999) in modeling the pile response from direct wave equation analyses. Lanzo et al. (2003) presented frequency and time domain analyses by using computer codes PROSHAKE, DESRAMOD and QUAD4M. They have considered viscous damping which is generally assumed to be of the Rayleigh type, i.e. stiffness- and mass proportional, or in a simplified form, only stiffness-proportional. They have shown the dependency of damping from frequency. On the

other hand, the numerical methods can be useful and implement easily.

Rajashree & Sitharam (2001) applied a FEM in order to present the nonlinear soil behavior by a hyperbolic relation for static load conditions and a modified hyperbolic relation which includes both degradation and gap for cyclic loads. They used an incremental-iterative procedure where the pile was idealized as beam elements and the soil as elasto-plastic spring elements. Klar and Frydman (2002) presented 3-D models and Winkler models based on the commercial 2-D finite difference code FLAC under static, seismic, and lateral dynamic loading. Karim et al. (2002) analyzed a saturated porous elastic soil layer under cyclic loading by using a 2-D mesh free Galerkin method by having periodic conditions. Liang et al. (2007) applied a 3-D FEM and presented the parametric study of laterally loaded drilled shafts in clay. A hyperbolic p-y criterion was developed for cohesive intermediate geometrical. Harada et al. (2008) employed a multi-Winkler model based on soil traction for nonlinear soil–foundation interaction during cyclic loading. The integration of the traction over the foundation area was efficiently treated numerically by employing the fiber element method. Al-Wakel et al. (2011) implemented a model of frequency-dependent damping by using 3-D FEM while a rectangular footing on saturated soil was subjected to cyclic and harmonic force. The coupled dynamic equations with an u-p formulation based on the dynamic consolidation theory were used to simulate the soil skeleton. The Beam on Nonlinear Winkler Foundation can be modeled in ABAQUS while the interaction nonlinearity can be accounted for. Trochanis (1991) presented the response of laterally loaded piles by using ABAQUS and compared the results with 3-D FEM. Boulanger et al (1999) employed ABAQUS to present the dynamic results of piles and validated the results with centrifuge experimental tests. Commercial software such as ABAQUS can be versatile, economical and friendly user software for various complicated conditions in a simple manner.

It may be noted that the existing literature on offshore monopile foundations as cited above presents experimental and theoretical solutions based on numerical or analytical approaches. To the best of our knowledge, no work has been reported till date that presents a comprehensive parametric study of offshore foundations by using FEM with presence of the pore pressure that is developed due to dynamic load. The influence of different parameters such as pore pressure, load amplitudes and frequencies, the bulk modulus of the grains, the permeability of the seabed and void ratio of the seabed, and Young's modulus of the matrix material are investigated. The FEM and a Kelvin-Voigt model are employed for analysis of a 2-D saturated soil model.

2 MODEL DESCRIPTION

Consider an axisymmetric solid circular cylinder with radius R, as shown in Figure 1. The arc-boundary which represents the common border between the solid cylinder and the saturated soil is subject to harmonically varying forced displacement with the cyclic frequency ω and applied in the horizontal (x) direction. The two-dimensional analysis of each individual soil layer is performed.

2.1 Soil modeling

The soil is considered as an isotropic and elastic material. For saturated soil, the permeability, specific weight and void ratio, porous bulk moduli (which encompass the bulk modulus of grains and the bulk modulus of fluid) are defined. The mesh consists of 4-noded quadrilateral elements with linear interpolation of the displacement and pore pressure (CPE4P).
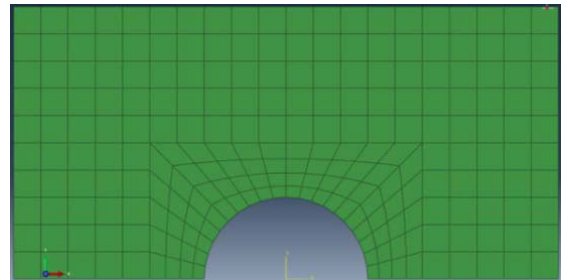

Figure 1: Two-dimensional finite-element model of an offshore wind turbine foundation and the surrounding soil.

2.2 Theoretical approach

The numerical calculation for dynamic analysis of offshore monopile foundations based on a one dimensional Kelvin-Voigt model by using FEM is presented. The dynamic analysis has been implemented within the framework of ABAQUS. Different model size for symmetry pile are applied. A numerical solution for the reaction force on the pile is given.
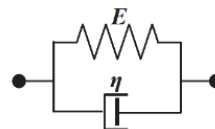

Figure 2: Kelvin-Voigt model.

In the Kelvin-Voigt model as shown in Figure 2, the equation of motion can be written as:

$$C\dot{x} + Kx = F. \tag{1}$$

Here C, K and F are the damping, stiffness and reaction force, respectively, while x and $\dot{x}$ are the displacement and the velocity. By applying sinusoidal force-displacement, the reaction force F could be in sinusoidal form with phase angle respect to applied displacement, however the amplitude of force and applied displacement are different. By calculating the phase angle from numerical results in ABAQUS (Dassault Systèmes Simulia Corp. 2012) and using the flowchart as shown in Figure 3, the damping and stiffness can be calculated.
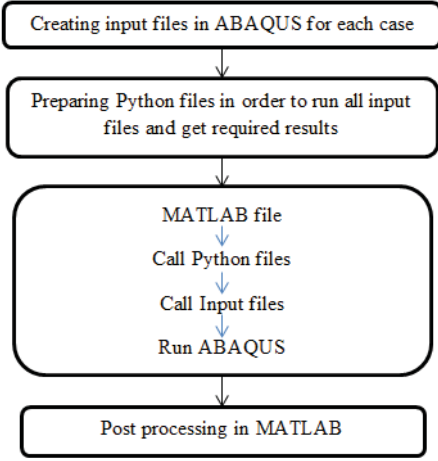
Figure 3: Flowchart of computer program.

2.3 Boundary conditions

The pore pressure and displacement at the exterior boundary should be zero. Symmetry of the solution should apply across the center line of the model, while for the semi-circle carve, the sinusoidal periodic displacement in horizontal direction is applied as shown in Figure 4.
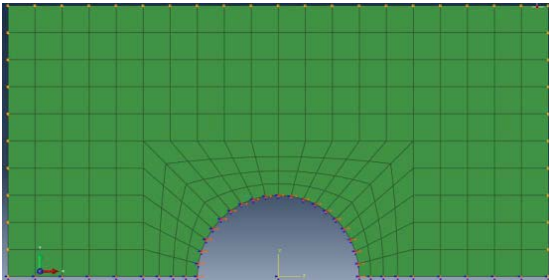
Figure 4: Boundary conditions for the soil block.

3 NUMERICAL RESULTS

For numerical illustration of the elastic solutions of this study, a solid cylinder with radius $R = 3.0$ m is considered. The material properties listed in Table 1 are considered. A soil block with a circular cavity subjected to sinusoidal periodic displacement is analyzed, using different geometry and soil properties in order to illustrate the effects of changes.

Table 1. Material properties of soil.

Young's modulus (N/m^2)	1×10^8
Poisson's ratio	0.25
Void ratio	0.50
Bulk modulus of grain (N/m^2)	3.6×10^{10}
Bulk modulus of fluid (N/m^2)	2×10^9

3.1 Results for different geometries

Figure 5 (top and middle) illustrates the damping and stiffness due to sinusoidal periodic load for different geometry of the soil block around the pile. It can be seen from Figure 5 that for each dimension of the model, the stiffness and damping have their maximum value for the smaller size of the model. It is seen that for large sizes of the model, the variations of the mentioned properties become small. As expected, the effect of the exterior boundary condition for large sizes of the model became smaller than those for a small model.
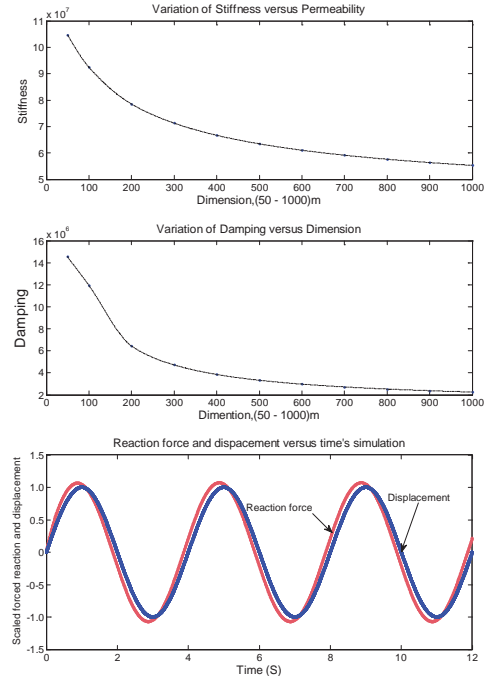
Figure 5: Variation of stiffness and damping versus model dimensions, and variation of scaled reaction force and displacement versus time.

The graphs in Figure 5 (top and middle) are calculated based on reaching steady state conditions. The simulation is carried for 12 s as shown in Figure 5 (bottom) and then by calculating the phase angle between two graphs the damping is determined. It is worth to mention that the stiffness and damping are calculated after two periods in order to have the steady state results. It can be concluded that a bigger model can make better results by avoiding the effect of outer boundary conditions. Thus, in the rest of the analyses the larger model of this study is considered.

3.2 Results for different void ratio

Figure 6 illustrates the variation of stiffness and damping due to periodic loading for different values of the void ratio. It is seen that the values of stiffness and damping decrease by increasing the void ratio. It is noted that the variation of damping versus void ratio is greater than the variation of the stiffness.
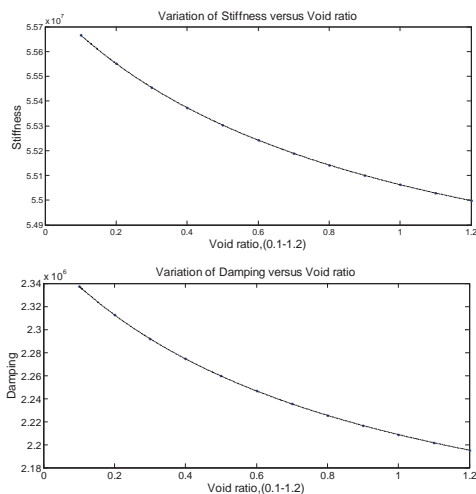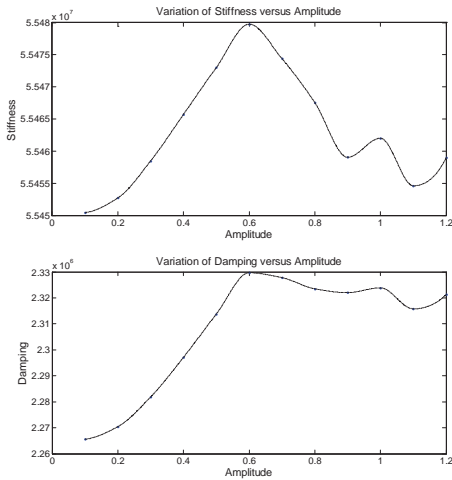

Figure 6: Variation of stiffness and damping versus variation of the void ratio.

3.3 Results for different permeability

The variation of stiffness and damping due to periodic load for saturated soil for different values of permeability are presented in Figure 7 (top and middle). As it can be seen the by increasing the permeability the damping increases, and for specific values of the permeability the maximum damping occurs, whereas for further increasing permeability the damping decreases. The stiffness decreases with increasing the permeability. A decrease of almost 30% can be identified. The following values of the permeability have initially been examined in the study: 0.5, 0.4, 0.2, 0.1, 0.07, 0.05, 0.03, 0.01, 0.005, 0.001, 0.0005, 0.0001, 0.00005, and 0.00001 (m/s). The behavior of damping makes awareness to investigate

the variation of damping using smaller increments in the permeability. The following values have been applied in Figure 7 (bottom): 0.01, 0.02, 0.03,… , 0.27, 0.028, 0.29, 0.30 (m/s). The graph suggests that the maximum damping for the soil material properties and pile geometry occurs for a permeability of 0.15.
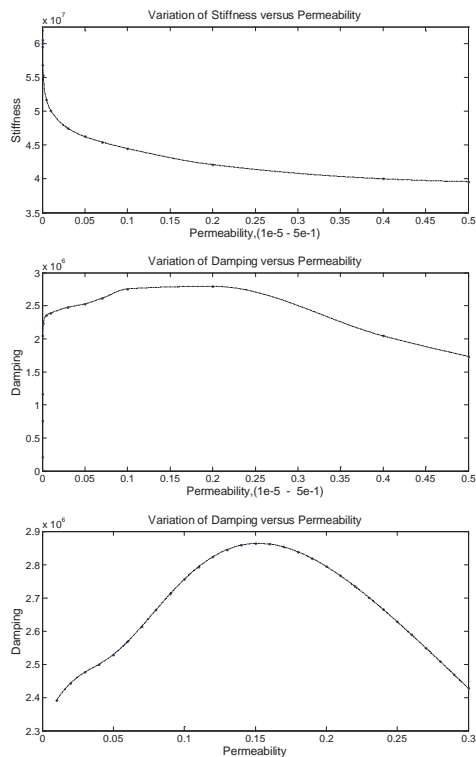
Figure 7: Variation of stiffness and damping versus variation of the permeability.

3.4 Results for different load frequencies

Figure 8 shows the variation of stiffness in the soil due to harmonic forced displacement with different values of the excitation frequency. It is evident that the dynamic soil stiffness increases with increasing load frequency in the entire range of frequencies.
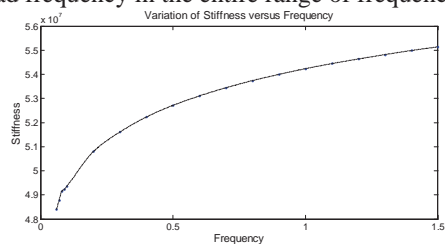
Figure 8: Variation of stiffness versus variation of the load frequency.

3.5 Results for different load amplitudes

Figure 9 illustrates the variation of stiffness and damping due to time-harmonic excitation with different values of load amplitudes. As it can be seen, the behavior of stiffness and damping are similar: by increasing load amplitudes, the stiffness and damping related to the soil increase up to the specific value of amplitude = 0.6 m. Hereafter they are going to decrease. It can be mentioned that the variations of the stiffness are very small, whilst the variations of damping are slightly greater with respect to the load amplitude variation.

Figure 9: Variation of stiffness and damping versus variation of the load amplitude.

3.6 Results for different grain bulk moduli

The variation of stiffness and damping due to harmonic loading for soil with different grain bulk moduli are presented in Figure 10. As expected the values of stiffness and damping increase with an increase of the grain bulk modulus. The relative variations of stiffness and damping are almost the same, and only small variations are observed.
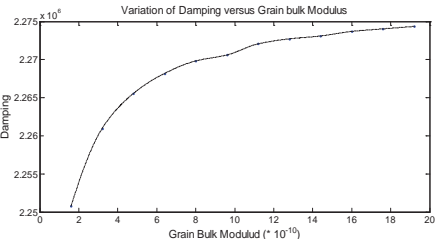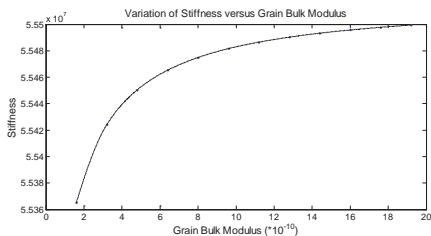
Figure 10: Variation of stiffness and damping versus different grain bulk modulus.

3.7 Results for different Young's moduli

It is evident from Figures 11(a) and 11(b) that the variation of stiffness and damping is almost linear versus the variation of Young's modulus.
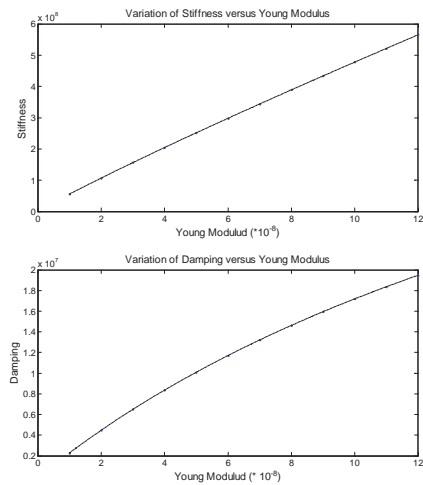
Figure 11: Variation of stiffness and damping versus different Young's moduli.

As expected, by increasing the Young's modulus the stiffness and damping in soil increase. It is worth to mention that the variation of stiffness is higher than the variation of damping versus the variation of Young's modulus. For the mentioned model, the relative variation of the stiffness is about 1.5 times higher than the relative variation of the damping. This implies that the stiffness is more sensitive than the damping with respect to variations of Young's modulus.

4 CONCLUSIONS

The dynamic response of isotropic elastic saturated soil is presented by using a finite-element model. The effects of model size, soil properties (such as Young's modulus, bulk modulus of grain, void ratio, and permeability), load frequency and amplitude on

the dynamic stiffness and soil damping are investigated.

Numerical results are presented by using the finite-element method by coding the input file and using Python scripting in ABAQUS and MATLAB. A sinusoidal forced displacement is applied and the simulation is carried out within 12 second.

Some general observations of this study can be summarized as follows:

- Dynamic stiffness and damping decrease with increase of void ratio and the variation of damping versus void ratio is greater than variation of stiffness versus void ratio.

- Damping increases to certain value for specific value of permeability and then decreases by increasing the permeability, whilst stiffness decreases by increasing permeability.

- Dynamic stiffness is more sensitive than damping with respect to variation of Young's modulus.

Results of the frequency-dependent damping and dynamic stiffness are similar and in the same line to the results reported in Chang et al. (2000) and Kazama & Nogami (1991), respectively.

5 ACKNOWLEDGEMENT

6 REFERENCES

Ahangar, M. & Bargi, K. & Sharifian, H. & Safarnezhad, M. 2011. Dynamic nonlinear behavior of fixed offshore jacket piles. *International journal of civil and structural engineering* 2(1) :260-269.

Al-Wakel, S.A.F. & Fattah, M.Y. & Karim, H.H. 2011. Dynamic Analysis of Foundations on Saturated Clay Using an Energy Absorbing Layer. *Eng. & Tech. Journal*, 29 (11):2189-2201.

Bea, R.G. 1992. Pile capacity for axial cyclic loading. *Journal of Geotechnical Engineering, ASCE,* 118(1)*:* 34-50.

Boulanger, R.W. & Curras, C.J. & Kutter, B.L. & Wilson, D.W. & Abghari, A. 1999. Seismic Soil-Pile-Structure Interaction Experiments and Analyses. *Journal of Geotechnical and Geoenvironmental Engineering*, *ASCE*, 125(9): 750-759.

Chang, D.W. & Roesset, J.M. & Wen, C.H. 2000. A time-domain viscous damping model based on frequency-dependent damping ratios. *Soil Dynamics and Earthquake Engineering* 19: 551-558.

Chang, D.W. & Yeh, S. H. 1999. Time-domain wave equation analysis of single piles utilizing transformed radiation damping. *Soils and Foundations, JGS* 39(2):31-44.

Dassault Systèmes Simulia Corp. (2012). *Abaqus 6.12 Analysis User's Manual*. Providence, RI, USA: Dassault Systèmes Simulia Corp.

Harada, T. & Nonaka, T. & Wang, H. & Magoshi, K. & Iwamura, M. 2008. A nonlinear dynamic soil foundation interaction model using fiber element method and its application to nonlinear earthquake response analysis of cable stayed bridge. *The 14th World Conference on Earthquake Engineering October 12-17 Beijing China.*

Karim, M.R. & Nogami, T. & Wang, J.G. 2002. Analysis of transient response of saturated porous elastic soil under cyclic loading using element-free Galerkin method. *Int. J. of Solids and Struct* 39: 6011- 6033.

Kazama, M. & Nogami, t. 1991. Effects of permeability and loading rate on dynamic stiffness of saturated soil, *GEO-Cost* 91. 3-6 *Sep.:459-462*.

Klar, A. & Frydman, S. 2002. Three-Dimensional Analysis of Lateral Pile Response using Two-Dimensional Explicit Numerical Scheme. *Journal of Geotechnical and Geoenvironmental Engineering*, ASCE, 128(9):775-784.

Lanzo, G. & Pagliaroli, A. & D'Elia, B. 2003. Numerical study on the frequency-dependent viscous damping in dynamic response analyses of ground. *Transactions on the Built Environment* 72, *WIT Press, www.witpress.com, ISSN* 1743-3509.

Liang, R. Y. &Shatnaw, E.S. & Nusaira, J. 2007. Hyperbolic P-Y Criterion for Cohesive Soils. *Jordan Journal of Civil Engineering* 1(1): 38-58.

Nogami, T. & Konagai, K. 1987. Dynamic response of vertically loaded nonlinear pile foundations, *Journal of Geotechnical and Geoenvironmental Engineering*, ASCE, 113(2):147-160.

Rajashree, S.S. & Sitharam T.G. 2001. Nonlinear finite element modeling of batter piles under lateral load. *Journal of Geotechnical and Geoenvironmental Engineering*, ASCE, 127(7) :604-612.

Trochanis, A.M. & Bielak, J. & Christiano, P. 1991. Three-dimensional Nonlinear Study of Piles. *ASCE Journal of* Geotechnical Engineering 117(3): 429–447.

Assessment of the dynamic behaviour of saturated soil subjected to cyclic loading from offshore monopile wind turbine foundations

Authors:
Mads Damgaard, Mehdi Bayat, Lars Vabbersgaard Andersen and Lars Bo Ibsen

C.1   Author's Right

Assessment of the dynamic behaviour of saturated soil subjected to cyclic loading from offshore monopile wind turbine foundations

M. Damgaard [a], M. Bayat [b,*], L.V. Andersen [b], L.B. Ibsen [b]

[a] Technology and Engineering Solutions, Vestas Wind Systems A/S, Hedeager 42, 8200 Aarhus, Denmark
[b] Department of Civil Engineering, Aalborg University, Sohngårdsholmsvej 57, 9000 Aalborg, Denmark

ABSTRACT

The fatigue life of offshore wind turbines strongly depends on the dynamic behaviour of the structures including the underlying soil. To diminish dynamic amplification and avoid resonance, the eigenfrequency related to the lowest eigenmode of the wind turbine should not coalesce with excitation frequencies related to strong wind, wave and ice loading. Typically, lateral response of monopile foundations is analysed using a beam on a nonlinear Winkler foundation model with soil–pile interaction recommended by the design regulations. However, as it will be shown in this paper, the guideline approaches consequently underestimate the eigenfrequency compared to full-scale measurements. This discrepancy leads the authors to investigate the influence of pore water pressure by utilising a numerical approach and consider the soil medium as a two-phase system consisting of a solid skeleton and a single pore fluid. In the paper, free vibration tests are analysed to evaluate the eigenfrequencies of offshore monopile wind turbine foundations. Since the stiffness of foundation and subsoil strongly affects the modal parameters, the stiffness of saturated soil due to pore water flow generated by cyclic motion of monopiles is investigated using the concept of a Kelvin model. It is found that the permeability of the subsoil has strong influence on the stiffness of the wind turbine that may to some extent explain deviations between experimental and computational eigenfrequencies.

© 2014 Elsevier Ltd. All rights reserved.

1. Introduction

For offshore wind turbines, the monopile foundation concept, in which a pile made of welded steel is driven open-ended into the soil, is often applied. For a variety of subsoil conditions, this type of foundation has proven to be cost-effective at shallow water. As an example, the Thanet and Bligh Bank wind farm consist of 3.0 MW turbines installed on monopile foundations in water depths between 15 and 30 m. As future offshore wind turbines with rated power values of 5–6 MW installed on monopile foundations are expected to be installed at greater water depths, the dynamic system response becomes highly sensitive to excitations with low frequency content.

Besides the static bearing capacity of wind turbines, the fatigue limit state is of paramount importance to investigate. To reduce the fatigue damage accumulation during the lifetime of wind turbine structures, amplification of the response must be avoided. In this regard, sufficient system stiffness is required to ensure that

the eigenfrequency f_1 related to the lowest eigenmode $\Phi^{(1)}$ of the wind turbine structure does not coalesce with excitations from the operation frequency of a three-blade turbine and waves. Fig. 1 illustrates the realistic spectra representing aerodynamic and hydrodynamic excitation for the North Sea and the excitation ranges 1P and 3P associated with the mass imbalances in the blades and shadowing effect from the wind each time a blade passes the tower, respectively. The forcing frequency 1P is the frequency of the rotor revolution and the 3P frequency is the frequency of blades passing the tower on a three-bladed turbine. The mass imbalance can be due to differences in the blade weight during installation or cracking in a blade where moisture finds its way. Three possible designs can be chosen for a wind turbine [2]: a very stiff structure with the eigenfrequency f_1 above 3P ("stiff–stiff"), the eigenfrequency f_1 in the range between 1P and 3P ("soft–stiff") or a very soft structure with the eigenfrequency f_1 below 1P ("soft–soft"). A "soft–stiff" wind turbine structure is often chosen in current practice because a huge amount of steel is required for a "stiff–stiff" structure. As the trend is to create larger turbines, rotor blades become longer, generator masses greater and hub heights higher. Thus, the rotation frequency and the first natural frequency will decrease. It may then seem impossible to
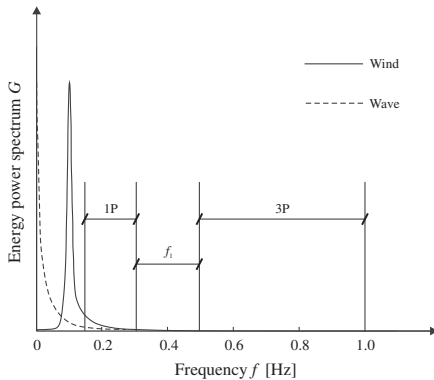
Fig. 1. Excitation range for a modern offshore three-bladed wind turbine structure [1].

design wind turbine structures as "soft–soft" structures, since the risk of the hydrodynamic frequency range falls into 1P is relatively high. Finally, it should be noted that ice breaking [3,4] can induce serve vibrations of offshore wind turbines with excitation frequencies close to the structural eigenfrequencies of offshore wind turbines. Evidently, this effect should only be considered relevant for wind turbines installed in cold regions.

The eigenfrequency f_1 depends on the stiffness of the foundation and tower as well as on the stiffness of the interaction between soil and foundation. In general, the stiffness of the soil–structure interaction is complicated to determine, since cyclic loading might lead to possible softening/hardening of the soil. Kausel [5] made an extensive review of some of the leading developments for solving soil–structure interaction problems. In this regard, finite element models are high-precision methods in simulation of soil–pile interaction problems. Klar and Frydman [6] presented 3-D models and Winkler models based on the commercial two-dimensional finite difference code FLAC under static, seismic, and lateral dynamic loading. In addition, Yegian and Wright [7], Randolph [8], Trochanis et al. [9] and Achmus et al. [10] used the finite element method (FEM) for analysing the dynamic response of pile-supported structures. Al-Wakel et al. [11] implemented a frequency-dependent damping model by using a 3-D FE model, where the saturated soil was subjected to cyclic and harmonic forces. Medina et al. [12] analysed the effect of the soil–structure interaction on the dynamic behaviour of piles. Impedances and kinematic interaction factors of the pile configurations were calculated using a coupled boundary-element/finite-element methodology.

However, since the FEM comes at the cost of great computation times, a beam on nonlinear Winkler foundation (BNWF) model, originally formulated by Winkler [13], is usually employed for design of monopile foundations due to its versatility and efficiency. The pile is modelled as a beam on a nonlinear foundation in which the interaction between pile and soil is modelled as a series of uncoupled springs. The spring stiffness is governed by the so-called p–y curves, where p and y are the resulting force per unit length in the horizontal direction and the corresponding displacement, respectively. Following this approach, Matlock et al. [14], Makris and Gazetas [15] and Nogami et al. [16] analysed the soil–pile interaction for different soil conditions. El Naggar and Novak [17,18] studied the lateral response of monopiles to transient dynamic loading. Based on inner and far field models accounting for the soil nonlinearity and wave propagation away from the pile, reasonable agreement between the developed model and field

tests was obtained. Further, El Naggar and Bentley [19] formulated p–y curves for dynamic soil–pile interaction and Kong et al. [20] presented a simplified method including the effect of separation between the pile and the soil. The last-mentioned has further been studied by Memarpour et al. [21], who developed a BNWF model that accounted for gap formations between pile and soil. Experimental investigations of the interaction between foundation and subsoil have been reported by Bhattacharya and Adhikari [22] and Lombardi et al. [23]. Based on a series of 1-g laboratory tests of a scaled wind turbine on a monopile foundation for different soil conditions, the eigenfrequency related to the lowest eigenmode was evaluated and successfully compared with BNWF models. Sørensen and Ibsen [24] and Damgaard et al. [25] used BNWF models to demonstrate the correlation between scour depths and eigenfrequencies of offshore wind turbines, whereas Barakat et al. [26], Low et al. [27], Fenton and Griffiths [28] and Andersen et al. [29] applied BNWF models for reliability-based soil–pile interaction. A further development of BNWF models for nonlinear dynamic soil–pile interaction was conducted by Allotey and El Naggar [30].

Several formulations of p–y curves exist for sand and clay. Originally, the formulations were developed as a consequence of the oil and gas industry's expansion of offshore platforms, where the soil–pile interaction became crucial to analyse. Design regulations such as API [31] and DNV [32] have adopted the p–y curve formulation for sand proposed by Murchison and O'Neil [33] based on the field tests presented by Cox et al. [34]. For soft and stiff clay, the p–y curve formulations recommended by the design regulations are based on the work performed by Matlock [35], Reese and Welch [36] and Dunnavant and O'Neill [37]. Overall, the p–y curve formulations are based on a number of field tests on fully instrumented flexible piles with significantly smaller slenderness ratio compared to offshore wind turbine foundations. Several assumptions of the derivations of the formulations can be questioned. In the authors' opinion, the most important ones are listed below:

- The soil is not treated as a continuum but as a series of discrete, uncoupled resistances. As a consequence, there is no rigorous description of 3-D failure and deformation mechanisms in the soil surrounding the pile.
- Using the BNWF model, the pile bending stiffness is employed when solving the governing equation. However, the spring stiffness representing the soil stiffness is independent on the pile properties, which is questionable.
- The p–y curve formulations were originally developed and verified for flexible piles with diameters up to 2 m. However, for offshore wind turbines, monopiles with diameters of 4–6 m exist. Hence, a pile which behaves rigidly will have a negative deflection at the pile toe. This deflection causes shearing stresses at the pile toe, which increase the total lateral resistance. In addition, rotations at the pile toe will provide a moment on the pile caused by vertical stresses acting on the pile toe, see Fig. 2. These effects are neglected in the p–y curve formulations.
- The p–y curve formulations are based on full-scale tests on piles installed in rather homogenous soil. However, piles are often installed in a stratum.
- The initial stiffness of the p–y curves is independent of the pile diameter. Sørensen et al. [38] provided an expression for the initial stiffness of sand that depended on the depth below soil surface, the pile diameter and Young's modulus of elasticity of the soil. Validated against laboratory tests, it was found that the initial stiffness of the p–y curves highly depends on the pile diameter.

As it will be shown in this paper, a BNWF model based on the incorporated p–y curves recommended by the design regulations
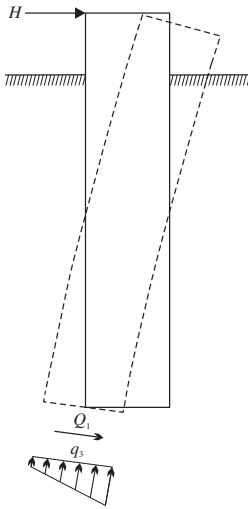
Fig. 2. Forces and stresses acting on the pile toe of a plugged monopile in case of rigid behaviour.

consequently underestimate the eigenfrequency f_1 related to the lowest eigenmode $\boldsymbol{\Phi}^{(1)}$ of offshore wind turbine structures installed on monopile foundations compared to full-scale measurements. The discrepancy might be caused by the above-mentioned assumptions and limitations of the current p–y curve formulations. However, it should be noted that cyclic loading is only in a very simple manner incorporated in the current p–y curve formulations, and the effects of pore fluid pressure build-up in the soil stratum are disregarded, *i.e.* the soil material is described as a single-phase system. Therefore, in order to ameliorate the current results based on the p–y curve method, the soil is treated as a fully saturated porous material, or matrix, where the fluid phase interacts with the stresses carried by the solid phase, *i.e.* the effective stresses. Despite of an offshore wind turbine structure is characterised with low eigenfrequencies, the cyclic behaviour of the structure provides pore pressure build-up in the soil in the relatively low frequency range. Hence, depending on the permeability of the bulk material constituted by the grain skeleton and the pore fluid, the soil material may be partially (un)drained. As it will be shown in this paper, the pore fluid pressure build-up in different soil strata has a significant effect on the soil stiffness—even for cohesionless soils. This in turn provides a dependency between the soil permeability, the soil stiffness and the eigenfrequency of the wind turbine structure.

The aim of this paper is to explain the dynamic behaviour of saturated soil subjected to steady-state vibrations. A thorough numerical investigation based on BNWF models and experimental tests have been carried out in order to evaluate the eigenfrequencies related to the lowest eigenmode of 54 offshore wind turbines. Furthermore, the concept of a Kelvin model is employed and combined with a two-dimensional FE model of the foundation and subsoil in order to illustrate the dependency between soil stiffness and permeability. This in turn makes it possible to analyse the dynamic response of a linear pore-elastic medium, which is used to explain the observed differences between the experimental and the numerical values of the eigenfrequencies of the wind turbine structures. It should be mentioned that the two-dimensional FE model is incorporated to get better results for two-dimensional p–y curves; however the volumetric dynamic flow is ignored.

Following the introduction, Section 2 contains the experimental modal analysis of the investigated offshore wind turbine structures. In addition, the section presents the computational eigenfrequencies based on the Winkler model and compares the results with the experimental tests. A FE model of a monopile placed in saturated soil is developed in Section 3. Finally, in Section 4 the paper is concluded.

2. Eigenfrequencies of offshore wind turbine structures

The eigenfrequency f_1 related to the lowest eigenmode $\boldsymbol{\Phi}^{(1)}$ of an offshore wind turbine and its substructure has a high impact on the dynamic behaviour of the system. A detailed knowledge of the expected frequencies of the excitation forces and of the eigenfrequencies of the wind turbine is crucial. In the following, a thorough data processing of 510 free vibration tests on 54 offshore wind turbine structures is presented. The estimated experimental eigenfrequencies $f_{1,i}$ related to the lowest eigenmode $\boldsymbol{\Phi}^{(1)}$ are supported by a BNWF model approach with p–y curve formulations recommended by API [31] and DNV [32]. Based on a piezocone penetration test for each wind turbine location, the section documents to what extent the recommended BNWF model approach is able to predict the measured eigenfrequencies $f_{1,i}$ related to the lowest eigenmode $\boldsymbol{\Phi}^{(1)}$.

2.1. Wind turbines and site conditions

The wind turbine structures are part of a wind park with a total of 100 Vestas V90–3.0 MW wind turbines located in the North Sea. The turbines are arranged with approximately 500 m between each other and divided into seven rows. The mean water level (MWL), *i.e.* the average height of the water surface, varies between 20 m and 30 m as indicated in Fig. 3.

2.2. Soil conditions

At each wind turbine location, a full-scale piezocone penetration test has been conducted in order to determine the soil properties. By use of the classification method proposed by Robertson [39], the soil unit weight γ is determined for each soil layer. The internal peak angle of friction φ' is found according to the procedure proposed by Bolton [40] with the relative density I_D determined by the expression given by Jamiolkowski et al. [41]. The undrained cohesion c_u is estimated using the total cone resistance q_c as suggested by Robertson et al. [42]. Because no boring profiles have been available, an empirical cone factor N_k equal to 15 has
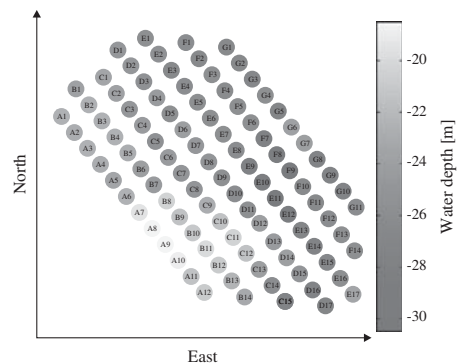

Fig. 3. Mean water level MWL for the investigated wind park.

been used to determine the undrained cohesion c_u. The soil conditions at the wind park consist of different layers that include cohesive and cohesionless soil. As an example, the stratification and properties are summarised in Table 1 for wind turbine location D9. The soil strengths are determined with a 50% quantile.

2.3. Pile and tower conditions

The foundation concept for all the investigated wind turbines is the well-proven monopile concept. The concept consists of a tubular steel pile section with a grouted transition piece. The diameter of the monopile is varying between 4.11 m and 4.9 m and the piles are driven between 21 m and 31 m into the soil. A nominal 80 mm grout annulus between the pile and the transition piece is utilised with an 8.6 m long overlap zone between the outside of the pile and the inside of the transition piece. For location D9, the outer pile diameter OD is 4.5 m, the pile length L is 51.2 m and the pile wall thickness t varies from 60 mm to 75 mm. The pile toe is located 49.7 m below the mean sea level leading to an embedded depth of 24.2 m. The tower is a tubular steel tower which consists of two sections that are bolted together through internal flange-bolt connections. The geometry of the pile, transition piece and tower for location D9 is shown in Fig. 4. The hub height is 54 m above MWL, where a rotor mass and nacelle mass of 42,653 kg and 70,000 kg, respectively, are placed. An oscillation damper is built into the top of the tower just beneath the nacelle. It consists of a pendulum partly immersed in high viscous oil and able to oscillate in the two horizontal directions. The mass of the damper is 6000 kg.

2.4. Free vibration tests

In the period September 2010 to February 2012, a total of 510 free vibration tests have been performed on 54 offshore wind turbines. By use of two accelerometers placed in the nacelle, the tower acceleration in the fore–aft direction y and the side–side direction x has been measured. Fig. 5 shows the raw output time domain signal for a free vibration test on turbine D9. The acceleration in the fore–aft direction a_y and the blade pitch angle θ_b are shown as functions of time t. A sampling frequency f_s of 10 Hz and an 8th order Butterworth low pass filter with a cut-off frequency $F_c = 4f_1$ has been used to establish a sufficiently high signal-to-noise ratio.

For each free vibration test, the damped eigenfrequency $f_{1,d}$ related to the lowest eigenmode $\boldsymbol{\Phi}^{(1)}$ is determined by making least-squares fitting to the crossing times of the resultant acceleration decay a_r. The undamped eigenfrequency f_1 is then determined by the following relation:

$$f_1 = \frac{f_{1,d}}{\sqrt{1 - \zeta_1^2}}, \tag{1}$$

where ζ_1 is the damping ratio related to the lowest eigenmode $\boldsymbol{\Phi}^{(1)}$ found by fitting a linear function to the natural logarithm of the identified peaks and valleys of the resultant acceleration decay a_r. To reduce the aerodynamic effects from the rotor blades when they

Table 1
Soil stratification and characteristic soil properties based on 50% quantile for wind turbine location D9.

	Depth (m)	φ_k' (°)	c_{uk} (kPa)
Loose sand	−5.3	33.2	–
Very stiff clay	−6.7	–	319.3
Very stiff clay	−12.5	–	247.1
Very hard clay	−39.0	–	1036.4

pitch out of the wind, the eigenfrequencies of the wind turbine are only derived from pitch angles θ_b higher than 80°.

2.5. Winkler model approach

The concept of a Winkler foundation model is adopted to estimate the undamped eigenfrequency f_1 related to lowest eigenmode $\boldsymbol{\Phi}^{(1)}$ of the investigated offshore wind turbines. The soil resistance is modelled as uncoupled linear springs with stiffness E_{py}^* acting on an elastic beam as shown in Fig. 6. According to Timoshenko [43], two coupled equations can be formulated to describe beam deflections:

$$G_p A_v \frac{d}{dz}\left(\frac{dy}{dz} - \psi\right) - E_{py}^* y = 0, \tag{2}$$

$$E_p I_{p,x} \frac{d^4 y}{dz^4} - N \frac{d^2 y}{dz^2} + E_{py}^* y = 0, \tag{3}$$

where G_p, A_v, E_p and $I_{p,x}$ are the shear modulus, effective shear area, Young's modulus and second moment of area of the structure, respectively. Further, ψ is the cross-sectional rotation of the structure, whereas y and N are the structural deflection and axial force, respectively. The structure is clamped in the vertical direction at the pile toe, *i.e.* no load transfer is taken into account in the vertical direction and $N = 0$.

The computational model relies on a FE approach, where the wind turbine structure is discretized into a number of 2D beam elements. For each degree of freedom (DOF), the beam element with the length L is exposed to a forced unit displacement or rotation, *cf.* Fig. 7. Hence, assuming that plane sections normal to the beam axis remain plane and normal to the beam axis during the deformation, the shape functions of a cubic spline Φ_i are given by

$$\boldsymbol{\Phi} = \begin{bmatrix} \Phi_1 \\ \Phi_2 \\ \Phi_3 \\ \Phi_4 \end{bmatrix} = \begin{bmatrix} 2\xi^3 - 3\xi^2 + 1 \\ (\xi^3 - 2\xi^2 + \xi)L \\ -2\xi^3 + 3\xi^2 \\ (\xi^3 - \xi^2)L \end{bmatrix}, \quad \xi = \frac{z}{L}. \tag{4}$$

Based on the strong formulation according to Eq. (3) with the axial deformation omitted, the weak formulation is obtained by multiplying Eq. (3) with an arbitrary function $v(z)$ and integrating over the element length L, *i.e.*,

$$\int_0^L v(z) \frac{d^2}{dz^2}\left(E_p I_{p,x} \frac{d^2 y}{dz^4}\right) dz + \int_0^L v(z) E_{py}^* y \, dz = 0. \tag{5}$$

Using the FE approximation $y(z) = \boldsymbol{\Phi a}$ and $v(z) = \boldsymbol{c}^T \boldsymbol{\Phi}^T$, where a_i is the nodal displacement/rotation and c_i is a constant, Eq. (5) may advantageously be rewritten in the form:

$$\boldsymbol{c}^T \int_0^L \frac{d^2 \boldsymbol{\Phi}^T}{dz^2} E_p I_{p,x} \frac{d^2 \boldsymbol{\Phi}}{dz^4} dz \boldsymbol{a} + \boldsymbol{c}^T \int_0^L \boldsymbol{\Phi}^T E_{py}^* \boldsymbol{\Phi} dz \boldsymbol{a}$$
$$= \boldsymbol{c}^T \boldsymbol{a} \boldsymbol{k}_{e,p} + \boldsymbol{c}^T \boldsymbol{a} \boldsymbol{k}_{e,py} = 0, \tag{6}$$

where $\boldsymbol{k}_{e,p}$ and $\boldsymbol{k}_{e,py}$ are the element stiffness matrices of the wind turbine structure and subsoil, respectively. Whereas $\boldsymbol{k}_{e,p}$ can be found analytically in the form [44],

$$\boldsymbol{k}_{e,p} = \frac{EI_{p,x}}{L^3} \begin{bmatrix} 12 & 6L & -12 & 6L \\ 6L & 4L^2 & -6L & 2L^2 \\ -12 & -6L & 12 & -6L \\ 6L & 2L^2 & -6L & 4L^2 \end{bmatrix}, \tag{7}$$

numerical integration is used to derive $\boldsymbol{k}_{e,py}$. Hence, rather than modelling the soil as a number of discrete springs connected to the element nodes, a consistent approach is used, where the soil is modelled as a continuous spring over each element. For each
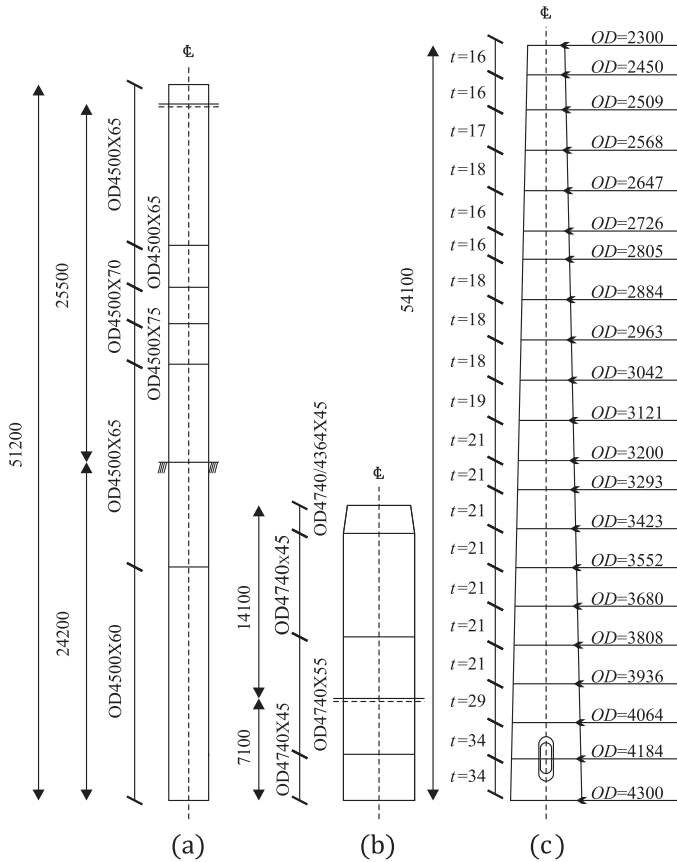
Fig. 4. Geometry of the offshore wind turbine structure at location D9 decomposed into: (a) monopile foundation, (b) transition piece, (c) tower. All dimensions are in millimetres. As an example, OD4740X45 corresponds to a section with outer diameter *OD* = 4740 mm and thickness *t* = 45 mm.
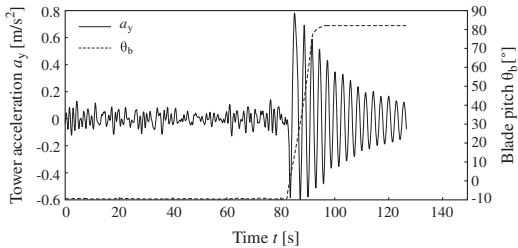

Fig. 5. Fore–aft acceleration a_y in the nacelle and pitch angle θ_b as functions of time t.

integration point along the element of the pile, E_{py}^* is evaluated and Simpson integration is used to determine $\mathbf{k}_{e,py}$. Keep in mind that this procedure is in contrast to calculations previously presented in the literature, where the soil is modelled as discrete springs acting in the finite element nodes, meaning that an accurate description requires a lot of elements. This is avoided by modelling the soil springs as being continuous over the elements.

The stiffness E_{py}^* depends on the soil properties. In this study, E_{py}^* is chosen as the initial slope of the p–y curves. Based on the findings from O'Neill and Murchison [45], API [31] and DNV [32] recommend the following expression for the initial stiffness E_{py}^* for piles located in sand:

$$E_{py}^* = \frac{dp}{dy}\bigg|_{y=0} = \frac{d}{dy} A p_u \tanh\left(\frac{kz}{A p_u} y\right)\bigg|_{y=0} = A p_u \frac{\frac{kz}{A p_u}}{\cosh^2\left(\frac{kz}{A p_u} y\right)}\bigg|_{y=0} = kz. \quad (8)$$

Here, p_u is the ultimate soil resistance, k is the initial modulus of subgrade reaction and z is the depth below the soil surface. A is a dimensionless factor depending on whether static or cyclic loading conditions are present. For static loading $A = (3.0 - 0.8\frac{z}{D}) \geqslant 0.9$, whereas for cyclic loading $A = 0.9$. However, as it can be observed from Eq. (8), the dimensionless factor A is cancelled out. For clayey soils, DNV [32] recommends to linearise the nonlinear p–y curves from the discretisation point given by the relative displacement $y/y_c = 0.1$ with ordinate value $p/p_u = 0.23$, where $y_c = 2.5\varepsilon_{50}D$. D is the pile diameter and ε_{50} is the strain corresponding to a stress of 50% of the ultimate stress in a laboratory stress–strain curve. P_u for clayey soil is given by
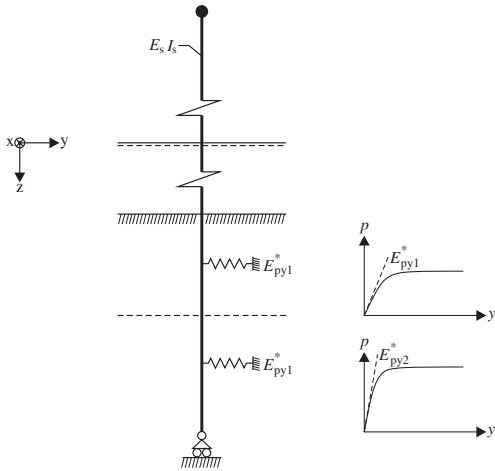
Fig. 6. Computational model for the determination of the undamped eigenfrequency f_1 related to the lowest eigenmode $\boldsymbol{\Phi}^{(1)}$.
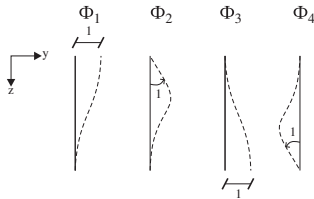

Fig. 7. Shape functions of a 2D beam element.

$$P_u = \max\left(\left(3 + \frac{\gamma'}{c_u}z + \frac{J}{D}z\right)c_u D; 9c_u D\right), \tag{9}$$

where γ is the submerged unit weight, c_u is the undrained shear strength and J is an empirical dimensionless parameter.

Using a similar approach, the structural element mass matrix $\boldsymbol{m}_{e,p}$ reads [44]

$$\boldsymbol{m}_{e,p} = \int_0^L \Phi^T \Phi \rho_p A_p dz = \frac{\rho_p A_p L}{420} \begin{bmatrix} 156 & 22L & 54 & -13L \\ 22L & 4L^2 & 13L & -3L^2 \\ 54 & 13L & 156 & -22L \\ -13L & -3L^2 & -22L & 4L^2 \end{bmatrix}, \tag{10}$$

where ρ_p, and A_p are the mass density and the section area of the structure, respectively. The mass of the nacelle and rotor is added as a concentrated mass in the top node. Likewise, masses of the flanges and internal equipment are added as concentrated masses. The monopile is assumed to be flooded, i.e. the mass of the water within the monopile is added as dead weight. Water around the monopile is applied as added mass according to DNV [32]. Hence, for each element below MWL, the added mass is determined in terms of the hydrodynamic inertia coefficient C_m, the outer area of the pile per unit length A_p, the pile length L_p and the water density ρ_w, i.e. $m = (C_m - 1)A_p L_p \rho_w$. $C_m = 1.2$ has been used in the current study. To account for the increased mass and stiffness in the presence of the grout annulus between the pile and the transition piece, an equivalent steel wall thickness is used.

Assembling the global system stiffness and mass matrices and applying the nodal boundary conditions, the following eigenvalue problem is solved:

$$\boldsymbol{M}_p \ddot{\boldsymbol{u}} + (\boldsymbol{K}_p + \boldsymbol{K}_s)\boldsymbol{u} = \boldsymbol{0}, \tag{11}$$

where $\boldsymbol{M}_p$ is the global structural stiffness matrix and $\boldsymbol{K}_p$ and $\boldsymbol{K}_s$ are the global stiffness matrices of the wind turbine and subsoil, respectively. $\boldsymbol{U}(t)$ is the generalised displacement and rotational vector. In order to find the undamped eigenfrequency f_k for the kth eigenmode $\boldsymbol{\Phi}^{(k)}$, a harmonic function is applied as a solution to Eq. (11)

$$u(t) = \mathrm{Re}\big(\boldsymbol{\Phi}^{(k)} e^{i\omega_k t}\big), \tag{12}$$

where it is used that the kth angular eigenfrequency ω_k of the harmonic motion $\boldsymbol{u}(t)$ is given by $\omega_k = 2\pi f_k$. Inserting Eq. (12) into Eq. (11) makes it possible to find the kth undamped eigenfrequency f_k and corresponding eigenmode $\boldsymbol{\Phi}^{(k)}$ by solving the frequency condition:

$$det\big((\boldsymbol{K}_p + \boldsymbol{K}_s) - \omega_k^2 \boldsymbol{M}_p\big) = 0. \tag{13}$$

The number of beam elements is based on a convergence test indicating that 140 elements and thereby system matrices with the dimension 282×282 are sufficient in order to evaluating the undamped eigenfrequency f_1 related to lowest eigenmode $\boldsymbol{\Phi}^{(1)}$.

2.6. Comparison of experimental and computational eigenfrequencies

For the experimental investigations, a minimum of five tests for each turbine is required to sustain a decent reliability level. Fig. 8 shows the comparison of the measured and computational eigenfrequencies $f_{1,i}$. As indicated, an apparent trend is observed, where all the measured eigenfrequencies are higher than the corresponding calculated values, i.e. the minimum, mean and maximum values of the measured undamped eigenfrequencies for each turbine are 2–13% higher as shown in Fig. 8a–c, respectively.

Keep in mind that soil properties are of a random nature characterised by a high degree of uncertainty related to the calibration of the soil characteristics. Nevertheless, a systematic tendency of underestimating the eigenfrequencies is observed that may not only be caused by the stochastic soil properties. Further, it should be noted that in case of fixed boundary conditions at the seabed, i.e. no inclusion of soil–structure interaction, the computational eigenfrequencies are all significantly higher than the corresponding measured values, cf. Fig. 9.

According to Sørensen and Ibsen [24] and Damgaard et al. [25], the measured eigenfrequencies are sensitive to sediment transportation at seabed, where scour effects are able to change the eigenfrequency f_1 related to the lowest eigenmode $\boldsymbol{\Phi}^{(1)}$ up to 8% due to compaction of the backfill material. The environmental effects have not been considered in the computational model. Nevertheless, the distinct tendency of underestimating the eigenfrequency f_1 may indicate that the soil stiffness is estimated too low. It is believed that the cyclic motion of the monopile generates a pore pressure for saturated soil. Since the bulk modulus of water is significantly higher than the bulk modulus of the matrix material, the soil stiffness will increase in this range. The postulate encourages the authors to investigate and illustrate the variation of the soil stiffness versus the soil permeability.

3. Computational model of saturated soil

In order to elucidate the difference between the measured and calculated eigenfrequencies, a two-dimensional poroelastic FE model subjected to a harmonic forced displacement is considered. Based on the FE approach and utilising a Kelvin model, the soil stiffness is determined.
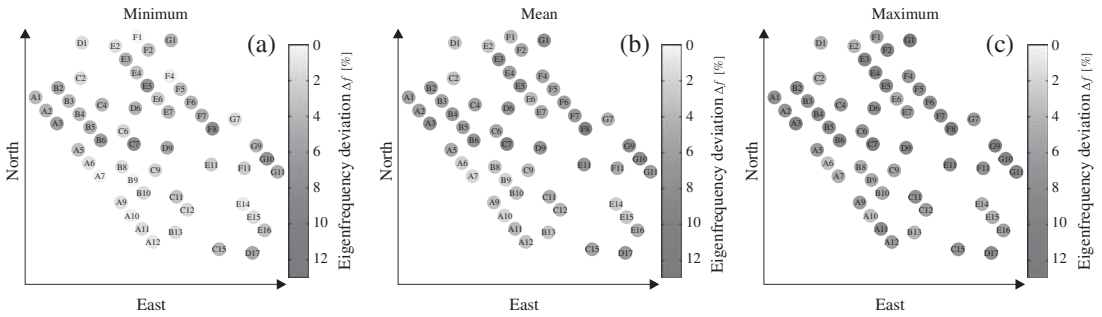
Fig. 8. Deviations between measured and calculated undamped eigenfrequencies $f_{1,i}$ related to the lowest eigenmode $\Phi^{(1)}$: (a) comparison with minimum values of measured data, (b) comparison with mean values of measured data, and (c) comparison with maximum values of measured data.

3.1. Model description

A two-dimensional axisymmetric solid circular cylinder with radius R, as shown in Fig. 11, is surrounded by saturated soil. The arc-boundary, which represents the common border between the solid pile and the saturated soil, is subjected to a harmonic sinusoidal forced displacement in the horizontal x-direction with the cyclic frequency ω in the time domain.

The soil is considered as an isotropic and poroelastic material. For the saturated soil, the Young's modulus E_s, the permeability k_s, the Poisson's ratio v_s, the specific weight γ, the void ratio e_s and the porous bulk moduli K_s and K_f (which encompass the bulk modulus of grains and the bulk modulus of fluid) are defined in order to incorporate the pore water pressure in the poroelastic medium. The mesh consists of 4-noded quadrilateral elements with linear interpolation of the displacement and pore pressure. The porous medium is modelled in ABAQUS [46] by attaching the FE mesh to the solid phase. Liquid can flow through this mesh. Here, it can be mentioned that while the pore pressure p is presents in the fluid and solid phase, the effective stresses σ'_{ij} are carried solely by the solid skeleton. Given that the solid phase only constitutes the fraction $(1 - n)$ of the entire matrix (n is the porosity), the total stress in the solid phase $\sigma_{s_{ij}}$ actually is: $\sigma_{s_{ij}} = \sigma'_{ij}/(1-n) + p\delta_{ij}$. Here δ_{ij} is the Kronecker delta and the pore pressure is considered positive in compression. By using the flowchart in Fig. 10, the desired properties can be calculated.

The inp format file and CPE4P element are employed to get the requested outputs from ABAQUS such as displacement and pore pressure. To reduce time consuming and avoid any mistakes it is better to do much of the simulation process automatically. In this regard and calculating desired results the Python program is employed so that it can be called from MATLAB and then executes ABAQUS. The post processing can be done with any other software. Here, the MATLAB is employed to call Python, which is why it is used for post processing.

The pore pressure and displacements are considered zero at the exterior boundary and the sinusoidal periodic displacement in the horizontal direction is applied for the semi-circle boundary. An illustration of the numerical model is shown in Fig. 11.
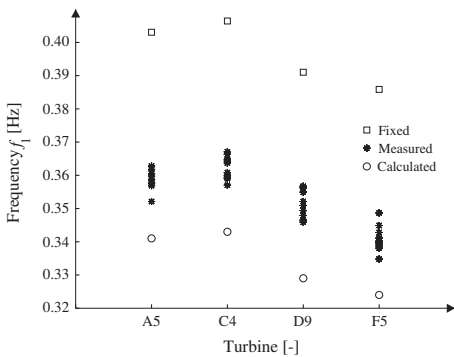

Fig. 9. Comparison of measured and calculated undamped eigenfrequencies $f_{1,i}$ related to the lowest eigenmode $\Phi^{(1)}$ for selected turbines. Calculated eigenfrequencies for fixed boundary conditions at the seabed is included.
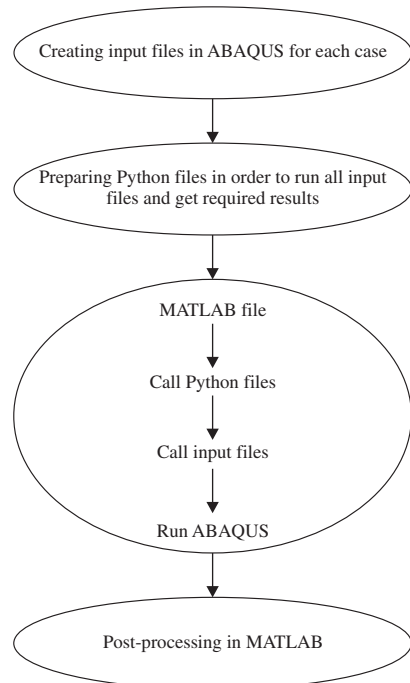

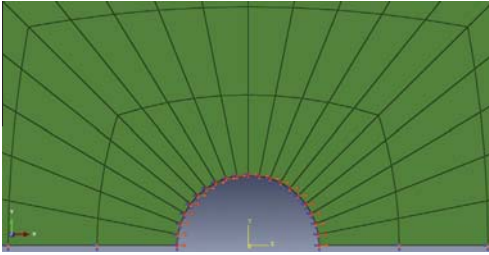**Fig. 10.** Flow chart of the computer program.

Fig. 11. Two-dimensional finite-element model of an offshore wind turbine foundation and the surrounding soil.

To illustrate the elastic solutions of this study, a solid cylinder with radius $R = 3.0$ m is considered. The material properties listed in Table 2 are used.

It should be noted that the values of Young's modulus E_s, Poisson's ratio v_s and void ratio e_s correspond to dense, well graded sand. The bulk modulus of grain K_s is valid for all quartz sands and about the same for other minerals.

3.2. Theoretical approach

For different values of soil permeability k covering different types of soil and excitation frequencies of the harmonic forced displacement f_{disp}, the aim is to evaluate to what extent the influence of pore water provides additional soil stiffness. Based on the FE model described in the previous section, the phase shift between the forced displacement and mean value of the reaction force at the semi-circle boundary can be determined in the time domain. Hence, the spring and dashpot constants of a Kelvin model can be determined for each soil permeability k_s and excitation frequency of the harmonic forced displacement f_{disp}, cf. Fig. 12. According to Newton's second law, the equation of motion for the Kelvin model reads:

$$\eta \dot{x} + \Delta x = F. \tag{14}$$

Here, η, Δ and F are the damping, stiffness and reaction force, respectively, while x and $\dot{x}$ represent the displacement and the velocity, respectively. For a periodic sinusoidal load, the external force $F(t)$ can be written as,

$$F(t) = \text{Im}\{F_0 e^{i\omega t}\} = F_0 \sin(\omega t), \tag{15}$$

where ω is the circular frequency of the load. If it is assumed that the force amplitude F_0 is real, the solution for the displacement $x(t)$ is now also written as,

$$x(t) = \text{Im}\{X e^{i\omega t}\} = x \sin(\omega t) \tag{16}$$

where X is real number. Substitution of Eqs. (15) and (16) into the differential equation, Eq. (14), provides:

$$(\eta \omega X \cos(\omega t) + \Delta \sin(\omega t))X = F_0 \sin(\omega t) \tag{17}$$

The left hand side of Eq. (17) can be written as:

$$\eta \omega X \cos(\omega t) + \Delta X \sin(\omega t) = X\Delta \left(\overbrace{\frac{\eta \omega}{\Delta}}^{\tan \varphi} \cos(\omega t) + \sin(\omega t) \right)$$

$$= \overbrace{\frac{\eta \omega x}{\cos(\varphi)}}^{F_{R0}} \sin(\omega t + \varphi)$$

$$= F_{R0} \sin(\omega t + \varphi) = F_R \tag{18}$$

The reaction force F_R at the semi-circle boundary is in a sinusoidal form with the phase angle φ. As an example, the reaction force F_R and forced displacement $x(t)$ are shown in Fig. 13 for one simulation. As earlier mentioned, by calculating the phase angle φ between the reaction force F_R and the forced-displacement $x(t)$ and having the amplitude of the reaction force F_{R0}, the stiffness Δ and the damping η can be determined from Eq. (18) for each time step. It is worth to mention that the stiffness is calculated after the first period in order to have the steady state results.

3.3. System stiffness for different values of soil permeability

Fig. 14 illustrates the trend of the non-dimensional stiffness Δ due to sinusoidal periodic loading for different geometries of the soil box around the pile. As expected, the behaviour of the two models is generally the same. This is especially the case for undrained conditions, where no dissipation effects are present. For increasing permeability k_s, higher deviation is obtained. In the following, a soil box dimension of 1000 m × 1000 m is used.

The variation of the non-dimensional stiffness Δ for different values of soil permeability k_s and frequencies of the forced displacement f_{disp} is presented in a semi-logarithmic plot in Fig. 15. The values of the excitation frequencies f_{disp} represent typical load frequencies acting on offshore wind turbines. Several interesting observations can be made:

- For low and high values of the soil permeability k_s, indicating fully undrained and drained soil behaviour, respectively, the stiffness Δ is independent of the frequency of the forced displacement f_{disp}.
- In the transient state between fully undrained and drained soil behaviour, the frequency of the forced displacement f_{disp} has a high influence on the stiffness Δ. For increasing forced displacement frequency $f_{disp} \in [0.01; 0.4]$ Hz, the pore pressure p in both the fluid and solid phase will increase resulting in a stiffness increase.
- Steady state conditions are reached for permeabilities $k_s > 1$ m/s, i.e. the static soil stiffness is represented for high values of k_s independent of the frequency of the forced displacement f_{disp}.

It might be argued that the higher stiffness in the clayey soils is already considered in the derivation of the p–y curves, because of undrained conditions. Probably, the interesting part of Fig. 15 can be related to quartz sands where the usual approach is not accurate. According to Section 2, the soil conditions for the investigated

Table 2
Material properties of the investigated saturated soil.

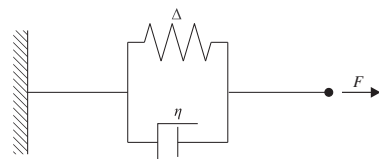|	
Young's modulus E_s (Pa)	1.9272×10^8
Poisson's ratio v_s (−)	0.28
Void ratio e_s (−)	0.50
Bulk modulus of grain K_s (Pa)	3.6×10^{10}
Bulk modulus of fluid K_f (Pa)	2×10^9

Fig. 12. Kelvin model consisting of a spring and a dashpot.
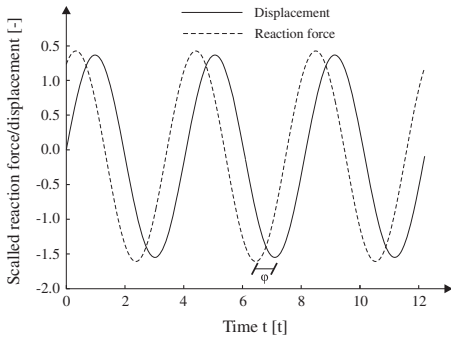
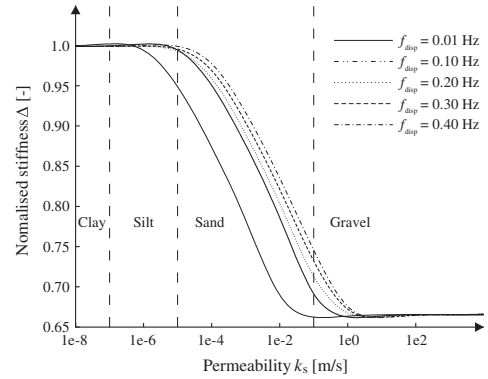**Fig. 13.** Variation of scaled reaction force and displacement versus time.

Fig. 15. Normalised stiffness Δ as a function of the permeability k_s for different excitation frequencies of the forced displacement f_{disp}.
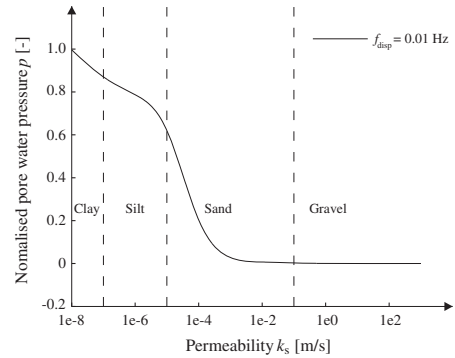
offshore wind turbine structures vary from clayey soils to sandy soils. As indicated in Fig. 15, the stiffness Δ for cohesionless soils is able to increase with approximately 23% when the frequency of the forced displacement increases from $f_{disp} = 0.01$ Hz to $f_{disp} = 0.40$ Hz. In addition, for sandy soils $k_s > 1e - 2$ m/s that govern the top layer of the investigated wind turbine locations, the permeability k_s has a high influence on the stiffness Δ that increases with approximately 50%. Since the eigenfrequency related to the lowest eigenmode f_1 for the investigated turbines is around 0.35 Hz, the cyclic behaviour of the foundations related to this mode provides a significant increase in the soil stiffness due to the fact that the pore pressure build-up only dissipates slowly. The effects are not accounted for in the p–y curve formulations recommend by the design regulations, which therefore may explain some parts of the observed deviations between calculated and measured eigenfrequencies.

It should be noticed from Fig. 15 that the rate of reduction of the normalised stiffness Δ versus increasing permeability k_s is the same for different values of excitation frequencies. Fig. 16 shows the normalised maximum pore pressure p versus permeability k_s for an excitation frequency $f_{disp} = 0.01$ Hz. As indicated, the change in the curvature of the variation between pore pressure p and permeability k_s corresponds very well to the change of the slope of variation between normalised stiffness Δ and permeability k_s according to Fig. 15. Hence, this substantiates the conclusion that the dramatically increase in the stiffness Δ for a sandy seabed is due to nearly undrained soil behaviour.
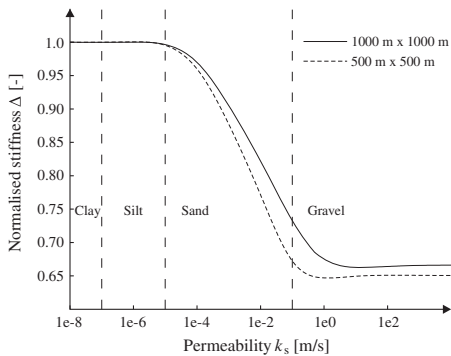

Fig. 16. Normalised pore water p as a function of the permeability k_s for an excitation frequency of the forced displacement $f_{disp} = 0.01$ Hz.
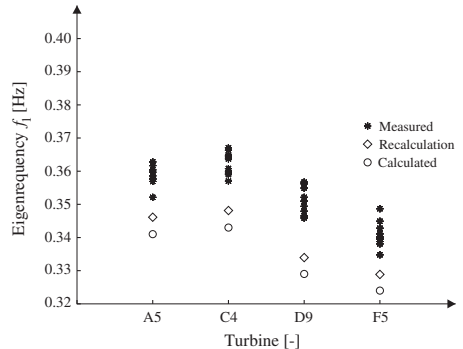

Fig. 17. Comparison of measured, calculated and recalculated undamped eigenfrequencies $f_{1,i}$ related to the lowest eigenmode $\Phi^{(1)}$ for selected turbines.

Recalculation of the undamped eigenfrequency f_1 related to the lowest eigenmode $\Phi^{(1)}$ with a stiffness increase as suggested in Fig. 15 has been performed. In this regard, the initial stiffness E_{py}^* of the implemented p–y curves for sand in the computational

Fig. 14. Normalised stiffness Δ as a function of the permeability k_s for different dimensions of the soil box around the pile.

model is increased with 20%. As indicated in Fig. 17, the recalculation of the eigenfrequency f_1 shows a better agreement between calculated and measured frequencies. A substantial improvement of the eigenfrequency f_1 related to the lowest eigenmode $\boldsymbol{\Phi}^{(1)}$ of approximately 29%, 27%, 22% and 29% is obtained for the four investigated wind turbines A5, C4, D9 and F5, respectively. Nevertheless, even though the soil stiffness is increased due to pore pressure generation during cyclic motion, deviations between recalculated and measured eigenfrequencies are still observed. The assumptions and limitations of the p–y curve formulations suggested by the design regulations as described in Section 1 may cause this tendency.

By considering a wide range of offshore wind turbines, further work can be carried out to generate more data to understand the dynamic behaviour of offshore structures with different kind of nonlinearity in material, soil–pile interaction and thermomechanical loading. Future work also is needed to consider the volumetric dynamic flow, especially in the case of a bucket foundation.

4. Conclusions

In this paper, the dynamic properties of offshore wind turbines are investigated. A through data processing on free vibration tests is performed in order to evaluate the eigenfrequency related to the lowest eigenmode. Utilising a Winkler model approach with p–y curve formulations recommended by the design regulations, the computational eigenfrequencies are compared with the experimental results. To strengthen the comparison, a two-dimensional finite element model of a pile placed in saturated soil is considered. For different frequencies of a forced displacement, the stiffness based on a Kelvin model is determined. Three interesting conclusions can be drawn:

- Based on 510 free vibration tests, it is found that the eigenfrequencies related to the lowest eigenmode of 54 offshore wind turbines are significantly higher than the ones obtained by a Winkler model. Deviations between 2% and 13% are obtained.
- The effect of pore pressure build-up seems to increase the soil stiffness significantly. Since the linear soil springs used for the Winkler model approach are based on few static and cyclic experimental tests of piles with a slenderness ratio of $L/D < 34.4$, the effects of the dynamic behaviour of saturated soil are neglected in the derivation. This in turn may to some extent explain the observed deviations between experimental and computational eigenfrequencies of the investigated offshore wind turbines.
- Based on a Winkler model, an increase of the soil stiffness in sandy soils due to pore pressure generation provides a significant improvement of the recalculated eigenfrequency.

Acknowledgement

References

[1] Leblanc C. Design of offshore wind turbine support structures – selected topics in the field of geotechnical engineering. PhD thesis. Denmark: Department of Civil Engineering, Aalborg University; 2009.
[2] Kühn M. Dynamics and design optimisation of offshore wind energy conversion systems. PhD thesis. Netherland: Delft university wind energy research institute; 2003.
[3] ISO 19902. Petroleum and natural gas industries – fixed steel offshore structures. The European Committee for Standardization, B-1050 Brussels; 2007.
[4] Tian Y, Huang Y. The dynamic ice loads on conical structures. Ocean Eng 2013;59:37–46.
[5] Kausel E. Early history of soil–structure interaction. Soil Dyn Earthquake Eng 2010;30(9):822–32.
[6] Klar A, Frydman S. Three-dimensional analysis of lateral pile response using two-dimensional explicit numerical scheme. J Geotech Geoenviron Eng, ASCE 2002;128(9):775–84.
[7] Yegian MK, Wright SG. Lateral soil resistance-displacement relationships for deep pile foundations in soft clays. In: Proceedings of the 5th annual offshore technology conference. Texas; 1973.
[8] Randolph MF. The response of flexible piles to lateral loading. Géotechnique 1981;31(2):247–59.
[9] Trochanis AM, Bielak J, Christiano P. Three-dimensional nonlinear study of piles. ASCE J Geotech Eng 1991;117(3):429–47.
[10] Achmus M, Yu-Shu Kuo, Abdel-Rahman K. Behavior of monopile foundations under cyclic lateral load. Comput Geotech 2009;36:725–35.
[11] Al-Wakel SAF, Fattah MY, Karim HH. Dynamic analysis of foundations on saturated clay using an energy absorbing layer. Eng Technol J 2011;29(11):2189–201.
[12] Medina C, Aznárez JJ, Padrón LA, Maeso O. Effects of soil–structure interaction on the dynamic properties and seismic response of piled structures. Soil Dyn Earthquake Eng 2013;53:160–75.
[13] Winkler E. Die Lehre von Elasticzitat und Festigkeit 1867.
[14] Matlock H, Foo SH, Bryant L. Simulation of lateral pile behavior. Proc, Earthquake Eng Soil Dyn, ASCE, New York 1978:600–19.
[15] Makris N, Gazetas G. Dynamic pile-soil–pile interaction. Part II: Lateral and seismic response. Earthquake Eng Struct Dyn 1992;21:145–62.
[16] Nogami T, Otani J, Konagai K. Nonlinear soil/pile interaction/model for dynamic lateral motion. J Geotech Eng/ASCE 1992;118(1):89–106.
[17] El Naggar M, Novak M. Nonlinear lateral interaction in pile dynamics. Soil Dyn Earthquake Eng 1995;14:141–57.
[18] El Naggar M, Novak M. Nonlinear analysis for dynamic lateral pile response. Soil Dyn Earthquake Eng 1996;15:233–44.
[19] El Naggar M, Bentley KJ. Dynamic analysis for laterally loaded piles and dynamic p–y curves. Can Geotech J 2000;37(6):1166–83.
[20] Kong D, Luan M, Ling X, Qiu Q. A simplified computational method of lateral dynamic impedance of single pile considering the effect of separation between pile and soils. In: Luan M, Zen K, Chen G, Nian T, Kasama K, editors. Recent development of geotechnical and geo-environmental engineering in Asia, PT: B. CT: 4th Asian joint symposium on geotechnical and geo-environmental engineering (JS-Dalian 2006). CY: NOV 23–25. CL: Dalian, PEOPLES R CHINA. UT: ISI:000279628900023; 2006. p. 138.
[21] Memarpour MM, Kimiaei M, Shayanfar M, Khanzadi M. Cyclic lateral response of pile foundations in offshore platforms. Comput Geotech 2012;42:180–92.
[22] Bhattacharya S, Adhikari S. Experimental validation of soil–structure interaction of offshore wind turbines. Soil Dyn Earthquake Eng 2011;31:805–16.
[23] Lombardi D, Bhattacharya S, Wood DM. Dynamic soil–structure interaction of monopile supported wind turbines in cohesive soil. Soil Dyn Earthquake Eng 2013;49:165–80.
[24] Sørensen SPH, Ibsen LB. Assessment of foundation design for offshore monopiles unprotected against scour. Ocean Eng 2013;63:17–25.
[25] Damgaard M, Ibsen LB, Andersen LV, Andersen JKF. Cross-wind modal properties of offshore wind turbines identified by full scale testing. J Wind Eng Ind Aerodyn 2013;116:94–108.
[26] Barakat SA, Malkawi AIH, Tahat RH. Reliability-based optimization of laterally loaded piles. Struct Saf 1999;21(1):45–64.
[27] Low BK, The CI, Tang WH. Stochastic nonlinear p–y analysis of laterally loaded piles. Proc of the eigth international conference on structural safety and reliability (ICOSSAR). Newport Beach, California; 2001. p. 17–22.
[28] Fenton G, Griffiths DV. Reliability-based deep foundation design. In Probabilistic applications in geotechnical engineering, GSP No. 170, proceedings of geo-denver 2007 symposium. Denver, CO: American Society of Civil Engineers. Fixity, Prague; 2007.
[29] Andersen LV, Vahdatirad MJ, Sichani MT, Sørensen JD. Natural frequencies of wind turbines on monopile foundations in clayey soils-probabilistic approach. Comput Geotech 2012;43:1–11.
[30] Allotey NEl, Naggar MH. Generalized dynamic Winkler model for nonlinear soil–structure interaction analysis. Can Geotech J 2008;45(4):560–73.
[31] API. Recommended practice for planning, designing and constructing fixed offshore platforms-working stress design. API RPZA-WSD, 20 ed. Washington, D.C., USA: American Petroleum Institute; 2000.
[32] DNV. Design of offshore wind turbine structures. DNV-OS-J101. Det Nordsee Veritas, Det Norske Veritas Classification A/S; 2010.
[33] Murchison JM, O'Neill MW. Evaluation of p–y relationships in cohesionless soils. Analysis and design of pile foundations. In: Proc of the symposium in conjunction with the ASCE National Convention; 1984. p. 174–91.
[34] Cox WR, Reese LC, Grubbs BR. Field testing of laterally loaded piles in sand. In: Proceedings of the sixth annual O_shore technology conference. Houston, Texas, Paper No. OTC 2079; 1974.
[35] Matlock H. Correlation for design of laterally loaded piles in soft clays. 2nd Offshore technology conference. Houston, Texas; 1970. p. 577–94.

[36] Reese LC, Welch RC. Lateral loading of deep foundation in sti_clay. J Geotech Eng, Div 1975;101(7):633–49.
[37] Dunnavant TW, O'Neill MW. Experimental *p–y* model for submerged stiff clay. J Geotech Eng 1989;115(1):95–114.
[38] Sørensen SPH, Ibsen LB, Augustesen AH. Effects of diameter on initial stiffness of *p–y* curves for large-diameter piles in sand. Numer Methods Geotech Eng NUMGE 2010:907–12.
[39] Robertson PK. Soil classification using the cone penetration test. Can Geotech J 1990;27(1):151–8.
[40] Bolton MD. The strength and dilatancy of sands. Geo-technique 1986;36(1):65–78.
[41] Jamiolkowski M, Lo Presti DCF, Manassero M. Evaluation of relative density and shear strength of sands from CPT and DMT. Soft Ground Construction 2001:201–38.

[42] Robertson PK, Lunne T, Powell JJM. Cone penetration testing in geotechnical practice. London: Blackie Acedemic & Professional; 1997.
[43] Timoshenko SP. Strength of materials, part II, advanced theory and problems, 2nd ed., 10th printing. New York: D. Van Nostrand; 1941.
[44] Cook RD, Malkus DS, Plesha ME. Concepts and applications of finite element analysis. 3rd ed. John Wiley & Sons; 1989.
[45] O'Neill MW, Murchison JM. An evaluation of *p–y* relationships in sands. Research Report No. GT-DF02-83, Dep of Civ Eng. TX, USA: University of Houston; 1983.
[46] Dassault Systèmes Simulia Corp. Abaqus 6.12 Analysis User's Manual. Providence, RI, USA: Dassault Systèmes Simulia Corp; 2012.

$p - y - \dot{y}$ curves for dynamic analysis of offshore wind turbine monopile foundations

Authors:
Mehdi Bayat, Lars Vabbersgaard Andersen and Lars Bo Ibsen

D.1   Author's Right

Journal author rights

In order for Elsevier to publish and disseminate research articles, we need publishing rights. This is determined by a publishing agreement between the author and Elsevier. This agreement deals with the transfer or license of the copyright to Elsevier and authors retain significant rights to use and share their own published articles. Elsevier supports the need for authors to share, disseminate and maximize the impact of their research and these rights, in Elsevier proprietary journals* are defined below:

For subscription articles	For open access articles
Authors transfer copyright to the publisher as part of a journal publishing agreement, but have the right to:	Authors sign an exclusive license agreement, where authors have copyright but license exclusive rights in their article to the publisher**. In this case authors have the right to:
• Share their article for Personal Use, Internal Institutional Use and Scholarly Sharing purposes, with a DOI link to the version of record on ScienceDirect (and with the Creative Commons CC-BY-NC- ND license for author manuscript versions)	• Share their article in the same ways permitted to third parties under the relevant user license (together with Personal Use rights) so long as it contains a CrossMark logo, the end user license, and a DOI link to the version of record on ScienceDirect.
• Retain patent, trademark and other intellectual property rights (including raw research data).	• Retain patent, trademark and other intellectual property rights (including raw research data).
• Proper attribution and credit for the published work.	• Proper attribution and credit for the published work.

http://www.elsevier.com/about/company-information/policies/copyright

p-y-$\dot{y}$ curves for dynamic analysis of offshore wind turbine monopile foundations

M. Bayat[*], L. V. Andersen, L.B. Ibsen

Department of Civil Eng., Aalborg University, 9000 Aalborg, Denmark

Abstract

The well-known p-y curve method provides soil-structure interaction that is independent of the load rate. In this paper an improved p-y curve method is proposed by considering the influence of the excitation frequency. For this purpose, a two-dimensional finite-element program is developed for analysis of a segment of an offshore monopile foundation placed in different depths. The intended use of the model is analyses of offshore wind turbines in operation where small-magnitude cyclic response is observed in addition to the quasi-static response from the mean wind force. The response to small-magnitude cyclic loading is analysed by employing coupled equations based on the $\mathbf{u}$-P formulation, i.e. accounting for soil deformation as well as pore pressure. Thus, the paper has focus on the effects of drained versus undrained behaviour of the soil and the impact of this behaviour on the stiffness and damping related to soil-structure interaction at different load frequencies. In order to enable a parameter study with variation of the soil properties, the constitutive model is purposely kept simple. Hence, a linear poroelastic material model with few material parameters is utilized. Based on the two-dimensional model, linear p-y-$\dot{y}$ curves are extracted for the lateral loading of monopiles subjected to cyclic loads. The developed code is verified with findings in the literature.

Keywords: Soil dynamics; Kelvin model; Cyclic load; Offshore foundation.

---

[*] Corresponding author. Tel.: +45 9940 8575; Fax: +45 3 9940 8552. *E-mail*: meb@civil.aau.dk

1. Introduction

A monopile consists of a tubular support structure that extends into the seabed; it is used for installations at water depths of up to 25-35 m [1]. Offshore wind turbine foundations are subjected to time-varying loads from waves, wind and ice, and during operation blade passage across the tower as well as imbalances in the rotor cause cyclic loading. In the literature, there are several approaches to decrease the computational costs and complexity of load analysis on offshore wind turbines [103-106] to satisfy design criteria and avoid failure. The dynamic loads may cause premature failure in the ultimate limit state or the fatigue limit state if resonance occurs or damping is low. The presented methods and computational models are not proved to actually provide reliable results for optimized design. Time-varying load such as cyclic load can cause ultimate and/or serviceability limit failures of offshore foundations. For example, ultimate limit failure of a scaled model wind turbine supported by a monopile in Kaolin clay has been observed by Lombardi et al. [107] by performing a series of laboratory tests. In order to have better appraisal of soil-structure interaction, the coupled flow and deformation associated with the motion of fluid and solid grain particles should be considered. Cyclic loading is an important aspect of offshore design because the environmental loading during extreme storm conditions generally dominates compared with the permanent loading [2]. Accurate predictions of dynamic response are a major design problem. Traditionally, the p-y curve method, which is based on modelling the pile as a beam on a series of uncoupled linear/nonlinear springs representing the interaction between soil and pile, is employed for analysis of pile deflections [3]. The soil-pile interaction is represented by the so-called p-y curves, where p is the resultant force per unit length of the pile and y is the corresponding displacement in the horizontal direction. Some theoretical works have been done to demonstrate the soil-pile interaction for different soil conditions subjected to different types of loading by [4-12]. Further, to validate and compare with theoretical results related to the p-y curve method, some

experimental investigations have been accomplished by [13-16]. Bouzid et al. [108] carried out cyclic triaxial tests followed by monotonic tests and used this to obtain the p-y curves. Some other design guidelines such as American Petroleum Institute (API) [17] and Det Norske Veritas (DNV) [18]/Risø [19] derived and present the formulations of p-y curves for sand and clay. The p-y curve method was developed for small-diameter (D = 0.32 m, D from 0.5 to 3 m), long, flexible and slender piles with length-to-diameter ratios (L/D) generally bigger than 12 in the oil and gas industry. Rigid monopiles with L/D < 12 and diameters from 3.5 to 7 m are typically used for offshore wind turbines. Offshore wind turbine structures are sensitive to rotations and dynamic changes in the pile-soil system. The effect of load rate is not concerned in the p-y curve method. In order to incorporate the effect of load frequency and pore pressure, the coupled equations are needed to illuminate the behaviour of different states in the soil. The other contentions for applying the p-y curve method for wind turbine monopile foundations are not presented for brevity. A literature review regarding to the p-y curve method has been performed by the same authors in their earlier study [20] and the most commonly used models for the p-y curves for liquefied soils were reviewed Dash et al. [109]. The Interested reader may refer to [20-22, 108, 109] and the references therein.

The frequency of cyclic load can impact on the stiffness and damping related to soil-structure interaction. LeBlanc *et al.* [23] studied the response of stiff piles in drained sandy soil subjected to cyclic lateral loading to develop a model for predicting pile rotations in response to repeated cyclic loading. It was established that the pile stiffness increased with the number of cycles, independent of relative density. In this research the effect of load frequency will be considered to introduce, p-y-$\dot{y}$ curves. The existing p-y curve method does not account for two phase material and excess pore pressure in the soil stratum during cyclic loading. In this study a combination of springs and dashpots are employed to interpret the poroelastic response and drive equivalent viscoelastic model. For

simplicity, the linear poroelastic model is employed. Consequently, a linear viscoelastic model in the reduced formulation can be represented. Serviceability requirements for offshore wind turbines allow rotations of 0.5° at the mudline, and soil behaviour is controlled by elasticity rather than plasticity. Essentially, small settlement and rotation of offshore foundations are controlled by viscous linear elastic behaviour [24]. The current design approach based on the p-y curve method disregards the effects of pore fluid pressure build-up in the soil stratum during cyclic loading. Therefore, the current design approach based on the p-y curve method might not be appropriate for monopile foundations. Current design practices need to be improved to be cost-effective and provide a safe and economical design.

Based on presented guidelines by API and DNV regarding to use the Winkler approach in design of monopiles, a set of unconnected springs at each depth is employed to model the soil and these springs are attached along the pile which is modeled as a beam. In this study the same approach is considered to reflect the effect of pore water pressure. By considering the plane strain condition an accurate results may not be obtained, but the presented results for the soil stiffness can be compared with those from the Winkler approach with no pore water. The seepage damping is another important output of this study. So, the purpose of the current research is to obtain a better understanding of the soil stiffness and damping due to saturated soil subjected to a cyclic loading- not to improve the p-y curve method. The stiffness of saturated soil due to pore water flow generated by cyclic motion of monopiles is investigated using the concept of a Kelvin model which combines springs and dashpots. In this manner, the results indicate the relative changes in soil stiffness due to the presence of pore water.

In order to have the effect of pore pressure and soil deformation, two-phase coupled equations are needed. Three famous coupled and dynamic formulations, based on the soil and pore fluid (water) displacements and the pore water pressure (PWP), are the $\mathbf{u} - P - \mathbf{U}$, $\mathbf{u} - P$, and $\mathbf{u} - \mathbf{U}$

equations, where $\mathbf{u}$, P, and $\mathbf{U}$ are the soil skeleton displacement, PWP, and pore water displacement, respectively [25]. Cheng and Jeremić [26] used a fully coupled, inelastic $\mathbf{u} - P - \mathbf{U}$ formulation to simulate the dynamic behaviour of piles in liquefiable soils subjected to seismic loading. In the $\mathbf{u} - P$ formulation, if the fluid phase is considered incompressible, then the Ladyzenskaja-Babuska-Brezzi (LBB) condition needs to be satisfied [27-29]. In this case, the element type for the displacement and pore pressure fields requires special consideration to prevent volumetric locking [30-31]. Considering this restriction, a simple model for numerical analyses is the $\mathbf{u} - P$ formulation that neglects the relative acceleration of the fluid with respect to the solid skeleton. This model is especially useful for low-frequency analysis. Zienkiewicz *et al.* [31] studied the transient and static response of saturated soil which they modeled as a two-phase material based on the $\mathbf{u} - P$ formulation for porous media. Pastor *et al.* [32] used a generalized plasticity approach to describe the behaviour of soil in the $\mathbf{u} - P$ formulation under transient loading. Oka *et al.* [33] applied the FEM and finite difference method (FDM) to investigate numerically the governing equations of soil skeleton and pore water, obtained through application of the $\mathbf{u} - P$ formulation. Karim *et al.* [34] analysed a saturated porous elastic soil layer under cyclic loading by using a 2-D mesh free Galerkin method and the $\mathbf{u} - P$ formulation by having periodic conditions. Tsai [35] examined the viscosity effect on consolidation of poroelastic soil due to groundwater table variation by using the $\mathbf{u} - P$ formulation. A viscoelastic consolidation numerical model was developed. Elgamal *et al.* [36-37] implemented the $\mathbf{u} - P$ model for a two-phase (solid-fluid) problem with multi-surface plasticity, using a finite element method (FEM) to highlight the effect of excitation frequency. Researchers have attempted to solve these coupled equations by various numerical methods [38-40]. Here, however, a two dimensional linear model will be employed to analyze a monopile segment at a given depth.

The proposed model and observation should be considered as an attempt at reconciling the traditional p-y curve method and applying cyclic load. In particular, the model is shown to possess reasonable results in presenting soil stiffness and damping curves over a frequency range relevant for offshore wind turbine. This study deals with a two-dimensional model of an offshore monopile foundation, surrounded by an elastic saturated soil and subjected to cyclic load. The plane strain condition is invoked and small deformation of the soil is assumed. The FEM and the $\mathbf{u} - P$ equations are employed to explore the effects of load frequency on the restoring and dissipative forces. Based on this, contributions to the force p from displacement y and velocity $\dot{y}$ of the pile are determined.

Following this introduction, Section 2 presents different sources of damping in offshore wind turbines and Section 3 contains the governing coupled $\mathbf{u} - P$ equations of the saturated soil. In Section 4, the numerical solution is validated by comparison to the other solutions. Further the model and methodology are described. The stiffness and damping of saturated soil that accounts for rate-dependent behaviour and a p-y-$\dot{y}$ curve method accounting for the load frequency is proposed in Section 5. Some concluding remarks are presented in Section 6.

2. Damping mechanisms

Total damping in offshore wind turbine system is included damping in turbine, tower, foundation and soil. It consists of structural damping, aerodynamic damping (related mainly to the blades) and also shadow damping (tower effect), damping due to water (hydrodynamic damping) and soil damping [41]. While most parts of damping are determined with a high reliability level, this is not the case for soil damping due to complex material behaviour of the soil [42]. There are different types of damping in soil: radiation (or geometric) damping due to the propagation of elastic waves into a larger area or volume; material (or internal) damping which is due to a local

conversion from mechanical energy into heat, induced by friction, viscous and hydrodynamic effects [43-44].

Hajiabadi and Lotfi [45] implemented FEM to analyze the damping for visco-elastic media. Xunqiang *et al.* [46] studied a 3-D damping by FEM in visco-elastic soil. Liang *et al.* [47] applied a 3-D FEM and presented a parametric study of laterally loaded drilled shafts in clay. A hyperbolic *p-y* criterion was developed for cohesive intermediate soil. Harada *et al.* [48] employed a multi-Winkler model based on soil traction for nonlinear soil–foundation interaction during cyclic loading. Viscous damping is commonly employed to capture damping at small strains and low load frequency which is using the first natural mode only [49] and the proposed formulation allowed the use of frequency dependent viscous damping using the full Rayleigh damping. This energy dissipation can be measured by the area of the hysteric loop for nonlinear or plastic material behaviour; it is called hysteretic damping and it is frequency independent [50]. Auersch [51] presented the stiffness and damping for pile foundations regarding to buildings in the elastic half-space by using the boundary element method (BEM). Carbonari *et al.* [52] presented soil–pile interaction and radiation damping by using FEM in the frequency domain. Al-Wakel *et al.* [53] implemented a frequency-dependent damping model by using a 3-D FE model and the unbounded domain was replaced by an absorbing layer of finite thickness with properties that appreciably reduced the wave reflection into bounded domain. The $\mathbf{u} - P$ equations for a foundation on saturated soil were used to simulate the soil skeleton and pore fluid responses. Medina *et al.* [54] estimated the damping for the pile by coupled BEM-FEM while dynamic and kinematic interaction effects were considered. Zania [55] performed a parametric study to determine the eigenfrequency and damping analytically. However, influence of pore water pressure on the soil stiffness and damping during dynamic loading of a monopile has, to the authors' awareness, not been the subject of systematic analysis so far.

3. Governing equations for saturated soil

The total momentum balance for the porous medium is:

$$\sigma_{ij,j} + \rho b_i = \rho \ddot{u}_i + \rho_f \ddot{w}_i \tag{1}$$

where σ_{ij} is the total stress tensor and $\sigma_{ij} = \sigma'_{ij} - \alpha P \delta_{ij}$. Here σ'_{ij} is the effective stress tensor, $\alpha = 1 - \frac{K_T}{K_S}$, where K_T and K_S are the total bulk moduli of the solid matrix and solid particles receptively, P is pore pressure and δ_{ij} is Kronecker's delta: $\delta_{ij} = 1$ when $i = j$, and $\delta_{ij} = 0$ when $i \neq j$. The density of the mixture is $\rho = (1 - n_p)\rho_s + n_p \rho_f$ where n_p, ρ_s and ρ_f are the porosity and the densities of the solid phase and fluid, respectively. Finally, $\ddot{u}_i$ and $\ddot{w}_i$ are the acceleration of the solid skeleton and pseudo-acceleration of the fluid phase relative to the skeleton. Comma subscript and dot superscripts denote derivatives with respect to spatial coordinates and time, respectively. The tensile component of stress and compressive component of pressure are assumed to be positive. The equation for the total coupled system can be written as

$$-P_{,i} - \frac{\dot{w}_i}{k} + \rho_f b_i = \rho_f \left(\ddot{u}_i + \frac{\ddot{w}_i}{n_p} \right) \tag{2}$$

where $k = \frac{k'}{g \rho_f}$, and k' is the hydraulic conductivity, which has the unit of velocity. Further, b_i is the body force per unit mass. The final equation is supplied by the mass conservation of the fluid flow:

$$\dot{w}_{i,i} + \alpha \dot{\epsilon}_{ii} + \frac{\dot{P}}{Q} = 0 \tag{3}$$

where $Q = Q_{sf} = \frac{K_S K_f}{K_S + K_f}$ is the total compression modulus. K_S and K_f are the solid and fluid bulk moduli, respectively [25].

3.1. Governing equation ($\mathbf{u} - P$ formulation)

The relative acceleration of the fluid with respect to the solid skeleton can be ignored for lower frequencies. Then Eq. (1) is rewritten as:

$$\sigma_{ij,j} + \rho b_i = \rho \ddot{u}_i \tag{4}$$

Substituting $\dot{w}_i$ from Eq. (2) into Eq. (3) by taking the derivate of Eq. (2) once with respect to direction i, and ignoring the relative acceleration of the fluid with respect to the solid skeleton, it is obtained that:

$$\left(k\left(-P_{,i} + \rho_f b_i - \rho_f \ddot{u}_i \right) \right)_{,i} + \alpha \dot{\epsilon}_{ii} + \frac{\dot{P}}{Q} = 0 \tag{5}$$

3.2. Boundary conditions

For a model which combines solid and fluid phases, the boundary conditions are defined based on traction, displacement, fluid flow and pore pressure as ($\Gamma = \Gamma_t \cup \Gamma_u$); ($\Gamma = \Gamma_w \cup \Gamma_P$):

$$\sigma_{ij} n_j = \bar{t}_i \qquad\qquad \text{on} \qquad \Gamma = \Gamma_t$$

$$u_i = \bar{u}_i \qquad\qquad \text{on} \qquad \Gamma = \Gamma_u$$

$$n_i \dot{w}_i = n_i k\left(-P_{,i} + \rho_f b_i \right) = \dot{\bar{w}}_n = -\bar{q}_n \qquad \text{on} \qquad \Gamma = \Gamma_w$$

$$P = \bar{P} \qquad\qquad \text{on} \qquad \Gamma = \Gamma_P \tag{6}$$

3.3. Numerical solutions of governing equations

By ignoring the acceleration term in Eq. (5), the FE system of equations for the $\mathbf{u} - P$ formulation can be written as [25]:

$$\begin{bmatrix} M_{KijL} & 0 \\ 0 & 0 \end{bmatrix} \begin{bmatrix} \ddot{\bar{u}}_{Lj} \\ \ddot{\bar{P}}_N \end{bmatrix} + \begin{bmatrix} 0 & 0 \\ Q_{LjM} & S_{MN} \end{bmatrix} \begin{bmatrix} \dot{\bar{u}}_{Lj} \\ \dot{\bar{P}}_N \end{bmatrix} + \begin{bmatrix} K_{KijL}^{ep} & -Q_{KiN} \\ 0 & H_{MN} \end{bmatrix} \begin{bmatrix} \bar{u}_{Lj} \\ \bar{P}_N \end{bmatrix} = \begin{bmatrix} f_{Ki}^u \\ f_M^P \end{bmatrix} \tag{7}$$

and

$$\begin{bmatrix} \boldsymbol{M} & 0 \\ 0 & 0 \end{bmatrix} \begin{bmatrix} \ddot{\overline{\boldsymbol{u}}} \\ \ddot{\overline{\boldsymbol{P}}} \end{bmatrix} + \begin{bmatrix} 0 & 0 \\ \boldsymbol{Q}^{\mathrm{Tran}} & \boldsymbol{S} \end{bmatrix} \begin{bmatrix} \dot{\overline{\boldsymbol{u}}} \\ \dot{\overline{\boldsymbol{P}}} \end{bmatrix} + \begin{bmatrix} \boldsymbol{K}^{\mathrm{ep}} & -\boldsymbol{Q} \\ 0 & \boldsymbol{H} \end{bmatrix} \begin{bmatrix} \overline{\boldsymbol{u}} \\ \overline{\boldsymbol{P}} \end{bmatrix} = \begin{bmatrix} \boldsymbol{f}^{\mathrm{u}} \\ \boldsymbol{f}^{\mathrm{P}} \end{bmatrix} \tag{8}$$

where

$$\mathbf{f}^{\mathrm{u}}: \mathrm{f}_{Ki}^{\mathrm{u}} = (\mathrm{f}_1^{\mathrm{u}})_{Ki} + (\mathrm{f}_2^{\mathrm{u}})_{Ki} ; \quad \mathbf{f}^{\mathrm{P}}: \mathrm{f}_M^{\mathrm{P}} = -(\mathrm{f}_1^{\mathrm{P}})_M + (\mathrm{f}_2^{\mathrm{P}})_M$$

and

$$\mathrm{f}_1^u = (\mathrm{f}_1^{\mathrm{u}})_{Ki} = \int_{\Gamma_t} N_K^{\mathrm{u}} \overline{\mathrm{t}}_i d\Gamma \, , \mathbf{f}_2^u = (\mathrm{f}_2^u)_{Ki} = \int_{\Omega} N_K^{\mathrm{u}} \rho \mathrm{b}_i d\Omega$$

$$\mathrm{f}_1^{\mathrm{P}} = (\mathrm{f}_1^{\mathrm{P}})_M = \int_{\Gamma_w} N_M^{\mathrm{P}} \overline{\mathrm{w}} d\Gamma \, , \mathbf{f}_2^{\mathrm{P}} = (f_2^{\mathrm{P}})_M = \int_{\Omega} N_{M,i}^{\mathrm{P}} k \rho_{\mathrm{f}} b_i d\Omega$$

$$\mathbf{M}: \mathrm{M}_{KijL} = \delta_{ij} \left(\int_{\Omega} N_K^{\mathrm{u}} \rho N_L^{\mathrm{u}} d\Omega \right) \, , \mathbf{Q}: \mathrm{Q}_{LjM} = \int_{\Omega} \alpha \, N_{L,j}^{\mathrm{u}} N_M^{\mathrm{P}} d\Omega$$

$$\mathbf{S}: \mathrm{S}_{MN} = \int_{\Omega} N_M^{\mathrm{P}} \frac{1}{Q} N_N^{\mathrm{P}} d\Omega \, , \mathbf{H}: \mathrm{H}_{MN} = \int_{\Omega} N_{M,i}^{\mathrm{P}} k N_{N,i}^{\mathrm{P}} d\Omega \tag{9}$$

In these equations, the solid displacement u_i and pore water pressure P have been approximated by using the shape functions and nodal values:

$$u_i = N_k^{\mathrm{u}} \overline{u}_{ki}^{nd} \tag{10}$$

$$P = N_l^{\mathrm{P}} \overline{P}_l^{nd} \tag{11}$$

Similar approximations are applied to $\dot{u}_i$ and $\dot{P}$ [25]. The FE formulation has been implemented in an in-house code programmed in MATLAB.

4. Verification and computational model

4.1. Verification of the developed code

In order to verify the developed code, the problem of one-dimensional consolidation under time-dependent loading is analyzed. Olson [56] presented the exact solution for the time-dependent loading defined in Fig. 1 and with the material properties listed in Table 1. The same were used by Samimi and Pak [100]. The numerical results obtained from Eqs. (15) and (16) can be verified by comparing variation of pore pressure over depth with the exact solution is reported by [56].

Table 1 near here

It should be noticed that the soil properties in Table 1 are only going to be implemented in the verification study for the one-dimensional consolidation problem.

4.1.1 Discretization in time domain

For time integration of the governing equation (8), the generalized Newmark technique is employed with Newton-Raphson iteration. Accordingly, the variables and their temporal derivatives in the time interval $[t_n, t_{n+1}]$ are given as:

$$\begin{cases} \ddot{\mathbf{u}}_{n+1} = a_0(\mathbf{u}_{n+1} - \mathbf{u}_n) - a_2\dot{\mathbf{u}}_n - a_3\ddot{\mathbf{u}}_n \Rightarrow \ddot{\mathbf{u}}_{n+1}^{(k)} = a_0\left(\mathbf{u}_{n+1}^{(k)} - \mathbf{u}_n\right) - a_2\dot{\mathbf{u}}_n - a_3\ddot{\mathbf{u}}_n \\ \dot{\mathbf{u}}_{n+1} = \dot{\mathbf{u}}_n + a_6\ddot{\mathbf{u}}_n + a_7\ddot{\mathbf{u}}_{n+1} \Rightarrow \dot{\mathbf{u}}_{n+1}^{(k)} = \dot{\mathbf{u}}_n + a_6\ddot{\mathbf{u}}_n + a_7\ddot{\mathbf{u}}_{n+1}^{(k)} \\ \mathbf{u}_{n+1}^{(k)} = \mathbf{u}_{n+1}^{(k-1)} + \Delta\mathbf{u}^{(k)} \end{cases} \tag{12}$$

and

$$\begin{cases} \dot{P}_{n+1} = a_8\dot{P}_n + a_9(P_{n+1} - P_n) \Rightarrow \dot{P}_{n+1}^{((k-1))} = a_8\dot{P}_n + a_9\left(P_{n+1}^{(k)} - P_n\right) \\ P_{n+1}^{(k)} = P_{n+1}^{(k-1)} + \Delta P^{(k)} \end{cases} \tag{13}$$

where

$$a_0 = 1/(\alpha_{ti}\Delta t^2), a_2 = 1/(\alpha_{ti}\Delta t), a_3 = 1/(2\alpha_{ti}) - 1, a_6 = \Delta t(1 - \delta_{ti}),$$

$$a_7 = \Delta t\delta_{ti}, a_8 = 1 - 1/\delta_{ti}, \ a_9 = 1/(\delta_{ti}\Delta t), \delta_{ti} \geq 0.5, \alpha_{ti} \geq 0.25(0.5 + \delta_{ti})^2 \tag{14}$$

Here Δt is the time step length and k is the iteration number counting locally in each time step [25 and 57]. Further, α_{ti} and δ_{ti} are the Newmark time integration constants. By considering the governing equation in t_{n+1} and implementing the variable at t_{n+1} in terms of the variable at t_n, as mentioned in Eqs. (12) and (13), the governing equation becomes:

$$\begin{bmatrix} \mathbf{M}a_0 + \mathbf{K} & -\mathbf{Q} \\ \mathbf{Q}^T a_0 a_7 & \mathbf{S}a_9 + \mathbf{H} \end{bmatrix} \begin{bmatrix} \Delta\mathbf{u}^{(k)} \\ \Delta P^{(k)} \end{bmatrix} = \begin{bmatrix} \mathbf{F}^{\mathrm{u}} \\ \mathbf{F}^{\mathrm{P}} \end{bmatrix} \tag{15}$$

where the equivalent forces are:

$$\mathbf{F}^{\mathrm{u}} = \mathbf{f}_{n+1}^{\mathrm{u}} - \mathbf{M}\left(a_0\left(\mathbf{u}_{n+1}^{(k-1)} - \mathbf{u}_n\right) - a_2\dot{\mathbf{u}}_n - a_3\ddot{\mathbf{u}}_n\right) + \mathbf{Q}P_{n+1}^{(k-1)} - \mathbf{K}\mathbf{u}_{n+1}^{(k-1)}$$

$$\mathbf{F}^{\mathrm{P}} = \mathbf{f}_{n+1}^{\mathrm{p}} - \mathbf{Q}^{\mathrm{Tran}}\left(\dot{\mathbf{u}}_n + a_6\,\ddot{\mathbf{u}}_n + a_7\left(a_0\left(\mathbf{u}_{n+1}^{(k-1)} - \mathbf{u}_n\right) - a_2\dot{\mathbf{u}}_n - a_3\ddot{\mathbf{u}}_n\right)\right) - \mathbf{S}\left(a_8\dot{P}_n + \right.$$

$$a_9\left(P_{n+1}^{(k-1)} - P_n\right)\right)\dot{P}_{n+1}^{(k-1)} - \mathbf{H}P_{n+1}^{(k-1)} \tag{16}$$

As it can be seen from the right hand side of Eqs. (15) and (16), the variables at time t_{n+1} are in terms of iteration $(k-1)$.

4.1.2 Comparing the results

In the one-dimensional consolidation problem (as shown in Fig. 1), a fully saturated soil layer with the height of (H =) 10 m is subjected to a step loading of 1 kPa on the top surface as considered by Samimi and Pak [100]. As shown in Fig. 1, this load is applied during a time period of 1 day and remains constant thereafter. Since the soil layer rests on a rigid impervious base and this is a one-dimensional problem, the boundary conditions are as follows: all boundaries are considered impermeable, except the upper surface which is considered free draining. In addition, the base is fixed against all displacements, while no movement along horizontal directions is allowed for the side boundaries, the same as considered by Samimi and Pak [100]. The excess pore pressure under consolidation in terms of the vertical position is expressed as (for further information, see [58]):

$$\begin{cases} T_v \leq T_c : P = \sum_{m=0}^{\infty} \frac{2q_c}{M^3 T_c}(1 - e^{-M^2 T_v})\sin(\frac{My}{H}) \\ T_v \geq T_c : P = \sum_{m=0}^{\infty} \frac{2q_c}{M^3 T_c}(e^{-M^2(T_c - T_v)} - e^{-M^2 T_v})\sin(\frac{My}{H}) \end{cases} \tag{17}$$

where $T_c = \frac{c_v\,t_c}{H^2}$, $T_v = \frac{t c_v}{H^2}$, $c_v = \frac{k}{m_v \gamma_w}$, $m_v = \frac{(1+v)(1-2v)}{E(1-v)}$, $M = (2m+1)\frac{\pi}{2}$, H is drainage distance. The excess pore pressure versus depth is very comparable to those of Samimi and Pak [100] as shown in Fig. 2. The diagram, in particular the axis definition, has been chosen such that a direct comparison with Fig. 4 in [100] is possible. As expected, the excess pore pressure at the top free surface of the model equals to zero at all times. Further, it is seen that with the increase of the load on the top surface of the model, the excess pore pressure at the bottom of the model gets the same

value as step loading for each time simulation when $T_v \leq T_c$. For example, if $t = 0.1$day then the excess pore pressure at the bottom is 0.1 kPa and equals to the step loading at $t = 0.1$day, and the same explanation can be mentioned for other time simulation when $T_v \leq T_c$. It is compatible with the concept of consolidation; by surcharging the load at the ground surface (the top surface of the model) the immediate increase of the pore water pressure will be equal to the increase of the total stress.

Fig. 1 near here

Fig. 2 near here

It can be added that the same geometry of the model as shown in Fig. 1 and a similar procedure for applying the step loading are presented by Xie and Wang [101] who made observations similar to those as shown in Fig. 2.

As it is described in [58], the coefficient of volume compressibility (m_v), the coefficient of permeability and the total stress on the element have high effect on the generated excess pore pressure. Based on the values presented in [100] for one-dimensional consolidation, the numerical results are found to be in good agreement with the exact solution as presented by Olson [56].

4.2. Computational model of saturated soil

In order to expound $p - y - \dot{y}$ curves based on the Kelvin model, a two-dimensional poroelastic FE model subjected to a harmonic forced displacement is employed to determine the damping and the soil stiffness in the saturated soil. In this study, the plain strain conditions are considered. The analysis is conducted using the material properties given in Table 2 with the reference case highlighted in bold format.

Table 2 near here

By considering the domain for variation of soil properties given in Table 2, it should be pointed out that some of the values do not represent realistic types of soil. Thus, some values for the soil porosity and Poisson's ratio are fictitious and do not have any physical meaning or/and real application, but are only included to provide to provide extreme cases.

4.2.1. Model description

A tubular monopile offshore foundation (Fig. 3), surrounded by an elastic saturated soil with radius R is considered. Harmonic sinusoidal forced displacement acting in the horizontal direction (y-direction) is applied to the common border between the saturated soil and solid pile. Small deformation of the soil is assumed and as indicated by Fig. 3 symmetry is considered with respect to the horizontal axis and the center line of the monopile.

Fig. 3 near here

The soil around solid pile is modelled as a poroelastic material with isotropic material properties as mentioned in Table 2. In order to reveal the effect of load frequency, eight different load frequencies are considered (as shown in Table 3) when the forced displacement is:

$$y(t) = y_0 \sin(2\pi f_{freq.}t) = \text{Real}(y_0 e^{i2\pi f_{freq.}t}), \qquad i = \sqrt{-1} \tag{18}$$

Table 3 near here

All our numerical results will be in normalized form and for each material property in Table 2 we will run eight simulations based on the different load frequencies as mentioned in Table 3, which means a total 1440 simulations.

In order to have stable results and avoiding any LBB conditions, the elements used for coupled analysis consist of 6-noded quadratic and 3-noded linear elements or 9-noded biquadratic and 4-noded bilinear elements for displacement and pore pressure fields, respectively, as shown in Fig. 4 [26].

The chosen mesh consists of 9-noded biquadratic and 4-noded bilinear elements for displacement and pore pressure fields, respectively. Fine meshes are generated close to the pile while coarse meshes are used far from the pile as shown in Fig 5a. The pore pressure, lateral flow and displacements are considered zero at the exterior boundary and the sinusoidal periodic displacement in the horizontal direction is applied for the semi-circle boundary at the soil-pile interface. An illustration of the boundary conditions is shown in Fig. 5b.

4.2.2 Theoretical approach

In order to investigate the influence of pore water pressure on soil behaviour, especially the stiffness and damping in different depths, different values of soil permeability, Young's modulus and porosity are considered (see Tables 3 and 5) when different excitation frequencies of the harmonic forced displacement are employed. Based on the FE formulation in Sections 2 and 3, the viscous damping which is linearly proportional to velocity can be observed by employing the Kelvin model (as shown in Figure 6).

Dynamic analysis for nonlinear system and material model is time consuming and costly. Therefore, linear analysis is valuable to estimate the behaviour of soil. If the load is considered sinusoidal with circular frequency (Ω), the force can be found as:

$$F(t) = F_0 \sin(\Omega t) \tag{19}$$

For a system with spring and dashpot the equation of motion can be represented as:

$$F(t) = k_{sp}y(t) + c_{dam}\dot{y}(t), \quad c_{damp} = \Omega c_{dam} \tag{20}$$

where F, k_{sp}, c_{dam}, y and $\dot{y}$ are force, stiffness, damping, displacement and velocity respectively. Substituting the applied load into the equation of motion, the displacement can be obtained as follows:

$$y = \frac{F_0}{k_{sp}\sec(\delta)}\sin(\Omega t - \delta) \tag{21}$$

where δ is the phase lag or phase delay in the spring-damper system and can be found as

$$\delta = \tan^{-1}\left(\frac{\Omega c_{dam}}{k_{sp}}\right) = \tan^{-1}\left(\frac{c_{damp}}{k_{sp}}\right) \tag{22}$$

The physical interpretation of phase shift is illustrated in Figure 7.

Fig. 7 near here

It can be mentioned that by applying the periodic sinusoidal load the displacement is also sinusoidal, but with phase shift, once the steady state has been reached (normally after the first period in the conducted FE analysis).

5. Numerical analysis

For numerical illustration of the elastic solutions of this study, a soil box with dimensions $80 \text{ m} \times 80 \text{ m}$ is considered with the pile radius, R, equal to 2 m. Poisson's ratio, porosity, shear modulus and permeability are varied one at a time in accordance with Table 2. Based on the geometry of the model, and for the reference case defined in Table 2, the static stiffness of the model is $k_{static}^{ref} = 8.7634 \times 10^8 \frac{N}{m^2}$, and for all values of Poisson's ratio listed in Table 2, the dimensionless static stiffnesses $(S_s(\nu) = \frac{k_{static}^{ref}}{G})$ are presented in Table 4 as:

Table 4 near here

The analysis is conducted using Kelvin model to find the dynamic soil stiffness and damping. Complex stiffness of model can be represented as:

$$k_{\text{com}} = k_{\text{sp}} + ic_{\text{damp}}, \qquad i = \sqrt{-1}, \qquad c_{\text{damp}} = \Omega c_{\text{dam}}$$

The real and imaginary parts of the complex stiffness are normalized by the static stiffness:

$$\text{Normalized stiffness} = \frac{\text{Real part of complex stiffness}}{\text{Static stiffness}} = \frac{k_{\text{sp}}}{k_{\text{static}}^{\text{ref}}}$$

$$\text{Normalized equivalent damping} = \frac{\text{Imaginary part of complex stiffness}}{\text{Static stiffness}} = \frac{c_{\text{damp}}}{k_{\text{static}}^{\text{ref}}}$$

5.1. Stiffness and damping analysis

5.1.1 Results for different Poisson's ratios

Figs. 8 and 9 illustrate the normalized soil stiffness and equivalent damping for different values of the load frequencies and Poisson's ratio. Poisson's ratio takes thirty values between 0.1 and 0.45. It is noted that Young's modulus is constant. Hence, the shear modulus decrease with the increase of Poisson's ratio.

Fig. 8 near here

In Fig. 8, the effect of Poisson's ratio on the soil stiffness is shown by fixing the value of the load frequency. It is seen that the stiff soil, with greater value of stiffness and small value of the Poisson's ratio, converts into the soft soil with the increase of the Poisson's ratio. By considering the constant Poisson's ratio and changing load frequency, it can be observed that the undrained condition occurs for high load frequency in comparison with the case by having low load frequency. It is seen that the effect of load frequency on stiffness decreases with the increase of Poisson's ratio.

Fig. 9 shows the variation of the equivalent soil damping versus Poisson's ratio in the presence of different load frequencies. It is seen that the normalized equivalent damping decreases with the increase of Poisson's ratio for all load frequencies. It is observed that the rate of decreasing

equivalent damping versus Poisson's ration is increased especially for the large values of the load frequency and Poisson's ratio.

Fig. 9 near here

Results of Figs. 8 and 9 can be summarized to conclude that the soil stiffness and equivalent damping decrease with the increase of the Poisson's ratio, the stiff soil converts into the soft soil.

5.1.2 Results for different porosities

The variation of normalized soil stiffness and equivalent damping with porosity for different values of the load frequencies are shown in Figures 10 and 11. The porosity takes twenty values between 0.0 and 0.45.

Fig. 10 near here

Fig. 10 illustrates the trend of the non-dimensional stiffness due to the harmonic sinusoidal forced displacement where different values of the porosity are considered. The soil stiffness for dense soil, with small value of porosity, decreases with the increase of porosity for high value of load frequency. But, the normalized stiffness slightly increases for low value of load frequency when the porosity is increased. This phenomenon can be explained by the presence of interactive effects between drained and undrained conditions for dynamic behaviour of soil. It can be noticed that the variation of normalized soil stiffness versus the load frequency is greater than the variation of soil stiffness versus porosity. It can be concluded the load frequency has high impact on dynamic behaviour of the porous medium.

Fig. 11 near here

The variation of equivalent damping with porosity for different values of load frequency is shown in Fig 11. The graphs in Fig. 11 suggest that the maximum equivalent damping occurs for dense sand (with small value of porosity) and it is not changing linearly with frequency. It is observed that the variation of the equivalent damping with porosity is much more noticeable for the

high value of the load frequency (for example, frequency = 0.2 Hz) in comparison with the variation of equivalent damping with porosity when the low load frequency is considered.

By comparing results from Figs. 8 and 10, it can be highlighted that the variation of Poisson's ratio is more important than the variation of the porosity in terms of their effect on the variation of the dynamic soil stiffness. When Young's modulus is kept constant but Poisson's ratio is at the same time increased, this leads to a decrease of the shear modulus and, as a results of this, a decrease of the stiffness related to soil-pile interaction. Regarding the small variation in stiffness caused by variation of the porosity, it should be remember that only one property of the soil is changed at a time. Thus, all results in Fig. 11 are based on the same values of Young's modulus, Poisson's ration, permeability and etc.

5.1.3 Results for different Young's moduli

Figs. 12 and 13 show the variation of non-dimensional soil stiffness and equivalent damping with Young's modulus by having different values for load frequencies. Young's modulus takes thirty values between 25 and 2500 MPa.

Fig. 12 near here

Fig. 13 near here

Semi-logarithmic plots in Figs. 12 and 13 show that variation of normalized soil stiffness and equivalent damping respectively for different values of load frequencies. It can be seen that the variation of soil stiffness is highly dependent on the load frequency especially for soft soil with low value of shear modulus. The soil equivalent damping increases with the increase of Young's modulus to its maximum value and then decreases.

5.1.4 Results for different permeability

Figs. 14 and 15, respectively show the variations of non-dimensional soil stiffness and equivalent damping with hydraulic conductivity for different values of load frequencies. The soil hydraulic conductivity takes values between 10^{-10} and $1 \, \mathrm{m/s}$.

Fig. 14 near here

Semi-logarithmic plots in Fig. 14 show variation of normalized stiffness for different values of soil hydraulic conductivity and load frequency. It is noticed that for low and high values of the hydraulic conductivity, undrained and drained conditions the soil occur is independent of load frequency. It is seen that the rate of soil stiffness reduction in the transient state between fully undrained and drained soil almost is the same. Based on the value of the soil hydraulic conductivity, it can be observed that sandy soil presents the stiffness reduction with the increase of soil hydraulic conductivity. This result is compatible to the one reported in Fig. 15 in [20].

Fig. 15 near here

Figs. 15 show the variation of equivalent damping versus the soil hydraulic conductivity for different values of load frequencies. For drained and undrained soil behaviour the equivalent damping takes zero value and the maximum value of equivalent damping occurs in between. The graphs of Fig. 15 suggest almost the same maximum equivalent damping for different values of load frequencies and hydraulic conductivities.

5.1.5 Results for different permeability

The normalized soil reaction based on the Kelvin model can be calculated as:

$$\text{soil reaction force} = p_{rec.} = k_{\mathrm{sp}} y + i c_{\mathrm{damp}} y \, , i = \sqrt{-1} \tag{35}$$

For a certain angular frequency the normalized reaction force corresponds to $k_{\mathrm{sp}} + i\Omega \, c_{\mathrm{dam}}$ with the amplitude equals $\sqrt{\left(k_{\mathrm{sp}}\right)^2 + (\Omega \, c_{\mathrm{dam}})^2}$. Fig. 16 shows the variations of non-dimensional soil reaction and load displacement and velocity for a certain value of load frequency (0.4 Hz). The

horizontal displacement takes the values: 0.00, 0.01, 0.02, 0.03, 0.04, 0.06, 0.08, 0.09, and 0.1 m while the other soil properties are taken from the reference case in Table 2.

Fig. 16 near here

As expected, the soil reaction for the high amount of the horizontal displacement is greater than those for small horizontal displacement due to higher spring reaction which is proportional to horizontal displacement. In order to make a clear distinguish between the reaction forces from spring and dashpot, the related reaction force due to damping is shown with negative slope. The relative slope of reaction forces regarding to spring and damper is 8.3171 (= 0.128/0.01539). The effect of different horizontal velocity can be realized from the fact that for large values of the velocity and displacement, the soil reaction increases with the increase of horizontal velocity linearly. This linear relation between the normalized reaction force and load amplitude validates our simulation as well.

5.2. Presenting $p - y - \dot{y}$ curves

In the following, results are presented with generalized stiffness and equivalent damping based on results from the previous section in order to be applicable for different soil properties and model geometries. Based on results for different hydraulic conductivities, the soil behaviour is going to change from undrained to drained state by increasing the hydraulic conductivity, and damping takes the maximum value in the transition phase between the drained and undrained cases. Therefore, the undrained properties might be illuminated somewhat by considering two material properties namely the shear modulus and Poisson's ratio. For a tubular circular pile segment of unit length, the soil stiffness is independent of the pile diameter, i.e. it is only a function of shear modulus and Poisson's ratio:

$$k_0 = G \, S_0(v)$$

The static stiffness (k_0) is normalized with respect to the shear modulus, and the variation of normalized static stiffness ($S_0(v)$) versus Poisson's ratio (v) is shown in Fig 17.

Fig. 17 near here

Fig. 8 shows the variation of dynamic stiffness normalized with respect to the static stiffness versus Poisson's ratio, while Fig. 17 shows the variation of static stiffness normalized with respect to the shear modulus versus Poisson's ratio. It can be mentioned that the results presented in Figs. 17 and 8 support each other. As it is seen in Fig. 8, when the load frequency equals to zero the dynamic stiffness gets the same value as the static stiffness. The straight line in Fig. 8 with the constant value 1.0 represents this behaviour. Fig. 17 shows that a perfectly incompressible soil by having a Poisson's ratio of 0.5 has the highest normalized static stiffness.

and also the stiffness in the undrained state can be written as:

$$S_u = S_{\text{undrained}} = G\, S_0(v_{\text{undrained}}), v_{\text{undrained}} = \frac{3K_u - 2G}{2(3K_u + G)}\,, \quad K_u = K_{undrained} = \left(\frac{n_p}{K_f} + \frac{1-n_p}{K_s}\right)^{-1}$$

Normalized global stiffness and damping and frequency are defined as:

Normalized global soil spring stiffness: $k = \frac{k_{\text{sp}} - k_0}{S_u - k_0}$

Normalized global equivalent soil damping: $\delta = \frac{c_{\text{dam}}}{S_u}$

Normalized frequency: $a = 2\pi f_{freq.}\, \frac{R^2}{k}\left(\frac{n_p}{Q_{\text{sf}}} + \frac{1}{D_z}\right), D_z = \frac{E(1-v)}{(1-2v)(1+v)}$

Figs. 18 and 19 show the maximum and minimum values of the non-dimensional global soil stiffness and equivalent soil damping values for different values of the non-dimensional frequencies. The Poisson's ratio, porosity and shear modulus are varying between [0.2 and 0.35], [0.1 and 0.4)] and [25 and 200] MPa, respectively. In order to present the variation of the normalized global soil stiffness and damping versus normalized frequency, several numerical analyses have been performed. As it is indicated in Fig. 18 the maximum normalized global

stiffness has been obtained for soil properties with shear modulus = 200 GPa, Poisson's ratio = 0.35 and porosity = 0.4 whilst the border for minimum normalized global stiffness occurs for another soil type with shear modulus = 25 GPa, Poisson's ratio = 0.2 and porosity = 0.1. For the mentioned interval for soil properties, the results for other combination of soil properties are between these minimum and maximum borders. The similar procedure has been carry out to present the border for maximum and minimum soil damping, as shown in Fig. 19.

Fig. 18 near here

Fig. 19 near here

The minimum and maximum values of that the normalized global soil stiffness and equivalent soil damping are varying between these two curves as shown in Figs. 18 and 19. The border for maximum soil stiffness and damping in Figs. 18 and 19 are obtained based on minimum and maximum values of soil properties such shear modulus, Poisson's ratio and porosity, respectively. And also, The border regarding to minimum soil stiffness and damping in Figs. 18 and 19 are obtained based on maximum and minimum values of soil properties such shear modulus, Poisson's ratio and porosity, respectively.

6. Conclusions

This research concerns the variation of soil stiffness and damping of offshore monopile wind turbine foundations subjected to lateral dynamic loads by using a two-phase model for the soil. The study explores the $p - y - \dot{y}$ curves to illustrate the dependency of the soil reactions on the load frequency. The coupled dynamic equations for an offshore monopile foundation as a rigid disc moving horizontally in an elastic saturated soil, using the $\mathbf{u} - P$ formulation under cyclic load and assuming plane strain, are developed. This preludes the effect of load frequency which can result

from pore pressure generation during cyclic motion. For different frequencies of forced displacement, the conclusions can be drawn as:

- The soil stiffness is independent of load rate when the hydraulic conductivity takes small or large values.

- The reduction of soil stiffness onsets in the transient region from silt to sandy soil and it occurs in sandy soil for all values of load frequencies (Fig. 14) that are relevant to offshore wind turbine monopile foundations. The maximum equivalent damping occurs in the transition region, mostly in the sandy soil regime, and the maximum damping moves toward the coarse soil region by increasing the load frequency (Fig. 15).

- Based on a Kelvin model rather than a Winkler model, the soil spring stiffness and equivalent soil damping diagrams are presented. These can be applied in p-y-$\dot{y}$ models for offshore monopile foundations.

7. References

[1] Lozano-Minguez E, Kolios A. J., Brennan F. P., Multi-criteria assessment of offshore wind turbine support structures. Renewable Energy 2011; 36: 2831-2837.

[2] Randolph. M. F., 2009: Offshore Design Approaches for Sub-Failure Cyclic Loading of Foundations. In: Mechanical behaviour of soils under environmentally induced cyclic loads. International Centre for Mechanical Sciences (CISM): Udine (Italy).

[3] Winkler E., 1867; "Die Lehre von Elasticzitat und Festigkeit (On Elasticity and Fixity). Prague.

[4] Matlock H., Foo S. H. C., Simulation of lateral pile behaviour under earthquake motion. 1978. Rep. to Chevron Oil Field Research Co.. La Habra, Calif, Dept. of Civil Engineering, University of Texas at Austin,Austin, Tex.

[5] Makris N., Gazetas G., Dynamic soil-pile interaction. part ii. lateral and seismic response. Earthquake Engineering and Structural Dynamics 1991; 21(2): 145-162.

[6] Nogami T., Kazama, M., Dynamic response analysis of submerged soil by thin layer element method. Soil Dynamics and Earthquake Engineering 1992; 11(1): 17-26.

[7] El-Naggar M. H., Novak, M, Nonlinear axial interaction in pile dynamics. Journal of Geotechnieal Engineering 1994; 120(4): 678-696.

[8] El-Naggar M. H., Novak, M., Nonlinear lateral interaction in pile dynamics. Soil Dynamics and Earthquake Engineering 1995; 14: 141-157.
[9] El-Naggar M. H., Bentley K. J., Dynamic analysis for laterally loaded piles and dynamic p-ycurves. Canadian Geotechnical Journal 2000; 37(6): 1166-1183

[10] Kong L. G., Zhang L. M., Rate-Controlled Lateral-load Pile Tests Using a Robotic Manipulator in Centrifuge. Geotechnical Testing Journal 2007; 30(3): 1-10, DOI: 10.1520/GTJ13138.

[11] Memarpour M. M., Kimiaei M., Shayanfar M., Khanzadi M., Cyclic lateral response of pile foundations in offshore platforms. Computers and Geotechnics 2012; 42:180-192.

[12] Damgaard M, Andersen L. V, Ibsen L. B., Computationally efficient modelling of dynamic soil-structure interaction of offshore wind turbines on gravity footings. Renewable Energy 2014; 68: 289-303.

[13] Bhattacharya S., Adhikari S., Experimental validation of soil–structure interaction of offshore wind turbines. Soil Dynamics and Earthquake Engineering 2011: 31: 805-816

[14] Lombardi D., Bhattacharya S., Modal analysis of pile-supported structures during seismic liquefaction. Earthquake Engineering and structural dynamics 2014; 43(1): 119-138.

[15] Sørensen , S. P. H., Ibsen, L. B. Assessment of foundation design for offshore monopiles unprotected against scour. Ocean Engineering 2013; 63: 17-25.

[16] Damgaard M., Ibsen L. B., Andersen L.V., Andersen J. K. F. Cross-wind modal properties of offshore wind turbines identified by full scale testing. Journal of Wind Engineering and Industrial Aerodynamics 2013; 116: 94-108.

[17] API. Recommended practice for planning, designing and constructing fixed offshore platforms-working stress design. API RPZA-WSD, 20 ed. Washington, D.C., USA: American Petroleum Institute; 2000.

[18] DNV. Design of offshore wind turbine structures. DNV-OS-J101. Det Norske Veritas Classification A/S, Høvik, Norway, 2011.

[19] DNV/Risø. Guidelines for design of wind turbines. Technical University of Denmark, National Laboratory for Sustainable Energy. Copenhagen: Det Norske Veritas/Risø, 2001.

[20] Damgaard M., Bayat M., Andersen L. V., Ibsen L, B., Assessment of the dynamic behaviour of saturated soil subjected to cyclic loading from offshore monopile wind turbine foundations. Computers and Geotechnics 2014; 61: 116-126.

[21] Randolph M. F., The response of flexible piles to lateral loading. Géotechnique 1981; 31(2): 247-259.

[22] Sørensen S. P. H., Ibsen L. B., Augustesen A. H., Effects of diameter on initial stiffness of p–y curves for large-diameter piles in sand. Numerical Methods in Geotechnical Engineering 2010; 907-912.

[23] LeBlanc C., Houlsby G., Byrne B., Response of stiff piles in sand to long-term cyclic lateral loading. Géotechnique 2010; 60(2): 79-90.

[24] Achmus M., Kuo, Y., Abdel-Rahman K., Behavior of monopile foundations under cyclic lateral load. Computers and Geotechnics 2009; 36: 725-735.

[25] Zienkiewicz O. C., Chan A. H. C., Pastor M., Schrefler B. A., Shiomi T., Computatioal Geomechanics with Special Reference to Earthquake Engineering 1990. John Wiley & Sons Ltd, England.

[26] Cheng Z., Jeremić B., Numerical modeling and simulation of pile in liquefiable soil. Soil Dynamics and Earthquake Engineering 2009; 29(11-12): 1405-1416.

[27] Brezzi F., 1974. On the existence, uniqueness, and approximation of saddle-point problems arising from Lagrange multipliers. RAIRO 1974; 8: 479-506.

[28] Ye X., Domain decomposition for a least-square finite element method for second order elliptic problem. Applied Mathematics and Computation 1998; 91(2-3): 233-242.

[29] Bathe K. J., The inf-sup condition and its evaluation for mixed finite element methods. Computers and Structures 2001; 79: 243 -252.

[30] Zienkiewicz O. C., Taylor, R.L., 2000. The finite element method. The basis, vol. 1, 5th ed. London: Butterworth Heinemann.

[31] Zienkiewicz OC, Chan AHC, Pastor M, Paul DK, and Shiomi T., Static and Dynamic Behavior of Soils: A Rational Approach to Quantitative Solutions: I. Fully Saturated Problems. Proceedings of the Royal Society London, Series A, Mathematical and Physical Sciences 1990; 429: 285-309.

[32] Pastor M., Zienkiewicz O. C., Chan, A. H. C., Generalized plasticity and the modeling of soil behavior, International Journal for Numerical and Analytical Methods in Geomechanics 1990; 14(3): 151-190.

[33] Oka F., Yashima A., Shibata T., Kato M., Uzuoka R., Fem-Fdm coupled liquefaction analysis of a porous soil using an elasto-plastic model. Applied Scientific Research 1994; 52: 209-245.

[34] Karim M. R., Nogami T., Wang, J. G., Analysis of transient response of saturated porous elastic soil under cyclic loading using element-free Galerkin method, International Journal of Solids and Structures 2002; 39: 6011-6033.

[35] Tsai T. L., Viscosity effect on consolidation of poroelastic soil due to groundwater table depression, Environ Geol 2009; 57: 1055-1064, DOI 10.1007/s00254-008-1391-0.

[36] Elgamal A., Yang Z., Parra, E., Computational modeling of cyclic mobility and post-liquefaction site response. Soil Dynamics and Earthquake Engineering 2002; 22: 259-271.

[37] Elgamal, A., Yang, Z., Parra, E., Ragheb, A., Modeling of cyclic mobility in saturated cohesionless soils. International Journal of Plasticity 2003; 19: 883-905.

[38] Lu J. F., Jeng D. S., Dynamic response of an offshore pile to pseudo-Stoneley waves along the interface between a poroelastic seabed and seawater. Soil Dynamics and Earthquake Engineering 2010; 30: 184-201.

[39] Maghoula P., Gatmiri B., Duhamela D., Boundary integral formulation and two-dimensional fundamental solutions for dynamic behavior analysis of unsaturated soils. Soil Dynamics and Earthquake Engineering 2011; 31: 1480-1495.

[40] Soares-Jr D., 2013. Iterative dynamic analysis of linear and nonlinear fully saturated porous media considering edge-based smoothed meshfree techniques. Computer Methods in Applied Mechanics and Engineering 2013; 253:, 73-88.

[41] EN 1991-1-4. Eurocode 1: Actions on Structures - Part 1-4: General Actions - Wind Actions, European Committee for Standardization, Brussels 2005.

[42] Damgaard M., Andersen J. K. F., Ibsen L. B., Andersen L. V., Natural Frequency and Damping Estimation of an Offshore Wind Turbine Structure, Proceedings of the Twenty-second (2012) International Offshore and Polar Engineering Conference, Rhodes, Greece, June 17–22, 2012, Copyright © 2012 by the International Society of Offshore and Polar Engineers (ISOPE), ISBN 978-1-880653-94–4 (Set); ISSN 1098-6189 (Set)

[43] Damgaard M, Zania V, Andersen L. V, Ibsen L. B. Effects of soil–structure interaction on real time dynamic response of offshore wind turbines on monopiles. Engineering Structures 2014; 75: 388-401.

[44] Andersen, L. V., 2006. Linear Elastodynamic Analysis. DCE Lecture Notes No 3. Aalborg University

[45] Hajiabadi M. R., Lotfi V., An effective approach for utilizing damping solvent extraction method in frequency domain. Soil Dynamics and Earthquake Engineering 2012; 38: 46-57.

[46] Xunqiang Y., Jianbo L., Chenglin W., Gao L., ANSYS implementation of damping solvent stepwise extraction method for nonlinear seismic analysis of large 3-D structures. Soil Dynamics and Earthquake Engineering 2013; 44: 139-152.

[47] Liang R. Y., Shatnawi E. S., Nusairat J., Hyperbolic P-Y Criterion for Cohesive Soils, Jordan Journal of Civil Engineering 2007; 1(1); 38-58.

[48] Harada T, Nonaka T., Wang H., Magoshi K., Iwamura M., A nonlinear dynamic soil foundation interaction model using fiber element method and its application to nonlinear earthquake response analysis of cable stayed bridge, The 14th World Conference on Earthquake Engineering October 12-17, 2008, Beijing, China.

[49] Youssef M. A., Hashash D. P., Viscous damping formulation and high frequency motion propagation in non-linear site response analysis, Soil Dynamics and Earthquake Engineering 2002; 22: 611-624.

[50] Gerolymos N., Gazetas, G., Development of Winkler model for static and dynamic response of caisson foundations with soil and interface nonlinearities, Soil Dynamics and Earthquake Engineering 2006; 26: 363-376.

[51] Auersch L., Wave propagation in the elastic half-space due to an interior load and its application to ground vibration problems and buildings on pile foundations. Soil Dynamics and Earthquake Engineering 2010; 30(10): 925-936.

[52] Carbonari S., Dezi F., Leoni G., Seismic soil–structure interaction in multi-span bridges: Application to a railway bridge, earthquake engineering and structural dynamics 2011; 40:1219-1239. DOI: 10.1002/eqe.1085

[53] Al-Wakel S. A. F., Fattah M. Y., Karim H. H., Dynamic Analysis of Foundations on Saturated Clay Using an Energy Absorbing Layer. Engineering & Technology 2001; 29(11): 2189-2201.

[54] Medina C, Aznarez J. J., Padron L. A., Maeso, O., A procedure for evaluating the soil-structure interaction effects on the system period and damping of pile-supported structures, compdyn 2013, 4th ECCOMAS Thematic Conference on Computational Methods in Structural Dynamics and Earthquake Engineering, M. Papadrakakis, N.D. Lagaros, V. Plevris (eds.), Kos Island, Greece, 12–14 June 2013

[55] Zania V., Natural vibration frequency and damping of slender structures founded on monopiles, Soil Dynamics and Earthquake Engineering 2014; 59: 8-20.

[56] Olson R. F., Consolidation under time-dependent loading. Journal Geotechnique Engineering (ASCE) 1977; 103: 55-60.

[57] Bathe K. J., The inf-sup condition and its evaluation for mixed finite element methods. Computers and Structuers 2001; 79: 243 -252.

[58] Das B. M., Advanced Soil Mechanics, Taylor & Francis 270 Madison Ave, New York, NY 10016, USA

List of figures

List of tables:

p-y-ẏ curves for dynamic analysis of offshore wind turbine monopile foundations

M. Bayat[*], L. V. Andersen, L.B. Ibsen
Department of Civil Eng., Aalborg University, 9000 Aalborg, Denmark

Table 1:

E =Young's modulus (kPa)	v = Poisson's ratio	Hydraulic conductivity (m/s)
$E = 104$	$v = 0.2$	5×10^{-7}

[*] Corresponding author. Tel.: +45 9940 8575; Fax: +45 3 9940 8552. *E-mail*: meb@civil.aau.dk

Table 2:

Hydraulic conductivity (m/s)	100 logarithmically spaced points between 10^{-10} and 10^{0}
Reference value	10^{-3}
Shear modulus (Pa)	30 logarithmically spaced points between 25×10^{6} and 25×10^{8}
Reference value	25×10^{7}
Porosity	20 linearly spaced points between decades 0 and 0.45
Reference value	0.25
Poisson's ratio	30 linearly spaced points between decades 0.1 and 0.45
Reference value	0.3
Solid phase bulk modulus (GPa)	36
Fluid phase bulk modulus (GPa)	2
Solid phase density (kg/m^3)	2650
Fluid density (kg/m^3)	1000

Table 3:

Load frequency, $f_{freq.}$(Hz)	0.0	0.001	0.01	0.05	0.1	0.2	0.3	0.4
Forced displacement amplitude, y_0(m)	0.1							

Table 4:

Poisson's ratio, ν	0	0.1	0.15	0.2	0.25	0.3	0.35	0.4	0.45
$S_s(\nu)$	2.8161	2.9584	3.0518	3.1672	3.3134	3.5054	3.7697	4.1599	4.8037

p-y-ẏ curves for dynamic analysis of offshore wind turbine monopile foundations

M. Bayat[*], L. V. Andersen, L.B. Ibsen
Department of Civil Eng., Aalborg University, 9000 Aalborg, Denmark

Fig. 1

[*] Corresponding author. Tel.: +45 9940 8575; Fax: +45 3 9940 8552. *E-mail*: meb@civil.aau.dk

Black Continuous Lines = Analytical
Red Dashed Lines = Numerical

Fig. 2

Fig. 3:

(a)

(i) Quadratic for u

(ii) Linear for p

(b)

(i) Biquadratic for u

(ii) Bilinear for p

Fig. 4

Fig. 5a

Forced displacement

Forced displacement

y

x
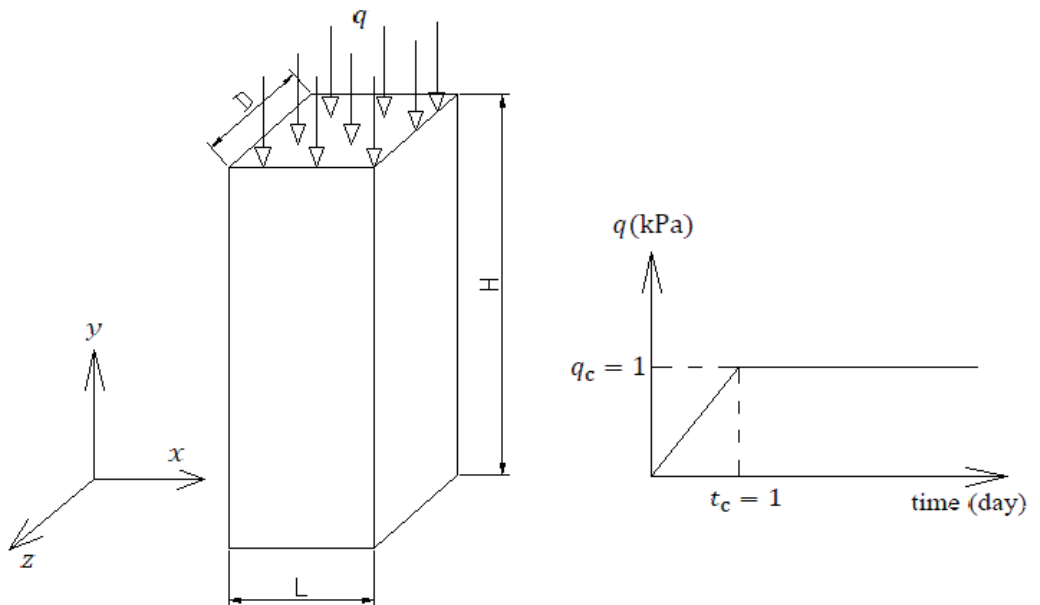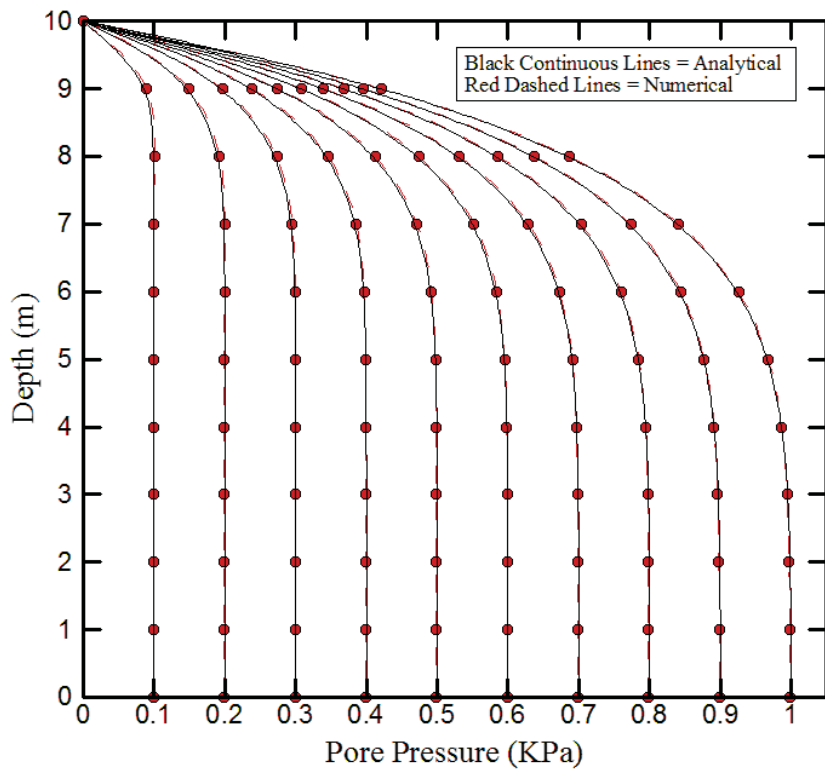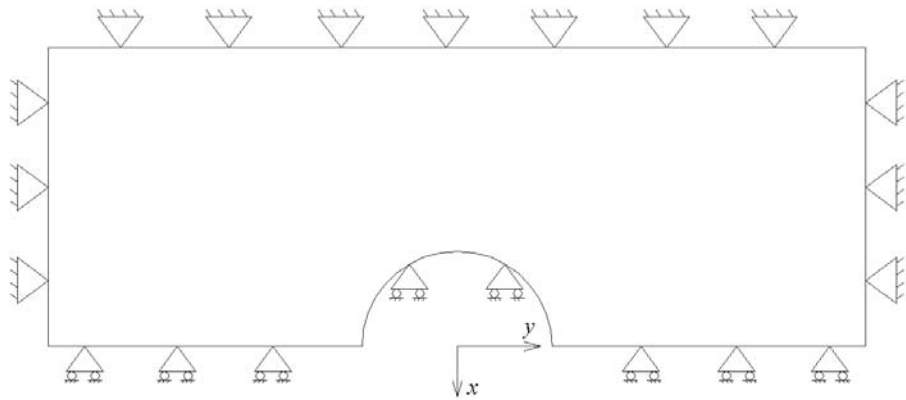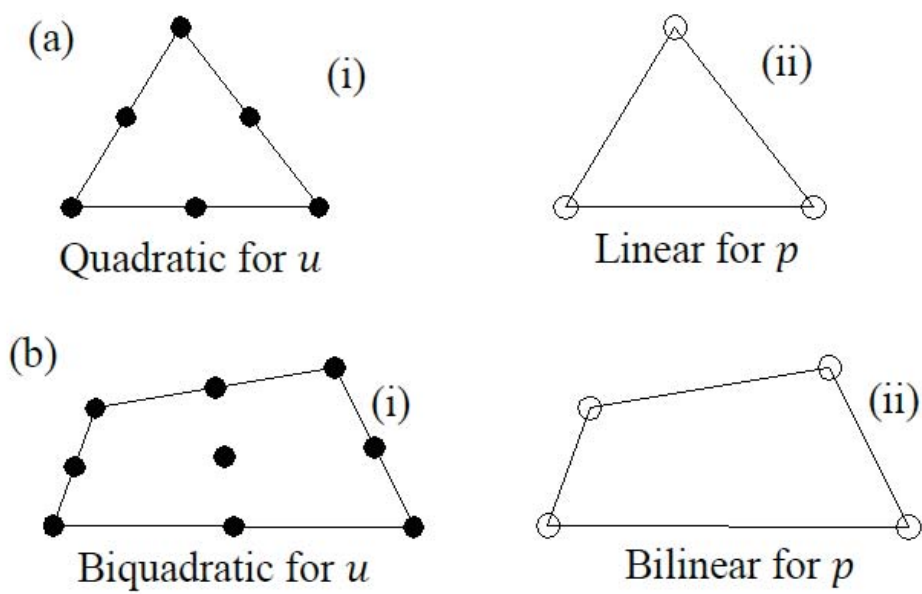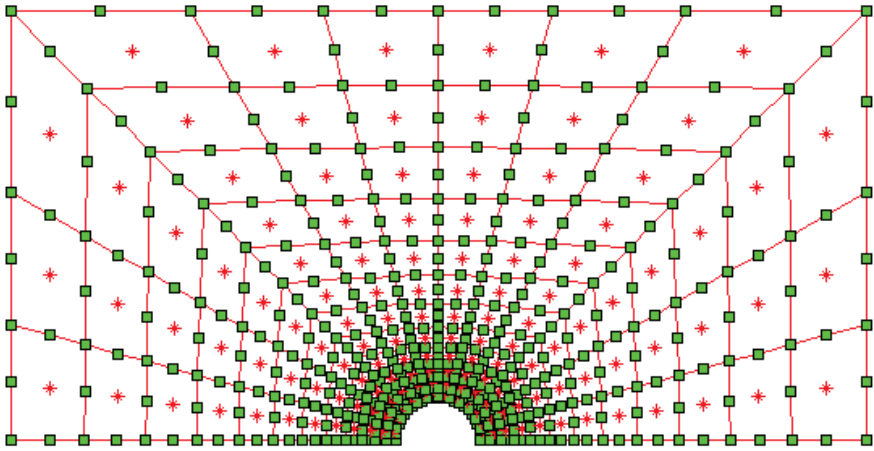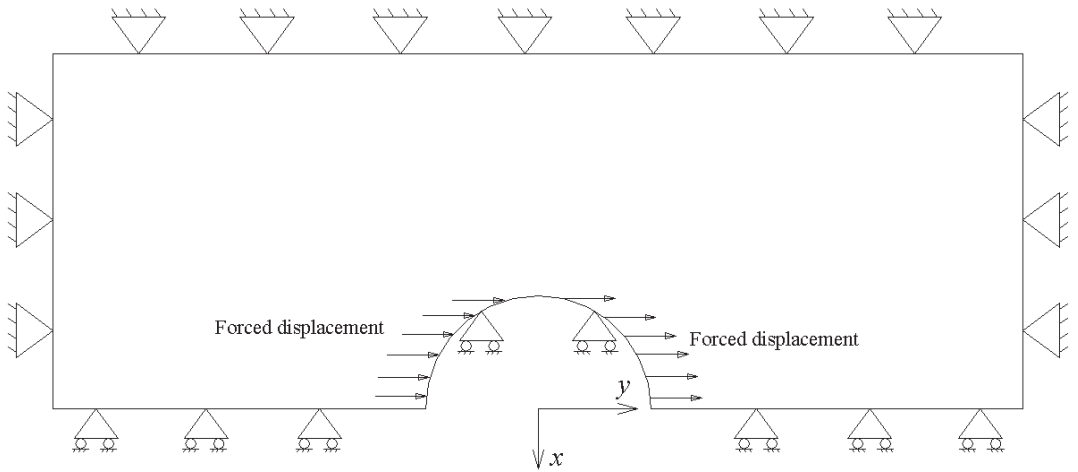
Fig. 5b
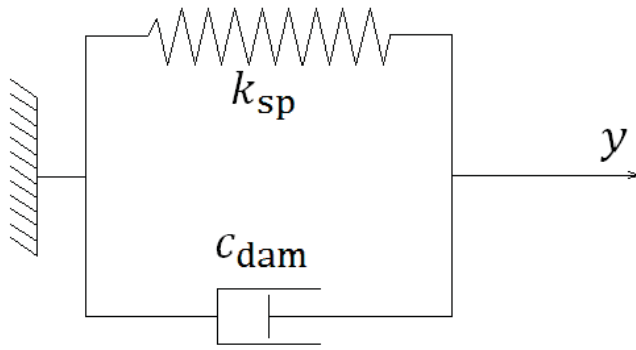
Fig. 6
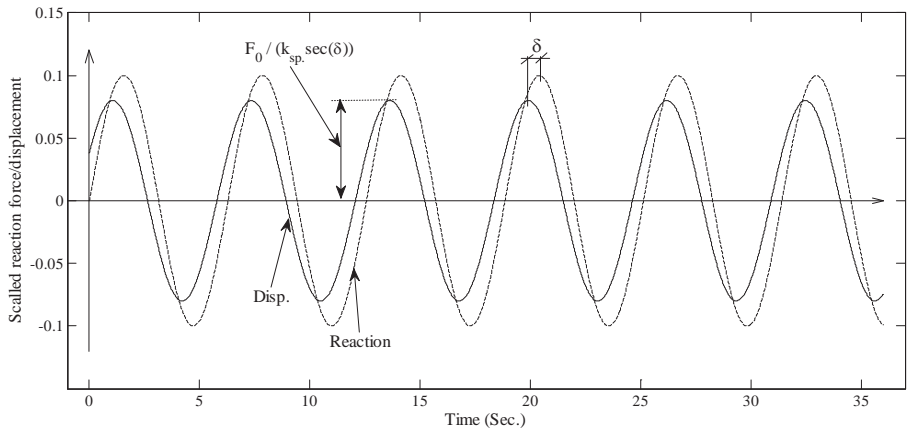
Fig. 7
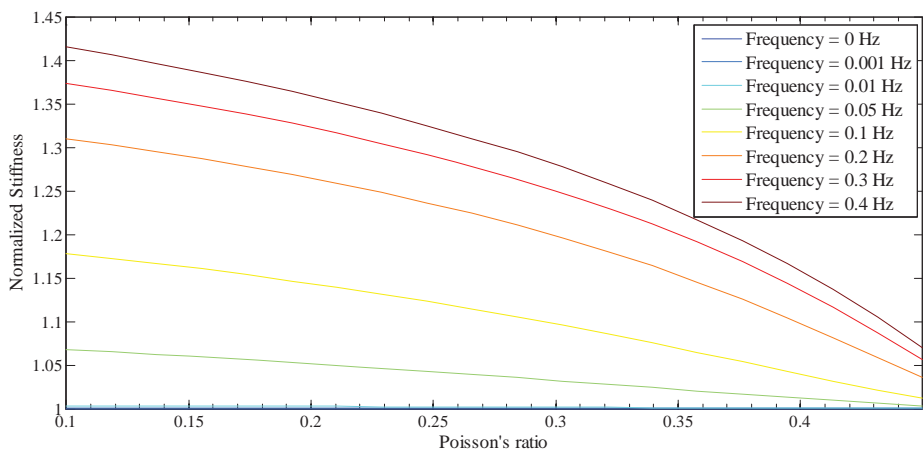
Fig. 8
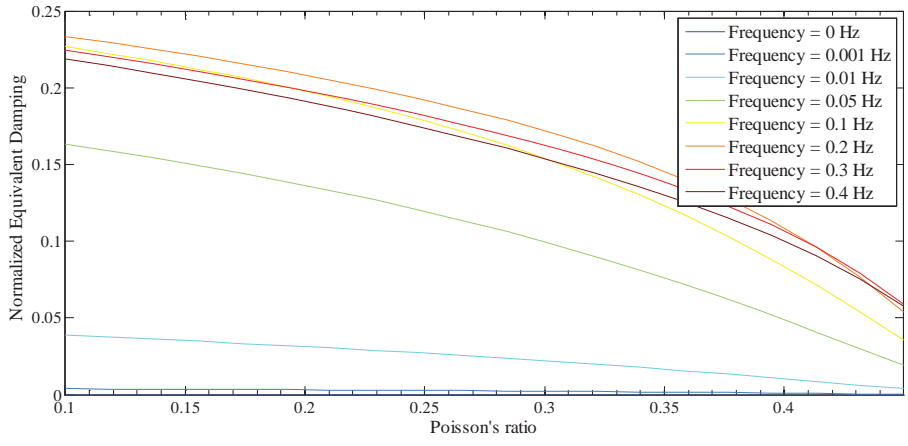
Fig. 9
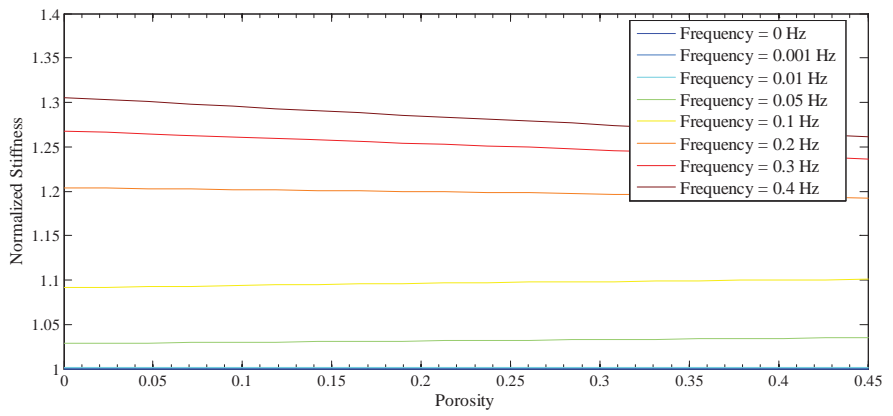
Fig. 10
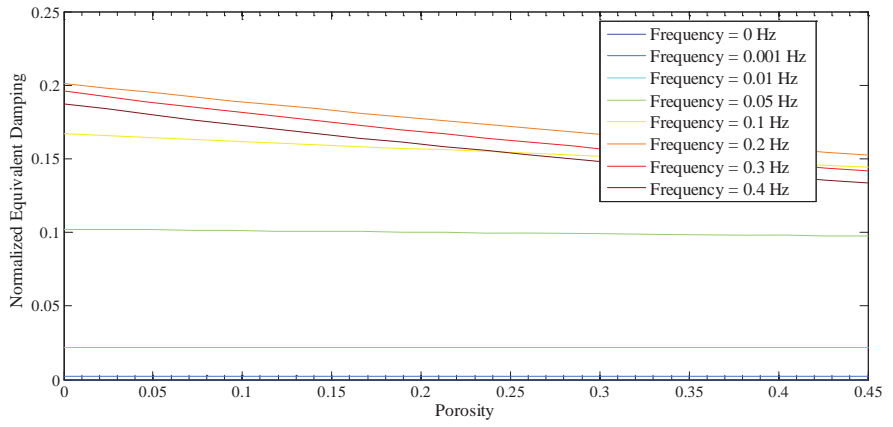
Fig. 11
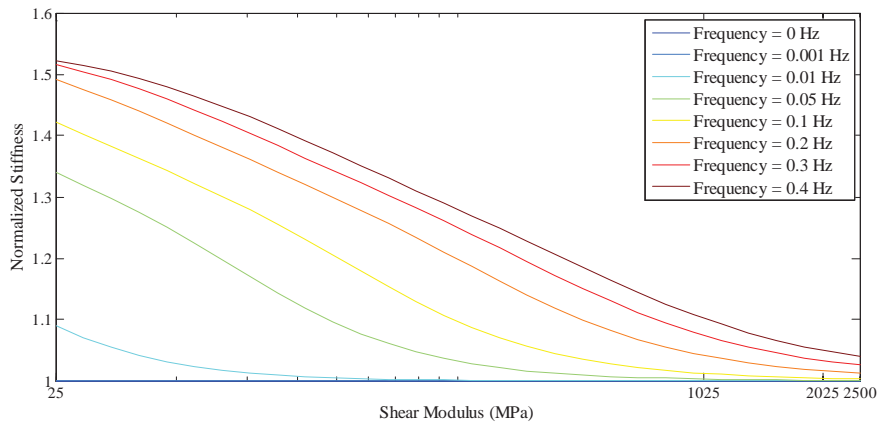
Fig. 12
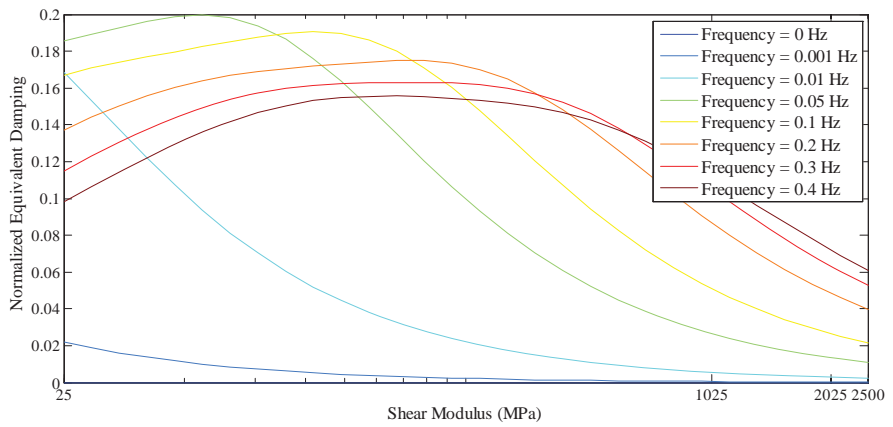
Fig. 13
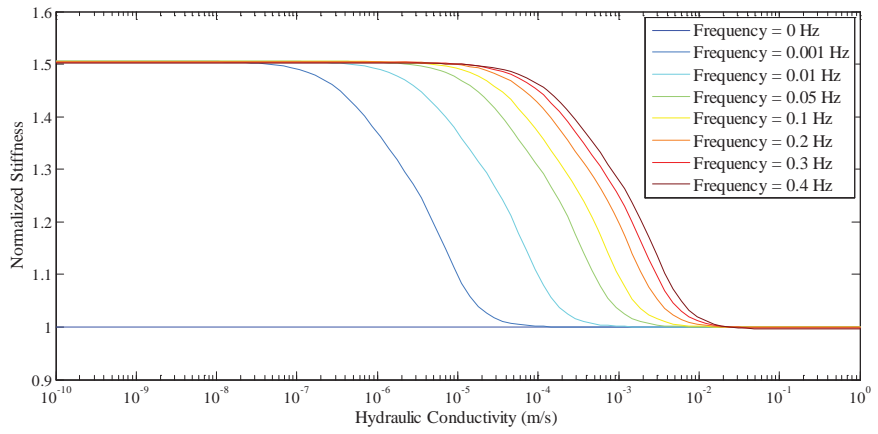
Fig. 14
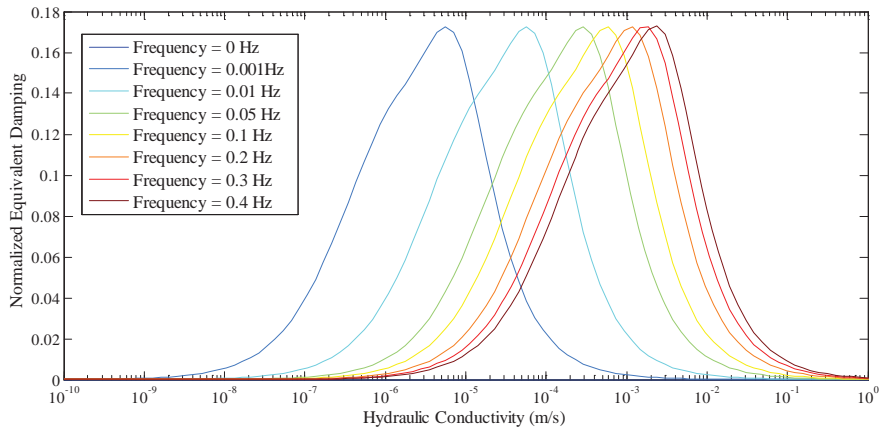
Fig. 15
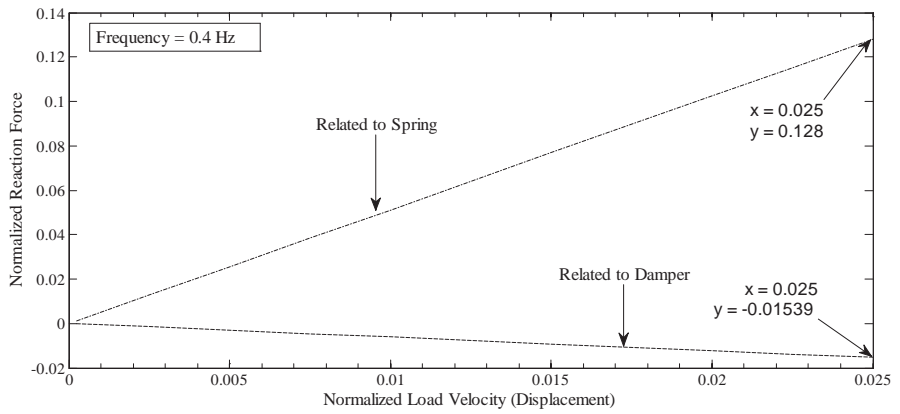
Fig. 16
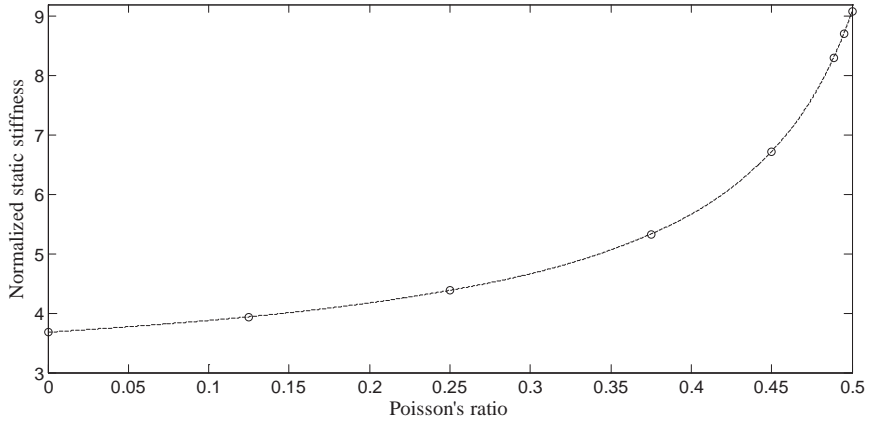
Fig. 17
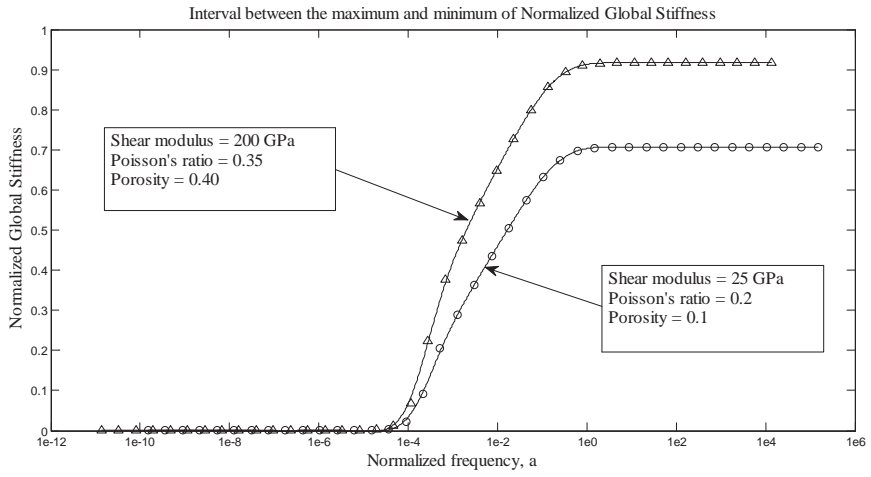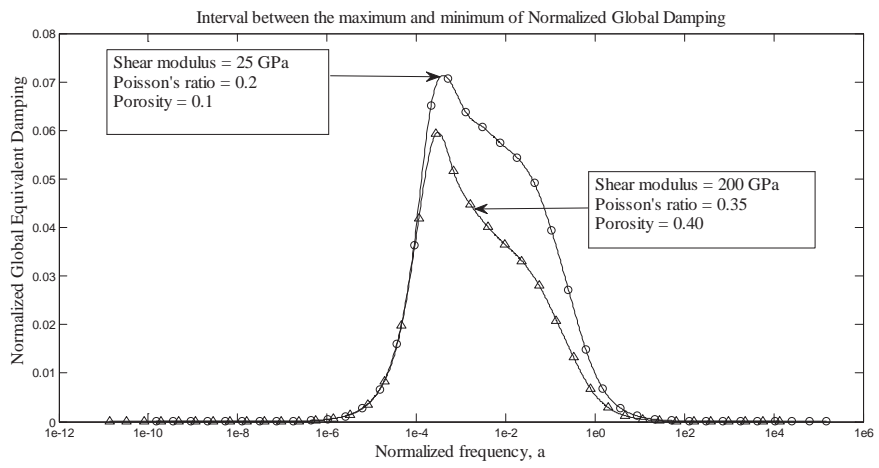
Interval between the maximum and minimum of Normalized Global Stiffness

Normalized Global Stiffness (y-axis)

Normalized frequency, a (x-axis)

Shear modulus = 200 GPa
Poisson's ratio = 0.35
Porosity = 0.40

Shear modulus = 25 GPa
Poisson's ratio = 0.2
Porosity = 0.1

Fig. 18

Fig. 19

Influence of pore pressure on dynamic response of offshore wind turbine using poroelastic model

Authors:

Mehdi Bayat, Lars Vabbersgaard Andersen, Lars Bo Ibsen and Johan Clausen

E.1 Author's Right

Journal author rights

In order for Elsevier to publish and disseminate research articles, we need publishing rights. This is determined by a publishing agreement between the author and Elsevier. This agreement deals with the transfer or license of the copyright to Elsevier and authors retain significant rights to use and share their own published articles. Elsevier supports the need for authors to share, disseminate and maximize the impact of their research and these rights, in Elsevier proprietary journals* are defined below:

For subscription articles	For open access articles
Authors transfer copyright to the publisher as part of a journal publishing agreement, but have the right to:	Authors sign an exclusive license agreement, where authors have copyright but license exclusive rights in their article to the publisher**. In this case authors have the right to:
• Share their article for Personal Use, Internal Institutional Use and Scholarly Sharing purposes, with a DOI link to the version of record on ScienceDirect (and with the Creative Commons CC-BY-NC- ND license for author manuscript versions) • Retain patent, trademark and other intellectual property rights (including raw research data). • Proper attribution and credit for the published work.	• Share their article in the same ways permitted to third parties under the relevant user license (together with Personal Use rights) so long as it contains a CrossMark logo, the end user license, and a DOI link to the version of record on ScienceDirect. • Retain patent, trademark and other intellectual property rights (including raw research data). • Proper attribution and credit for the published work.

http://www.elsevier.com/about/company-information/policies/copyright

Influence of pore water in the seabed on dynamic response of offshore wind turbines on monopiles

M. Bayat[a,*], L. V. Andersen[a], L. B. Ibsen[a], J. Clausen[a]

[a]*Department of Civil Engineering, Aalborg University, Sofiendalsvej 11, 9200 Aalborg SV, Denmark*

Abstract

The well-known $p - y$ curve method provides soil-structure interaction that does not account for the pore pressure effect for dynamic analysis of offshore wind turbines (OWTs). However, in order to avoid conservatism, the dynamic structural response must be analyzed using reliable estimations. The turbine is introduced using a simplified model with the purpose of assessing the modal damping due to pore water flow around the monopile. In this paper the effect of pore pressure is illustrated by implementing a poroelastic model to present more realistic dynamic properties and compare them with results obtained by the $p - y$ curve method. For this purpose, two different finite-element programs are developed and combined for analyzing an offshore monopile foundation placed in different depths. The response to cyclic loading is analyzed by employing a Winkler foundation model based on nonlinear $p - y$ curve method. Moreover, a two-phase system consisting of a solid skeleton and pore fluid, based on $\mathbf{u} - P$, is implemented to perform free vibration tests to evaluate the eigenfrequencies. Here, $\mathbf{u}$ is grain displacement and P is pore water pressure. Since the stiffness of foundation and subsoil strongly affects the modal parameters of the combined structure and soil, the stiffness of saturated soil, accounting for pore pressure generated by cyclic motion of monopiles is investigated using the concept of a Kelvin model. A simple model of an OWT foundation is constructed with equivalent masses, dashpots and springs providing the foundation response at the pile-cap level by using Winkler and Kelvin

---

[*] Corresponding author. Tel.: +4599408575; *E-mail*: meb@civil.aau.dk (or) Bayat.me@gmail.com

models. The calculated soil stiffness from the Winkler and Kelvin models are compared in presentence of soil damping for Kelvin model.

1. Introduction

Several foundation concepts such as monopile, suction caisson, jacket, tripod and gravity foundations have been developed for offshore wind turbines (OWTs). The monopile foundation is analyzed in this paper, since it is the far most used foundation concept for OWTs. A monopile foundation consists of a tubular support structure that extends into the seabed. Offshore wind turbine foundations (OWTFs) are subjected to time-varying loads from waves, wind and ice, and during operation blade passage across the tower as well as imbalances in the rotor cause cyclic loading. It is vital to capture the integrated effect of the total loads. However, the total loading can be significantly less than the sum of the constituent loads. This is because the loads are not coincident, and because of the existence of different kinds of damping such as aerodynamic and soil damping which damp the motions due to the loads. The overall weight of the modern wind turbines is minimized, which makes it more flexible and corollary more sensitive to dynamic excitations at low frequencies. Based on Det Norske Veritas (DNV) [1]/Risø [2] as a design guideline, the deformation of a monopile can be calculated by using the Winkler approach; hence, the soil is modeled as non-linear springs attached along the pile, and the pile is modeled as beam elements. In the lateral direction, the non-linear springs represent the relationship between the lateral deflection distance y, and the mobilized resistance from the surrounding soil p [3]. This method has not been demonstrated to provide reliable results for OWTFs subjected to dynamic and cyclic loads. In order

to have better assessment of soil-structure interaction, the coupled flow and deformation associated with the motion of fluid and solid grain particles should be considered. For slender piles, the $p - y$ curve method has been implemented to account for soil-pile interaction [4-12] and theoretical results are compared by experimental investigation [13-16]. Some other design guidelines such as American Petroleum Institute (API) [3] and DNV [1]/Risø [2] derived and presented the formulations of $p - y$ curves for sand and clay. Application of the $p - y$ curve method for OWTFs has many short comings which refer to [17-19]. Firstly, monopiles are not slender. They have length-to-diameter ratio of 5-7 and usually exhibit "toe kick", whereas slender piles have no movement at the toe (bottom). Secondly, as further addressed in this paper, the effect of pore pressure is not comprised in the $p - y$ curve method. In order to include the effect of pore pressure, coupled equations for the soil and pore fluid are needed.

In this context, the estimation of a liable first natural frequency of the combined foundation and turbine structure is presented. To avoid dynamic amplification of the response, the first natural frequency of the wind turbine structure, including its foundation, must lie within a narrow range. Unfortunately, accurate and realistic natural frequencies cannot be quantified by a $p - y$ curve method. Several studies have presented dynamic response and calculated natural frequencies of OWTs based on single-phase soil model and the $p - y$ curve method. Traditionally, simplified soil stiffness functions ($p - y$ curves) are developed for small-diameter piles, not accounting for dynamics and representing the soil stiffness incorrectly for monopiles. The damping is also not very well predicted in this traditional approach. The inaccuracy in prediction of soil stiffness and damping implies significant safety margins in design. Therefore, additional modelling and research into this field is required. In this research the effect of pore pressure and damping will be considered to estimate the first three natural frequencies. The existing $p - y$ curve method does not account for

pore pressure build-up in the soil. In this study a combination of springs and dashpots are employed to interpret the visco-elastic response of pile-soil interaction.

In order to have the effect of pore pressure and soil deformation, two-phase coupled equations are needed. Three general coupled and dynamic formulations, based on the soil and pore fluid (water) displacements and the pore water pressure, are the $\mathbf{u} - P - \mathbf{U}$, $\mathbf{u} - P$, and $\mathbf{u} - \mathbf{U}$ equations, where $\mathbf{u}$, P, and $\mathbf{U}$ are the soil skeleton displacement, pore water pressure (PWP), and pore water displacement, respectively [20]. Cheng and Jeremić [21] used a fully coupled, inelastic $\mathbf{u} - P - \mathbf{U}$ formulation to simulate the dynamic behavior of piles in liquefiable soils subjected to seismic loading. In the $\mathbf{u} - P$ formulation, if the fluid phase is considered incompressible, then the Ladyzenskaja-Babuska-Brezzi (LBB) condition needs to be satisfied [22-24]. In this case, the element type for the displacement and pore pressure fields requires special consideration, to prevent volumetric locking [25-27]. Considering this restriction, a simple model for numerical analyses is the $\mathbf{u} - P$ formulation that neglects the relative acceleration of the fluid with respect to the solid skeleton. This model is especially useful for low-frequency analysis. Zienkiewicz *et al.* [27] studied the transient and static response of saturated soil, which they modeled as a two-phase material based on the $\mathbf{u} - P$ formulation for porous media. Pastor *et al.* [28] used a generalized plasticity approach to describe the behavior of soil in the $\mathbf{u} - P$ formulation under transient loading. Elgamal *et al.* [29-30] implemented the $\mathbf{u} - P$ model for a two-phase (solid-fluid) problem with multi-surface plasticity, using a finite element method (FEM) to highlight the effect of excitation frequency. Researchers have attempted to solve these coupled equations by various numerical methods [31-33]. Here, however, a two dimensional linear model will be employed to analyze a monopile segment at a given depth.

The characteristics of OWTFs are not fully understood. The proposed model and observation should be considered as an attempt at reconciling the traditional $p - y$ curve method and applying

cyclic load. In particular, the model is shown to possess reasonable results in presenting soil stiffness and damping curves over an applicable frequency range. This study deals with a selected wind turbine structure to estimate the first eigenfrequency for seabed conditions, by use of a Winkler foundation model.

Furthermore, the concept of a Kelvin model is employed and combined with a two-dimensional FE model of the foundation, surrounded by an elastic saturated soil and subjected to cyclic load in order to illustrate the dependency between soil stiffness and permeability. This in turn makes it possible to analyze the dynamic response of a linear pore-elastic medium by implementing a two phase model in incorporation of $\mathbf{u} - P$ equations. It should be mentioned that the two-dimensional FE model assume plane strain and plane flow; thus the volumetric dynamic flow is ignored. Further, small deformation of the soil is assumed. The FEM in the $\mathbf{u} - P$ equations is employed to explore the effects of pore pressure and calculate the seepage damping.

The outline of the paper is as follows: Section 2 presents the modeling concept and the methods of analysis are presented in Section 3. This includes natural frequency analysis, extraction of equivalent masses, dashpots and springs at pile cap as well as cross modal damping ratios. The model discretization is presented in Section 4. A monopile foundation is analyzed based on Winkler and Kelvin models which take into account the effect of pore pressure in Section 5. Some concluding remarks are presented in Section 6.

2. Modeling Concept

In this study, the FEM is employed to investigate a laterally loaded monopile by assuming that the pile and tower act as a Bernoulli–Euler beam.

2.1. Soil-pile interaction model and equilibrium equations

2.1.1. Winkler model

DNV-J101 [1] proposes the Winkler approach to describe the soil-pile interaction based on attaching non-linear springs along the pile. The pile is modeled as beam elements, see Figure 1.

<div align="center">

Figure 1 near here

</div>

The governing differential equation for the considered pile and tower as a Bernoulli–Euler beam for static and dynamic cases are given by:

Static, nonlinear: $E_{\mathrm{TP}}I_{\mathrm{TP,x}}\dfrac{d^4y}{dx^4} + E_{py}y = 0$ (1a)

Dynamic, linear: $E_{\mathrm{TP}}I_{\mathrm{TP,x}}\dfrac{\partial^4 y}{\partial x^4} + M_{\mathrm{TP}}\dfrac{\partial^2 y}{\partial t^2} + E_{py}^* y = 0$ (1b)

where E_{TP} , $I_{\mathrm{TP,x}}$ and M_{TP} are Young's modulus, second moment of area and mass of the structure (Tower/pile), respectively. Further, y is the structural deflection. E_{py} and E_{py}^* are the secant and initial stiffness (modulus) of the $p - y$ curve.

The $p - y$ curves for friction soils according to DNV-J101 [1] can be calculated based on mentioned items in Figure 2. where p_u is the theoretical ultimate lateral soil capacity, y is the lateral deflection, x is the depth measured below the soil surface (mudline). In API and DNV k is determined based on the internal angle of friction or relative density of the sand. A is a factor to account for static or cyclic loading (Reese *et al.* [34]).

<div align="center">

Figure 2 near here

</div>

In order to do a modal analysis of offshore wind turbines, linear analysis needs to be performed. Therefore, the soil stiffness used in the calculation needs to be linearized. It is assumed that the steel is in linear range, hence the stiffness of that can be described with Young's modulus. And also, it is common to estimate the initial spring stiffness E_{py}^* by linearizing the nonlinear $p - y$ curves suggested by DNV [1,2]. Theoretically, the linearizing can be done by use of either the initial soil

stiffness from the nonlinear uncoupled soil springs or from the secant and tangent soil stiffness when the turbine is producing power at the nominally rated output level. However, studies regarding cyclic loading of piles made by Klinkvort [35] and Roesen and Thomassen [36] indicate that the unloading-reloading path almost follows the initial stiffness E_{py}^* of the virgin curve. Despite decreasing secant stiffness during cyclic loading, it seems sensible for a modal analysis of offshore wind turbines to determine the spring stiffness from the initial stiffness of the nonlinear $p - y$ curve formulation. The linearization of the curves can be seen in Figure 3.

Figure 3 near here

The linearized stiffness for sand layers is equal to the initial slope of the $p - y$ curve. By differentiating the $p - y$ curve relationship for piles in cohesionless soils according to DNV [1,2], the initial stiffness E_{py}^* is given by:

$$E_{py}^* = \frac{\partial p}{\partial y}\bigg|_{y=0} = \frac{\partial p}{\partial y}\left(Ap_u \tanh\left(\frac{kx}{Ap_u}y\right)\right)\bigg|_{y=0} = kx \tag{2}$$

when $y = 0$, E_{py} is equal to the initial stiffness, $E_{py}^* = kx$. Hence, the initial stiffness of the $p - y$ curve is assumed independent of the pile geometry.

2.1.2.   Kelvin model

In order to illuminate the effect of pore pressure on soil behaviour, especially stiffness and damping in different depths, the Kelvin model is utilized based on the FE code for $\mathbf{u} - P$ equations. A two-dimensional poroelastic FE model subjected to a harmonic forced displacement is considered. In the Kelvin model (as shown in Figure 4), a system with a spring and a dashpot is considered to calculate the soil stiffness and damping in each integration point. The governing linear equation reads:

Figure 4 near here

Dynamic, linear, Kelvin: $E_{TP}I_{TP,x}\dfrac{\partial^4 y}{\partial x^4} + M_{TP}\dfrac{\partial^2 y}{\partial t^2} + E_{py}^* y + E_{p\dot{y}}^*\dfrac{\partial y}{\partial t} = 0$ (3)

The spring stiffness, E_{py}^*, is not the one proposed by API. It depends on whether drained or undrained or intermediate conditions are presented during the considered cyclic motion and will, together with the damping, $E_{p\dot{y}}^*$, be calculated from FE model based on a $\mathbf{u} - P$ formulation.

2.2. Coupled equations based on the $\mathbf{u} - P$ formulation

The 2D FE code has developed to solve the coupled equations. The total momentum balance for the porous medium reads:

$$\sigma_{ij,j} + \rho b_i = \rho\ddot{u}_i + \rho_f\ddot{w}_i \qquad (4)$$

where σ_{ij} is the total stress tensor and $\sigma_{ij} = \sigma'_{ij} - \alpha P\delta_{ij}$. Here σ'_{ij} is the effective stress tensor, $\alpha = 1 - \dfrac{K_T}{K_S}$, where K_T and K_S are the total bulk modulus of the solid matrix and solid particles receptively, P is pore pressure and δ_{ij} is Kronecker's delta: $\delta_{ij} = 1$ when $i = j$, and $\delta_{ij} = 0$ when $i \neq j$. The density of mixture is $\rho = (1 - n_p)\rho_s + n_p\rho_f$ where n_p, ρ_s and ρ_f are the porosity and the densities of the solid phase and fluid (water), respectively. Finally, $\ddot{u}_i$ and $\ddot{w}_i$ are the acceleration of the solid skeleton and pseudo-acceleration of the fluid phase relative to the skeleton. Comma subscript and dot superscripts denote derivatives with respect to spatial coordinates and time, respectively. The tensile component of stress and compressive component of pressure are assumed to be positive. The equation of the total coupled system can be written as

$$-P_{,i} - \frac{\dot{w}_i}{k} + \rho_f b_i = \rho_f\left(\ddot{u}_i + \frac{\ddot{w}_i}{n_p}\right) \qquad (5)$$

where $= \dfrac{k'}{g\rho_f}$, and k' is the hydraulic conductivity, which has the same unit as velocity. Further, $\mathbf{b}_i$ is the body force per unit mass. The final equation is supplied by the mass conservation of the fluid flow:

$$\dot{w}_{i,i} + \alpha\dot{\epsilon}_{ii} + \frac{\dot{P}}{Q} = 0 \tag{6}$$

where $Q = Q_{sf} = \frac{K_s K_f}{K_s + K_f}$ is the total compression modulus. K_S and K_f are the solid and fluid bulk moduli, respectively[37-39].

2.2.1. Governing equation ($\mathbf{u} - P$ formulation)

The relative acceleration of the fluid with respect to the solid skeleton can be ignored for lower frequencies. Then, Eq. (4) is rewritten as:

$$\sigma_{ij,j} + \rho b_i = \rho\ddot{u}_i \tag{7}$$

Substituting for $\dot{w}_i$ from Eq. (5) into Eq. (6) by taking derivate once, and ignoring the relative acceleration of the fluid with respect to the solid skeleton, it is obtained that:

$$\left(k\left(-P_{,i} + \rho_f b_i - \rho_f\ddot{u}_i\right)\right)_{,i} + \alpha\dot{\epsilon}_{ii} + \frac{\dot{P}}{Q} = 0 \tag{8}$$

For a model which combines solid and fluid phases, the boundary conditions are defined based on traction, displacement, fluid flow and pore pressure as shown in Figure 5. The pore pressure and displacements are considered zero at the exterior boundary and forced displacement in the horizontal direction is applied for the semi-circle boundary at the soil-pile interface. The soil stiffness and damping for a given depth is calculated by implementing FEM.

Figure 5 near here

2.2.2. Elements used for coupled analysis

In order to have stable results for pore pressure and avoiding any LBB conditions, the elements used for coupled analysis should consist, for example, of 6-noded quadratic and 3-noded linear elements or 9-noded biquadratic and 4-noded bilinear elements for displacement and pore pressure fields respectively as shown in Figure 6a [39]. Thus, the interpolation order for P is one lower than the interpolation order for $\mathbf{u}$.

The mesh consists of 9-noded biquadratic and 4-noded bilinear elements for displacement and pore pressure fields, respectively. Fine meshes are generated close to the pile while coarse meshes are used when it is far from the pile as shown in Figure 6b.

Figure 6b near here

2.3. Beam finite element description

The OWT is modelled as an Euler-Bernoulli beam and discretized into finite segments. The Winkler and Kelvin approaches used to represent the soil stiffness. DNV[1] suggests that the pile is modeled as beam elements and soil reaction along the monopile is considered as horizontal springs which act at the nodes. A beam element with two degrees of freedom (DOF), i.e. the horizontal translation and the in-plane rotation at each node, is chosen. Two FE procedures are working simultaneously to describe the behaviour of the OWT. A beam theory is considered for the OWT and for each integration point a Kelvin model is employed to present the soil damping and stiffness.

Two steps are implemented to discretize the pile and tower system based on beam theory. At first, master nodes are defined and located where there is a change in geometry of the structure (tower/pile), at mudline and also at sea level (waterline). In the second step, the master elements are divided into a number of two-noded elements with cubic interpolation of the transfer displacement and C_1 continuity. In order to consider a proper sub element length L_{elem}, convergence tests need to be done. The convergence tests are considered to examine the deflection of the monopile/OWT and also the maximum value of shear force and moment in the system. An example on a convergence test is shown in Figure 7.

Figure 7 near here

As it can be seen in Fig. 7, convergence of the maximum shear force is reached for an element length of 1 m. It can be mentioned that based on geometry and material properties the maximum length of an element cannot be larger than 7 m for the model presented in this study. The number of beam elements based on the convergence test is 121 and thereby system matrices with the dimensions 244×244 are sufficient to evaluate the first three undamped eigenfrequencies while f_1 related to the lowest eigenmode $\Phi^{(1)}$.

For simplicity, the rotor and nacelle masses are considered as a concentrated mass at the top point of the tower. Similarly, masses of the flanges are evaluated as concentrated masses. The monopile is assumed to be flooded, *i.e.* the mass of the water within the monopile is added as dead weight. Water around the monopile is applied as added mass according to DNV [1,2].

In this study, by considering admissible element size and applying more integration points for each element, the soil can be modelled as a continuous spring over each element by employing the Simpson rule. In this method the discrete springs connected to nodes for element with short length, which requires a lot of elements, is disregarded. For each integration point along the element of the pile, E_{py}^* is evaluated based on 2-D FE model and Simpson integration is used to determine $\mathbf{K}_{soil}$.

From the Kelvin model, the soil stiffness is calculated in each depth and these values are used instead of the obtained soil stiffness from the Winkler model to present the natural frequency of the OWT.

3. Methods of Analysis

3.1. Natural frequency analysis

Assembling the global system stiffness and mass matrices and applying the boundary conditions, the following eigenvalue problem is solved:

$$\mathbf{M}_{TP}\ddot{\mathbf{U}}(t) + (\mathbf{K}_{TP} + \mathbf{K}_{soil})\mathbf{U}(t) = 0 \tag{9}$$

11

where $\mathbf{M}_{TP}$ is the global structural (tower and pile) mass matrix, $\mathbf{K}_{TP}$ and $\mathbf{K}_{soil}$ are the global wind turbine structural and subsoil stiffness matrices, respectively. $\mathbf{U}(t)$ is the generalized DOF vector which contains displacements and rotations at the nodes. In order to find the undamped eigenfrequency f_a for the ath eigenmode $\Phi^{(a)}$, a harmonic function is applied as a solution to Eq. (9).

$$\mathbf{U}(t) = \Phi^{(a)}\text{Re}\left(q_a(t)e^{j\omega_a t}\right), j = \sqrt{-1} \tag{10}$$

Note that $\Phi^{(a)}$ is real and $q_a(t)$ is the modal coordinate. where it is used that the ath angular eigenfrequency ω_a of the harmonic motion $\mathbf{U}(t)$ is given by $\omega_a = 2\pi f_a$. Inserting Eq. (10) into Eq. (9) makes it possible to find the ath undamped eigenfrequency f_a and corresponding eigenmode $\Phi^{(a)}$ by solving the frequency condition:

$$\det\left((\mathbf{K}_{TP} + \mathbf{K}_{soil}) - \omega_a^2 \mathbf{M}_{TP}\right) = 0$$

(11)

it is noted that added mass from the soil is not accounted for. Only the mass inside the tubular pile is assumed to move with the pile.

3.2. Equivalent masses, dashpots and springs at pile cap

In order to obtain the eigenfrequency of the structure–foundation–soil system, an equivalent model has been calibrated to the pile head response. A simple model of a wind turbine has been generated. The base of the turbine tower is fixed to the monopile cap. Figure 8 shows a simple equivalent mass-dashpot-spring (EMDS) model.

Figure 8 near here

For a monopile and surrounding soil the equivalent stiffness ($\mathbf{K}_{cap}$) can be derived from the inverse of the flexibility at the pile cap. It can be shown as:

Case 1: Static

$$\mathbf{K}_{\text{sys}}^{\text{stat}} \, \mathbf{U} = \mathbf{F} \; \rightarrow \mathbf{K}_{\text{cap}}^{\text{stat}} \tag{12a}$$

$$\mathbf{K}_{\text{sys}}^{\text{stat}} = \mathbf{K}_{\text{pile}} + \mathbf{K}_{\text{soil}}^{\text{stat}} \tag{12b}$$

$\mathbf{K}_{\text{sys}}^{\text{stat}}$ is the stiffness of the pile-soil system, including the stiffness of the monopile and soil.

Case 2: Dynamic (cyclic for soil)

$$\mathbf{K}_{\text{sys}}(\omega) \, \mathbf{U}(\omega) = \mathbf{F}\,(\omega) \rightarrow \mathbf{K}_{\text{cap}}(\omega)\,; \quad \mathbf{K}_{\text{sys}}(0) = \mathbf{K}_{\text{sys}}^{\text{stat}}\,, \; \mathbf{K}_{\text{soil}}(0) = \mathbf{K}_{\text{soil}}^{\text{stat}} \tag{13a}$$

$$\mathbf{K}_{\text{sys}}^{\text{stat}} = \mathbf{K}_{\text{pile}} + \mathbf{K}_{\text{soil}}^{\text{stat}} \tag{13b}$$

By implementing the general stiffness and using the same procedure, the EMDS can be calculated as:

For Winkler model based on API:

$$\mathbf{D}_{\text{sys}}^{\text{w}}(\omega) \, \mathbf{U}(\omega) = \mathbf{F}(\omega) \; \rightarrow \mathbf{D}_{\text{cap}}^{\text{w}}(\omega) \rightarrow \mathbf{M}_{\text{cap}}^{\text{w}}(\omega) \tag{14a}$$

$$\mathbf{D}_{\text{sys}}^{\text{w}}(\omega) = \mathbf{K}_{\text{sys}}^{\text{stat}} - \omega^2 \mathbf{M}_{\text{sys}}\,; \tag{14b}$$

$$\mathbf{D}_{\text{sys}}^{\text{w}}(\omega) = \mathbf{K}_{\text{pile}} + \mathbf{K}_{\text{soil}}^{\text{stat}} - \omega^2 \mathbf{M}_{\text{sys}}\,; \tag{14c}$$

For Kelvin model based on poroelasticity:

$$\mathbf{D}_{\text{sys}}^{\text{k}}(\omega) \, \mathbf{U}(\omega) = \mathbf{F}(\omega) \; \rightarrow \; \mathbf{D}_{\text{cap}}^{\text{k}}(\omega) \rightarrow \mathbf{C}_{\text{cap}}^{\text{k}}\,(\omega) \text{and } \mathbf{M}_{\text{cap}}^{\text{k}}(\omega) \tag{15a}$$

$$\mathbf{D}_{\text{sys}}^{\text{k}}(\omega) = \mathbf{K}_{\text{sys}}(\omega) + \mathrm{j}\omega\mathbf{C}_{\text{sys}}(\omega) - \omega^2\mathbf{M}_{\text{sys}}\,; \quad \mathbf{C}_{\text{sys}}(0) = 0, \quad \mathrm{j} = \sqrt{-1} \tag{15b}$$

$$\mathbf{D}_{\text{sys}}^{\text{k}}(\omega) = \mathbf{K}_{\text{pile}} + \mathbf{K}_{\text{soil}}(\omega) + \mathrm{j}\omega\mathbf{C}_{\text{soil}}(\omega) - \omega^2\mathbf{M}_{\text{sys}}\,; \quad \mathbf{C}_{\text{soil}}(0) = 0 \tag{15c}$$

$\mathbf{C}_{\text{sys}}$ is calculated based on the calculated damping of soil from the Kelvin model and it takes zero value for the Winkler model and the structural damping has not been included. Hence, damping due to seepage of pore water can be quantified directly, since it is the only dissipation in the system. $\mathbf{M}_{sys}$ equals to the monopile mass. By applying a unit force or moment at the pile cap one at the time, the (dynamic) flexibility matrix, can be calculated. Next, $\mathbf{D}_{\text{cap}}$ is found as the real part of the inverse of the (complex) flexibility matrix at the pile cap. By comparing $\mathbf{D}_{\text{cap}}$ and $\mathbf{K}_{\text{cap}}$, the mass ($\mathbf{M}_{\text{cap}}$) at the pile cap can be calculated as:

$$\mathbf{M}_{cap}^{w} = \frac{\mathbf{K}_{cap}^{stat} - \mathbf{D}_{cap}^{w}(\omega)}{\omega^2}, \qquad \mathbf{M}_{cap}^{k} = \frac{\mathbf{K}_{cap}(\omega) - \text{Re}(\mathbf{D}_{cap}^{k}(\omega))}{\omega^2} \tag{16}$$

The equivalent dashpot at the pile cap ($\mathbf{C}_{cap}$) can be obtained from the imaginary part of the inverse of the complex flexibility matrix at the pile cap. It can be mentioned that the soil stiffness calculated from the Winkler and Kelvin models takes different values because of the presence of pore pressure in the FE model used to derive the Kelvin model. The equivalent mass, damping and stiffness at the pile cap obtained by the Winkler and Kelvin models can be represented as:

$$\text{Equivalent mass based on Winkler model} \quad = \mathbf{M}_{cap}^{w} = \begin{bmatrix} (m_{cap}^{w})_{11} & (m_{cap}^{w})_{12} \\ (m_{cap}^{w})_{21} & (m_{cap}^{w})_{22} \end{bmatrix} \tag{16a}$$

$$\text{Equivalent mass based on Kelvin model} \quad = \mathbf{M}_{cap}^{k} = \begin{bmatrix} (m_{cap}^{k})_{11} & (m_{cap}^{k})_{12} \\ (m_{cap}^{k})_{21} & (m_{cap}^{k})_{22} \end{bmatrix} \tag{16b}$$

$$\text{Equivalent stiffness based on Winkler model} = \mathbf{K}_{cap}^{w} = \begin{bmatrix} (k_{cap}^{w})_{11} & (k_{cap}^{w})_{12} \\ (k_{cap}^{w})_{21} & (k_{cap}^{w})_{22} \end{bmatrix} \tag{16c}$$

$$\text{Equivalent stiffness based on Kelvin model} = \mathbf{K}_{cap}^{k} = \begin{bmatrix} (k_{cap}^{k})_{11} & (k_{cap}^{k})_{12} \\ (k_{cap}^{k})_{21} & (k_{cap}^{k})_{22} \end{bmatrix} \tag{16d}$$

$$\text{Equivalent dashpot based on Kelvin model} \quad = \mathbf{C}_{cap}^{k} = \begin{bmatrix} (c_{cap}^{k})_{11} & (c_{cap}^{k})_{12} \\ (c_{cap}^{k})_{21} & (c_{cap}^{k})_{22} \end{bmatrix} \tag{16e}$$

In order to treat frequency-dependent soil stiffness properly, an iteration procedure is implemented as explained in the following. By first using the API model presented above, the natural frequency of a wind turbine and the equivalent pile-cap system are calculated based on the Winkler model. By implementing the obtained frequency and initial soil stiffness from the $p - y$ curve (API) as an initial guess for the Kelvin model, the reaction force at the interface is calculated based on the Kelvin model and using the poroelastic soil model to find the soil stiffness and damping for each layer. Then, by using the soil stiffness calculated from the Kelvin model, the natural frequency is calculated and compared with the natural frequency which was used as the input for the Kelvin model. Iteration procedure is performed until the natural frequency based has converged.

3.3. Extraction of Modal Damping

The surrounding soil around the pile is modeled as poroelastic material with isotropic material properties. In order to reveal the effect of pore pressure, the harmonic forced displacement is considered as:

$$\text{Forced displacement} = y(t) = y_0 \sin(\Omega t) \quad , \quad \Omega = 2\pi f \tag{17}$$

Damping in the soil consists of hysteretic, seepage and geometrical damping. Hysteretic and geometrical damping can have important roles when there is nonlinear material behaviour and large load frequency ($f > 0.5$ Hz), respectively, but it is disregarded in the presented analysis. Based on the FE formulation, the seepage provides viscous damping linearly proportional to the velocity of the moving soil. For each pile segment, the spring stiffness and viscous damping constant of an equivalent Kelvin model (see Figure 9) can be extracted.

Figure 9 near here

The reaction force at the interface between the pile and soil can be represented as:

$$p = k_{sp.}y + \mathrm{j}c_{dam.}\dot{y} \ , \quad \mathrm{j} = \sqrt{-1} \ , \qquad k_{sp.} = \mathrm{E}_{py}^* \qquad\qquad c_{dam.} = \mathrm{E}_{p\dot{y}}^* \tag{18}$$

where y and $\dot{y}$ are displacement and velocity respectively. The real and imaginary part of the reaction force is used to obtain the stiffness and damping in the equivalent Kelvin model. The constructed damping matrix based on the seepage damping is a non-classical matrix and thus the modal damping matrix is not diagonal. The cross modal damping ratios ζ_{ab} are calculated as:

$$\mathbf{\Phi}_a^T(\omega)\mathbf{C}_{sys}(\omega)\mathbf{\Phi}_b(\omega) = c_{ab}(\omega) = 2\zeta_{ab}(\omega)\sqrt{\omega_a\omega_b m_a(\omega)m_b(\omega)} \tag{19}$$

$\mathbf{\Phi}_a(\mathbf{\Phi}_b)$ and m_a (m_b) are the undamped eigenmode and modal mass for mode a (b). The iteration procedure is implemented to get the desired results for the frequency dependent cross modal damping ratio.

4. Discretization of model

4.1. Geometry and material properties of OWT

In this study a Vestas V90-3.0MW OWT with a nacelle height of 61.98 m above the mean sea level has been considered. The total length of the tubular pile and the transition piece is equal to 45.24 m and the outer pile diameter (OD) is 4.3 m. The pile wall thickness varies from 35 mm to 71 mm as shown in Fig. 5a. The pile cap is located 7.74 m below the mean sea level leading to an embedded depth of 29.5 m (see Table 1). The tower is a tubular steel tower which consists of twenty-five sections while two adjacent sections are bolted together through internal flange-bolt connections. The rotor mass and nacelle mass are 38,400 kg and 70,600 kg, respectively. The geometry of the offshore wind turbine monopile foundation is presented in Table 1.

Table 1 near here

To account for the increased mass and stiffness in the presence of the grout annulus between the pile and the transition piece, an equivalent steel wall thickness is used for section 3 of the pile.

The tower is placed on the transition piece 8 m above the mean sea level. Young's modulus, Poisson's ratio and mass density for the tower equal to 210 GPa, 0.3 and 7850 kg/m^3, respectively. The tower is conical and its wall thickness wall varies from 15 mm to 26 mm as shown in Figure 10.

Figure 10 near here

4.2. Geometry and material properties of surrounding soil

It is assumed the lateral soil stiffness represented by nonlinear springs based on $p - y$ curve method (see Figure 11). And also, a two-dimensional model based on the Kelvin model represents the pile-soil interaction by having a spring and dashpot for each layer (as shown in Fig. 4).

Three different soil types namely loose, medium and dense sand are considered. The mudline is started at -7.74m and ended at -51.74m. The material properties of loose, medium and dense sand are listed in Table 2.

Table 2 near here

4.3. Geometry of 2-D poroelastic model in each depth

The soil damping and stiffness in the saturated soil are determined based on the Kelvin model. A two-dimensional poroelastic FE model subjected to a harmonic forced displacement is employed in order to obtain the stiffness and damping properties to be applied within the Kelvin model. In this study, plane strain is considered and as illustrated in Fig. 4, the properties (stiffness and damping) are found per unit length. A tubular monopile offshore foundation (Figure 12) for a given depth, surrounded by an elastic saturated soil with radius R is considered. The soil box used in the present analysis has the horizontal dimensions 1000 m × 1000 m and the slices are 1 m thick. The R is 2.15 m. A harmonic sinusoidal forced displacement in the horizontal direction is applied to the border between the saturated soil and the pile. Small deformation of the soil is assumed and symmetry is considered with respect to the horizontal direction orthogonal to the forced displacement.

Figure 12 near here

5. Numerical results

The following subsections elucidate the Winkler model, the difference between the Winkler and Kelvin models and the effect of pore pressure when the Kelvin model is employed. The analysis is conducted using three cases, namely loose, medium and dense sandy soil. Cyclic and modal analyses are performed to determine the deformation and the first three natural frequencies. The effect of pore pressure is highlighted by doing a parametric study.

5.1. Results based on the Winkler model

The results presented in this section contain the pressure on the pile, variation of the shear force and moment along the OWT structure, mode shapes and natural frequencies of OWTs where there is loose sand, based on the API recommendation for cyclic load.

Figure 13 near here

The final displacement for whole structure is shown in Fig. 13. The maximum displacement occurs at the top of tower.

The horizontal soil pressure along the pile is seen in Figure 14, left. The pressure is continues and takes a change of sign along the pile.

Figure 14 near here

As it can be seen, the maximum soil pressure occurs close to mudline.

The variation of moment and shear force in the OWT structure is shown in Figure 15.

Figure 15 near here

The modal analysis has been done to present the first three natural frequencies and mode shapes as shown in Figure 16.

Figure 16 near here

5.2. Comparison between Winkler and Kelvin model

Three different soil types' namely loose, medium and dense sandy soil have been considered to compare the results from the Winkler and Kelvin models. The natural frequencies obtained from the modal analysis based on the API Winkler model are considered as an initial guess for the Kelvin model.

5.2.1. Variation of initial stiffness with the monopile depth

Based on API recommendation, the initial soil stiffness for each type of soil is varying with depth linearly as shown in Figure 17.

<center>**Figure 17 near here**</center>

The calculated initial soil stiffness is used to find the variation of shear modulus in the poroelastic FE model in order to have the same soil type for the Winkler and Kelvin models.

The natural frequencies, cross modal damping ratio, equivalent mass, dashpot and stiffness at pile cap are presented for different soil types.

5.2.2. Loose sand

The first three natural frequencies are compared in Table 3 for loose sand besides the cross modal damping ratio. The calculated natural frequencies based on the Kelvin model are greater than those calculated by the Winkler model.

<center>**Table 3 near here**</center>

The difference between natural frequencies obtained by the Kelvin and Winkler models becomes greater with the increase of mode number. The cross modal damping ratio can take negative or positive value for each mode which indicates the energy can transfer between modes in both directions.

The calculated EMDS extracted from the Winkler and Kelvin models are presented in Table 4.

<center>**Table 4 near here**</center>

The equivalent stiffness at pile cap from both methods (Winkler and Kelvin) has almost the same values whereas the equivalent Winkler mass is greater than those from Kelvin model. By considering these results for equivalent masses, the corresponding Kelvin frequencies are greater than those from Winkler model.

5.2.3.   Medium dense sand

Table 5 shows the first three natural frequencies obtained by the Winkler and Kelvin models for medium dense sand. The EMDS models are presented in Table 6.

<div align="center">**Table 5 near here**</div>

The same outcomes can be observed when the soil type is changed from loose to medium. In comparison between loose and medium dense sand it is seen that the damping ratio becomes smaller for medium dense sandy soil. Also the calculated natural frequencies for medium dense sandy soil are greater than those for loose sandy soil. As expected these results indicate higher soil stiffness for medium dense sandy soil.

<div align="center">**Table 6 near here**</div>

The equivalent stiffness for loose (medium dense) soil calculated by the Winkler are independent of mode shape whilst the equivalent mass does not have the same behaviour. The equivalent damping for medium dense sandy soil is smaller than that for loose sandy soil, whereas the equivalent mass is greater than those for loose sandy soil.

5.2.4.   Dense sand

The dynamic properties of dense sand such as natural frequencies, EMDS based on the Winkler and Kelvin models are presented in Tables 7 and 8.

<div align="center">**Table 7 near here**</div>

<div align="center">**Table 8 near here**</div>

In comparison with the other types of soil, the dense soil provides minimum damping and cross modal damping ratio which indicates for undrained conditions the damping is going to decrease. The calculated natural frequencies are greater than those for the other types of soil.

It is noted that the equivalent masses at the pile cap obtained by the Winkler model is greater than those obtained by the Kelvin model. The greater soil stiffness results in the smaller mass at the pile cap.

5.3. Effect of hydraulic conductivity

The variation of normalized soil damping and stiffness versus different values of hydraulic conductivity for the first mode of the saturated loose sandy soil are presented in Figs. 18 and 19. The soil damping and stiffness are normalized based on static stiffness in each soil layer.

It is seen in Figure 18 that for an artificial soil when the hydraulic conductivity is increased the soil damping increases and then decreases. Further, it can be seen that for undrained and drained conditions, the damping is close to zero and for a certain value of the hydraulic conductivity it reaches maximum.

<center>**Figure 18 near here**</center>

As illustrated in Fig. 19, the same trend is clear when the equivalent damping components for the cap are normalized with the equivalent corresponding stiffness components.

<center>**Figure 19 near here**</center>

<center>**Figure 20 near here**</center>

The semi-logarithmic plots in Figure 20 show variations of normalized stiffness for different values of soil hydraulic conductivity in different depths. It is noticed that for low and high values of hydraulic conductivity, the soil stiffness is approaches asymptotic values corresponding to undrained and drained conditions, respectively. The transition between fully undrained and drained conditions happens within nearly the same range of hydraulic conductivities for all layers. It can be observed that the transition takes place in sandy soil. This result is compatible to the one reported in Fig. 15 in [17].

6. Conclusions

The paper investigates the natural vibration characteristics and dynamic response of a 3.0 MW offshore wind turbine installed on a monopile foundation. In this regard, the finite element method is implemented to determine the soil stiffness and damping. The Winkler and Kelvin approaches are employed to evaluate the dynamic soil-pile interaction. In order to predict the soil stiffness and damping, a two-phase model is established for the soil in each layer corresponding to an integration point in the pile model. The two-dimensional coupled dynamic equations for a circular disc in an elastic saturated soil, using the $\mathbf{u} - P$ formulation under cyclic load with plane strain conditions, are employed. A further simplification, equivalent masses, dashpots and springs have been calibrated to the response of the pile and implemented at the base of the turbine support structure (i.e. at the monopile cap). Due to its simplicity, such a model is adequate for analysis of wind turbines by aero-elastic codes such as FLEX, FAST or HAWC [40-42]. However, it has to be kept in mind that the model only accounts for seepage damping in the soil.

For different soil types, the interesting conclusions can be drawn as:

- Contrary to the results of the equivalent soil stiffness at pile cap the equivalent dashpots and masses at pile cap are highly dependent on the soil type.

- The soil stiffness reduction in the transition region from undrained to drained states occurs for the hydraulic permeability in the range corresponding to sandy soil. The maximum damping occurs in the transition region, mostly in sandy soil.

- In comparison between loose, medium dense and dense sandy soil it is seen that the damping ratio becomes smaller for medium dense and dense sandy soil. Furthermore, as expected the natural frequencies for dense sandy soil are greater than those the other soil types.

7. References

[1] DNV. Design of offshore wind turbine structures. DNV-OS-J101. Det Nordske Veritas, Det Norske Veritas Classification A/S; 2010.

[2] DNV/Risø. Guidelines for design of wind turbines. Technical University of Denmark, National Laboratory for Sustainable Energy. Copenhagen: Det Norske Veritas/Risø 2001.

[3] Winkler E. Die Lehre von Elasticzitat und Festigkeit. 1867.

[4] Matlock H, Foo SHC. Simulation of lateral pile behaviour under earthquake motion. Rep. to Chevron Oil Field Research Co.. La Habra, Calif, Dept. of Civ. Engrg., University of Texas at Austin,Austin, Tex. 1978.

[5] Makris N, Gazetas G. Dynamic soil-pile interaction. part II lateral and seismic response. Earthquake Engineering and Structural Dynamics 1991; 21(2):145-162.

[6] Nogami T, Kazama M. Dynamic response analysis of submerged soil bt thin layer element method. Int. J. soil dynamics and Earthq Engrg 1992; 11(1):17-26.

[7] El-Naggar MH, Novak M. Nonlinear axial interaction in pile dynamics. Journal of Geotechnieal Engineering 1994; 120(4):678-696.

[8] El-Naggar MH, Novak M. Nonlinear lateral interaction in pile dynamics. Soil Dynamics and Earthquake Engineering 1995; 14:141-157.

[9] El-Naggar MH, Bentley KJ. Dynamic analysis for laterally loaded piles and dynamic $p - y$ curves. Canadian Geotechnical Journal 2000; 37(6):1166-1183.

[10] Kong LG, Zhang LM. Rate-Controlled Lateral-load Pile Tests Using a Robotic Manipulator in Centrifuge. Geotechnical Testing Journal, 30(3): Paper ID GTJ13138

[11] Memarpour MM, Kimiaei M, Shayanfar M, Khanzadi M. Cyclic lateral response of pile foundations in offshore platforms. Computers and Geotechnics 2012; 42:180-192.

[12] Damgaard M, Andersen LV, Ibsen LB. Computationally efficient modelling of dynamic soil-structure interaction of offshore wind turbines on gravity footings. Renewable Energy 2014; 68: 289-303.

[13] Bhattacharya S, Adhikari S. Experimental validation of soil–structure interaction of offshore wind turbines. Soil Dynamics and Earthquake Engineering 2011;31:805-816.

[14] Lombardi D, Bhattacharya S. Modal analysis of pile-supported structures during seismic liquefaction. Earthquake Engineering and Structural Dynamics 2014;43(1):119-138.

[15] Sørensen SPH, Ibsen LB. Assessment of foundation design for offshore monopiles unprotected against scour, Ocean Engineering 2013;63:17-25.

[16] Damgaard M, Ibsen LB, Andersen LV, Andersen JKF. Cross-wind modal properties of offshore wind turbines identified by full scale testing, J. WindEng.Ind.Aerodyn 2013;116:94-108.

[17] Damgaard M, Bayat M, Andersen LV, Ibsen LB. Assessment of the dynamic behaviour of saturated soil subjected to cyclic loading from offshore monopile wind turbine foundations. Computer and Geotechnique 2014;61: 116-126.

[18] Randolph MF. The response of flexible piles to lateral loading. Géotechnique, 1981;31(2):247-259.

[19] Sørensen SPH, Ibsen LB, Augustesen AH. Effects of diameter on initial stiffness of p–y curves for large-diameter piles in sand. Numer Methods Geotech Eng. NUMGE 2010:907–12.

[20] Zienkiewicz OC, Chan AHC, Pastor M, Schrefler BA, Shiomi T. Computatioal Geomechanics with Special Reference to Earthquake Engineering. 1999 John Wiley & Sons Ltd, England.

[21] Cheng Z. Jeremić B. Numerical modeling and simulation of pile in liquefiable soil. Soil Dyn. Earthq. Eng. 2009;29:1405-1416.

[22] Brezzi F. On the existence, uniqueness, and approximation of saddle-point problems arising from Lagrange multipliers. RAIRO. 1974;8:479-506.

[23] Ye X. Domain decomposition for a least-square finite element method for second order elliptic problem. Appl. Math. Comput. 1998;91:233-242.

[24] Bathe KJ, The inf-sup condition and its evaluation for mixed finite element methods. Comput. Struct. 2001;79:243-252.

[25] Zienkiewicz OC. The finite element method The basis. Taylor, R.L., 2000;1: 5th ed. London: Butterworth Heinemann.

[26] Zienkiewicz OC, Chan AHC, Pastor M, Paul DK, Shiomi T. Static and dynamic behavior of soils: a rational approach to quantitative solutions. I. Fully saturated problems. Proc. R. Soc. Lond. A. 1990;429:285-309.

[27] Zienkiewicz OC, Chan AHC, Pastor M, Paul DK, Shiomi T. Static and Dynamic Behavior of Soils: A Rational Approach to Quantitative Solutions: I. Fully Saturated Problems. Proceedings of the Royal Society London, Series A, Mathematical and Physical Sciences, 1990;429:285-309.

[28] Pastor M, Zienkiewicz OC, Chan AHC. Generalized plasticity and the modeling of soil behavior, Int. J. Numer. Anal. Meth. Geomech. 1990;14:151-190.

[29] Elgamal A. Yang Z. Parra E. Computational modeling of cyclic mobility and post-liquefaction site response. Soil Dyn. Earthq. Eng. 2002;22:259-271.

[30] Elgamal A. Yang Z. Parra E, Ragheb A. Modeling of cyclic mobility in saturated cohesionless soils. Int. J. Plasticity 2003;19:883-905.

[31] Lu JF, Jeng DS, Dynamic response of an offshore pile to pseudo-Stoneley waves along the interface between a poroelastic seabed and seawater. Soil Dyn. Earthq. Eng. 2010;30:184-201.

[32] Maghoula P, Gatmiri B, Duhamela D. Boundary integral formulation and two-dimensional fundamental solutions for dynamic behavior analysis of unsaturated soils. Soil Dyn. Earthq. Eng. 2011;31:1480-1495.

[33] Soares D. Iterative dynamic analysis of linear and nonlinear fully saturated porous media considering edge-based smoothed meshfree techniques. Comput. Method. Appl. M. 2013;253:73-88.

[34] Reese, L. C., W. R. Cox, and F. D. Koop Analysis of Laterally Loaded Piles in Sand. Offshore Technology Conference. Paper Number OTC 2080, 1974: May 6-8.

[35] Klinkvort RT. Centrifuge modelling of drained lateral pile - soil response Application for offshore wind turbine support structures, Ph.D. thesis. Department of Civil Engineering Technical University of Denmark (Denmark); 2012.

[36] Roesen HR, Thomassen K. Small-Scale Laterally Loaded Non-Slender Monopiles in Sand. Master thesis. Department of Civil Engineering, Aalborg University (Denmark); 2010.

[37] Jeremic' B. Lecture notes on computational geomechanics: inelastic finite elements for pressure sensitive materials. University of California, Davis; 2013.

[38] Bayat M, Ghorashi S.Sh, Amani J, Andersen LV, Ibsen LB, Rabczuk T, Zhuang X, Talebi H. Recovery-based error estimation in the dynamic analysis of offshore wind turbine monopile foundations, Computers and Geotechnics 70 (2015) 24-40.

[39] Zienkiewicz OC, Chan AHC, Pastor M, Schrefler BA, Shiomi T. Computatioal Geomechanics with Special Reference to Earthquake Engineering. 1999 John Wiley & Sons Ltd, England.

[40] Øye S. FLEX4 – simulation of wind turbine dynamics. In: Pedersen B, editor. State of the art of aeroelastic codes for wind turbine calculations. Denmark: Lyngby; 1996. p. 71–6.

[41] Jonkman J, Buhl M. Fast user's guide, Technical report NREL/EL-500-38230. National Renewable Energy Laboratory, Colorado, United States of America; 2005.

[42] Larsen T, Hansen A. Aeroelastic effects of large blade deflections for wind turbines. In: DU of Technology, editor. The science of making torque from wind. Roskilde, Denmark. p. 238–46.

Caption of Figures

Fig. 1: Winkler model approach and definitions of $p - y$ curves [1].

Fig. 2: DNV-J101 $p - y$ formulas for sand [1].

Fig. 3: Linear stiffness of sandy soil

Fig. 4: Kelvin model consisting of a spring and a dashpot in each depth

Fig. 5: Model description with applied load and boundary conditions

Fig. 6a: Elements used for coupled analysis, displacement (**u**) and pressure (*P*) formulation (a) (i) quadratic for **u**; (ii) linear for *P*; (b) (i) biquadratic for **u***;* (ii) bilinear for *P* [39]

Fig. 6b: Model description

Fig. 7: Convergence test

Fig. 8: Equivalent mass-dashpot-spring (EMDS) model at pile cap

Fig. 9: Kelvin model consisting of a spring and a dashpot

Fig. 10: Geometry of the wind turbine structure decomposed into: (a) pile; (b) transition piece; (c) tower. All dimensions are in millimeters.

Fig. 11: Numerical representation of the considered offshore wind turbine for a modal analysis

Fig. 12: Configuration of a monopile foundation for a given depth

Fig. 13: Displacement of whole wind turbine structure

Fig. 14: Variation of soil pressure on pile

Fig. 15: Variation of moment and shear force along the OWT's structure

Fig. 16: The first three natural frequencies and mode shapes of OWT structure

Fig. 17: Variation of initial soil stiffness with depth for different types of soil

Fig. 18: Variation of normalized damping versus hydraulic conductivity

Fig. 19: Variation of normalized equivalent damping versus hydraulic conductivity

Fig. 20: Variation of Normalized stiffness versus Hydraulic conductivity for different depths

Caption of Tables

Table 1: Geometry and material property of pile

Table 2: Geometry and material property of surrounded soil

Table 3: Natural frequencies based on the Winkler and Kelvin models and damping ratio for loose sandy soil

Table 4: The equivalent masses, dashpots and springs at pile cap and corresponding natural frequencies based on the Winkler and Kelvin models for loose sandy soil

Table 5: Natural frequencies based on the Winkler and Kelvin models and damping ratio for medium dense sandy soil

Table 6: The equivalent masses, dashpots and springs at pile cap and corresponding natural frequencies based on the Winkler and Kelvin models for medium dense sandy soil

Table 7: Natural frequencies based on the Winkler and Kelvin models and damping ration for dense sandy soil

Table 8: The equivalent masses, dashpots and springs at pile cap and corresponding natural frequencies based on the Winkler and Kelvin models for dense sandy soil

Influence of pore water in the seabed on dynamic response of offshore wind turbines on monopiles

M. Bayat[a,*], L. V. Andersen[a], L. B. Ibsen[a], J. Clausen[a]

[a]*Department of Civil Engineering, Aalborg University, Sofiendalsvej 11, 9200 Aalborg SV, Denmark*
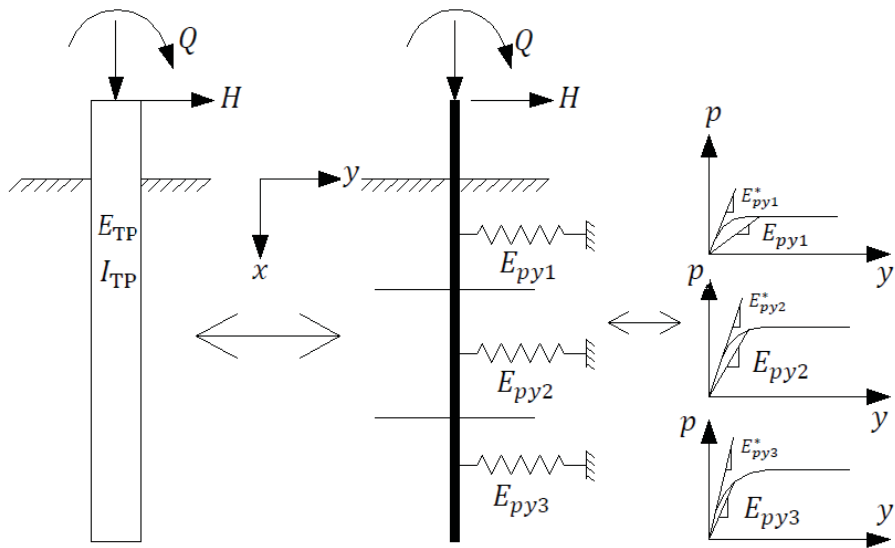
Figure 1

_____

[*] Corresponding author. Tel.: +4599408575; *E-mail*: meb@civil.aau.dk (or) Bayat.me@gmail.com

Static loading

$$p = A\, p_u \tanh\left(\frac{kx}{A\, p_u} y\right)$$

$$A = \left(3 - 0.8\frac{x}{D}\right) \geq 0.9$$

Cyclic loading

$$p = A\, p_u \tanh\left(\frac{kx}{A\, p_u} y\right)$$

$$A = 0.9$$
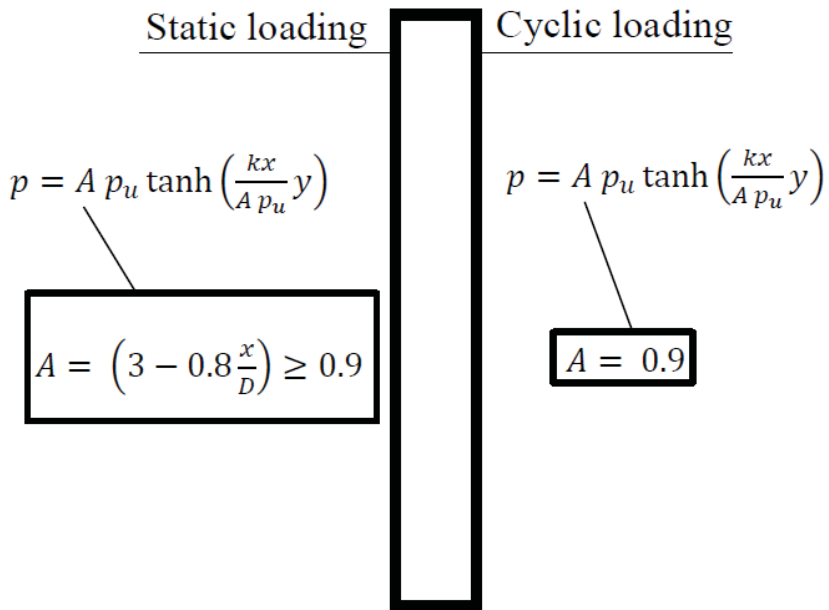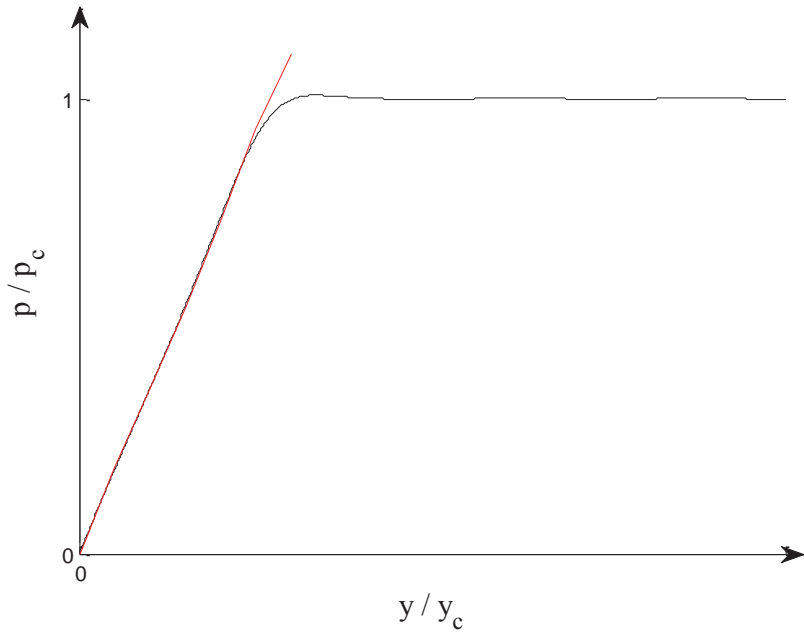
Figure 2

Figure 3

Figure 4

Figure 5

(a)

(i)

Quadratic for u

(ii)

Linear for p

(b)

(i)

Biquadratic for u

(ii)

Bilinear for p
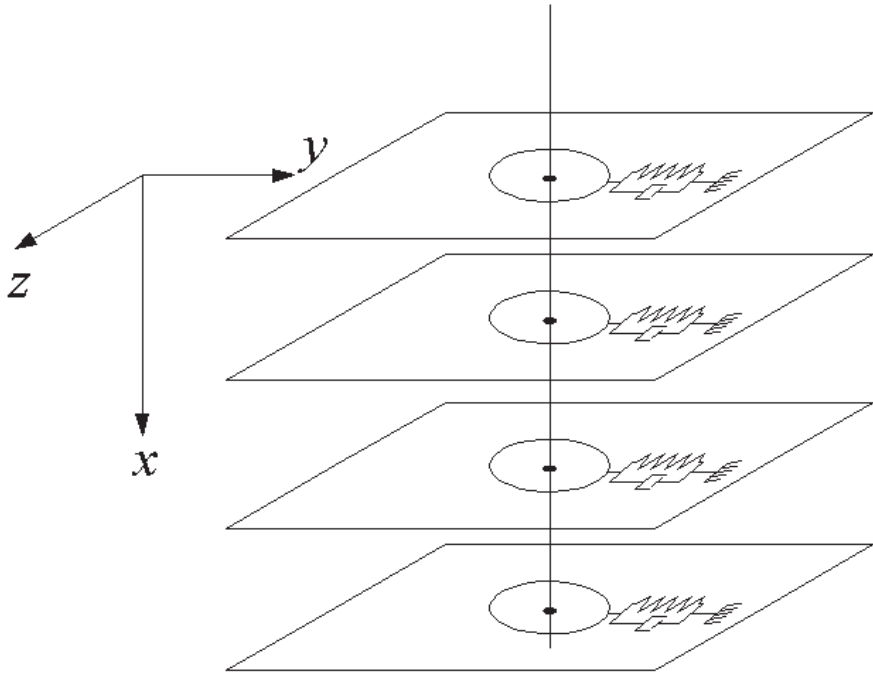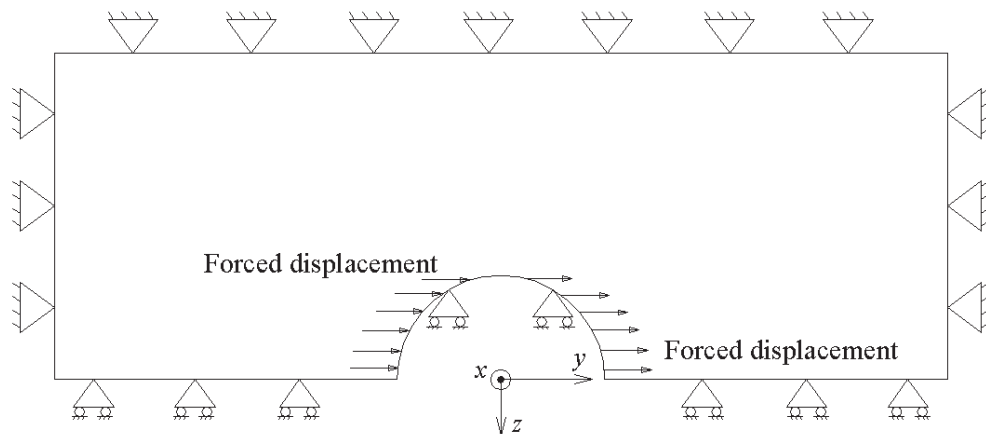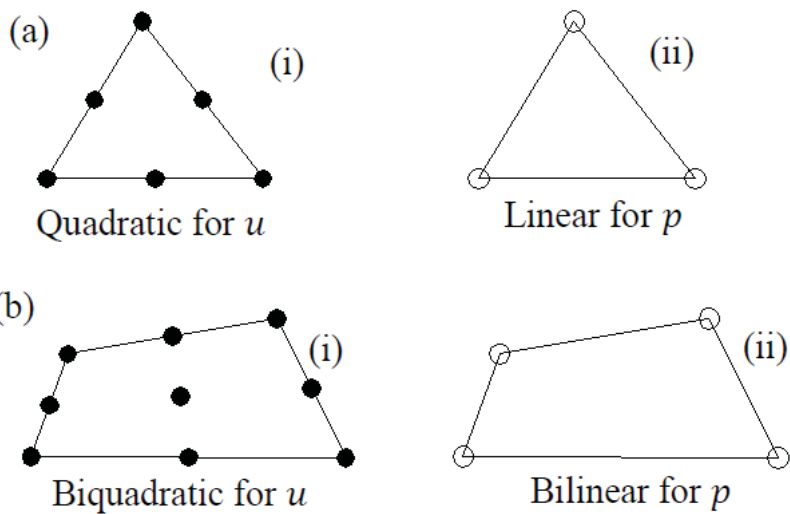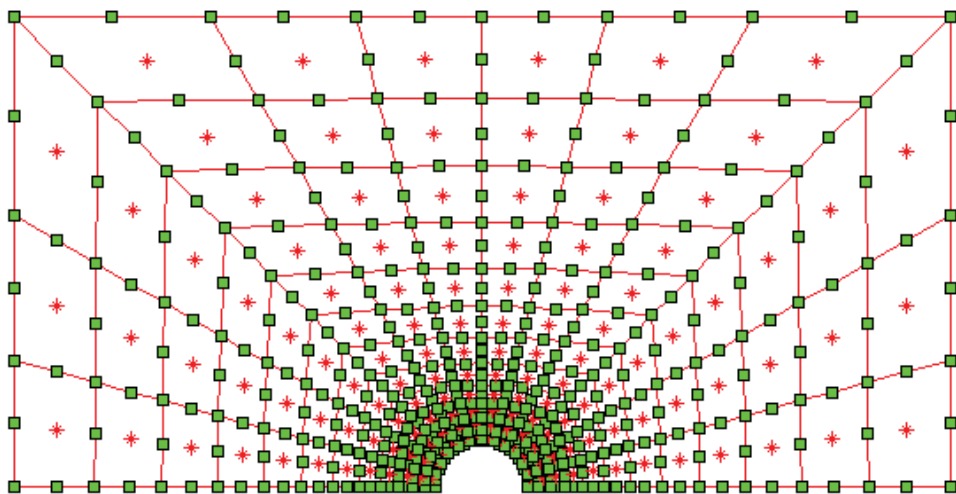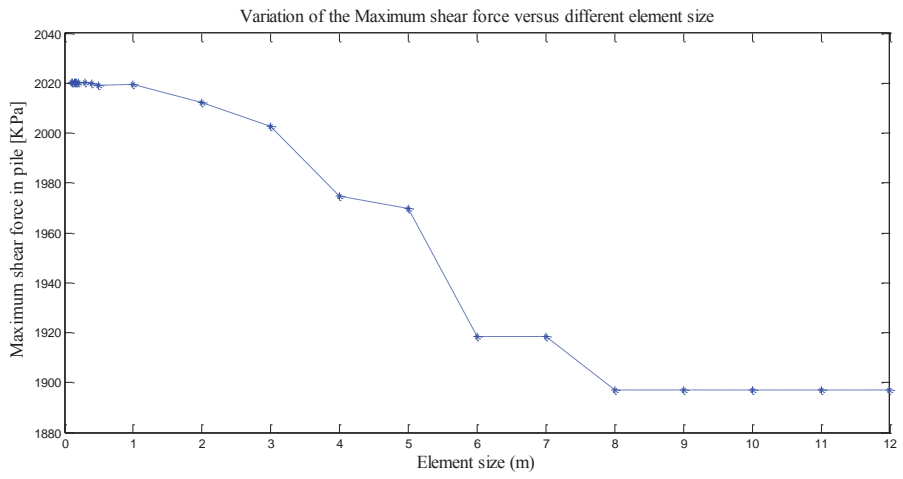
Figure 6a

Figure 6b

Figure 7
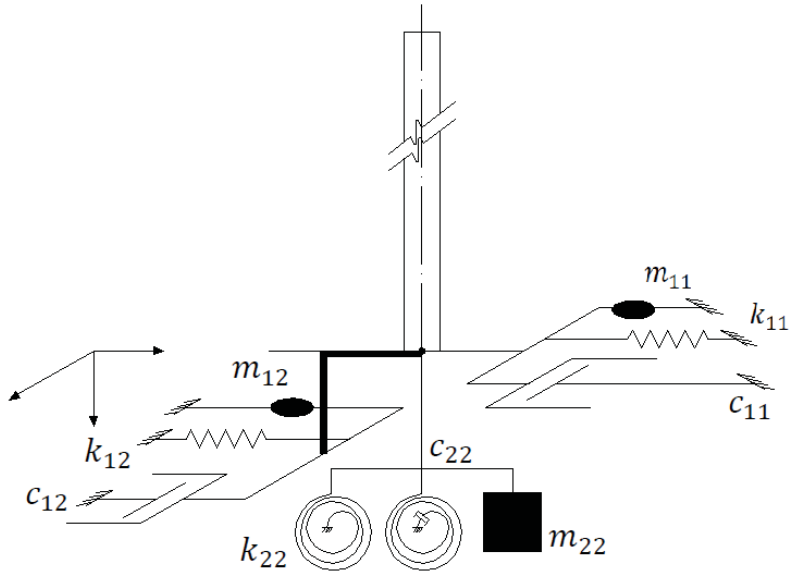
Figure 8
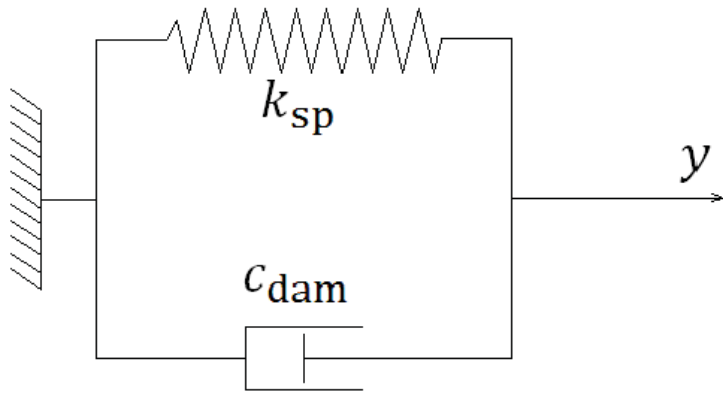
Figure 9
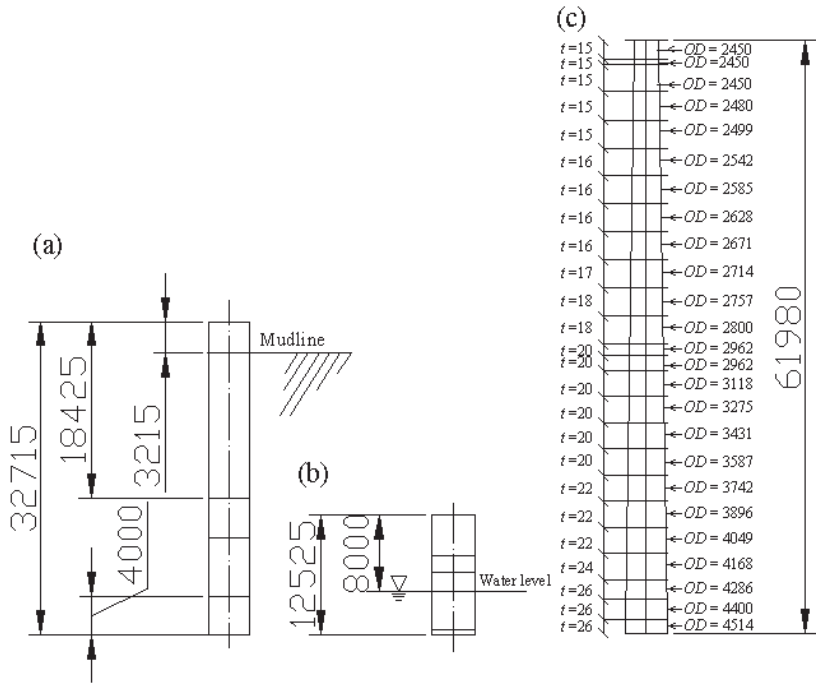
Figure 10
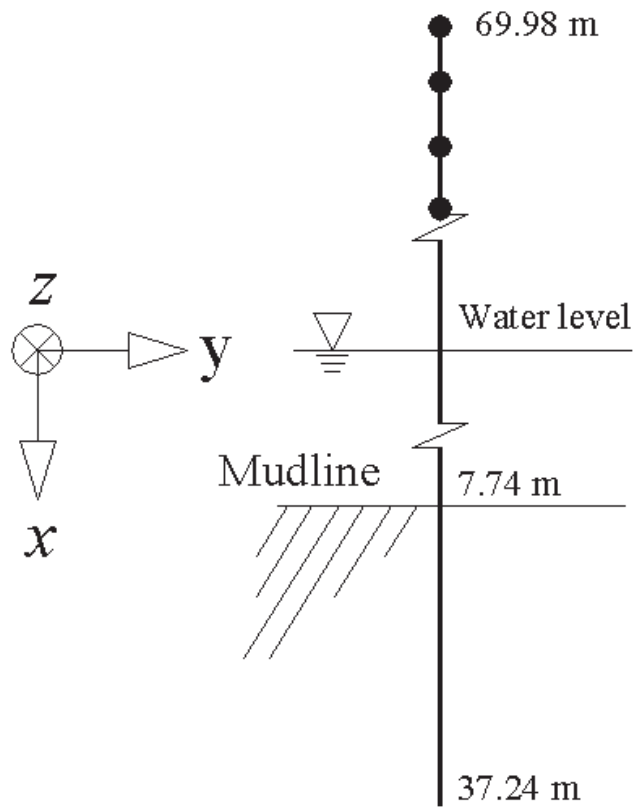
Figure 11
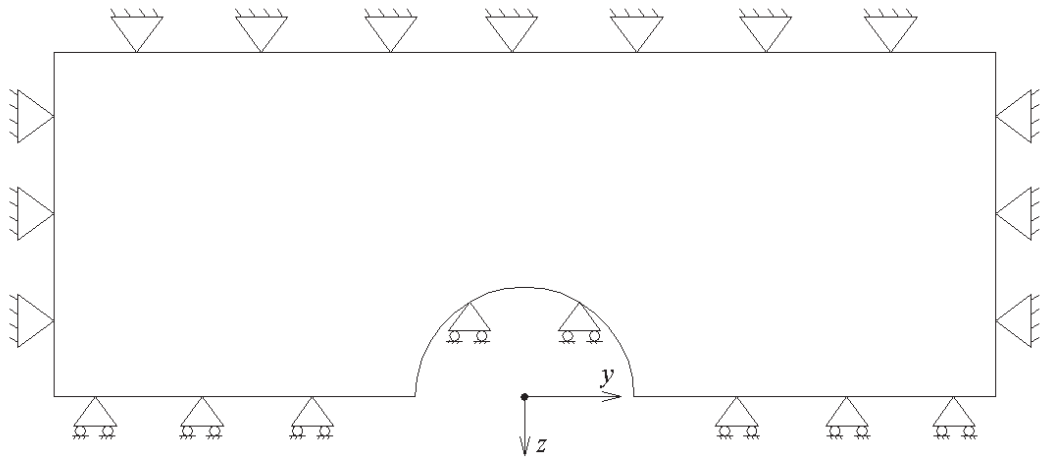
Figure 12
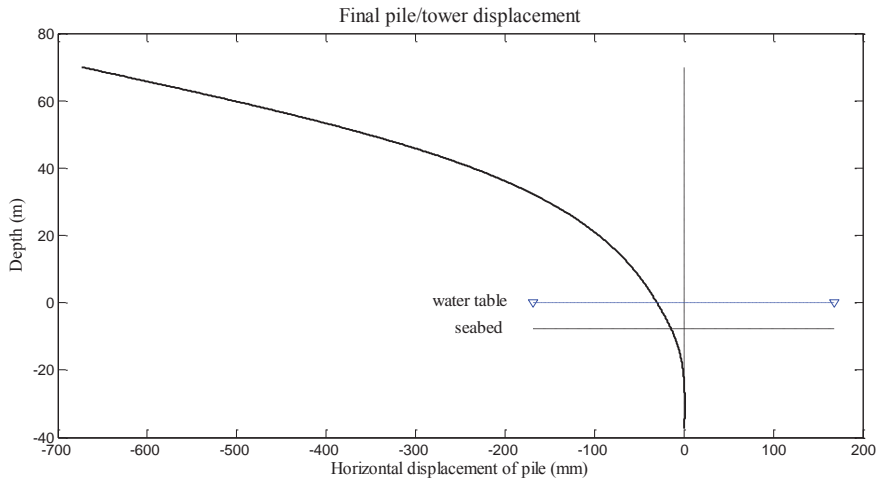
Figure 13
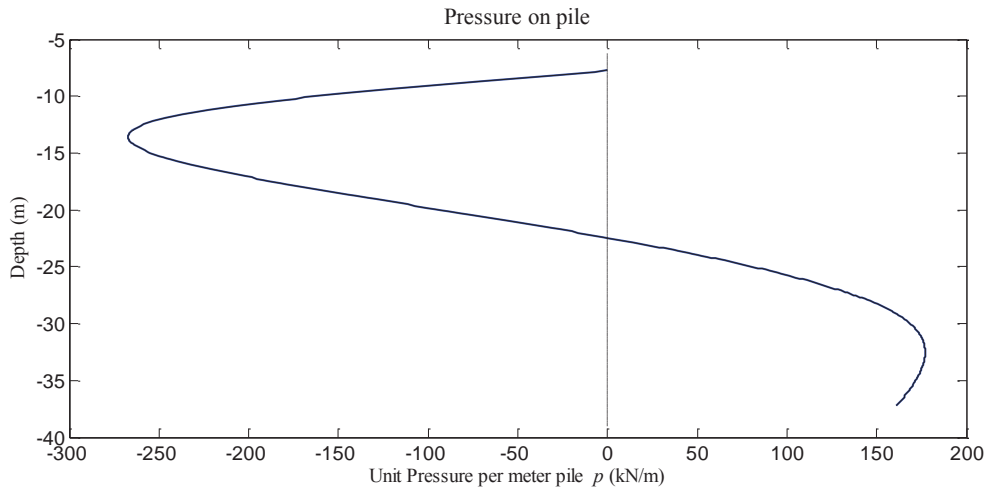
Figure 14
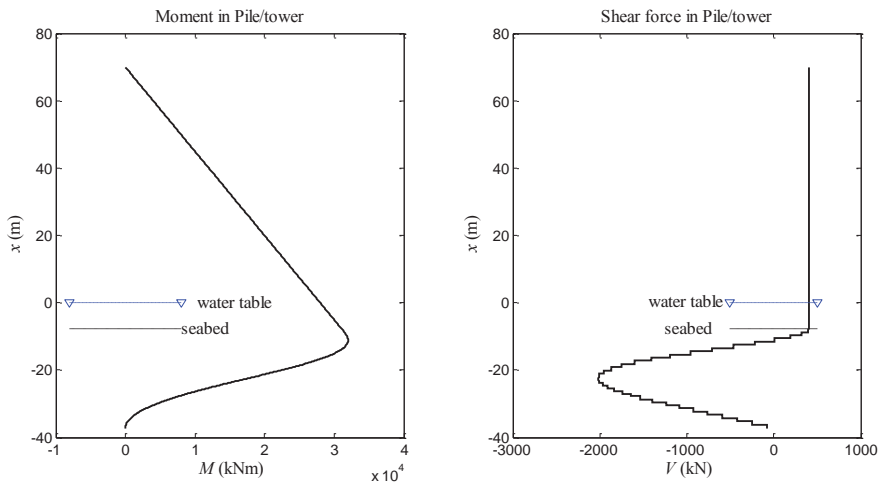
Figure 15
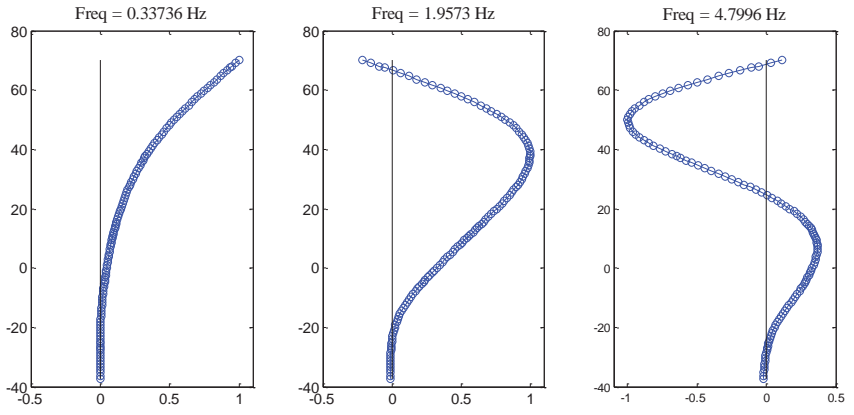
Figure 16
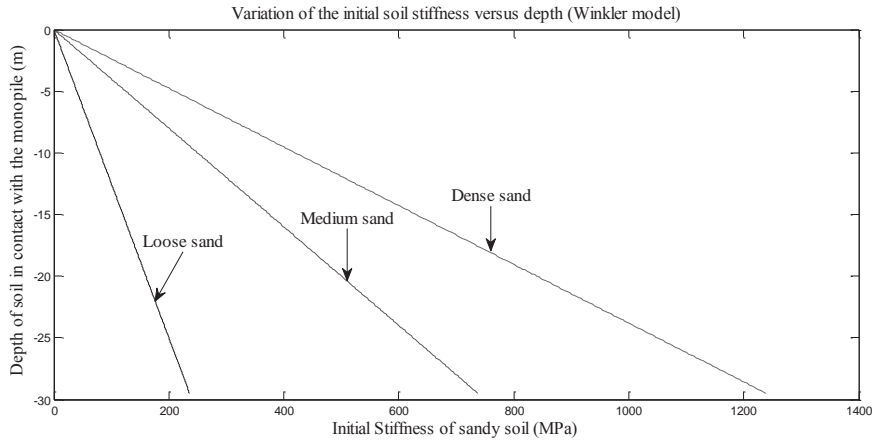
Figure 17
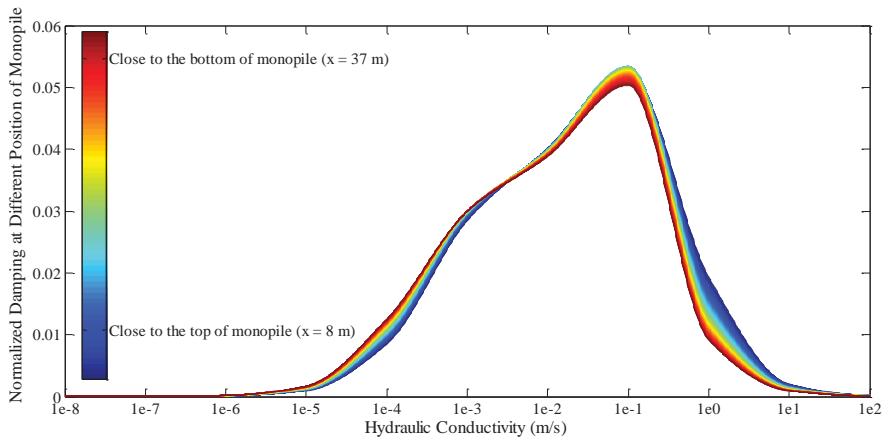
Figure 18
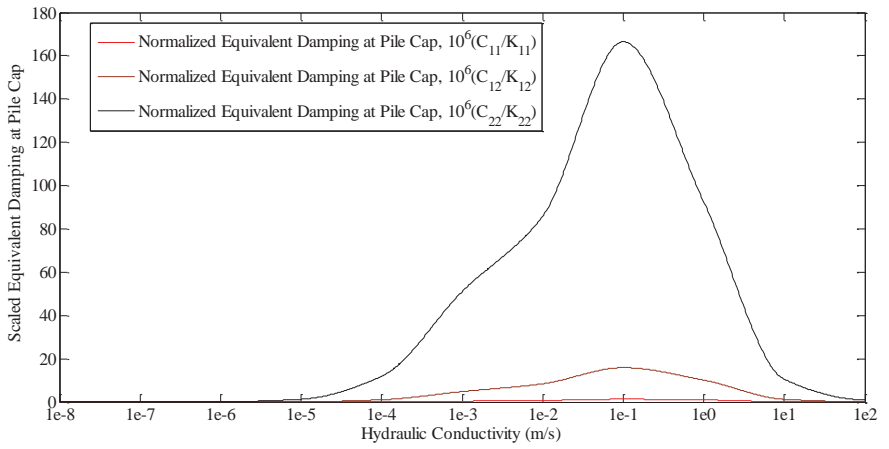
Figure 19
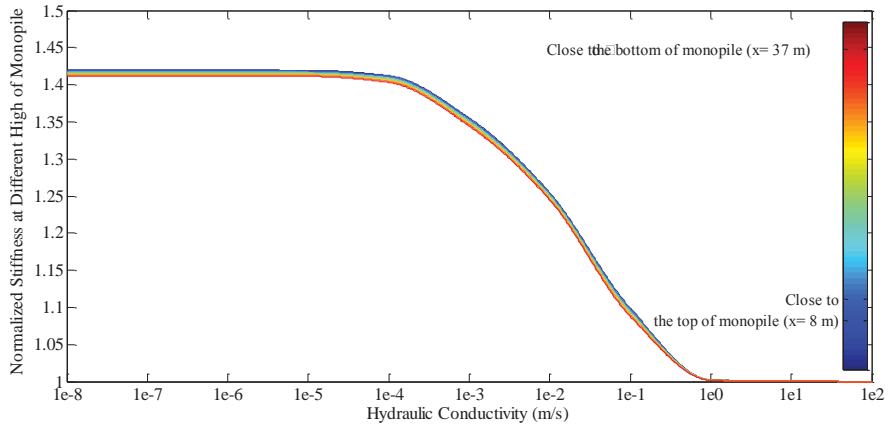
Figure 20

Influence of pore water in the seabed on dynamic response of offshore wind turbines on monopiles

M. Bayat[a,*], L. V. Andersen[a], L. B. Ibsen[a], J. Clausen[a]

[a]*Department of Civil Engineering, Aalborg University, Sofiendalsvej 11, 9200 Aalborg SV, Denmark*

Table 1

Geometry of the tubular pile								
	Section							
	1	2	3	4	5	6	7	8
Upper-Boundary (m)	-8	-3.695	-1.95	4.05	4.525	22.95	27.1	33.24
Lower-Boundary (m)	-3.695	-1.95	4.05	4.525	22.95	27.1	33.24	37.24
outer pile diameter (m)	4.5	4.54	4.54	4.54	4.3	4.3	4.3	4.3
Density (kg/m^3)	7850	7850	8331.3	9117.9	7850	7850	7850	7850
Thickness (m)	0.035	0.05	0.1088	0.07089	0.045	0.043	0.035	0.045

[*] Corresponding author. Tel.: +4599408575; *E-mail*: meb@civil.aau.dk (or) Bayat.me@gmail.com

Table 2

Soil's specifications	Type of Sand		
	Loose	Medium	Dense
Friction angle	$30°$	$36°$	$40°$
Effective unit weight (N/m^3)	8160	10200	12750
Hydraulic Conductivity (m/s)	1×10^{-2}	1×10^{-4}	1×10^{-5}
Upper-Boundary (m)	7.740		
Lower-Boundary (m)	51.74		

Table 3

Mode	API Model	Kelvin model		
	Frequency (Hz)	Frequency (Hz)	Cross modal damping ratio $\times\ 10^3$		
1	0.3374	0.3405	$\xi_{11} = 0.59704$	$\xi_{12} = 2.7182$	$\xi_{13} = -3.7632$
2	1.9573	2.0309	$\xi_{21} = -0.2762$	$\xi_{22} = 1.3246$	$\xi_{23} = 1.9928$
3	4.7997	4.9656	$\xi_{31} = 0.0866$	$\xi_{32} = -0.45507$	$\xi_{33} = 0.77448$

Note: The header row above "Loose sand" spans the full table.

Table 4

Model	Mode	$K_{cap}, C_{cap}, M_{cap}$								
		K_{11}	K_{12}	K_{22}	C_{11}	C_{12}	C_{22}	M_{11}	M_{12}	M_{22}
		$\times 10^9$			$\times 10^8$			$\times 10^4$		
Kelvin model ($\mathbf{u} - P$ based per mode)	1	0.66181	4.7098	54.773	0.04262	0.20594	1.19626	2.7640	5.8050	8.6251
	2	0.68271	4.8124	55.370	0.00539	0.02793	0.16890	3.6314	11.766	53.368
	3	0.68954	4.8504	55.612	0.0013639	0.0074447	0.04737	3.6334	11.785	53.590
Winkler model (API)	1	0.550	4.178	51.685				3.9069	13.545	65.554
	2	0.550	4.178	51.685				3.9070	13.546	65.557
	3	0.550	4.178	51.685				3.9074	13.549	65.575

Loose sand, (Equivalent Mass, Spring and Dashpot at Pile Cap)

Table 5

Mode	API Model	Kelvin model		
	Frequency (Hz)	Frequency (Hz)	Cross modal damping ratio $\times 10^4$		
1	0.3479	0.3506	$\xi_{11} = 0.5814$	$\xi_{12} = 2.7261$	$\xi_{13} = 4.0362$
2	2.1832	2.2458	$\xi_{21} = -0.070395$	$\xi_{22} = 0.34240$	$\xi_{23} = 0.54037$
3	5.322	5.4797	$\xi_{31} = 0.01749$	$\xi_{32} = -0.09131$	$\xi_{33} = 0.16039$

Medium sand

Table 6

Medium dense sand, (Equivalent Mass, Spring and Dashpot at Pile Cap)										
Model	Mode	$K_{cap}, C_{cap}, M_{cap}$								
		K_{11}	K_{12}	K_{22}	C_{11}	C_{12}	C_{22}	M_{11}	M_{12}	M_{22}
		$\times 10^9$			$\times 10^8$			$\times 10^4$		
Kelvin model (u − P based per mode)	1	1.3866	7.7608	70.483	0.013804	0.06087	0.31763	2.7737	6.7667	22.443
	2	1.3876	7.7655	70.510	0.000357	0.001588	0.008366	2.8631	7.3342	26.482
	3	1.3876	7.7657	70.511	0.0000605	0.0002691	0.0014191	2.8633	7.335	26.486
Winkler model (API)	1	1.125	6.764	65.848				3.0661	8.405	32.430
	2	1.125	6.764	65.848				3.0661	8.406	32.431
	3	1.125	6.764	65.848				3.0663	8.406	32.435

Table 7

Mode	API Model	Kelvin model		
	Frequency (Hz)	Frequency (Hz)	Cross modal damping ratio $\times 10^{-5}$		
1	0.3518	0.3543	$\xi_{11} = 0.8166$	$\xi_{12} = $ -3.8906	$\xi_{13} = $ 5.9967
2	2.2741	2.3320	$\xi_{21} = 0.09057$	$\xi_{22} = 0.4455$	$\xi_{23} = $ 0.72636
3	5.5544	5.7102	$\xi_{31} = $ -0.02327	$\xi_{32} = $ -0.1212	$\xi_{33} = $ 0.2163

Dense sand

Table 8

Model	Mode	$\mathbf{K_{cap}, C_{cap}, M_{cap}}$								
		K_{11}	K_{12}	K_{22}	C_{11}	C_{12}	C_{22}	M_{11}	M_{12}	M_{22}
		$\times 10^9$			$\times 10^8$			$\times 10^4$		
Kelvin model (u − P based per mode)	1	1.8970	9.5693	78.309	0.002948	0.011748	0.055391	2.5757	5.9264	19.183
	2	1.8970	9.5695	78.310	0.0000687	0.000274	0.0012946	2.5788	5.9436	19.295
	3	1.8970	9.5695	78.310	0.00001146	0.00004575	0.0002161	2.5788	5.9439	19.296
Winkler model (API)	1	1.541	8.349	73.217				2.758	6.790	23.518
	2	1.541	8.349	73.217				2.7576	6.790	23.518
	3	1.541	8.349	73.217				2.7577	6.790	23.521

Loose sand, (Equivalent Mass, Spring and Dashpot at Pile Cap)

APPENDIX F
Influence of pore pressure on dynamic response of offshore wind turbine using poroelastic model

F.1 Author's Right

http://www.elsevier.com/about/company-information/policies/copyright

Research Paper

Recovery-based error estimation in the dynamic analysis of offshore wind turbine monopile foundations

CrossMark

M. Bayat [a,*], S.Sh. Ghorashi [b,c], J. Amani [c], L.V. Andersen [a], L.B. Ibsen [a], T. Rabczuk [c,d], X. Zhuang [e], H. Talebi [b]

[a] Department of Civil Eng., Aalborg University, 9000 Aalborg, Denmark
[b] Graduiertenkolleg 1462, Berkaer Straße 9, 99423 Weimar, Germany
[c] Department of Civil Engineering, Bauhaus University Weimar, Weimar, Germany
[d] School of Civil, Environmental and Architectural Engineering, Korea University, Republic of Korea
[e] Department of Geotechnical Engineering, Tongji University, Shanghai 200092, China

ARTICLE INFO

ABSTRACT

Offshore wind turbine foundations are affected by cyclic loads due to oscillatory kinematic loads, such as those from wind, waves, and earthquakes. Monopiles are often used as a foundation concept for offshore windmill turbines. In this study, coupled dynamic equations with the $\mathbf{u} - P$ formulation for low-frequency load are considered for an offshore wind turbine monopile foundation, to present the response in terms of pore water pressure (PWP), stress and strain distribution in an elastic porous medium at regions around the monopile foundation. Different stress recovery techniques based on the Zienkeiwicz–Zhu (ZZ) error estimator namely, super-convergent patch recovery (SPR), weighted super-convergent patch recovery (WSPR), and L_2-projection techniques are also investigated to recover the stresses at nodal points in the finite element method. To estimate errors in the time domain when performing transient simulations, three recovery processes are used with different meshes. The convergence of the dynamic problem is also studied. The results are verified with findings in the literature, revealing that the time period of effective stresses follows the applied load frequency. In conclusion, the history of the shear stress can have an important effect on the shear stress distribution, making it asymmetric in the time domain.

© 2015 Elsevier Ltd. All rights reserved.

1. Introduction

Recent developments in offshore industries, such as offshore wind turbine foundations and structures for oil and gas extraction, have led to a growing demand for realistic predictions of the dynamic behavior of offshore structures. Offshore wind farms are receiving increasing attention in the quest for renewable sources of energy. As one option for wind turbines, the offshore monopile foundation plays a key role in offshore wind farm design. Monopile foundations bear loads from the seabed and waves, as well as loads that act on the turbine above sea level. Offshore windmill foundations comprise a major part (15–25%) of the total cost of the whole wind turbine structure.

Accomplishing a safe and cost-effective design for offshore monopile foundations requires that dynamic analyses be performed. The dynamic response varies significantly in time and is affected by different parameters, such as the inertia and damping

of the monopile structure, and the stiffness and damping of the underlying soil. To achieve the desired results, the soil should be appropriately modeled. Numerical analysis can be the most approachable and straightforward method for dynamic analysis [64,33,1,51,26,13]. Biot [7] offered an important and interesting soil model, establishing governing equations of porous media based on a continuum formulation [7,8]. Zienkiewicz and Shiomi [68] modified the equations of motion in an innovative way, presenting a model for the soil skeleton and pore fluid media that is useful in the numerical context.

Three coupled and dynamic formulations, based on the soil and pore fluid (water) displacements and the pore water pressure (PWP), are the $\mathbf{u} - P - \mathbf{U}, \mathbf{u} - P$, and $\mathbf{u} - \mathbf{U}$ equations, where $\mathbf{u}, P$, and $\mathbf{U}$ are the soil skeleton displacement, PWP, and pore water displacement, respectively [67]. Cheng and Jeremić [11] used a fully coupled, inelastic $\mathbf{u} - P - \mathbf{U}$ formulation to simulate the dynamic behavior of piles in liquefiable soils subjected to seismic loading. In the $\mathbf{u} - P$ formulation, if the fluid phase is considered incompressible, then the Ladyzenskaja–Babuska–Brezzi (LBB) condition needs to be satisfied ([9,62,6,2]). In this case, the element type

* Corresponding author. Tel.: +45 9940 8575.
E-mail addresses: meb@civil.aau.dk, bayat.me@gmail.com (M. Bayat).

for the displacement and pore pressure fields requires special consideration, to prevent volumetric locking [65,67]. The restrictions imposed by the LBB condition exclude the use of elements with equal order interpolation for pressures and displacements. This difficulty can be solved by implementing appropriate stabilization techniques such as the fractional step algorithm which was developed for soil mechanics by Pastor et al. [41]. Later, the generalized fractional step method proposed by Pastor et al. [42], was modified by Li et al. [34]. Recently, Soares et al. [50] described an edge-based smoothed meshfree technique by presenting an independent spatial discretization for each phase of the model. Considering this restriction for monolithic algorithm, a simple model for numerical analyses is the $\mathbf{u} - P$ formulation that neglects the relative acceleration of the fluid with respect to the solid skeleton. This model is especially useful for low-frequency analysis. The contribution of the solid acceleration is neglected in the fluid mass balance; this omission was investigated by Chan [10], who found the omitted contribution to be insignificant.

Prevost [45] incorporated a semi-discrete finite element (FE) procedure with an implicit–explicit time integration algorithm to analyze wave propagation in fluid-saturated porous media, which was modeled in the $\mathbf{u} - P$ format. Zienkiewicz et al. [66] studied the transient and static response of saturated soil, which they modeled as a two-phase material based on the $\mathbf{u} - P$ formulation for porous media. Pastor et al. [43] used a generalized plasticity approach to describe the behavior of soil in the $\mathbf{u} - P$ formulation under transient loading. Elgamal et al. [19,20] implemented the $\mathbf{u} - P$ model for a two-phase (solid–fluid) problem with multi-surface plasticity, using a finite element method (FEM) to highlight the effect of excitation frequency.

Researchers have attempted to solve these coupled equations by various numerical methods. For example, Lu and Jeng [35] investigated the porous soil which governed by the $\mathbf{u} - P$ formulation, using the boundary element method. Maghoul et al. [37] applied a boundary integral formulation for dynamic behavior analysis of unsaturated soils. Khoshghalib and Khalili [30] used a meshless radial point interpolation to solve the fully coupled Biot's equations. Soares [49] formulated an edge-based smoothed weak meshless formulation by Delaunay triangulation to perform an iterative dynamic analysis of linear and nonlinear fully saturated porous media. Zhang et al. [63] formulated a coupling material point method to predict the dynamic response of saturated soil and the contact/impact behavior between saturated porous media and solid bodies. Samimi and Pak [47] solved the $\mathbf{u} - P$ formulation by applying the Element-Free Galerkin method. Irzal et al. [27] implemented an isogeometric analysis to predict the behavior of a deformable fluid-saturated porous medium, using non-uniform rational B-splines.

To improve the efficiency of numerical approaches, it is important to calculate and reduce the errors. For as long as physical events have been computationally simulated, the numerical error of such calculations has been a major concern. Discretization error is inherent in these simulations, arising from the discretization process of the continuum domain. As a result, not all of the information characterized by the partial differential or integral equations can be obtained. Especially for the dynamic analysis of complex problems with many degrees of freedom, adaptive refinement procedures need to be used. This requirement is because of the limitations of the speed and memory of available computers. The mesh size should be refined in regions where there are large gradients in the changes between the nodal variables. The error can be in conjunction with the adaptive refinement procedure to obtain the desired accuracy for design purposes with less computational effort.

In 1910, Richardson [46] presented the first report of a practical approach for estimating numerical error, utilizing the finite difference method. Subsequent researchers used the FEM for this purpose. The FEM has a well-developed theory for error estimation. To date, many reliable methods for estimating the error in the global energy norm have been proposed, using either residuals- or recovery-based methods. Tang and Sato [53,54] and Tang and Shao [55] studied error estimation and adaptive mesh refinement on seismic liquefaction, seeking to improve the numerical results for large deformation in a soil–pile interaction problem. They used a FE and finite difference coupled dynamic method for liquefaction analysis of saturated soil. The $\mathbf{u} - P$ formulation was used for the governing equations, which described the coupled problem in terms of soil skeleton displacement and excess pore water pressure. Nazem et al. [39] used an h-adaptive FEM to tackle the penetration and indentation problems of geomechanics in the presence of inertial forces. They compared three alternative error estimation techniques, based on the energy norm, the Green–Lagrange strain, and the plastic dissipation.

Earlier studies on offshore monopile foundation have considered three-dimensional simulation (see e.g. [14,33]), and several authors have emphasized the importance of using a non-linear material model [24,52]. However, in this study the ZZ error estimator is applied for a two-dimensional (2D) model with an elastic constitutive model. These simplifying assumptions make some shortcomings such as ignoring bending of pile, different drainage paths and dilatancy out of the plane. But in order to investigate small displacements and get some desired outputs such as the estimation of the regions with higher numerical error, the 2D model may be applicable. Also, serviceability requirements for offshore wind turbines only allow rotations of $0.5°$ at the mudline. For such small rotations, soil behavior is controlled by elasticity rather than plasticity. Essentially, small settlement and rotation of foundations are controlled by linear elastic soil behavior as it was mentioned by Achmus et al. [1].

In the dynamic analysis of monopile foundations, complex changes occur in the displacement, stress, and pore pressure fields of the $\mathbf{u} - P$ coupled equations due to the fluid–soil interaction. The error must be estimated to identify zones that are affected by insufficient mesh size. To the best of the authors' knowledge, no dynamic analysis of offshore foundations has been performed by considering different stress recovery techniques-namely, super-convergence path recovery (SPR), weighted super-convergence path recovery (WSPR), and L_2-projection to implement the Zienkiewicz–Zhu (ZZ) error estimation. The mentioned post-processing procedures have not been employed for the coupled $\mathbf{u} - P$ equations which can highlight the distinction of the present study. Moreover, the convergence rates are compared for the different recovery procedures. Thus, it motivates the authors to perform comprehensive error estimation for the coupled $\mathbf{u} - P$ equations. Indeed, it then paves the way to implement different adaptive refinement procedures based on the implemented error estimation methods, finally leading to the lower computational costs for modeling two phase media such as saturated soil.

This study considers a 2D offshore monopile foundation (Fig. 1), surrounded by a linear-elastic saturated soil and subjected to cyclic load. The plane strain condition is invoked by having small deformation of the soil. Symmetry is assumed with respect to the horizontal axis and the center line of the monopile. This work aims to investigate the effects of stress recovery techniques on the ZZ error estimation in the time domain, by employing the FEM in the $\mathbf{u} - P$ equations. Displacement and pore water pressure fields are investigated in the time domain for a saturated soil.

Following this brief introduction, Section 2 contains the governing coupled $\mathbf{u} - P$ equations of the saturated soil and its FEM discretization process. The recovery-based ZZ error estimation and the SPR, WSPR, and L_2-projection stress recovery procedures are addressed in Section 3. The time discretization of the coupled
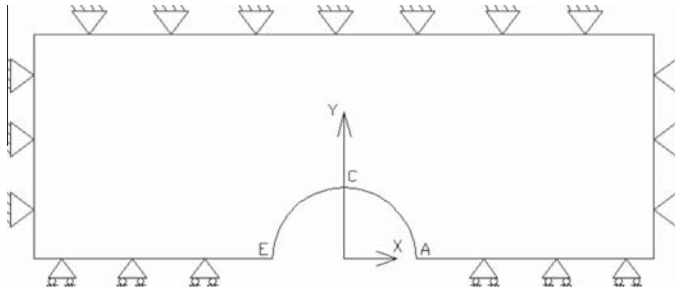
Fig. 1. Configuration of a monopile foundation.

equations using the generalized Newmark integration method is described in Section 4. In Section 5, two benchmark examples are solved, and the numerical solution is validated by comparison to the exact analytical solution. A monopile foundation is analyzed while considering four meshing configurations. The convergence rate of the problem is calculated, and the error estimation processes are compared. Some concluding remarks are discussed in Section 6.

2. Governing equations of saturated soil

The total moment balance of porous media is [67]:

$$\sigma_{ij,j} + \rho b_i = \rho \ddot{u}_i + \rho_f \ddot{w}_i \tag{1}$$

where σ_{ij} is the total stress tensor and $\sigma_{ij} = \sigma'_{ij} - \alpha P \delta_{ij}$. Here σ'_{ij} is the effective stress tensor. For isotropic materials, $\alpha = 1 - \frac{K_T}{K_S}$, where K_T is the total bulk modulus of the solid matrix, and K_S is the bulk modulus of the solid particles. For most soil mechanics problems, because K_S of the solid particle is much larger than the bulk modulus of the whole material, $\alpha \approx 1$ can be assumed. δ_{ij} is Kronecker delta: $\delta_{ij} = 1$ when $i = j$, and $\delta_{ij} = 0$ when $i \neq j$. The tensile component of stress and compressive component of pressure,are assumed to be positive. The density of the mixture is $\rho = (1 - n_p)\rho_s + n_p\rho_f$ where n_p, ρ_s and ρ_f are the porosity and the densities of the solid phase and fluid, respectively. b_i is the body force per unit mass, u_i and $\ddot{u}_i$ are the displacement and acceleration of the solid skeleton, respectively; and w_i, $\dot{w}_i$ and $\ddot{w}_i$ are the pseudo-displacement, pseudo-velocity and pseudo-acceleration, respectively, of the fluid phase relative to the skeleton of solid. The equation of the total coupled system can be written as:

$$-P_{,i} - \frac{\dot{w}_i}{k} + \rho_f b_i = \rho_f \left(\ddot{u}_i + \frac{\ddot{w}_i}{n_p} \right) \tag{2}$$

where $k = \frac{k'}{g\rho_f}$, and k' is the permeability in Darcy's law, which has the same unit as velocity. P and g are pore pressure and gravity acceleration respectively. The final equation is supplied by the mass conservation of the fluid flow [67]:

$$\dot{w}_{i,i} + \alpha \dot{\epsilon}_{ii} + \frac{\dot{P}}{Q} = 0 \tag{3}$$

where $Q = Q_{sf} = \frac{K_S K_f}{K_S + K_f}$ is the total compression modulus. K_S and K_f are the solid and fluid compression moduli, respectively. $\dot{P}$ and $\dot{\epsilon}_{ii}$ are the time derivative of the pore pressure and strain respectively.

2.1. Governing equation (**u** − P formulation)

For lower frequencies, the relative acceleration ($\ddot{w}_i$) of the fluid with respect to the solid skeleton is ignored. Then, Eq. (1) reduces to:

$$\sigma_{ij,j} + \rho b_i = \rho \ddot{u}_i \tag{4}$$

By combining Eqs. (2) and (3) and ignoring the relative acceleration of the fluid with respect to the solid skeleton, the governing equation of the fluid mass balance becomes:

$$\left(k \left(-P_{,i} + \rho_f b_i - \rho_f \ddot{u}_i \right) \right)_{,i} + \alpha \dot{\epsilon}_{ii} + \frac{\dot{P}}{Q} = 0 \tag{5}$$

2.1.1. Boundary conditions

The boundary conditions are $(\Gamma = \Gamma_t \cup \Gamma_u)$; $(\Gamma = \Gamma_w \cup \Gamma_P)$:

$$
\begin{aligned}
\sigma_{ij}n_j &= \bar{t}_i & \text{on} \quad \Gamma = \Gamma_t \\
u_i &= \bar{u}_i & \text{on} \quad \Gamma = \Gamma_u \\
n_i \dot{w}_i = n_i k(-p_{,i} + \rho_f b_i) &= \dot{\bar{w}} = -\bar{q} & \text{on} \quad \Gamma = \Gamma_w \\
P &= \bar{P} & \text{on} \quad \Gamma = \Gamma_P
\end{aligned}
\tag{6}
$$

where $\bar{t}_i$, $\bar{u}_i$, $\bar{q}$ and $\bar{P}$ are boundary traction, displacement, flow and pore pressure, respectively.

2.2. Discretization process of governing equations

By neglecting the acceleration term in Eq. (5) and discretizing, the FE system of equations for the **u** − P formulation, which is based on earlier work by Zienkiewicz and Shiomi [68], can be written in tensor index form:

$$
\begin{bmatrix} M_{KijL} & 0 \\ 0 & 0 \end{bmatrix} \begin{bmatrix} \ddot{u}_{Lj} \\ \ddot{P}_N \end{bmatrix} + \begin{bmatrix} 0 & 0 \\ Q_{LjM} & S_{MN} \end{bmatrix} \begin{bmatrix} \dot{u}_{Lj} \\ \dot{P}_N \end{bmatrix} + \begin{bmatrix} K^{ep}_{KijL} & -Q_{KiN} \\ 0 & H_{MN} \end{bmatrix} \begin{bmatrix} \bar{u}_{Lj} \\ \bar{P}_N \end{bmatrix} = \begin{bmatrix} f^u_{Ki} \\ f^P_M \end{bmatrix}
\tag{7}
$$

and

$$
\begin{bmatrix} \mathbf{M} & 0 \\ 0 & 0 \end{bmatrix} \begin{bmatrix} \ddot{\bar{u}} \\ \ddot{\bar{P}} \end{bmatrix} + \begin{bmatrix} 0 & 0 \\ \mathbf{Q}^T & \mathbf{S} \end{bmatrix} \begin{bmatrix} \dot{\bar{u}} \\ \dot{\bar{P}} \end{bmatrix} + \begin{bmatrix} \mathbf{K}^{ep} & -\mathbf{Q} \\ 0 & \mathbf{H} \end{bmatrix} \begin{bmatrix} \bar{u} \\ \bar{P} \end{bmatrix} = \begin{bmatrix} \mathbf{f}^u \\ \mathbf{f}^P \end{bmatrix}
\tag{8}
$$

where

$$\mathbf{f}^u : f^u_{Ki} = (f^u_1)_{Ki} + (f^u_2)_{Ki}, \quad \mathbf{f}^P : f^P_M = -\left(f^P_1\right)_M + \left(f^P_2\right)_M$$

and

$$
\begin{aligned}
&\mathbf{f}^u_1 \leftrightarrow (f^u_1)_{Ki} = \int_{\Gamma_t} N^u_K \bar{t}_i d\Gamma, \quad \mathbf{f}^u_2 \leftrightarrow (f^u_2)_{Ki} = \int_{\Omega} N^u_K \rho b_i d\Omega \\
&\mathbf{f}^P_1 \leftrightarrow \left(f^P_1\right)_M = \int_{\Gamma_w} N^P_M \bar{w} d\Gamma, \quad \mathbf{f}^P_2 \leftrightarrow \left(f^P_2\right)_M = \int_{\Omega} N^P_{M,i} k\rho_f b_i d\Omega \\
&\mathbf{M} \leftrightarrow M_{KijL} = \delta_{ij} \left(\int_{\Omega} N^u_K \rho N^u_L d\Omega \right), \quad \mathbf{Q} \leftrightarrow Q_{LjM} = \int_{\Omega} \alpha N^u_{L,j} N^P_M d\Omega \\
&\mathbf{S} \leftrightarrow S_{MN} = \int_{\Omega} N^P_M \frac{1}{Q} N^P_N d\Omega, \quad \mathbf{H} \leftrightarrow H_{MN} = \int_{\Omega} N^P_{M,i} k N^P_{N,i} d\Omega \\
&\mathbf{K}^{ep} \leftrightarrow K^{ep}_{KijL} = \int_{\Omega} N^u_{K,m} D_{imjq} N^u_{L,q} d\Omega
\end{aligned}
\tag{9}
$$

In these equations, the solid displacement u_i and pore water pressure P can be approximated by using the shape functions and nodal values:

$$u_i = N_K^u \bar{u}_{ki}^{nd} \tag{10}$$

$$P = N_l^P \bar{P}_l^{nd} \tag{11}$$

Similar approximations are applied to $\dot{u}_i$ and $\dot{P}$. For more details, please see the note by Jeremic [28].

3. Error estimation

To check the accuracy of numerical solutions based on the classical energy norm, error estimation methods are used. These methods can be categorized into two classes: residuals-based and recovery-based. In residual-based methods, the residuals of a differential equation and its boundary conditions are considered as error criteria. In recovery-based methods, the gradient of the solution is used.

The ZZ error estimator [69–71] is a recovery-based method that is used in conjunction with the SPR technique at each patch to improve the accuracy of the error estimate. The error of the FE approximation $\bar{u}$ with respect to the exact solution u_{ex} is:

$$e = u_{ex} - \bar{u} \tag{12}$$

and the error of the flux (proportional to the gradient of u) is:

$$e_\sigma = \sigma_{ex} - \bar{\sigma} \tag{13}$$

The stresses $\bar{\sigma} = \mathbf{DB\bar{u}}$ are obtained from FEM procedure at the Gauss points where $\mathbf{D}$ is the material constitutive matrix and $\mathbf{B}$ is the strain-interpolation matrix that contains first-order partial derivatives of shape functions with respect to the physical coordinates. The stresses at the Gauss points are extrapolated to nodes by using shape functions.

The energy error norm $\|e\|$ is defined as follows [70–72]:

$$\|e^{Z92}\| = \left\{ \int_\Omega (\sigma_{ex} - \bar{\sigma})^T (\sigma_{ex} - \bar{\sigma}) d\Omega \right\}^{1/2} \tag{14a}$$

$$\|e^{Z95}\| = \left\{ \int_\Omega (\sigma_{ex} - \bar{\sigma})^T \mathbf{D}^{-1} (\sigma_{ex} - \bar{\sigma}) d\Omega \right\}^{1/2} \tag{14b}$$

where σ_{ex} and $\bar{\sigma}$ are the exact and FEM stresses, respectively. However, these definitions are nearly useless because the exact solutions for u and σ are almost always unknown.

To use the above equations for error estimation, the recovered stresses σ^* must be calculated. The ZZ error estimator is effective and economical for evaluating errors and driving adaptive mesh refinement. Field derivatives and fluxes computed from FE solutions do not possess inter-element continuity, and they have low accuracy at nodes and element boundaries. It is well known that the calculated FE stresses at the Gauss points based on nodal displacement do not have continuity between elements [70,71]. The main objective of the recovery process is to overcome this difficulty and make a smoothed continuous stress field between elements. Derivatives and fluxes are more accurate at super-convergent (Gauss) points compared to other points within the element. Moreover, as the element size decreases, the values at super-convergent points converge more quickly to the true stress values. Thus, an accurate value σ^* of the stress σ at the nodes can be recovered by interpolating between the stresses at the gauss points in a patch around the node.

Therefore, the global error $\|e_{es}\|$ can be estimated as,

$$\|e_{es}^{Z92}\| = \left\{ \int_\Omega (\sigma^* - \bar{\sigma})^T (\sigma^* - \bar{\sigma}) d\Omega \right\}^{1/2} \tag{15a}$$

$$\|e_{es}^{Z95}\| = \left\{ \int_\Omega (\sigma^* - \bar{\sigma})^T \mathbf{D}^{-1} (\sigma^* - \bar{\sigma}) d\Omega \right\}^{1/2} \tag{15b}$$

If the exact solution is available, the error of recovery procedure $\|e_R\|$ can be defined as [70–72]:

$$\|e_R^{Z92}\| = \left\{ \int_\Omega (\sigma_{ex} - \sigma^*)^T (\sigma_{ex} - \sigma^*) d\Omega \right\}^{1/2} \tag{16a}$$

$$\|e_R^{Z95}\| = \left\{ \int_\Omega (\sigma_{ex} - \sigma^*)^T \mathbf{D}^{-1} (\sigma_{ex} - \sigma^*) d\Omega \right\}^{1/2} \tag{16b}$$

The global energy norm E_{norm} can be defined as:

$$E_{norm}^{Z92} = \left\{ \int_\Omega \sigma^T \sigma d\Omega \right\}^{1/2} \tag{17a}$$

$$E_{norm}^{Z95} = \left\{ \int_\Omega \sigma^T \mathbf{D}^{-1} \sigma d\Omega \right\}^{1/2} \tag{17b}$$

The relative error is estimated as follows:

$$e_{rel} = \frac{\|e\|}{\sqrt{\|e\|^2 + E_{norm}^2}} * 100 \tag{18}$$

3.1. Super-convergence path recovery

The theory of super-convergence is that to have more accurate results in Gauss points to recover the results at nodal points and the rate of convergence has a maximum value. The technique states that if the gradients at some points are super-convergent, then any gradient field resulting from a polynomial fit to these values will be super-convergent. To use the SPR technique for post-processing FE derivatives, the mesh is partitioned into sub-domains (or "patches"), and a continuous polynomial expansion is assumed over these patches [70,71]. An element patch is selected as a group of elements surrounding a typical vertex node. In constructing a patch, it is possible that the boundary vertex will lead to patches of insufficient size. An approach is to choose only patches on internal nodes and to evaluate the boundary nodal values from the adjacent interior patches. The advantage of SPR is that the number of smoothing equations to be solved for each patch is modest, and the recovery is only performed for each vertex node.

After analysis, a patch is defined for each vertex of a node inside the domain as the union of elements sharing the node. The recovered solution can be obtained for each component by $\sigma^* = \mathbf{Pa}$, where $\mathbf{P}$ are polynomials defined as follows:

$$\begin{aligned} \mathbf{P} &= \begin{bmatrix} 1 & x & y \end{bmatrix}, \quad m = 3, \quad \text{first order} \\ \mathbf{P} &= \begin{bmatrix} 1 & x & y & x^2 & xy & y^2 \end{bmatrix}, \quad m = 6, \quad \text{second order} \\ \mathbf{P} &= \begin{bmatrix} 1 & x & y & x^2 & xy & y^2 & x^3 & x^2y & xy^2 & y^3 \end{bmatrix}, \quad m = 10, \\ &\quad \text{third order} \end{aligned} \tag{19}$$

and $\mathbf{a} = \begin{bmatrix} a_1 & \dots & a_m \end{bmatrix}$ is an unknown vector. Using least squares fitting, polynomial expansion to the set of super-convergent (gauss) points can be written as:

$$\mathbf{I} = \sum_{i=1}^{ng} (\sigma^* - \bar{\sigma})^2 = \sum_{i=1}^{ng} (\mathbf{Pa} - \bar{\sigma})^2 \tag{20}$$

where ng is the number of gauss points in the patch. Minimization of the error function $\mathbf{I}$ with respect to the unknown parameters $\mathbf{a}$ leads to:

$$\sum_{i=1}^{ng} \mathbf{P}^T \mathbf{Pa} = \sum_{i=1}^{ng} \mathbf{P}^T \bar{\sigma} \tag{21}$$

Evaluating the unknown vector $\mathbf{a}$ from the above equations with respect to the global coordinates for higher order elements often leads to singularities in left-hand side (LHS) of the equation.

To alleviate the ill-conditioning issue, it is convenient to normalize the coordinates to the local coordinates of the patch. When the unknown parameters $\mathbf{a}$ are obtained, the smoothed values at any particular node inside the patch can easily be found by inserting the coordinates into Eq. (20).

3.2. Weighted super-convergence path recovery

The WSPR method is a modified version of the SPR for modeling high-gradient regions, such as cracks, by implementing weighting parameters to obtain more realistic values of error. In the standard SPR technique, all sampling points have similar properties in the patch, which may yield to significant errors, particularly at the edges of a crack [29]. For elements located on high-gradient regions with insufficient sampling points, the points of the nearest patch must be used, with the definition of a weight function for the SPR procedure. In this case, the error function $\mathbf{I}$ can be written as follows:

$$\mathbf{I} = \sum_{i=1}^{ng}[w_i(\boldsymbol{\sigma}^* - \bar{\boldsymbol{\sigma}})]^2 = \sum_{i=1}^{ng}[w_i(\mathbf{Pa} - \bar{\boldsymbol{\sigma}})]^2 \quad (22)$$

One of the most common weighting factors that can be used in solid mechanics problems is the distance between the recovered nodal point and the sampling point. In this paper, the weighting parameter is defined as $w_i = 1/\sqrt{r_i}$, where r_i is the distance of each sampling point from the vertex node that is being recovered. Minimizing $\mathbf{I}$ with respect to the unknown vector $\mathbf{a}$,

$$\sum_{i=1}^{ng} w_i^2 \mathbf{P}^T \mathbf{Pa} = \sum_{i=1}^{ng} w_i^2 \mathbf{P}^T \bar{\sigma}_i \quad (23)$$

3.3. L_2-projection recovery

The error function for the L_2-projection recovery is defined as,

$$\mathbf{I} = \int_{\Omega} (\boldsymbol{\sigma}^* - \bar{\boldsymbol{\sigma}})^2 d\Omega = \int_{\Omega} (\mathbf{Pa} - \bar{\boldsymbol{\sigma}})^2 d\Omega \quad (24)$$

As was done with the SPR technique, the above equation is minimized and re-arranged to generate:

$$\int_{\Omega} \mathbf{P}^T \mathbf{Pa} d\Omega = \int_{\Omega} \mathbf{P}^T \bar{\sigma} d\Omega \quad (25a)$$

Then the unknown vector $\mathbf{a}$ can be found as

$$\mathbf{a} = \mathbf{A}^{-1}\mathbf{b}; \quad \mathbf{A} = \int_{\Omega} \mathbf{P}^T \mathbf{P} d\Omega, \quad \mathbf{b} = \int_{\Omega} \mathbf{P}^T \bar{\sigma} d\Omega \quad (25b)$$

The matrix $\mathbf{A}$ has the same order as the number of the terms used in the polynomial $\mathbf{P}$. Using the numerical integration in Eq. (25b) is similar to the Eq. (21) with the difference that each term is affected by an element area and the weighting coefficient. Therefore, in the L_2-projection method, the recovered stresses, $\boldsymbol{\sigma}^*$, are affected by the size of the connected elements to the patch surrounding the particular assembly node. For example for nine node elements as shown is Fig. 2, the nodal recovered stress $\boldsymbol{\sigma}^*$ belong to a polynomial expansion ($\mathbf{Pa}$) with the same order as $\mathbf{P}$. A patch surrounding the particular assembly node represents a union of elements containing this vertex node.

In Fig. 2 the center of the figure represents the patch assembly point. The interested reader can find more details in Zienkiewicz and Zhu [70,71]. In the real world, most problems fail when they reach the maximum tensile strength\shear stress. The ZZ error estimation is formulated based on the primary and recovered stresses, using the FEM over the elements. The stresses are functions of the displacements that, in turn, are affected by the PWP, heat changes, etc. Hence, error estimation only over the stresses
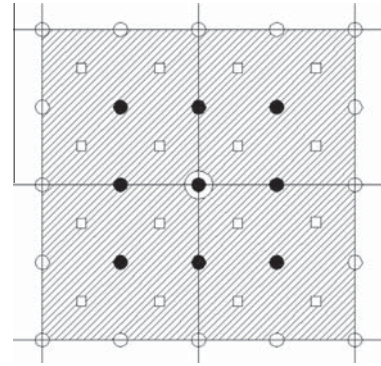

Fig. 2. Computation of superconvergent values for 9 node elements, □ Gauss point. ● Nodal values determined by the recovery procedure.

can reveal the error when examining the material behavior under the applied loading with the discretized mesh. Thus, it is possible to achieve a desired accuracy by using the adaptive refinement procedure.

4. Time integration procedure

For time discretization of the governing Eq. (8), the generalized Newmark technique is employed with the Newton–Raphson iteration. Accordingly, the problem variables and their temporal derivatives in the time interval of $[t_n, t_{n+1}]$ are given as:

$$\begin{cases} \ddot{\mathbf{u}}_{n+1}^{(k)} = \ddot{\mathbf{u}}_n + \Delta\ddot{\mathbf{u}}_n \Rightarrow \ddot{\mathbf{u}}_{n+1}^{(k-1)} + \Delta\ddot{\mathbf{u}}^{(k)} = \ddot{\mathbf{u}}_n + \Delta\ddot{\mathbf{u}}_n \Rightarrow \Delta\ddot{\mathbf{u}}_n = \ddot{\mathbf{u}}_{n+1}^{(k-1)} \\ +\Delta\ddot{\mathbf{u}}^{(k)} - \ddot{\mathbf{u}}_n \\ \dot{\mathbf{u}}_{n+1} = \dot{\mathbf{u}}_{n+1} + \Delta t\ddot{\mathbf{u}}_n + \beta_1\Delta t(\ddot{\mathbf{u}}_{n+1}^{(k-1)} + \Delta\ddot{\mathbf{u}}^{(k)} - \ddot{\mathbf{u}}_n) \\ \mathbf{u}_{n+1} = \mathbf{u}_n + \Delta t\dot{\mathbf{u}}_n + \frac{1}{2}\Delta t^2\ddot{\mathbf{u}}_n + \frac{1}{2}\beta_2\Delta t^2(\ddot{\mathbf{u}}_{n+1}^{(k-1)} + \Delta\ddot{\mathbf{u}}^{(k)} - \ddot{\mathbf{u}}_n) \end{cases} \quad (26)$$

and

$$\begin{cases} \dot{p}_{n+1}^{(k)} = \dot{p}_{n+1}^{(k-1)} + \Delta\dot{p}^{(k)} = \dot{p}_n + \dot{p}_n \Rightarrow \Delta\dot{p}_n = \dot{p}_{n+1}^{(k-1)} + \Delta\dot{p}^{(k)} - \dot{p}_n \\ p_{n+1} = p_n + \Delta t\dot{p}_n + \bar{\beta}_1\Delta t(\dot{p}_{n+1}^{(k-1)} + \Delta p^{(k)} - \dot{p}_n) \end{cases} \quad (27)$$

where Δt is the time step length. It should be noted that for linear-elastic stress–strain behavior a single iteration solves the problem exactly and the superscript k in Eqs. (26) and (27) is unnecessary [67]. The approximation is stable unconditionally when [67]:

$$\beta_2 \geqslant \beta_1 \geqslant \frac{1}{2} \quad \text{and} \quad \bar{\beta}_1 \geqslant \frac{1}{2} \quad (28)$$

By considering the governing equation in t_{n+1} and implementing the variable at t_{n+1} in terms of the variable at t_n, as mentioned in Eq. (27), the governing equation becomes:

$$\begin{bmatrix} \mathbf{M} + \frac{1}{2}\beta_2\Delta t^2\mathbf{K} & -\bar{\beta}_1\Delta t\mathbf{Q} \\ -\bar{\beta}_1\Delta t\mathbf{Q}^T & -\mathbf{S} - \bar{\beta}_1\Delta t\mathbf{H} \end{bmatrix} \begin{bmatrix} \Delta\ddot{u}^{(k)} \\ \Delta\dot{p}^{(k)} \end{bmatrix} = \begin{bmatrix} \mathbf{F}^u \\ -\mathbf{F}^p \end{bmatrix} \quad (29)$$

where the equivalent forces are:

$$\mathbf{F}^u = f_{n+1}^u - \mathbf{M}\ddot{u}_{n+1}^{(k-1)} + \mathbf{Q}\left(p_n + \Delta t\dot{p}_n + \bar{\beta}_1\Delta t\left(\dot{p}_{n+1}^{(k-1)} - \dot{p}_n\right)\right)$$
$$\quad - \mathbf{K}\left(\mathbf{u}_n + \Delta t\dot{\mathbf{u}}_n + \frac{1}{2}\Delta t^2\ddot{\mathbf{u}}_n + \frac{1}{2}\beta_2\Delta t^2\left(\ddot{\mathbf{u}}_{n+1}^{(k-1)} - \ddot{\mathbf{u}}_n\right)\right)$$
$$\mathbf{F}^p = f_{n+1}^p - \mathbf{Q}^T\left(\dot{\mathbf{u}}_n + \Delta t\ddot{\mathbf{u}}_n + \beta_1\Delta t\left(\ddot{\mathbf{u}}_{n+1}^{(k-1)} - \ddot{\mathbf{u}}_n\right)\right) - S\dot{p}_{n+1}^{(k-1)}$$
$$\quad - \mathbf{H}\left(p_n + \Delta t\dot{p}_n + \bar{\beta}_1\Delta t\left(\dot{p}_{n+1}^{(k-1)} - \dot{p}_n\right)\right) \quad (30)$$

5. Validation and numerical results

5.1. Validation

The results of this paper are verified with the exact solution reported by Olson [40] for one-dimensional consolidation under time-dependent loading, with Young's modulus $E = 104$ kPa, Poisson's ratio $v = 0.2$, and permeability $= 5 \times 10^{-7}$ m/s, and step loading = 1 kPa on the top surface. The load is applied during a time period of 1 day and remains constant thereafter (Fig. 3). Olson [40] expressed the excess pore pressure in terms of the vertical position. All boundaries are considered impermeable, except for the upper surface that is free draining (for further information, see Das [16]). According to this solution, the excess pore pressure of consolidation is expressed as:

$$\begin{cases} T_v \leqslant T_c : p = \sum_{m=0}^{\infty} \frac{2q_c}{M^3 T_c} \left(1 - e^{-M^2 T_v} \right) \sin \left(\frac{My}{H} \right) \\ T_v \geqslant T_c : p = \sum_{m=0}^{\infty} \frac{2q_c}{M^3 T_c} \left(e^{-M^2 (T_c - T_v)} - e^{-M^2 T_v} \right) \sin \left(\frac{My}{H} \right) \end{cases} \quad (31)$$

where $T_c = \frac{c_v t_c}{H^2}$, $T_v = \frac{t c_v}{H^2}$, $c_v = \frac{k}{m_v \gamma_w}$, $m_v = \frac{(1+v)(1-2v)}{E(1-v)}$, $M = (2m + 1) \frac{\pi}{2}$, E is Young modulus, v is Poisson's ratio, and H is drainage distance.

Fig. 4a and b shows the excess pore pressure plotted versus depth as symbol points. The results of this study are very comparable to those of Olson [40].

For further assessment, a saturated porous seabed of finite thickness subjected to progressive wave loading is considered and a comparison of the FE solution with an exact solution reported by Hsu and Jeng [25] is made. The wavelength $(L_{wl}) = 324$ (m), wave period $(T_{wl}) = 15.0$ s, shear modulus $(G_{seabed}) = 10^7$ N/m^2 and permeability $= 10^{-4}$ m/s are used (see Fig. 5). The moving boundary conditions in time and space are taken from the analytical solution to obtain the FE solution. Interested readers may refer to Ulker and Rahman [56] and Ulker et al. [57] for more details about the exact solution and required boundary conditions.

Hsu and Jeng [25] presented the variation of dimensionless stresses and pore pressure versus dimensionless seabed thickness in Fig. 6 for saturated seabed when the surface subject to $p = p_0 e^{i\left(\frac{2\pi}{L_{wl}}x - \frac{2\pi}{T_{wl}}t\right)}$, x and t are the horizontal coordinate and time respectively. Based on normalizing the results based on p_0, the value of that is considered as unit (for more details refer to [56] and [58]). Graphs of non-dimensionalized stresses and pore pressure against thickness as obtained from FEM are given in Fig. 6.
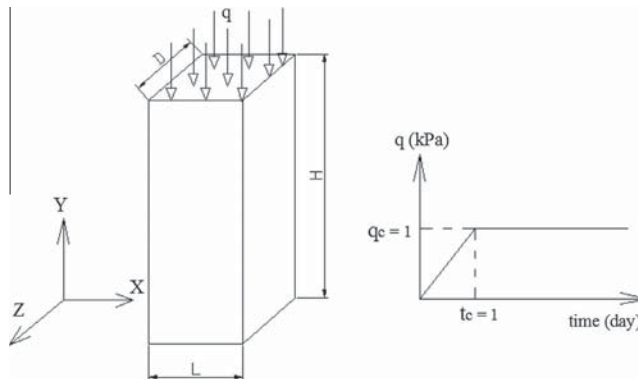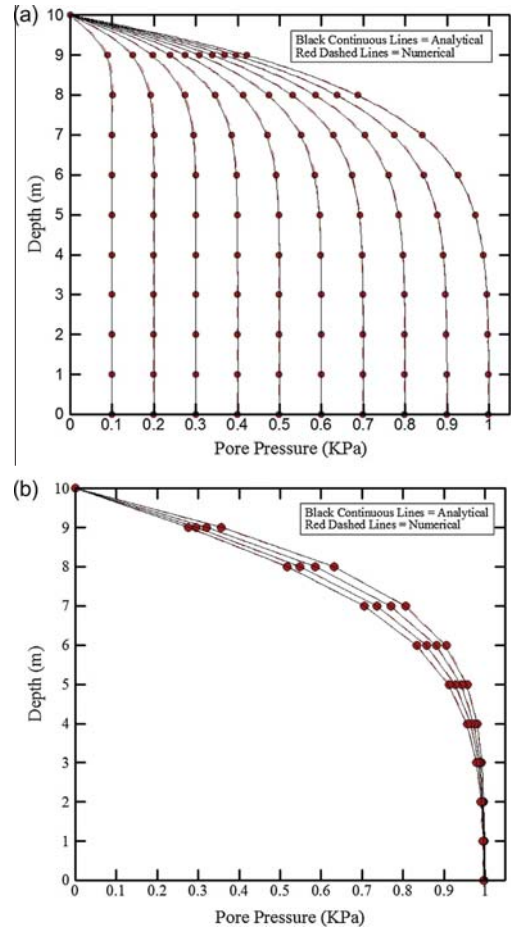

Fig. 4. Excess pore water pressure change along the depth for different times. Symbols line is solution of the present study. Continuous lines are from Olson [40]. (a) $t < tc$. (b) $t > tc$.

Fig. 3. One-dimensional consolidation problem under time-dependent loading.

It can be seen that the results of this study are well- compatible with those of Hsu and Jeng [25].

5.2. Numerical results

5.2.1. Response of the monopile foundation under dynamic cyclic displacement

To illustrate the linear-elastic stress–strain behavior of the saturated soil around the monopile numerically, a 2D model with the plane strain condition is applied to the presented formulation for an axisymmetric solid circular cylinder with radius R, as shown in Fig. 7. The arc-boundary (or semi-circle boundary), which represents the common border between the solid cylinder and saturated soil, is subject to harmonically varying forced displacement ($u = 0.1 \sin(\pi t/2)$) with cyclic frequency ω and applied forced

displacement is in the horizontal (x) direction the same as considered by Damgaard et al. [15], as shown in Fig. 8.

The 2D analysis of each soil layer is performed based on the material properties presented in Table 1.

Typically, offshore monopile wind turbines have diameters of 4–6 m [15]. However, recent research for water depths above 40 m has shown that monopiles with diameters up to 10 m might be applicable and economically feasible [48]. A monopile with diameter 6 m is considered in this study. The behavior of the monopile foundation can change from flexible to rigid, depending on the pile material properties and its geometry, embedded length, the applied load and also soil material properties. The dimensionless pile flexibility factor is therefore defined [44] and investigated by many researchers such as Doherty and Gavin [18], Vonmarie [59] and Haiderali and Madabhushi [22] just to mention a few. This pile flexibility factor is [44]:
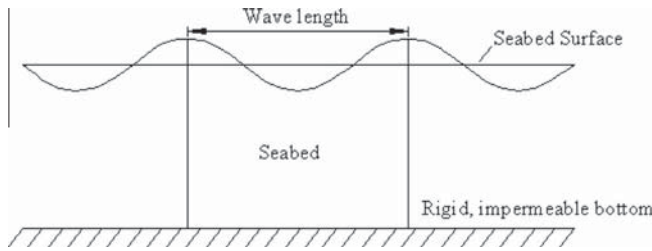

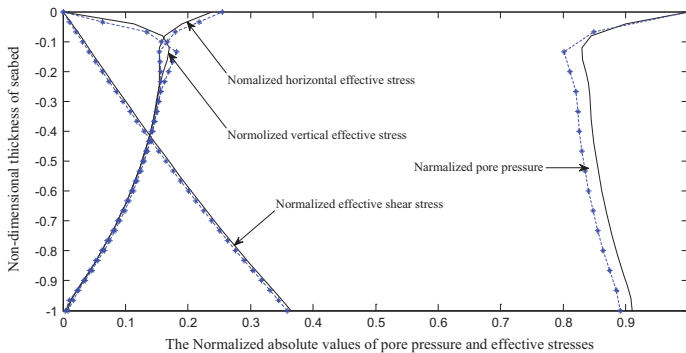**Fig. 5.** Geometry of seabed with finite thickness under harmonic wave load.

Fig. 6. Distribution of the dimensionless pore pressure and stresses versus the nondimensional seabed thickness for a fully saturated porous bed. Calculated results from 25 in solid lines, and present study in dashed lines (*).
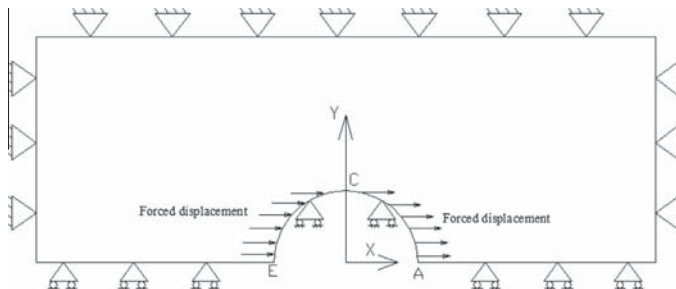

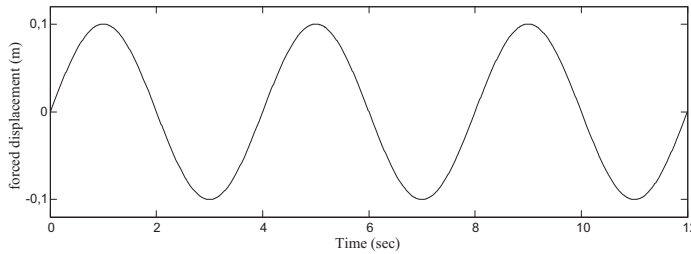**Fig. 7.** Model description of the monopile with applied load and boundary conditions.

Fig. 8. Applied forced displacement versus time.

Table 1
Material properties of soil and pile.

Young's modulus (N/m^2)	1×10^8
Poisson's ratio	0.25
Void ratio	0.50
Bulk modulus of grain (N/m^2)	3.6×10^{10}
Bulk modulus of fluid (N/m^2)	2×10^9
Density of grain (kg/m^2)	2000
Density of fluid (kg/m^2)	1000
Permeability (m/s)	10^{-7}
Pile radius (m)	3

Pile flexibility factor

$$= \frac{\text{Pile Young's modulus} \times \text{Pile moment of inertia}}{\text{Soil Young's modulus} \times \text{Embedded monopile length}^4}$$

Based on the value of the flexibility factor, the pile behavior can be varied from flexible to stiff pile. Rigid pile defines for flexibility factor greater than 0.01. Based on current design practices, offshore monopile wind foundations need to be cost-effective and provide rigid piles with a safe, stable, and economical design (Vonmarie, [59]). For monopile offshore foundations, rigid body motion is more pronounced than the pile deformation especially when there is large pile diameter [23]. Therefore, a rigid monopile is considered in this study.

In this study, by considering plane strain conditions a rigid monopile with radius $R = 3$ m is considered. According to design regulations Det Nordske Veritas [17], normally a steel pile with Modulus of elasticity, $E = 210,000$ N/mm^2 and Poisson's ratio, $v = 0.3$ is considered for the monopile foundation in industry [17]. Here, by considering the rigid arc-boundary for the monopile, the pile properties do not affect the response of the saturated surrounding soil. For small vibration amplitudes, considered in this study, full contact between the soil and the pile is assumed. Thus, the interface is not modeled explicitly. Instead the boundary of the soil towards the pile is subject to forced cyclic displacements.

Simulations are done for 12 s, which represents three periods of harmonic forced displacement. The monopile model is solved using four different rectangular meshes, with 96, 144, 272, and 480 elements. To satisfy the LBB condition, the second-order rectangular mesh (Q9) is selected for the displacement field and the first-order rectangular mesh (Q4) for the pressure field. Nodes for the pressure field are selected on the nodes constructed for the displacement field [67]. Varying time steps are considered for pore pressure propagation; a small time step is considered for the primary steps, and the time step is then increased.

In the following sections, the results are presented for a mesh configuration with 480 elements. In order to have the desired boundaries and passing the outgoing wave motions through the
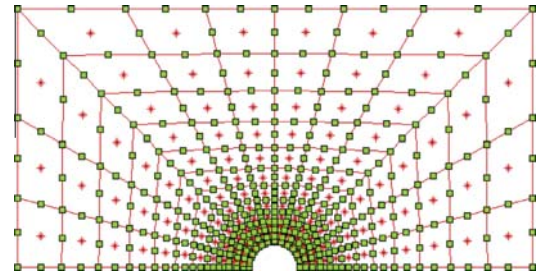

Fig. 9. Model description.

boundary in FEM simulation, the bounded domain problems should be such that the energy crosses them without reflection from model boundaries towards the structure. To treat this, large model size, artificial or transmitting boundaries and damping solvent stepwise extraction methods and boundary element method based on applied load and desired outputs can be applied and employed Andersen [3], Li et al. [32], Andersen et al. [4], and Xunqiang et al. [61]. Many different methods have been reported in the literature to present and model absorbing boundary conditions such as Lysmer and Kuhlemeyer [36], Bamberger et al. [5] and Krenk and Kirkegaard [31]. In this study based on the applied load and medium load frequency and considered pile geometry a large model size is employed. The problem is discretized with fine mesh close to the pile and the dimensions of the whole model are 200 m × 200 m. Time steps for plotting are selected based on the cyclic displacement applied to the problem. The dynamic results are mainly presented for the second and third simulation periods, which provide more stable results compared to the first period.

The chosen mesh consists of 9-noded biquadratic and 4-noded bilinear elements for displacement and pore pressure fields, respectively. Fine meshes are generated close to the pile while coarse meshes are used far from the pile as shown in Fig. 9. The pore pressure, lateral flow and displacements are considered zero at the exterior boundary and the sinusoidal periodic displacement in the horizontal direction is applied for the semi-circular boundary at the soil–pile interface. An illustration of the boundary conditions is provided in Fig. 7.

As shown in Fig. 7, the symmetry of the problem has been exploited by introducing appropriate boundary conditions at the plane of symmetry.

Fig. 10 illustrates the shear stress in the plane of symmetry for different time simulations in the second cycle of forced displacement (4 < time < 6 s).

Imposing prescribed displacement in presence of symmetry boundary conditions with respect to the center line of the pile
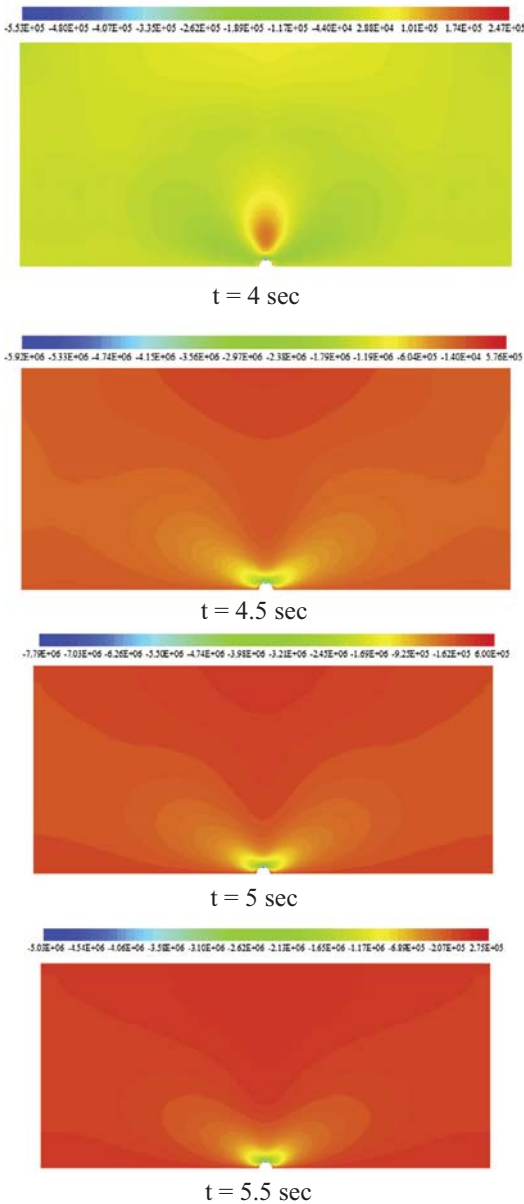
t = 4 sec

t = 4.5 sec

t = 5 sec

t = 5.5 sec

Fig. 10. Time sequence contours of the shear stress (N/m²) in four time simulations for the symmetry plane of a soil system.

(Y-axis) and moving boundary conditions (as shown in Fig. 7) justify the symmetric shear stress distribution with respect to the Y-axis. At the times 4 and 6 s, the direction of shear stress is changed based on changing the direction of imposed displacement (see Fig. 8), and the absolute value of the difference between the minimum and maximum shear stresses is almost the same. The absolute amount of shear stress increases with time as the pile moves in a positive direction (4 < time < 5 s) along the horizontal axis.

t = 4 sec

t = 5 sec
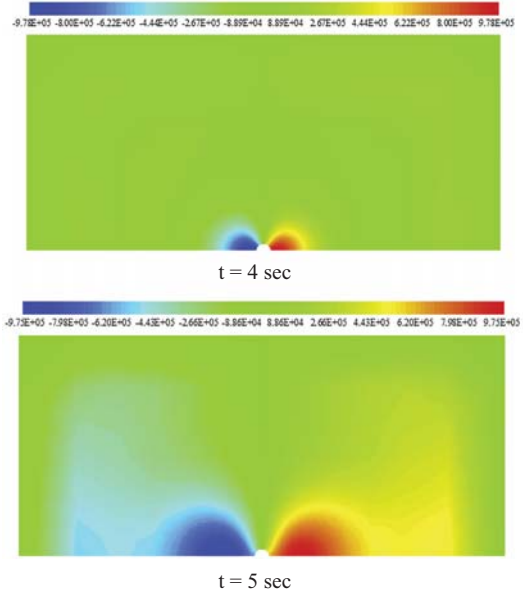
Fig. 11. Time sequence contours of the pore pressure (N/m²) in two different time simulations for the symmetry plane of a soil system.

For the reverse direction, the shear stress decreases until the pile is relocated to the center (5 < time < 6 s). According to the numerical analysis, the same behavior can be seen as the pile moves to LHS and arrives at the origin (6 < time < 8 s). As expected, the results for times of 4, 4.5, 5, and 5.5 s are very similar to those for 6, 6.5, 7, and 7.5 s, respectively.

The absolute value of maximum shear stress always occurs at the middle of semi-circle boundary (point C), with a small difference in the results. In other words, the absolute values of the maximum shear stress at the corresponding times are not exactly the same. These values are obtained by the time integration of the generalized Newmark method. Moreover, the use of a non-uniform mesh may introduce small numerical errors in the results, leading to small differences in the results at each time step. The shear stress at the center line (Y-axis) has both positive and negative shear stress values at all times. This phenomenon can be justified and explained by the presence of applied imposed displacement and soil movement. Close to the pile, the soil follows the direction of the pile's movement; far from the pile, the soil moves in the opposite direction.

Fig. 11 shows the PWP distribution for different time simulations.

By indicating the positive compression pore pressure the anti-symmetry pore pressure distribution with respect to the Y-axis is seen in Fig. 11. Plane stress, symmetry and moving boundary conditions indicate the zero normal stresses at point C; only shear stress exists at this point, without any normal stress, which leads to a value of zero pressure for every time step. These contours suggest that the pore pressure distribution is more concentrated close to the pile when it is located at the origin, whereas it is dispersed in a large area when the pile reaches the maximum distance from the origin (Fig. 11a and b).

Two interesting observations in Figs. 8 and 9 are the significant shearing and excess pore pressure generation adjacent to the pile.

Fig. 12 shows the pore pressure generation during the dynamic simulation.

The behaviors of the time-varying pressure and the forced-displacement load are similar, but the period of the pressure is smaller than that of the applied load, $T_{pressure} < 4$ s, for the first period. The first maximum (or minimum) at point A (or point E) is smaller than that for the rest of the time simulation because the dynamic simulation is not yet stabilized. Accordingly, the contours shown in Figs. 8 and 9 are taken for time >4 s. The results for the second period are much more stable than those for the first period. Although the results for the third period are better compared to the second period, the second and third period results have almost the same maximum and minimum values, just with decreased oscillations in the third period. Results for points A and E clearly have the same trend, but in opposite directions. Moreover, the maximum (or minimum) pore pressure does not occur at the maximum (or minimum) displacement time.

Fig. 13 shows the normal effective stresses at points A and E (in Fig. 7) during the time simulation.

The normal effective stress at nodes A and E display opposing behaviors. The absence of external loads in Y direction justify that the normal stress in the horizontal direction should be higher than the normal stress in the Y direction. The normal stresses in the horizontal and in plane perpendicular directions at point A (or E) are in tension or compression at each time. In addition, the maximum (or minimum) normal stress is achieved when the pile has the maximum (or minimum) displacement. Importantly, the period of effective stress in first time period is the same as the applied load, in contrast with the pore pressure behavior shown in Fig. 12.

Fig. 14 shows the shear stress at point C as a function of time.

The shear stress at point C changes with time in the same manner as the applied forced-displacement load. The maximum (or minimum) shear stress occurs when the displacement is maximum (or minimum). The shear stress is zero when the pile is located at the origin based on disappearing of the displacement.

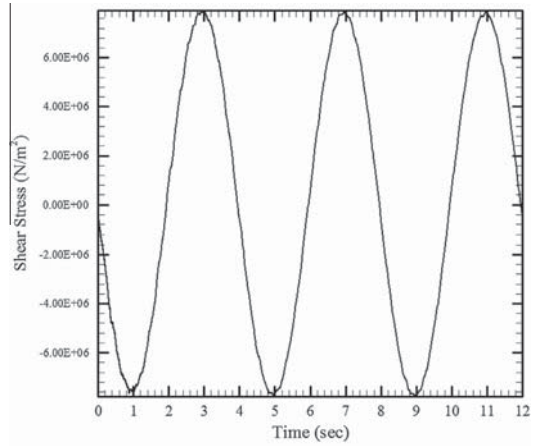**Fig. 12.** Variation of the pore pressures (N/m²) at the corner of the pile (points A and E) versus time.

Fig. 14. Variation of the shear stress (N/m²) at the middle of semi-circle boundary (point C) versus time.

Fig. 13. Variation of the effective stresses (N/m²) at the corner of the pile (points A and E) versus time.
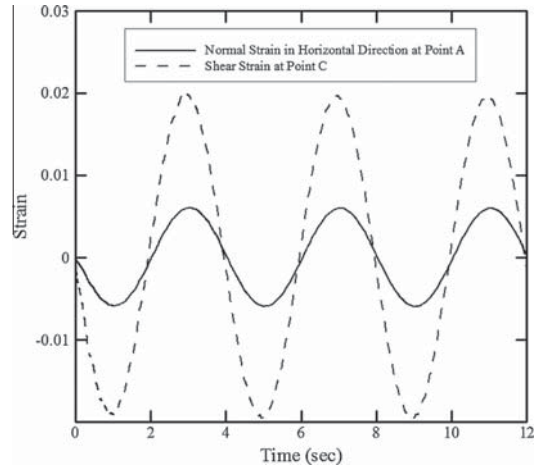

Fig. 15. Variation of the strains at the corner and middle of the semi-circle boundary (point A and C) versus time.

Fig. 15 shows the normal and shear strains as a function of time for points A and C.

The pile undergoes the maximum normal and shear strains (at points A and C) when it reaches to the absolute maximum displacement. Moreover, the general observations for the effective stress at point A and shear stress at point C are valid for normal and shear strains and points A and C. These results are indicated by Figs. 12 and 11 for corresponding points. At the time with zero shear strain at point C in Fig. 15 indicates the zero shear stress in Fig. 14. And also, the time for zero normal strain at point A in Fig. 15 corresponds to maximum distance of pile from center which indicates maximum pore pressure and subsequently the effective stress for the corresponding time should be zero. This observation is indicated by Fig. 13 by indicating effective stress at point A.

Fig. 16 shows the pore pressures on a semi-circular boundary (where is interaction between soil and pile) for different time simulations.

The point C in Fig. 7 indicates $X = 0$ in Fig. 15, the point C has zero pore pressure for all simulation times which is vindicated by presented results in Fig. 11. The horizontal coordinate of semi-circle nodes (X) are changing between -3 and 3 (m). It is found that the pressures along the semi-circular line have zero value when time is about 5.35 and 7.35 s. An anti-symmetric behavior is seen when the pile rocks to the LHS or RHS. The variation in PWP on the semi-circular line changes linearly with time. For the second period of simulation, the maximum pore pressure occurs around 4.5 or 6.5 s. Accounting for the behavior of the pore pressure, this phenomenon can be explained by the presence of the porous media movement. Fig. 12 may be referred to for more details. The period of time-variant pore pressure is reduced in the first period.

Fig. 17 depicts the normal stress in the horizontal direction on a semi-circular curve for different time simulations.

The normal stress is zero at point C and is anti-symmetric with respect to the Y axis, which is confirmed by results in Fig. 16, for the whole simulation time. At 4 s, the normal stress changes from compression to tensile stress at the semi-circular boundary where $X = 2.6$ (or -2.6) m. This phenomenon can be explained by the presence of interactive effects between the movement of grain particles and the fluid phase. This effect can also be seen at other times, when the behavior of the normal stress appears sinusoidal.
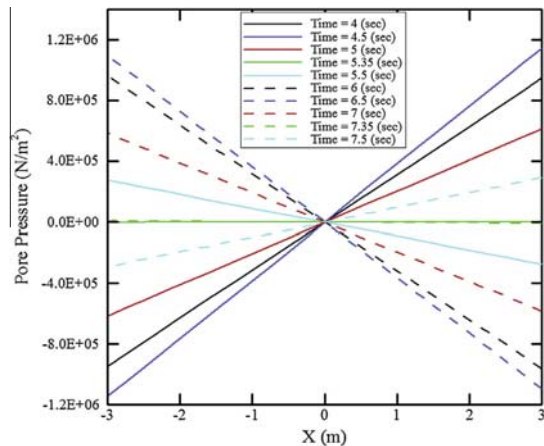
As expected, when the pile moves in a positive horizontal direction ($4 < time < 5$ s), the normal stress in front of the pile is negative. As the time increases, the absolute value of the normal stress increases to a maximum value. For the reverse direction ($5 < time < 6$ s), it decreases. The same behavior can be seen for the other side of the pile. The maximum (minimum) effective normal stress in the horizontal direction is obtained at the maximum (minimum) displacement of the pile. Comparing Figs. 14 and 15 while also considering Fig. 12, it can be observed that because the time in the first cycle changes with respect to the other pore pressure cycles, the maximum effective stress and minimum pore pressure do not coincide at the same time.

Fig. 18 shows the shear stresses along the semi-circular line of the pile for different time steps.

The maximum shear stress occurs at point C, where the pore pressure and effective stresses are zero (refer to Figs. 14 and 15). By considering the couple equation of motion which represented the effect of pore pressure on stress field and considering the
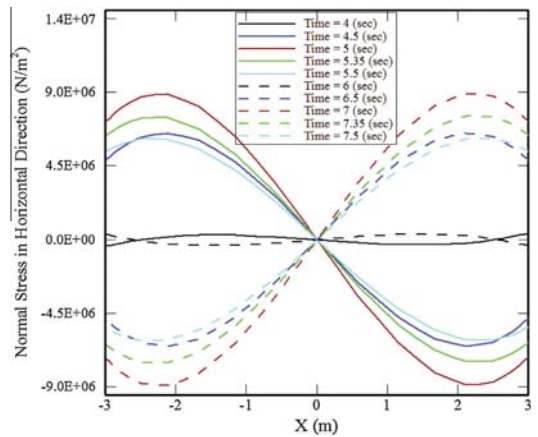

Fig. 17. Variation of the normal stress (N/m²) in the horizontal direction on a semi-circular pile line for different time simulations.

Fig. 16. Variation of the pore pressure (N/m²) on a semi-circular pile line for different time simulations.

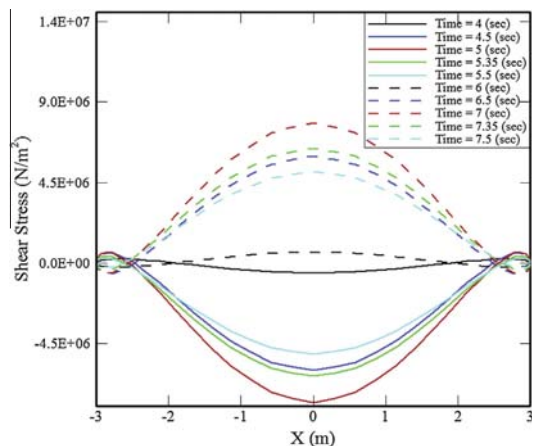**Fig. 18.** Variation of the shear stress (N/m²) on a semi-circular pile line for different time simulations.

results for pore pressure (Fig. 14), these effects justify that the shear stress changes around the monopile as shown in Fig. 18. The shear stress behavior for 4 < time < 5 s is comparable with that for 6 < time < 7 s and larger than those for 5 < time < 6 s and 7 < time < 8 s. As a result of the time history of shear stress, the absolute value of the shear stress duration at 4 < time < 5 s is greater than at 5 < time < 6 s. The zero-value shear stress point moves to RHS (LHS) when the pile moves to the RHS (LHS). Accounting for the boundary condition, this phenomenon can be explained by the high resistance of the saturated soil when the pile is located at the center compared to when the pile is moving to the LHS or RHS of the origin.

5.2.2. ZZ error estimation of the monopile foundation and saturated isotropic seabed of finite thickness

Fig. 19a and b illustrates the variation of the energy norm (E_{norm}) using FE nodal and Gauss point stresses ($\bar{\sigma}$) respectively for the whole system by using the ZZ formulation over time (see Fig. 19).

The behavior of the energy norm is periodic in the time domain, as is the case with the normal and shear stresses. The energy norm starts at a zero value when the displacement is zero. During movement, it does not return to the zero value because of the interaction between the grain particles and fluid. In the following equation, the time period of the energy norm is half that of the displacement. The energy norm reaches its maximum (or minimum) at maximum (or minimum) displacement. The Eq. (17b) is numerically implemented to plot Fig. 17b as:

$$\left(E_{norm}^{Z95}\right)_{ng} = \left\{\int_{\Omega} \bar{\sigma}^T \mathbf{D}^{-1} \bar{\sigma} d\Omega\right\}^{1/2}$$
$$= \sqrt{\sum_{iel=1}^{nel} \sum_{ig=1}^{ng} \left[\bar{\sigma}_{ig}^T \mathbf{D}^{-1} \bar{\sigma}_{ig}\right] \cdot |J_{ig}| \cdot w_{ig}} \qquad (32)$$

where ng is the number of gauss points per element and nel is the total number of elements.

Fig. 20 shows the error norm ($\|e_s\|$) based on Eq. (15) obtained using different recovery procedures.

In order to investigate the behavior of energy norm the model with 96 elements is considered. The trend for the error norm based on difference between FEM and recovery stresses is approximately the same as the trend for the pile displacement. In first period, the
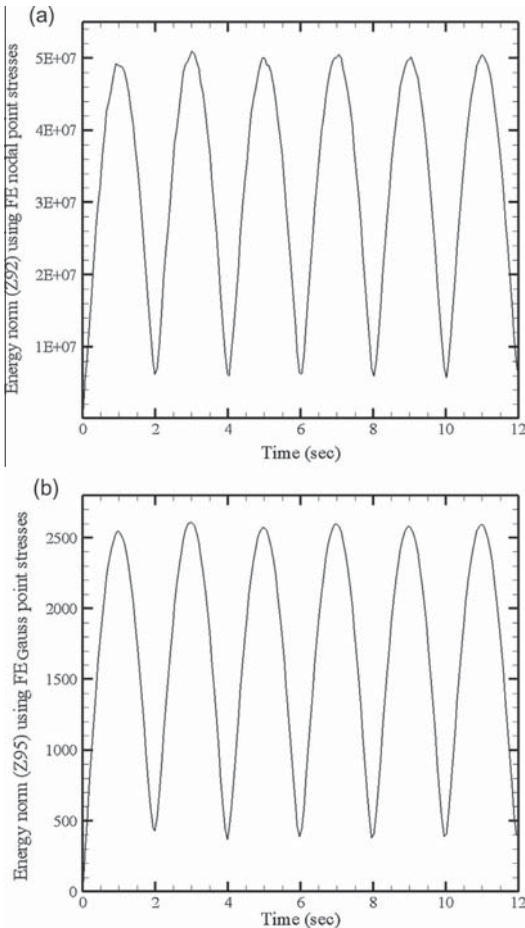

Fig. 19. Variation of the energy norm (E_{norm}) using finite element nodal and gauss point stresses versus time for the monopile model.
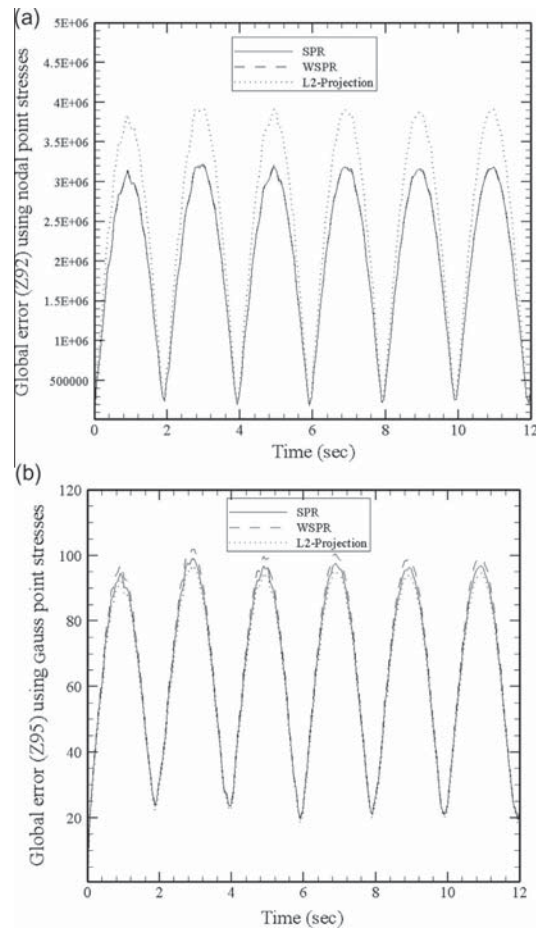

Fig. 20. Variation of the global error norm ($\|e_{es}\|$) by the SPR, WSPR, and L_2-projection methods versus time for the monopile model.

global error is not stabilized numerically based on the way of time integration, time step and applied oscillating boundary conditions; for second and subsequent periods, the maximum and minimum global error values are nearly the same. The error norm in Fig. 18b based on Eq. (15b) is calculated as follows:

$$\left(\|e_{es}^{Z95}\|\right)_{ng} = \sqrt{\int_{\Omega} (\boldsymbol{\sigma}^* - \bar{\boldsymbol{\sigma}})^T \mathbf{D}^{-1} (\boldsymbol{\sigma}^* - \bar{\boldsymbol{\sigma}}) d\Omega}$$

$$= \sqrt{\sum_{iel=1}^{nel} \sum_{ig=1}^{ng} \left[\left(\boldsymbol{\sigma}_{ig}^* - \bar{\boldsymbol{\sigma}}_{ig}\right)^T \mathbf{D}^{-1} \left(\boldsymbol{\sigma}_{ig}^* - \bar{\boldsymbol{\sigma}}_{ig}\right) \right] \cdot |J_{ig}| \cdot w_{ig}}$$

$$(33)$$

It is observed from Fig. 18b that the difference between FEM and L$_2$-projection recovery Gauss point stresses is smaller than difference between FEM and other recoveries results. Fig. 18a demonstrates that the SPR recovery nodal stresses take smaller global error in comparison to other methods. The result from Fig. 18a is similar to the one reported in Zienkiewicz and Zhu [70–72].

Fig. 21 compares the relative errors with the four configurations using the L$_2$-projection method.

The Eqs. (15b) and (17b) are implemented to calculate the relative errors by using Gauss point stresses. It shows that the numerical error decreases as the number of elements increases.

To quantify the efficiency and accuracy of the recovery procedures for analyzing a monopile foundation under cyclic displacement, the convergence rate and convergence curve in the time domain are calculated using the ZZ error, based on the SPR, WSPR and L$_2$-projection recovery procedures using the four mesh configurations (see Fig. 22).

The convergence rate is close to 0.5 however it takes greater value for SPR in comparison to that for L$_2$-projection recovery technique. For an FE optimal convergence can be obtained with $CN^{-p/d}$, where C is a positive constant number, N is the number of degrees of freedom, and d is the dimension of the problem [12]. In this paper, $p = 2$ and $p = 1$ for the displacement and pore pressure fields, respectively. It can be noticed that it is compatible with the theoretical convergence rate which depends on the applied polynomial degree in the FE approximation for the linear element (in this case $p = 1$) as it was mentioned by Tang and Sato [53] and Nadal et al. [38].
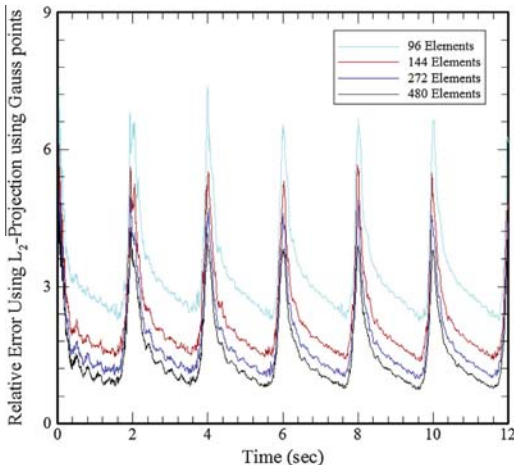
The second benchmark as shown in validation section is implemented to present the error estimation using SPR, WSPR and L$_2$-projection techniques. The developed FE mesh is generated and visualized using the open source mesh generator Gmsh [21] in order to introduce irregular mesh. Simulations are performed for 15 s which is the wave period of harmonic surface wave pressure. Fig. 23 compares the global error norm ($\|e_{es}\|$) with the three different stress recovery techniques by using Eq. (15b).

Here again the difference between the FEM and recovered gauss point stresses by L$_2$-projection is smaller than other recovery methods.

By using Eq. (16a) the global recovery error norm e_R for nodal stresses based on SPR, WSPR and L$_2$-projection techniques is presented in Fig. 24.

It shows that the calculated energy norm by considering SPR recovered stresses takes smaller values compared to those with
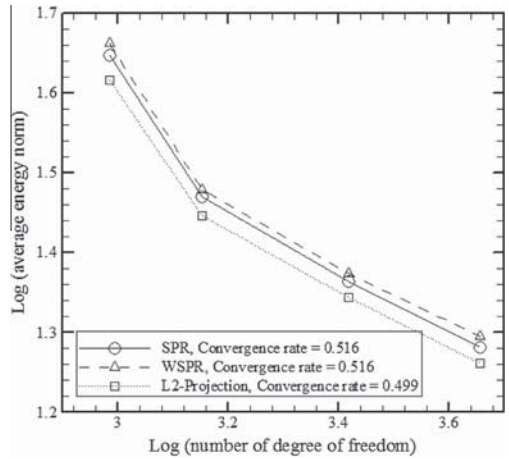

Fig. 22. Rate of Convergence of different stresses recovery procedures for monopile model.

Fig. 21. Variation of the relative errors (e_{rel}) by four different meshes (96, 144, 272, and 480 elements) versus time for the monopile model.
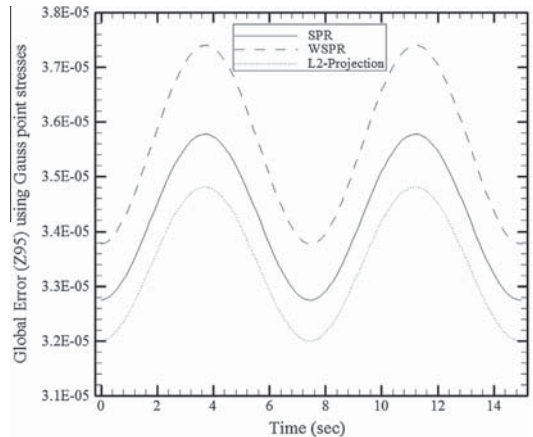

Fig. 23. Variation of the global error norm ($\|e_{es}\|$) by the SPR, WSPR, and L$_2$-projection methods versus time for the seabed model with regular mesh.

L_2-projection. This result is similar to the one reported in Zienkiewicz and Zhu [70–72].

By considering the Fig. 24, the related error ($\|e_R\|$) contours within the geometry has been illustrated in Fig. 25.

It is seen that the maximum error occurs on the surface of the model. Based on the dynamic load on the surface this contour changes with time.

Fig. 24a and b shows the global error norm ($\|e_{es}\|$) and the global recovery error norm $\|e_R\|$ for the model with irregular mesh by considering Eqs. (15b) and (16a), respectively.

The effect of using regular and irregular meshing can be shown by comparing the difference between recovered and exact stresses as shown in Figs. 21 and 24a (and also Figs. 22 and 24b). It is seen that the irregular mesh has greater difference between the exact and recovered stresses at nodal/Gauss point compared to that with regular mesh.

In the seabed model with finite thickness, another irregular mesh that is based on formulations presented by Xuan et al. [60] is considered. The coordinates of interior nodes (x', y') are:

$$\begin{cases} x' = x + (2r_c - 1)\alpha_{ir}\Delta x \\ y' = y + (2r_c - 1)\alpha_{ir}\Delta y \end{cases} \tag{34}$$

where x and Δx (y and Δy) are initial regular node coordinates and element sizes in the x-direction (and y-direction), respectively. Further, r_c is a random number between 0 and 1.0, and
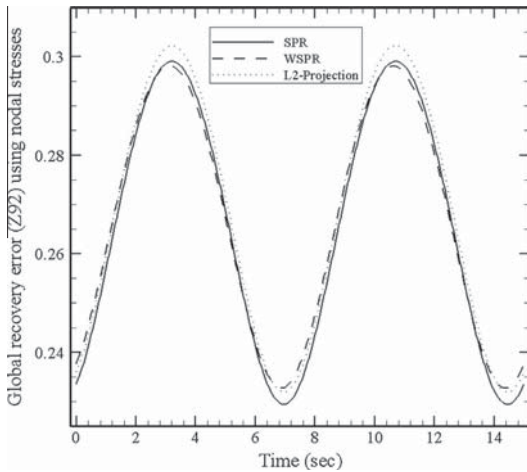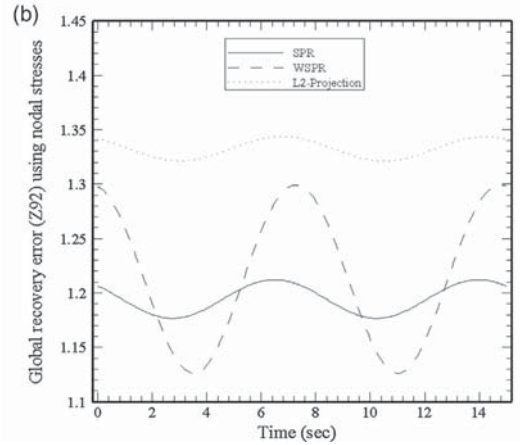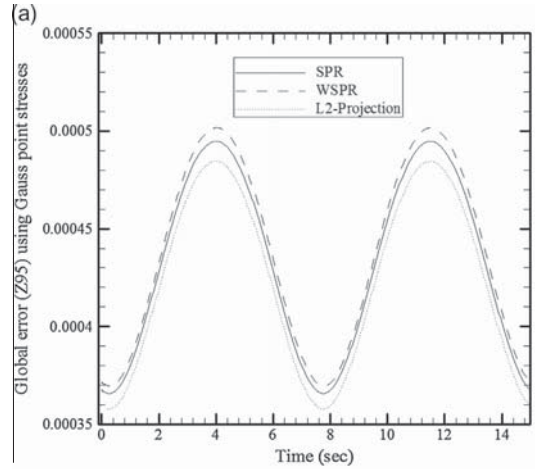

Fig. 24. Variation of the global recovery error norm $\|e_R\|$ by the SPR, WSPR, and L_2-projection methods versus time for the seabed model with regular mesh.

Fig. 26. Variation of the global error norm by the SPR, WSPR, and L_2-projection methods versus time for the seabed model with irregular mesh (b) based on ($\|e_{es}\|$) (b) based on $\|e^R\|$.

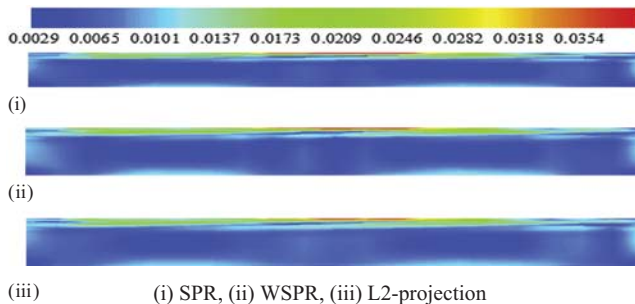(i) SPR, (ii) WSPR, (iii) L2-projection

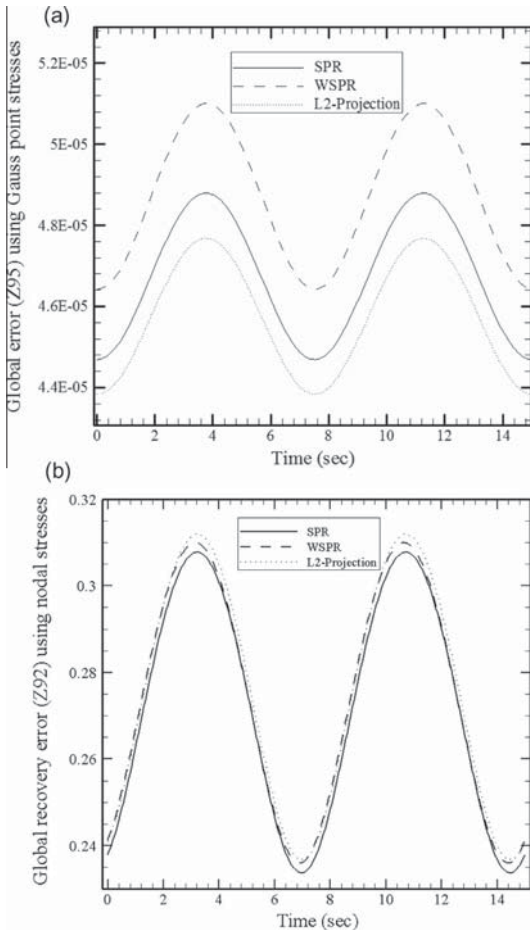**Fig. 25.** The error norm ($\|e^R\|$) contours within the geometry.

Fig. 27. Variation of the global error norm by the SPR, WSPR, and L_2-projection methods versus time for the seabed model with irregular mesh when $\alpha_{ir} = 0.2$ (b) based on ($\|e_{es}\|$) (b) based on $\|e^R\|$.
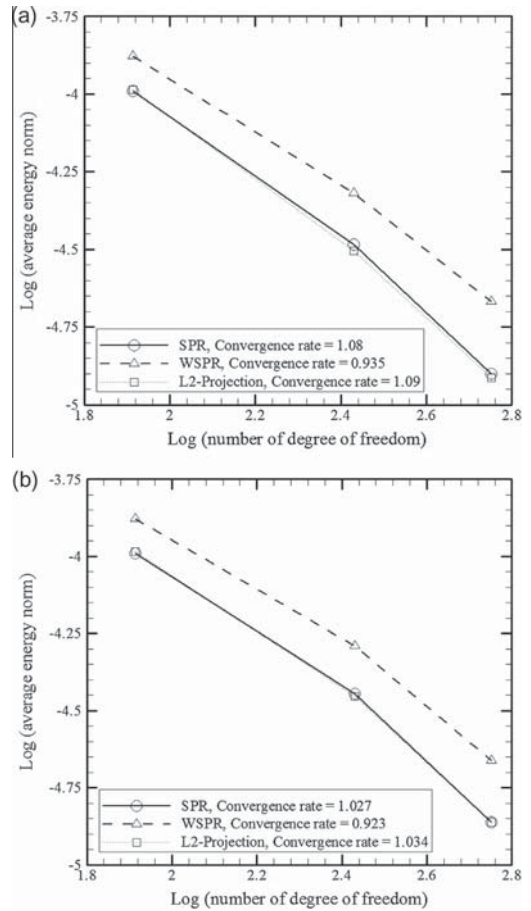
Fig. 28. Rate of Convergence of different stresses recovery procedures for the seabed model (a) with regular mesh (b) with irregular mesh when $\alpha_{ir} = 0.2$.

$\alpha_{ir} \in [0, 0.5]$ is an irregularity factor controlling the shape of the elements.

By using Eqs. (15b) and (16a), the global error norm ($\|e_{es}\|$) and the global recovery error norm $\|e_R\|$ for the model with irregular mesh when $\alpha_{ir} = 0.2$ are shown in Fig. 25a and b, respectively (see Fig. 27).

Here again, the seabed model with irregular mesh has greater global error norm and global recovery error norm in comparison to the correspond results in Fig. 23 for the model with regular mesh which is compatible with the results by Xuan et al. [60]. Furthermore, the global recovery error takes smaller values when the SPR recovered stresses are implemented, which is similar to the results given by Zienkiewicz and Zhu [70–72].

The convergence curve and convergence rate in the time domain are presented and calculated using the ZZ error, based on the SPR, WSPR and L_2-projection recovery procedures as shown in Fig. 28 by considering regular and irregular meshes for the seabed model.

A convergence rate is close to 1. These results follow the formula by Craig et al. [12] and compatible by earlier results reported

by Tang and Sato [53] and Nadal et al. [38]. It can be mentioned that the absolute value of displacement and stresses are just function of the vertical variable as it was mentioned by Ulker and Rahman [56] and Hsu and Jeng [25]. It is seen from Fig. 26b that for the model with irregular mesh (when $\alpha_{ir} = 0.2$) the convergence rate is slightly smaller than those for model with regular mesh as shown in Fig. 26a. This result is similar to the one reported by Xuan et al. [60].

6. Conclusions

This paper explores numerical results for 2D coupled dynamic equations for an offshore monopile foundation in a saturated soil with linear-elastic stress–strain behavior, using the $\mathbf{u} - P$ formulation under cyclic load with conditions of axis-symmetry and plane strain. Three recovery procedures, SPR, WSPR, and L_2-projection, are implemented to recover the stresses on nodes and to capture the ZZ error estimate. Results in the time domain are quantified and compared. For these analyses, the FEM is used with appropriate elements for the displacement and pore pressure fields, the generalized Newmark time integration is applied with the Newton–Raphson procedure.

Some specific observations of this study can be summarized as follows:

- The distributions of the pore pressure and stresses have an important role in the behavior of the saturated soil. Close to the monopile, the soil follows the direction of movement of the pile; however, far from the pile, the soil moves in an opposite direction (Figs. 8 and 9).

- For a given simulation time, the difference between the minimum and maximum shear stress values is constant. The maximum (or minimum) shear stress occurs at the center line of the model (the in plane perpendicular line at point C) and varies harmonically with the corresponding behavior of the load (Fig. 14). The direction of the shear stress at the center line (Y-axis) is independent of the direction of movement; it always takes both positive and negative values (Figs. 12 and 8).

- The time periods for all effective quantities (for points A, and E) are the same as those for the applied load (Fig. 13), whereas the time for the first cycle of periodic pressure is smaller than that for the applied load (Fig. 12).

- The convergence rate is 0.5 for all presented recovery procedures applied for solving the coupled dynamic equations for the monopile model. This result is compatible with that reported by Tang and Sato [53] reported for saturated porous soil.

- The global error norm ($\|e^R\|$) takes smaller value for SPR recovery stresses in comparison to L_2-projection technique (Figs. 22, 24b and 25b). This result is similar to the presented result by Zienkiewicz and Zhu [70,71].

Acknowledgements

References

[1] Achmus M, Kuo YS, Abdel-Rahman K. Behavior of monopile foundations under cyclic lateral load. Comp Geotech 2009;36:725–35.

[2] Amani J, Afshar MH, Aisipour M. Mixed discrete least squares meshless method for planar elasticity problems using regular and irregular nodal distributions. Eng Anal Bound Elem 2012;36:894–902.

[3] Andersen LV. Linear elastodynamic analysis, DCE Technical Memorandum No. 3. Aalborg University; 2006.

[4] Andersen LV, Ibsen LB, Liingaard MA. Impedance of bucket foundations: torsional, horizontal and rocking motion. In: Papadrakakis M, Topping BHV, editors. Proceedings of the sixth international conference on engineering computational technology. Athens (Greece); 2008.

[5] Bamberger A, Chalindars B, Joly P, Roberts JE, Teron JL. Radiation boundary conditions for elastic wave propagation. SIAM J Scient Statist Comput 1988;9(6):1016–49.

[6] Bathe KJ. The inf–sup condition and its evaluation for mixed finite element methods. Comp Struct 2001;79:243–52.

[7] Biot MA. Theory of propagation of elastic waves in a fluid-saturated porous solid. I. Low-frequency range. J Acoust Soc Am 1956;28:168–78.

[8] Biot MA. Mechanics of deformation and acoustic propagation in porous media. J Appl Phys 1962;33:1482–98.

[9] Brezzi F. On the existence, uniqueness, and approximation of saddle-point problems arising from Lagrange multipliers. Revue française d'automatique informatique recherche opérationnelle (RAIRO) Analyse numérique 1974;8:129–51.

[10] Chan AHC. A unified finite element solution to static and dynamic in geomechanics, Ph.D. thesis. University College of Swansea (England); 1988.

[11] Cheng Z, Jeremić B. Numerical modeling and simulation of pile in liquefiable soil. Soil Dyn Earthq Eng 2009;29:1405–16.

[12] Craig AW, Ainsworth M, Zhu JZ, Zienkiewicz OC. h and h-p version error estimation and adaptive procedures from theory to practice. Eng Comp 1989;5:221–34.

[13] Cuéllar P. Pile foundations for offshore wind turbines: numerical and experimental investigations on the behavior under short-term and long-term cyclic loading, Ph.D. thesis. Technical University of Berlin (Germany); 2011.

[14] Cuéllar P, Mira P, Pastor M, José A, Merodo F, Baeßler M, et al. A numerical model for the transient analysis of offshore foundations under cyclic loading. Comp Geotech 2014;95:75–86.

[15] Damgaard M, Bayat M, Andersen LV, Ibsen LB. Assessment of the dynamic behaviour of saturated soil subjected to cyclic loading from offshore monopile wind turbine foundations. Comp Geotech 2014;61:116–26.

[16] Das BM. Advanced soil mechanics. 3rd ed. 270 Madison Ave, New York (NY 10016, USA): Taylor & Francis; 2008.

[17] Det Norske Veritas (DNV). Design of offshore wind turbine structures. DNV-OS-J101. Det Norske Veritas Classification A/S, Høvik (Norway); 2011.

[18] Doherty P, Gavin K. Laterally loaded monopile design for offshore wind farms. Proceedings of the ICE - Energy 2012;165(1):7–17.

[19] Elgamal A, Yang Z, Parra E. Computational modeling of cyclic mobility and post-liquefaction site response. Int J Soil Dynam Earthq Eng 2002;22:259–71.

[20] Elgamal A, Yang Z, Parra E, Ragheb A. Modeling of cyclic mobility in saturated cohesionless soils. Int J Plast 2003;19:883–905.

[21] Geuzaine C, Remacle JF. GMSH: a three-dimensional finite element mesh generator with built-in pre- and post-processing facilities. Int J Numer Meth Eng 2009;79(11):1309–31. <http://geuz.org/gmsh/>; 2014.

[22] Haiderali A, Madabhushi G. Three-dimensional finite element modelling of monopiles for offshore wind turbines. In: Proceedings of the world congress on advances in civil, environmental, and materials research. Seoul; 2012. p. 3277–95.

[23] Haiderali A, Cilingir U, Madabhushi G. Lateral and axial capacity of monopiles for offshore wind turbines. Ind Geotech J 2013;43(3):181–94.

[24] Hededal O, Klinkvort R. A new elasto-plastic spring element for cyclic loading of piles using the p–y curve concept. Numer Meth Geotech Eng: NUMGE Trondheim 2010:883–8.

[25] Hsu JRC, Jeng DS. Wave-induced soil response in an unsaturated anisotropic of finite thickness. Int J Numer Anal Meth Geomech 1994;18:785–807.

[26] Ibsen LB, Barari A, Larsen KA. Modified vertical bearing capacity for circular foundations in sand using reduced friction angle. Ocean Eng 2012;47:1–6.

[27] Irzal F, Remmers JJC, Verhoosel CV, Borst Rd. Isogeometric finite element analysis of poroelasticity. Int J Numer Anal Meth Geomech 2013;37:1891–907. http://dx.doi.org/10.1002/nag.2195.

[28] Jeremic' B. Lecture notes on computational geomechanics: inelastic finite elements for pressure sensitive materials. University of California, Davis; 2013.

[29] Khoei AR, Azadi H, Moslemi H. Modeling of crack propagation via an automatic adaptive mesh refinement based on modified SPR technique. Eng Fract Mech 2008;75:2921–45.

[30] Khoshghalib A, Khalili N. A stable meshfree method for fully coupled flow-deformation analysis of saturated porous media. Comp Geotech 2010;37:789–95.

[31] Krenk S, Kirkegaard PH. Local tensor radiation conditions for elastic waves. J Sound Vib 2001;247(5):875–96.

[32] Li J, Lin G, Chen J. An improved numerical time-domain approach for the dynamic damfoundation-reservoir interaction analysis based on the damping solvent extraction method. In: The 14th world conference on earthquake engineering. Beijing (China); 2008. p. 1–8.

[33] Li M, Zhang H, Guan H. Study of offshore monopile behaviour due to ocean waves. Ocean Eng 2011;38:1946–56.

[34] Li XK, Han XH, Pastor M. An iterative stabilized fractional step algorithm for finite element analysis in saturated soil dynamics. Comp Meth Appl Mech Eng 2003;192:3845–59.

[35] Lu JF, Jeng DS. Dynamic response of an offshore pile to pseudo-Stoneley waves along the interface between a poroelastic seabed and seawater. Int J Soil Dynam Earthq Eng 2010;30:184–201.

[36] Lysmer J, Kuhlemeyer RL. Finite dynamic model for infinite media. J Eng Mech Div, ASCE 1969;95(4):859–78.

[37] Maghoula P, Gatmiri B, Duhamela D. Boundary integral formulation and two-dimensional fundamental solutions for dynamic behavior analysis of unsaturated soils. Int J Soil Dynam Earthq Eng 2011;31:1480–95.

[38] Nadal E, Ródenas JJ, Albelda J, Tur M, Tarancón JE, Fuenmayor FJ. Efficient finite element methodology based on cartesian grids: application to structural shape optimization. Abst Appl Anal 2013;2013:1–19. Article ID 953786.

[39] Nazem M, Kardani M, Carter P, Sheng D. A comparative study of error assessment techniques for dynamic contact problems of geomechanics. Comp Geotech 2012;40:62–73.

[40] Olson RF. Consolidation under time-dependent loading. J Geotech Eng Div (ASCE) 1977;103:55–60.

[41] Pastor M, Li T, Liu X, Zienkiewicz OC. Stabilized low-order elements for failure and localization problems in undrained soils and foundations. Comp Meth Appl Mech Eng 1999;174:219–34.

[42] Pastor M, Li T, Liu X, Zienkiewicz OC, Quecedo M. A fractional step algorithm allowing equal order of interpolation for coupled analysis of saturated soil problems. Mech Cohes-Frict Mater 2000;5:511–34.

[43] Pastor M, Zienkiewicz OC, Chan AHC. Generalized plasticity and the modeling of soil behavior. Int J Numer Anal Meth Geomech 1990;14:151–90.

[44] Poulos H. Behavior of laterally loaded piles: I-single piles. J Soil Mech Found Div 1971;97(SM5):711–31.

[45] Prevost JH. Wave propagation in fluid-saturated porous media: an efficient finite element procedure. Soil Dynam Earthq Eng 1985;4:183–202.

[46] Richardson LF. The approximate arithmetical solution by finite differences of physical problems. Philos Trans Roy Soc Lond. Ser A, Contain Pap Math Phys Charact (Lond) 1910;210:307–57.

[47] Samimi S, Pak A. Three-dimensional simulation of fully coupled hydro-mechanical behavior of saturated porous media using Element Free Galerkin (EFG) method. Comp Geotech 2012;46:75–83.

[48] Scharff R, Siems M. Monopile foundations for offshore wind turbines—solutions for greater water depths. Steel Construct 2013;6(1):47–53.

[49] Soares Jr D. Iterative dynamic analysis of linear and nonlinear fully saturated porous media considering edge-based smoothed meshfree techniques. Comp Meth Appl Mech Eng 2013;253:73–88.

[50] Soares Jr D, Großeholz G, Estorff OV. A more flexible and effective analysis of porous media considering edge-based smoothed meshfree techniques. Comput Mech 2014;53:1265–77.

[51] Sørensen SPH, Ibsen LB. Assessment of foundation design for offshore monopiles unprotected against scour. Ocean Eng 2013;63:17–25.

[52] Tahghighi h, Konagai K. Numerical analysis of nonlinear soil–pile group interaction under lateral loads. Soil Dynam Earthq Eng 2007;27: 463–74.

[53] Tang X, Sato T. Adaptive mesh refinement and error estimate for 3-D seismic analysis of liquefiable soil considering large deformation. J Nat Disas Sci 2004;26:37–48.

[54] Tang X, Sato T. H-adaptivity applied to liquefiable soil in nonlinear analysis of soil–pile interaction. Soil Dynam Earthq Eng 2005;25(7):689–99.

[55] Tang X, Shao Q. Numerical simulation on seismic liquefaction by adaptive mesh refinement due to two recovered fields in error estimation. Soil Dynam Earthq Eng 2013;49:109–21.

[56] Ulker MBC, Rahman MS. Response of saturated and nearly saturated porous media: different formulations and their applicability. Int J Numer Anal Meth Geomech 2009;33:633–64.

[57] Ulker MBC, Rahman MS, Guddati MN. Wave-induced dynamic response and instability of seabed around caisson breakwater. Ocean Eng 2010;37: 1522–45.

[58] Ulker MBC, Rahman MS, Jeng DS. Wave-induced response of seabed: various formulations and their applicability. Appl Ocean Res 2009;31:12–24.

[59] Vonmarie MC. Static and dynamic response of monopiles for offshore wind turbines, Master Thesis. University of Wisconsin-Madison (United States); 2011.

[60] Xuan HN, Bordas S, Nguyen-Dang H. Smooth finite elements: incompressibility, accuracy, superconvergence, singularities and selective integration. Int J Numer Meth Eng 2008;74(2):175–208.

[61] Xunqiang Y, Jianbo L, Chenglin W, Gao L. Analysis implementation of damping solvent stepwise extraction method for nonlinear seismic analysis of large 3-d structures. Soil Dynam Earthq Eng 2013;44:139–52.

[62] Ye X. Domain decomposition for a least-square finite element method for second order elliptic problem. Appl Math Comput 1998;91:233–42.

[63] Zhang HW, Wanga KP, Chen ZZ. Material point method for dynamic analysis of saturated porous media under external contact/impact of solid bodies. Comp Meth Appl Mech Eng 2009;198:1456–72.

[64] Zhang Y, Jeng DS, Gao FP, Zhang JS. An analytical solution for response of a porous seabed to combined wave and current loading. Ocean Eng 2013;57:240–7.

[65] Zienkiewicz OC, Taylor RL. The finite element method. The basis, 5th ed., vol. 1. London: Butterworth Heinemann; 2000.

[66] Zienkiewicz OC, Chan AHC, Pastor M, Paul DK, Shiomi T. Static and dynamic behavior of soils: a rational approach to quantitative solutions. I. Fully saturated problems. Proc Roy Soc Lond. Ser A, Math Phys Sci 1990;429:285–309.

[67] Zienkiewicz OC, Chan AHC, Pastor M, Schrefler BA, Shiomi T. Computational geomechanics with special reference to earthquake engineering. England: John Wiley & Sons Ltd.; 1999. ISBN 978-0-471-98285-2.

[68] Zienkiewicz OC, Shiomi T. Dynamic behaviour of saturated porous media; the generalized Biot formulation and its numerical solution. Int J Numer Anal Meth Geomech 1984;8:71–96.

[69] Zienkiewicz OC, Zhu JZ. A simple error estimator and adaptive procedure for practical engineering analysis. Int J Numer Meth Eng 1987;24:337–57.

[70] Zienkiewicz OC, Zhu JZ. The superconvergent patch recovery and a posteriori error estimators. Part 2. Error estimates and adaptivity. Int J Numer Meth Eng 1992;33:1365–82.

[71] Zienkiewicz OC, Zhu JZ. The superconvergent path recovery and a posteriori error estimators. Part 1. The recovery technique. Int J Numer Meth Eng 1992;33:1331–64.

[72] Zienkiewicz OC, Zhu JZ. Superconvergence and the superconvergent patch recovery. Finite Elem Anal Des 1995;19:11–33.

SUMMARY

The present thesis concerns soil–structure interaction affecting the dynamic structural response of offshore wind turbines with focus on soil stiffness and seepage damping due to pore water flow generated by cyclic motion of a monopile. The thesis aims to improve modelling of the dynamic interaction between the foundation and the soil and illustrates the dynamic response of offshore wind turbines at different load frequencies based on mathematical and numerical approaches.

The stiffness and seepage damping has been investigated using the concept of a Kelvin model which combines springs and dashpots. An appropriate model based on considering the effect of dynamic behaviour of soil–structure interaction has been explored. In this regard, the coupled equations for porous media have been employed in order to account for soil deformation as well as pore pressure. The effects of drained versus undrained behaviour of the soil and the impact of this behaviour on the stiffness and damping related to soil–structure interaction at different load frequencies have been illustrated. Based on the poroelastic and Kelvin models, more realistic dynamic properties have been presented by considering the effect of load frequency for the lateral loading of monopiles subjected to cyclic loads.